How to cope with stress: Elucidating mRNP packaging by the characterization of stress induced mRNPs

Dissertation

zur Erlangung des Doktorgrades der Naturwissenschaften
(Dr. rer. nat.)
am Fachbereich 08 für Biologie und Chemie
der Justus-Liebig-Universität Gießen

vorgelegt von Johanna Franziska Seidler

Gießen,
Dezember 2022

Die vorliegende Arbeit wurde am Institut für Biochemie (Fachbereich 08) der Justus-Liebig-Universität Gießen, unter Leitung von Prof. Dr. Katja Sträßer, erstellt.

Dissertation eingereicht am: 20.12.2022

Erstgutachter: Prof. Dr. Katja Sträßer
Fachbereich 08: Biologie und Chemie
Institut für Biochemie
Justus-Liebig-Universität Gießen

Zweitgutachter: Apl. Prof. Dr. Elena Evguenieva-Hackenberg
Fachbereich 08: Biologie und Chemie
Institut für Mikrobiologie und Molekularbiologie
Justus-Liebig-Universität Gießen

Danksagung

Als erstes würde ich mich gerne bei Katja Sträßer dafür bedanken, dass ich die letzten Jahre in ihrer Arbeitsgruppe forschen durfte. Danke für das Vertrauen, dass du mir entgegenbringst und für die Freiheit meiner Neugier nachgehen zu können. Danke für die zahlreichen mRNP Meetings und deine positive Art.

Des weiteren geht mein Dank an mein Prüfungskomitee. Vielen Dank an Apl. Prof. Elena Hackenberg, dass Sie sich die Zeit genommen und mein Zweitgutachten erstellt hat. Ich bin sehr froh, dass auch Prof. Dr. Reinhard Dammann und Prof. Dr. Tilman Borggrefe zugesagt haben, Teil meiner Prüfungskommission zu sein. Vielen Dank für eure Zeit!

Ich würde mich gerne bei allen Mitgliedern der AG Sträßer bedanken, die meinen Weg bis hierhin begleitet haben. Wenn ich an meinen Anfang zurückdenke, will ich mich als erstes bei Nataliia für die gute Einarbeitung und den resultierenden positiven Start in meine PhD Zeit bedanken. Danke an Kristin und Laura, die nicht nur meine Kolleginnen, sondern auch meine Freundinnen geworden sind. Danke für eure Hilfe, Unterstützung und die schönen Zeiten, die wir zusammen verbracht haben. Auch bei Jeanette würde ich mich sehr gerne bedanken. Ohne dich wäre das Stress-Projekt nicht so möglich gewesen. Auch wenn hier noch viele Fragen offen sind, hoffe ich, dass wir das Projekt gemeinsam abschließen können. Danke, dass du trotz all meiner Anforderungen immer mitgezogen hast und ich viel in der Zusammenarbeit mit dir lernen durfte.

Ich würde mich auch gerne bei den Mitgliedern der AG Kilchert bedanken. Als erstes würde ich mich gerne bei Cornelia bedanken, dass sie immer ein offenes Ohr für mich hatte und auch für ihre Unterstützung beim Korrigieren meiner schriftlichen Arbeit. Darüber hinaus noch ein besonderer Dank an Nadine und Jacqueline, die mir bei zahlreichen Fragen und Problemen geholfen haben.

Ich möchte mich auch bei Prof. Dr. Gert Bange bedanken. Er hat mir gegenüber eine meiner heutigen Grundüberzeugungen als erster in Worte gefasst: „Wissenschaft sollte Spaß machen!“. Danke, dass du mir das mit auf den Weg gegeben hast. Ich hoffe, dass ich das nie vergesse und mir den Spaß behalten kann.

Als letztes möchte ich mich bei meiner Familie bedanken. Danke für euer Verständnis dafür, wie viel Zeit ich in meine Arbeit investiere. Besonders möchte ich mich bei meinen Eltern bedanken, dass sie immer versucht haben mir mit Fragen und Ratschlägen zur Seite zu stehen. Danke, dass ihr immer ein offenes Ohr für

meine Unigeschichten, Zukunftsplanungen und Sorgen habt. Danke für eure Hilfe, besonders in den letzten Monaten, und vor allem danke dafür, dass ihr mich immer dabei bestärkt habt diesen Weg einzuschlagen.

Contents

1. Zusammenfassung

Ein Merkmal eukaryotischer Zellen ist die Unterteilung der Zelle mittels Membranen in unterschiedliche Kompartimente. Im Zellkern wird die DNA in Boten-RNA (mRNA) transkribiert, die mRNA prozessiert und bereits cotranskriptionell von RNA-bindenden Proteinen in ein Boten-Ribonukleoprotein-Partikel (mRNP) verpackt. Korrekt prozessierte und verpackte mRNPs werden durch die Kernpore ins Cytoplasma transportiert, wo die Translation erfolgt. Obwohl viele Proteine bekannt sind, die in *Saccharomyces cerevisiae* für den mRNA-Export aus dem Zellkern benötigt werden (z.B. Hpr1, Yra1 und Nab2), ist die genaue Zusammensetzung und Struktur eines export-kompetenten mRNPs immer noch unklar. Da vorherige Studien zeigten, dass vielle der bekannten mRNA-Export-Faktoren nicht essentiell für den Export von Hitzestress-mRNAs sind, sind für Hitzestress-mRNAs nicht nur die Struktur und Stöchiometrie, sondern auch die enthaltenen Proteine eines export-kompetenten, nukleären Hitzstress-mRNPs unbekannt.
Das erste Ziel dieser Arbeit ist die Aufreinigung von einem nukleären, transkript-spezifischen mRNP um die exakte Zusammensetzung eines Hitzestress-mRNPs zu bestimmen und die Strukturaufklärung zu ermöglichen. Um das zu erreichen, werden zuerst alle nukleären mRNPs mittels des nukleären Cap-Binding-Komplex angereichert und anschließend alle mRNPs eines spezifischen Transkripts aufgereinigt. In dieser Arbeit wurde die Aufreinigung mittels Antisense-Oligonukleotiden und aptamer-basierte Reinigungsmethoden getestet. Obwohl für die Reinigung eines nukleären mRNPs, das die hochtranskribierte *CCW12* mRNA beinhaltet, eine hohe Reinheit und die Mitreinigung bekannter nukleärer RNA-bindender Proteine erzielt werden konnte, war das für die Hitzeschock-mRNA *SSA4* nicht der Fall. In zukünftigen Studien soll der Fokus auf die Identifizierung von mRNA-bindenden Proteinen gerichtet werden, die am Export von Hitzestress-mRNA beteiligt sind.
Während Hitzestress-mRNAs bei erhöhten Temperaturen aus dem Nukleus exportiert werden, akkumulieren viele andere mRNAs im Zellkern. Das zweite Ziel dieser Arbeit ist es zu untersuchen, ob die Akkumulierung von mRNAs im Nukleus eine generelle Stressantwort darstellt und wie diese zu Stande kommt. Bei zwei Dritteln der getesteten Stressbedingungen konnte eine Akkumulation von mRNA beobachtet werden. In einer vorherigen Studie konnte gezeigt werden, dass die Kinase Slt2 essentiell für den mRNA-Export-Block unter Hitzestress ist [Carmody et al., 2010]. Hier konnte allerdings kein genauer Zusammenhang zwis-

chen der Aktivierung von Slt2 und der Akkumulation von mRNA im Zellkern für unterschiedliche Stressbedingungen festgestellt werde. Um den Einfluss der Aktivierung von Slt2 auf Proteine des mRNA-Exports zu untersuchen, wurde eine Phosphoproteom-Analyse in einem *SLT2*-Deletionsstamm durchgeführt und abweichende Phosphorylierungsmuster in bekannten mRNA-bindenden Proteinen entdeckt. Mutationen der phosphorylierten Aminosäuren in drei mRNP-Komponenten zeigten eine Auswirkung auf den mRNA-Export-Block unter Hitzestress. So führt die Mutation von Yra1 und Nab2 zu einer Reduktion und die Mutation von Hpr1 zu einer Erhöhung der mRNA im Zellkern. Wie genau sich die Phosphorylierung dieser Proteine auf ihre Funktion auswirkt und auf welche Weise dies den mRNA-Export-Block beeinflusst, muss in zukünftigen Studien weiter untersucht werden.

2. Summary

In eukaryotic cells, transcription and translation are spatially separated and take place in the nucleus and the cytoplasm, respectively. Therefore, the transcribed messenger RNA (mRNA) needs to be exported from the nucleus for subsequent translation. Already during transcription mRNA-binding proteins are recruited and package the mRNA into a messenger ribonucleoprotein particle (mRNP). Only correctly processed and packaged mRNA will be exported through the nuclear pore complex into the cytoplasm. Although many components of the a nuclear mRNP are known (eg. Hpr1, Yra1, Nab2), the exact composition and structure remains unknown. During exposure to heat stress, *Saccharomyces cerevisiae* accumulates bulk mRNA within the nucleus, whereas heat shock mRNAs are exported. Until today it is not precisely known how these stress reactions are mediated. However, the dissociation of known mRNA export adaptors from the RNA seems to be a key feature.

The aim of this study is the purification of a nuclear heat shock mRNP to elucidate mRNP composition and structure. For this purpose, a two-step purification strategy was applied, in which enrichment of all nuclear mRNPs by purification of the nuclear cap-binding complex was followed by a subsequent RNA purification step to enrich transcript-specific nuclear mRNPs. The purification of RNA was performed with an antisense oligonucleotide or different aptamer-based approaches. Even though the purification methods yielded a high enrichment of nuclear mRNPs containing the highly transcribed *CCW12* mRNA, this was not the case for the purification of the heat shock mRNP containing *SSA4* mRNA. In future studies, the focus for heat shock mRNPs will be shifted to the identification of the proteins forming the heat shock mRNP.

Heat stress causes the accumulation of bulk mRNA within the nucleus. The second aim of this study is to investigate if this accumulation of poly(A)-RNA is a common stress reaction and how the cell mediates the nuclear mRNA export block. A nuclear poly(A)-RNA accumulation was not observed for all tested stresses. A previous study showed that the kinase Slt2 is essential for the mRNA export block during stress [Carmody et al., 2010]. However, no direct correlation between activation of Slt2 and the accumulation of mRNA for the different stresses tested could be observed in this study. In this work, a comparative phosphoproteome analysis was carried out to identify differential phosphorylation of known nuclear mRNA-binding proteins in a *slt2* mutant. Deletion of *SLT2* led to differentially phosphorylation of many proteins linked to mRNA export. Phosphorylation site mutants of nuclear mRNP components revealed that preventing phosphorylation of the Yra1 and Nab2 reduces the nuclear mRNA retention while a phosphomimicry mutant of Hpr1 increases nuclear poly(A)-RNA accumulation upon heat stress. Further studies are needed to understand by which mechanism the different mutants alter mRNA accumulation and how exactly the mRNA export block is mediated.

3. Introduction

mRNA biogenesis

A hallmark of eukaryotic cells is the compartmentalization of the cell separating the nucleus from the cytoplasm. This spatially separates transcription and translation and makes it necessary to transport the protein-coding messenger RNA (mRNA) from the nucleus to the site of translation in the cytoplasm. The DNA is transcribed in mRNA within the nucleus by RNA polymerase II (RNAPII), processed (capped, spliced and polyadenylated) and packaged into a messenger ribonucleoprotein particle (mRNP). Only a correctly processed and packaged mRNA is transported into the cytoplasm. The formation of a mRNP occurs in parallel to the transcription of the mRNA due to the recruitment of many RNA-binding proteins to transcribing RNAPII. The main platform of recruitment is the C-terminal domain (CTD) of Rpb1, the largest subunit of RNAPII [Corden et al., 1985, Liu et al., 2010]. The CTD consists of repeats of a heptapeptide with the consensus sequence YSPTSPS. The CTD of *Saccharomyces cerevisiae*, hereafter referred to as yeast, harbors 26 repeats while higher eukaryotes have more repeats. The CTD undergoes various changes in phosphorylation through one cycle of transcription [Tietjen et al., 2010, Mayer et al., 2010, 2012a]. During transcription initiation the residues S5 and S7 are phosphorylated. S5 and S7 phosphorylation decreases when RNAPII enters elongation, which is accompanied by phosphorylation at the residues S2 and Y1. The phosphorylation of Y1 and S2 decreases at the site of polyadenylation and termination, respectively. The specific phosphorylation pattern of the CTD plays a crucial role in the recruitment of many proteins involved in chromatin remodeling, pre-mRNA processing and mRNP formation [Cho et al., 1997, Ng et al., 2003, Meinel et al., 2013]. Other recruitment platforms beside the CTD are the nascent mRNA itself [Meinel et al., 2013, Tuck and Tollervey, 2013] and a C-terminal region (CTR) of the general transcription elongation factor Spt5, which also comprises repeats that can be phosphorylated during transcription [Lindstrom et al., 2003, Mayer et al., 2012b].

The first processing step of a nascent mRNA is capping of its 5' end, which is required to protect the mRNA from exonucleolytic degradation [Furuichi et al., 1977]. The capping enzymes are recruited to S5-phosphorylated CTD during transcription initiation [Cho et al., 1997, Fabrega et al., 2003]. The capping requires a RNA triphosphatase (Cet1), a RNA guanyltransferase Ceg1 and a guanine-N7

methyltransferase (Abd1) [Mao et al., 1995, Cho et al., 1998]. Cet1 removes the γ-phosphate of the 5' end to generate a diphosphate. In a second step, Ceg1 transfers a GMP from a GTP to the 5' diphosphate of the nascent mRNA. Abd1 transfers a methyl group to the N-7 of the guanosine [Mao et al., 1995]. The created m7G cap is bound by the nuclear cap binding complex (CBC) which consists of the subunits Cbp20 and Cbp80. Cbp20 binds directly to the m7G cap and Cbp80 stabilizes this interaction. The nuclear CBC participates in the recruitment of other mRNA processing factors during mRNA processing and mRNP maturation [Flaherty et al., 1997, Andersen et al., 2013, Pabis et al., 2013]. After the export of the mRNA into the cytoplasm the nuclear CBC is replaced by the eukaryotic initiation factor eIF4E [Fortes et al., 2000].

The next major step in pre-mRNA processing is splicing. During splicing the non-coding sequences (introns) of a pre-mRNA are removed from in between the coding sequences (exons), which are ligated back together. In contrast to humans, only a minority of genes in yeast contain introns [Hooks et al., 2014]. An example for a gene possessing an intron is *YRA1* (Yeast RNA annealing protein 1) [Portman et al., 1997]. Splicing occurs cotranscriptionally and is mediated by the spliceosome. The spliceosome consists of the U1, U2, U5 and U4/U6 small nuclear RNP (snRNP) and non-snRNP proteins. Each snRNP in turn comprises a snRNA, seven Sm proteins and particle-specific proteins [Séraphin, 1995, Rauhut et al., 2016, Plaschka et al., 2017]. Each intron/exon boundary is marked by a splice site (ss). These 5' and 3' ss, plus a branch site (BS), define the binding sites for the splicesome. To sum up the major splicing steps, the U1 snRNP is recruited to the 5'ss [Séraphin et al., 1988]. The branch point-binding protein Msl5 binds the BS, while the protein Mud2 binds downstream of the BS [Kistler and Guthrie, 2001, Jacewicz et al., 2015]. In a following step, the U2 snRNP binds the BS while Msl5 is displaced (A complex) [Gozani et al., 1998]. The formation of the A complex involves the helicases Prp5 and Sub2 [Kistler and Guthrie, 2001]. Afterwards, the U4/U6/U5 snRNP is recruited (B complex) [Plaschka et al., 2017]. Structural rearrangements lead to the dissociation of U1 and U4 snRNP and formation of the active spliceosome (Bact complex) [Rauhut et al., 2016]. The intron is removed by two transesterification reactions. In the first reaction, a nucleophilic attack is performed from the 2'OH group of the BS adensoine on the 5' ss. This leads to the formation of a lariat structure. In a second step, the 3'OH group of the 3'ss carries out a nucleophilic attack on the 5'exon. This results in the ligation of both exons and the release of the intron [Zaug et al., 1983, Cech, 1987]. Many other proteins are also important for correct splicing. For example, the proteins Gbp2 and Hrb1, which bind to pre-mRNA and the spliceosome, function in surveillance of splicing and mark incorrect spliced RNAs for degradation [Hackmann et al., 2014].

After correct splicing has been completed, the last processing step of the nascent mRNA is the 3'end processing. The process is carried out by the cleavage and polyadenylation factor (CPF), which is recruited to the transcription site due to binding of 3' end processing factors such as Pcf11 to the S2-phosphorylated CTD. In addition, binding to the polyadenylation site of the nascent mRNA and to the CTR of Spt5 plays a significant role in recruitment of the CPF complex. CPF is a multiprotein complex that includes a nuclease, a polymerase, and a phosphatase/ATP module [Casañal et al., 2017]. The mRNA is cleaved, followed by a polyadenylation step conducted by the CPF polymerase module protein Pap1. After this, the Pab1-dependent polyadenylation nuclease (PAN) shortens the poly(A) tail to a defined length of 60 to 80 nt in yeast [Brown and Sachs, 1998]. The poly(A) tail is bound by poly(A)-binding proteins like Pab1 (Poly(A)-binding protein) and Nab2 (Nuclear abundant polyadenosine (poly(A)) RNA-binding protein 2) which are involved in regulating the length of the poly(A) tail by stabilization and prevention of readenylation [Hector et al., 2002, Viphakone et al., 2008, Kelly et al., 2010].
This very brief summary of transcription and maturation of mRNA only mentions some key steps of mRNP biogenesis, but already here the extend of factors involved and tightly controlled steps become apparent. All these steps need to be carried out correctly before the mature mRNA can be transported into the cytoplasm. Nevertheless, packaging of an export competent mRNP takes place simultaneously.

Nuclear mRNP assembly and export

After the mRNA has been transcribed and processed, it needs to be exported from the nucleus to the cytoplasm where translation takes place. The export of mRNA from the nucleus is a mechanism that is conserved from humans to yeast [Sträßer et al., 2002]. The formation of an export-competent mRNP starts already cotranscriptionally with recruitment of TREX complex components to the transcription site. The TREX complex couples transcription and export and consists of the heteropentameric THO complex (Hpr1, Tho2, Mft2, Tex1, Thp2), the Serine-Arginine-rich (SR)-like proteins Gbp2 and Hrb1, and the RNA export factors Sub2 and Yra1. The THO complex is recruited to the transcription site by binding to the S2-S5 phosphorylated CTD of RNAPII and the nascent RNA [Meinel et al., 2013]. Recruitment of the THO complex is necessary to promote efficient transcription elongation [Chavez et al., 2000, Mason and Struhl, 2005]. Deletion of THO components cause defects in transcription, mRNA export and can lead to a hyperrecombination phenotype [Chavez et al., 2001, Chavez and

Aguilera, 1997, Jimeno et al., 2002].
In recent years, several groups published structures of the yeast and human THO complex together with other TREX components [Ren et al., 2017, Schuller et al., 2020, Pühringer et al., 2020, Xie et al., 2021, Chen et al., 2021]. It could be shown that in yeast the THO-Sub2 complex forms a dimer while a tetramer is formed in humans. The THO complex assembles around its largest subunit Tho2. Gbp2 interacts with the THO complex via its RS and RRM domain [Xie et al., 2021]. In the THO-Gbp2 complex the RRM domain of Gbp2 is located closely to the C-terminal domain of Tho2. Therefore, it was postulated that the THO complex functions as platform to facilitate loading Gbp2 onto the mRNP. The SR-like proteins Gbp2 and Hrb1 are important for the export of correctly spliced mRNA [Hackmann et al., 2014]. It could be shown that in the absence of Gbp2 and Hrb1, unspliced pre-mRNA is exported into the cytoplasm. After splicing, correctly spliced mRNAs are bound by the adapters Gbp2 and Hrb1 which in turn aid in the recruitment of the export receptor Mex67 and shuttle together with the mRNA to the cytoplasm.
Sub2 and its human homologe UAP56 are DEAD-box RNA helicases. However, Sub2 belongs to a subfamily of DEAD-box helicases that harbors a DECD instead of the classical DEAD sequence defining this RNA helicase family [Fan et al., 2001]. Sub2 and UAP56 were identified originally as proteins involved in mRNA splicing [Fleckner et al., 1997, Noble and Guthrie, 1996]. Further research highlighted the importance of Sub2 in many other processes. Overexpression of Sub2 and a thermosensitive mutant were shown to cause an mRNA export block in yeast, indicating the importance of Sub2 for mRNA export [Sträßer and Hurt, 2001]. Depletion of Sub2 leads to genomic instability and increased formation of DNA-RNA hybrids during transcription (R-loops) [Domínguez-Sánchez et al., 2011]. The genomic instability caused by mutations of Sub2 could be rescued by Hpr1 overexpression, while the overexpression of Sub2 in turn is able to rescue the genomic instability caused by deletion of *HPR1* [Fan et al., 2001]. The recently published structures of the THO complex and Sub2 suggest that the THO complex functions as a kind of platform to place Sub2 for Yra1 loading [Schuller et al., 2020]. Interaction with Tho2 causes a half-open conformation of Sub2 while interaction with RNA and the C-terminus of Yra1 leads to a closed conformation [Ren et al., 2017, Xie et al., 2021]. In addition, it was found that the THO complex and Yra1 can stimulate the RNA-dependent ATPase activity of Sub2 [Ren et al., 2017, Chen et al., 2021].

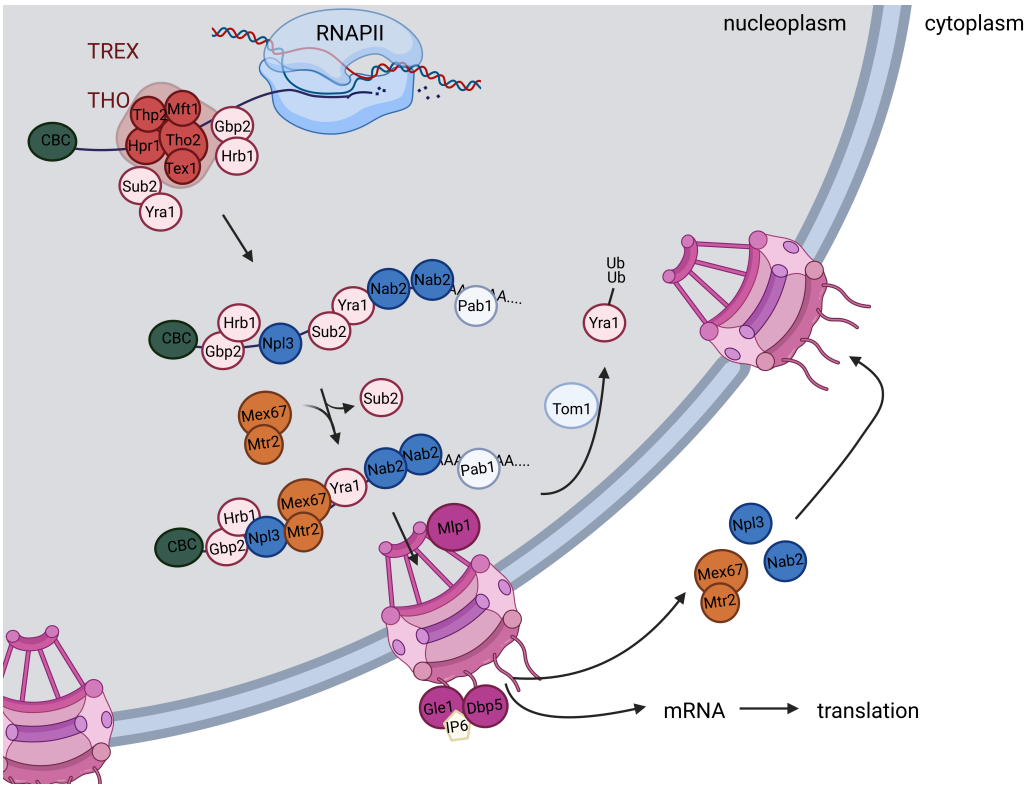

Figure 3.1: **mRNA export from nucleus** Schematic representation depicting the major steps of nuclear mRNA export. The TREX complex (red) binds cotranscriptionally to the nascent mRNA together with other adaptor proteins that are no TREX components (eg.Nab2 and Npl3, blue). Sub2 dissociates from the complex, which allows recruitment of the export receptor Mex67-Mtr2 (orange) to the mRNP. Tom1 (light blue) ubiquitinylates Yra1 causing its dissociation from the mRNP. The RNA is exported to the NPC (pink) and the mRNP is remodeled at the cytoplasmic site of the NPC by Dbp5, which leads to the dissociation of RNA-binding proteins. The RNA-binding proteins are reimported and can facilitate another round of mRNA export. Created with BioRender.com. Ub = ubiquitin

Yra1 is a nuclear protein that possesses an annealing activity and is conserved from yeast to humans (ALY/REF) [Portman et al., 1997]. It consists of an RRM domain, an N- and C-variable part and an N- and C-box [Portman et al., 1997, Stutz et al., 2000, Shchepachev et al., 2019] (Figure 5.20 A). The N- and C-terminus build the binding sites for Pcf11 [Johnson et al., 2009], Sub2 and Mex67 [Sträßer and Hurt, 2001, Ren et al., 2017, Schuller et al., 2020]. First, it was postulated that the THO complex recruits Sub2 to transcribed genes, which in turn recruits Yra1 [Sträßer and Hurt, 2001, Sträßer et al., 2002]. This mechanism was also described for THO, UAP56 and ALY in metazoans [Luo et al., 2001, Kiesler et al., 2002]. Later it was proposed that Yra1 is first recruited to the transcription site by Pcf11, then transferred to Sub2 [Johnson et al., 2009]. Taken together, these data indicate recruitment of Yra1 over multiple pathways to the transcription site. However, Yra1 and the THO complex stimulate the ATPase activity of Sub2, which

could lead to the release of Sub2 from the mRNP, which allows the binding of Yra1 to the mRNA exporter Mex67 and the formation of a ternary Yra1-Mex67-Nab2 complex [Ren et al., 2017, Sträßer and Hurt, 2001, Iglesias et al., 2010]. Yra1 is ubiquitinylated by the E3 ubiquitin ligase Tom1 and thereby released from the nuclear mRNP before being exported through the NPC [Iglesias et al., 2010].
Mex67 (NXF1 in humans) builds a dimer together with Mtr2 (p15 in humans). This heterodimer functions as mRNA exporter [Segref et al., 1997, Hurt et al., 2000] and is recruited to the mRNA via several adapter proteins. Besides the recruitment via the TREX complex as described above, the adapter proteins Nab2 and Npl3 [Gilbert and Guthrie, 2004] can recruit mRNA to Mex67.
Npl3 is a SR-like protein which is mainly localized in the nucleus [Wilson et al., 1994], but shuttles with the mRNA to the cytoplasm. This is regulated by a phosphorylation cycle. Cytoplasmic Npl3 is phosphorylated in one of its eight SR motifs (S411) by Sky1, which allows the import into the nucleus by the importer Mtr10 [Gilbert et al., 2001]. In the nucleus Npl3 is dephosphorylated by Glc7, which allows the association with mRNA and interaction with Mex67 [Gilbert and Guthrie, 2004]. However, Npl3 can also be phosphorylated by other kinases [Dermody et al., 2008, Smolka et al., 2007]. Besides Npl3´s function in mRNA export, it is known to have many additional functions in chromatin modification, transcription, splicing, R-loop prevention and translation [Baierlein and Krebber, 2013, Bucheli and Buratowski, 2005, Dermody et al., 2008, Kress et al., 2008, Pérez-Martínez et al., 2020].
The other mRNA export adapter which is not part of the TREX complex is Nab2. Nab2 was identified as protein that binds to nuclear polyadenylated RNAs [Anderson et al., 1993]. Similar to Npl3, Nab2 is also involved in many different processes like transcription, poly(A) tail length control, mRNP formation, mRNA export and RNAPIII transcription [Anderson et al., 1993, Batisse et al., 2009, Gallardo et al., 2003, Reuter et al., 2015]. The C-terminus of Nab2 contains seven Zinc finger (ZnF) domains that mediate binding to polyadenylated RNA (ZnF5, ZnF6, ZnF7) (Figure 5.22 A) [Anderson et al., 1993, Aibara et al., 2017]. In turn RNA binding results in dimerization of Nab2 [Aibara et al., 2017]. Furthermore, Nab2 contains a PY-NLS and RGG domain which are thought to be important for the reimport of Nab2 via the importer Kap104 [Aitchison et al., 1996, Marfatia et al., 2003, Soniat et al., 2013]. At its N-terminus Nab2 possesses a PWI-like domaine, [Szymczyna et al., 2003] which is important for nuclear export by mediating the interaction of Nab2 with Mlp1 (Myosin-Like Protein 1). Mutagenesis studies identified Phe73 as the main interacting amino acid with the C-terminal domain of Mlp1 [Grant et al., 2008, Fasken et al., 2008]. In addition, the N-terminus also functions in the interaction with Gfd1 (Good For Dbp5 protein 1), a high

copy suppressor of *rat8-2* mutant (Rat8 = Dbp5) that interacts with Rip1 (Rieske Iron-sulfur Protein 1/Nup42) and Dbp5 (DEAD box protein 5) at the cytoplasmic site of the nuclear pore complex (NPC) [Christine A. Hodge et al., 1999, Suntharalingam et al., 2004, Zheng et al., 2010]. It was also found that Nab2 interacts directly with Mex67 [Iglesias et al., 2010]. This interaction is promoted by Yra1 by forming a ternary complex. Also an interaction of Nab2 with the THSC/TREX-2 complex was observed, indicating another link of Nab2 to nuclear mRNA export [Gallardo et al., 2003].
The THSC/TREX2 complex is another conserved, multiprotein complex which couples transcription and mRNA export [Fischer et al., 2002, Gallardo et al., 2003, Rodríguez-Navarro et al., 2004, Fischer et al., 2004]. It consists of Sac3, Thp1, Sem1, Cdc31 and the SAGA histone acetylase complex component Sus1. It tethers the mRNP to the NPC by interacting with NUPs and the export-receptor Mex67/Mtr2 [Fischer et al., 2002].
In summary, it was shown that the TREX complex, Nab2 and Npl3 can recruit the mRNA to the export-receptor Mex67/Mtr2, but how does a export-competent mRNP really look like? As described above, formation of a nuclear mRNP starts with transcription. After capping, the nuclear CBC is recruited to the nascent transcript followed by the splicing machinery. In parallel, the TREX complex is recruited and Npl3 binds to prevent premature 3´end processing [Meinel et al., 2013, Bucheli and Buratowski, 2005]. The polyadenylation machinery and polyA-binding proteins like Nab2 are required for correct 3´end processing. All the involved proteins are recruited by the CTD, the CTR, the nascent transcript and through protein-protein interactions. Therefore, the assembly of nuclear mRNPs is a very complex, highly regulated and dynamic process. Although, many proteins and processes involved are known the exact composition and structure of nuclear mRNPs and their remodeling processes remain unknown.

mRNA transport through the nuclear pore

If an export-competent mRNP is formed the mRNA needs to be exported through the NPC into the cytoplasm. The TREX complex, Nab2 and Npl3 all take place in the recruitment of the mRNP to the mobile NUP and export receptor Mex67/Mtr2. In addition, Nab2 and Npl3 bind to Mlp1 and Yra1 to Mlp1 and Mlp2 [Fasken et al., 2008, Green et al., 2003, Vinciguerra et al., 2005, Bangs et al., 1998] locating the export-competent mRNP to the NPC. The NPC is a multi-protein complex consisting of multiple copies of around 30 nuclear pore proteins (nucleoporins or NUPs) [Rout et al., 2000, Alber et al., 2007] (Figure 3.2). The proteins form a channel through the nuclear envelope with eight-fold symmetry including several

substructures. It can be roughly divided into the inner ring with the central transport channel surrounded by the cytoplasmic and nuclear ring and the peripheral elements, the nuclear basket and the cytoplasmic filaments.
The nuclear basket consists of the phenylalanine and glycine (FG)-rich NUPs Nup1, Nup2 and Nup60 and the structural component Mlp1 and Mlp2 [Rout et al., 2000]. In yeast, however, not all NPC possess a nuclear basket [Galy et al., 2004]. Also an *MLP1 MLP2* double deletion is viable and shows only a slight mRNA export block but unspliced RNAs can be found in the cytoplasm in these cells. This leads to the understanding of the nuclear basket as platform for processing and quality control of nuclear mRNAs allowing a selective transport of fully mature mRNAs [Galy et al., 2004, Vinciguerra et al., 2005]. Single molecule methods now added the model of periphery-scanning of a mRNP which is prolonged by the nuclear basket. It was found that deletion of *MLP1* as well as mutations of Nab2 preventing the interaction of both proteins alters periphery scanning and leads to the release of mRNPs back into the nucleoplasm [Saroufim et al., 2015].

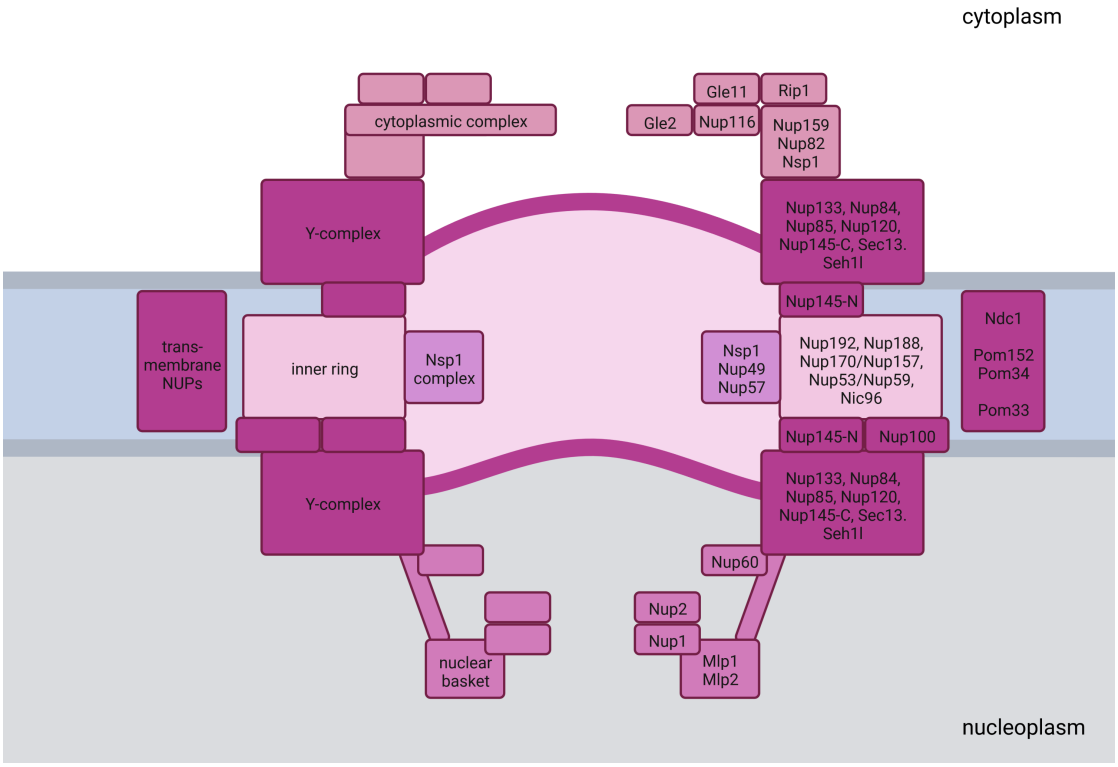

Figure 3.2: **Schematic representation of the NPC** The schematic representation of the NPC shows the main NUPs from *S. cerevisiae*. On the right site the different NUPs are listed. On the left site the names of the corresponding subcomplexes are labeled. The composition of the NPC was illustrated after Beck and Hurt [2017]. Created with BioRender.com.

The central channel of the NPC is lined with many FG-NUPs that interact transiently with nuclear transport receptors with low affinity allowing transport through the NPC [Rexach and Blobel, 1995, Sträßer et al., 2000]. Also the nuclear and cytoplasmic parts of the NPC contain FG-NUPs with several having redundant functions [Rout et al., 2000, Strawn et al., 2004, Alber et al., 2007]. Mex67/Mtr2 was described as mobile nucleoporin [Derrer et al., 2019] that binds to the FG-repeats of NUPs and thereby exports the mRNA through the NPC [Segref et al., 1997, Sträßer et al., 2000, Hurt et al., 2000, Derrer et al., 2019]. To that end, Mex67 possesses a C-terminal nuclear transport factor 2-like domain, containing two nuclear export signal motifs mediating the interaction with FG-repeat NUPs [Grant et al., 2002, Thakurta et al., 2004].
The cytoplasmic filament comprises besides others the FG-NUP Nup159. This localizes the helicase Dbp5 to the cytoplasmic side of the NPC [Schmitt et al., 1999, Christine A. Hodge et al., 1999, Weirich et al., 2004]. Dbp5 is another DEAD-box helicase that is important for nuclear mRNA export. While Dbp5 can be recruited to the nascent mRNP and shuttle through the NPC [Snay-Hodge et al., 1998, Christine A. Hodge et al., 1999, Estruch and Cole, 2003], it is mainly localized at the cytoplasmic side. It consists of two RecA domains connected by a linker and an N-terminal domain (Figure 5.24). At the cytoplasmic face of the NPC, Dbp5 interacts with Gle1 and inositol-6-phosphate (IP6), which stimulate its ATPase activity [Christine A. Hodge et al., 1999, Weirich et al., 2006]. This leads to the remodeling of the exported mRNP causing the release of Mex67 and Nab2 from the mRNP [Lund and Guthrie, 2005, Adams and Wente, 2020]. Afterwards, dissociated export factors can be reimported and facilitate another round of nuclear mRNA export.

How yeast copes with stress

Adaptation to external stimuli is essential for survival. Therefore, yeast possesses many mechanisms to protect the cell from stress and ensure survival when exposed to stress. One example how the cell triggers a stress response is the cell wall integrity pathway (CWI) (Figure 3.3). Membrane-spanning mechanosensors are responsible for stress detection. The most important sensors are Wsc1 and Mid2 [Ketela et al., 1999] and deletion of Wsc1 sensor results in cell lysis above 37°C [Gray et al., 1997, Verna et al., 1997, Jacoby et al., 1998]. Upon activation the sensors activate the GTPase Rho1 through the GDP/GTP-exchange factor Rom2 [Philip and Levin, 2001]. Rho1 in turn activates Pkc1 (Protein kinase C) [Kamada et al., 1996]. Pkc1 activates a mitogen-activated protein kinase (MAPKs) cascade. The MAPK kinase kinase Bck1 [Lee and Levin, 1992] phosphorylates the

MAPK kinases Mkk1 and Mkk2 [Irie et al., 1993]. Both can in turn activate the MAPK Suppressor of the LyTic phenotype (Slt2/Mpk1) [Martin et al., 1993, Lee et al., 1993]. Slt2 is a mainly nuclear localized kinase with many verified targets that plays a role in cell wall biogenesis, actin cytoskeleton dynamics, cell cycle progression, mitochondrial inheritance and many more [Mazzoni et al., 1993, Du et al., 2006, Li et al., 2010, Mascaraque et al., 2013, Moreno-Torres et al., 2015, Ahmadpour et al., 2016].

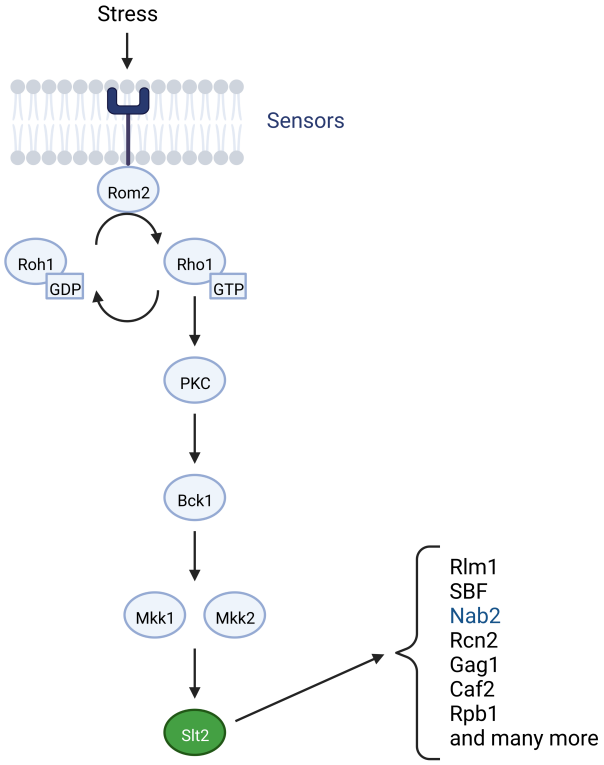

Figure 3.3: **Schematic representation of the major components that are involved in the CWI pathway stress response.** Representation of the main components of the CWI pathway. The MAPK cascade activates the MAPK Slt2 (green). Some selected targets of Slt2 are mentioned. Created with BioRender.com.

To mention only some verified targets: Slt2 activates the transcription factor Rlm1 which triggers the main transcriptional response needed to survive cell wall stress including Slt2 and Rlm1 itself [Jung and Levin, 1999]. The SBF complex, comprising Swi4 and Swi6, is also activated by Slt2 and leads to the activation of the transcriptional program controlling G1/S-phase transition [Kim et al., 2008]. Slt2 can also phosphorylate Y1 of Rpb1 to upregulate the transcription of stress-induced genes [Yurko et al., 2017]. Another target is the translation initiation repressor Caf20 [Mascaraque et al., 2013]. Caf20 inhibits translation of mRNAs involved in cell cycle, cell morphogenesis and intracellular signaling [Alonso-Rodríguez et al., 2016, Castelli et al., 2015]. Also, traffic from the Golgi to the vacuole is influenced

by the CWI pathway through the Slt2 target Gag1 (Golgi-associated protein 1) [Alonso-Rodríguez et al., 2016].
In addition to Rlm1 and the SBF complex, other transcription factors have been identified that mainly act in the activation of the heat stress response. One is the heat shock factor 1 (Hsf1), the others are Msn2 and Msn4. Hsf1 is an essential protein, which is constitutively phosphorylated but gets hyperphosphorylated upon heat stress [Sorger and Pelham, 1988]. The activated Hsf1 homotrimer recognizes the promoter region of its targets by binding to heat shock elements (nGAAn)[Sorger and Pelham, 1987, Amin et al., 1988, Yamamoto et al., 2005]. To activate transcription, Hsf1 recruits the mediator complex, which in turn interacts with RNAPII [Kim and Gross, 2013]. Msn2 and Msn4 are transcription factors also known to activate a general stress response. Upon hyperphosphorylation the proteins are activated and relocate to the nucleus [Görner et al., 1998, Garreau et al., 2000]. Within the nucleus, Msn2/4 bind to stress-responsive elements STRE (CCCCT) [Marchler et al., 1993] in the promoters of their target genes and activate transcription [Martínez-Pastor et al., 1996, Schmitt and Mcentee, 1996]. Msn2/4 are negatively regulated by the cAMP-PKA pathway, which prevents their nuclear localization [Boy-Marcotte et al., 1998, Smith et al., 1998]. It was found that even without stress Msn2/4 migrate from the cytoplasm to the nucleus in an oscillatory manner indicating a regulatory feedback loop mediated by kinases and phosphatases [Jacquet et al., 2003]. Boy-Marcotte et al. [1999] tried to distinguish between Hsf1 and Msn2/4 transcription response. They found that Hsf1 leads mainly to the transcription of chaperons [Boy-Marcotte et al., 1999] while the transcription factors Msn2/4 causes the expression of enzymes involved in carbon metabolism and antioxidant enzymes. However, there are genes as *HSP26* and *HSP12* where both transcription factors can activate transcription [Boy-Marcotte et al., 1999, Amorós and Estruch, 2001].
The changed transcription upon heat stress in yeast causes among others the expression of heat shock proteins (HSPs). In yeast the major HSPs are Hsp104, Hsp90, Hsp70, Hsp60, Hsp30 and Hsp26 which in general function as chaperones [Reading et al., 1989, Parselt et al., 1991, Régnacq and Boucherie, 1993, Nathan et al., 1997, Glover and Lindquist, 1998]. Hsp70 prevents protein aggregation by binding hydrophobic surfaces of denatured proteins. In complex with Hsp40 and Hsp104, they can also reactivate denatured proteins and lead to the disaggregation of larger protein complexes after removal of the stressor [Glover and Lindquist, 1998]. Several genes encode for the 70 kDa Hsp70 protein; one of them is *SSA4*. The *SSA4* promoter contains heat shock elements leading only to a low level of transcription without stress treatment [Boorstein and Craig, 1990].
As already mentioned, to survive stress exposure, a massive change in the tran-

scriptome [Varol et al., 2018] occurs. However, besides the change in transcription, a major change in translation can also be observed. A reduced mRNA-binding could be detected for factors involved in 43S complex recruitment and scanning which was postulated to block translation initiation upon heat stress [Bresson et al., 2020]. The inhibition of mRNA translation and polysomes disassembly, leads to the formation of cytoplasmic stress granules [Kedersha et al., 2002]. Stress granules are membraneless, solid-like amorphous aggregates formed upon stress treatment [Kroschwald et al., 2015]. They contain many translation initiation factors, the 40S ribosome, RNA-binding proteins (e.g. Pab1), disagregases/chaperones (eg. Hsp104) and polyadenylated mRNA [Kedersha et al., 2002, Kroschwald et al., 2015, Cherkasov et al., 2015, Khong et al., 2017]. It was proposed that stress granules serve as storage for capped and polyadenylated mRNAs so that they are protected from degradation and can be translated immediately after removal of the stressor [Kroschwald et al., 2015].
Besides the formation of stress granules, P-bodies can be observed upon stress treatment. P-bodies are dynamic assemblies of translationally inactive mRNAs and proteins involved in translation repression and mRNA turnover. In yeast several proteins are found to serve as marker for P-bodies including Dcp1, Dcp2, Edc3, Dhh1, Pat1, Lsm1, Xrn1, Ccr1 and Pop2 [Teixeira and Parker, 2007]. Originally thought to be sites of mRNA degradation, recent findings suggest that P-bodies are storage sites for translationally repressed mRNAs [Hubstenberger et al., 2017, Horvathova et al., 2017]. While in mammalian cells P-bodies can be observed even without stress [Souquere et al., 2009], in yeast they are only visible upon stress treatment [Buchan et al., 2008, Wang et al., 2018]. Stress granules and P-bodies are two distinct assemblies even though some proteins are present in both. In yeast cells, they seem to largely overlap during microscopy experiments [Buchan et al., 2008]. However, the exchange of mRNA between this assemblies is only very marginal [Wilbertz et al., 2019].

Nuclear mRNA export under stress

It has been known for a while that stress treatment leads to an accumulation of bulk mRNA within the nucleus, whereas heat shock mRNAs are exported from the nucleus (Figure 3.4). It was shown that the accumulation of mRNA occurs in response to various stress treatments like heat stress, ethanol treatment and glucose starvation [Saavedra et al., 1996, Heinrich et al.]. However, it still remains elusive how the cell mediates the mRNA export block. It was shown that under heat stress many of the known mRNA export adapters described above dissociate from the mRNA [Zander et al., 2016]. Nab2 and Yra1 accumulate in nuclear foci in an

Mlp1 dependent manner upon heat stress and glucose starvation [Carmody et al., 2010, Heinrich et al.]. Gbp2 was found to aggregate under heat stress [Wallace et al., 2015]. The adapter Npl3 it was postulated to be transiently localized to the cytoplasm under heat stress, as increased cytoplasmic localization was found for the *npl3-27* mutant (E409K point mutation) at 37°C and 42°C [Krebber et al., 1999]. The export receptor Mex67 remains localized at the nuclear rim upon heat stress [Carmody et al., 2010, Adams and Wente, 2020].

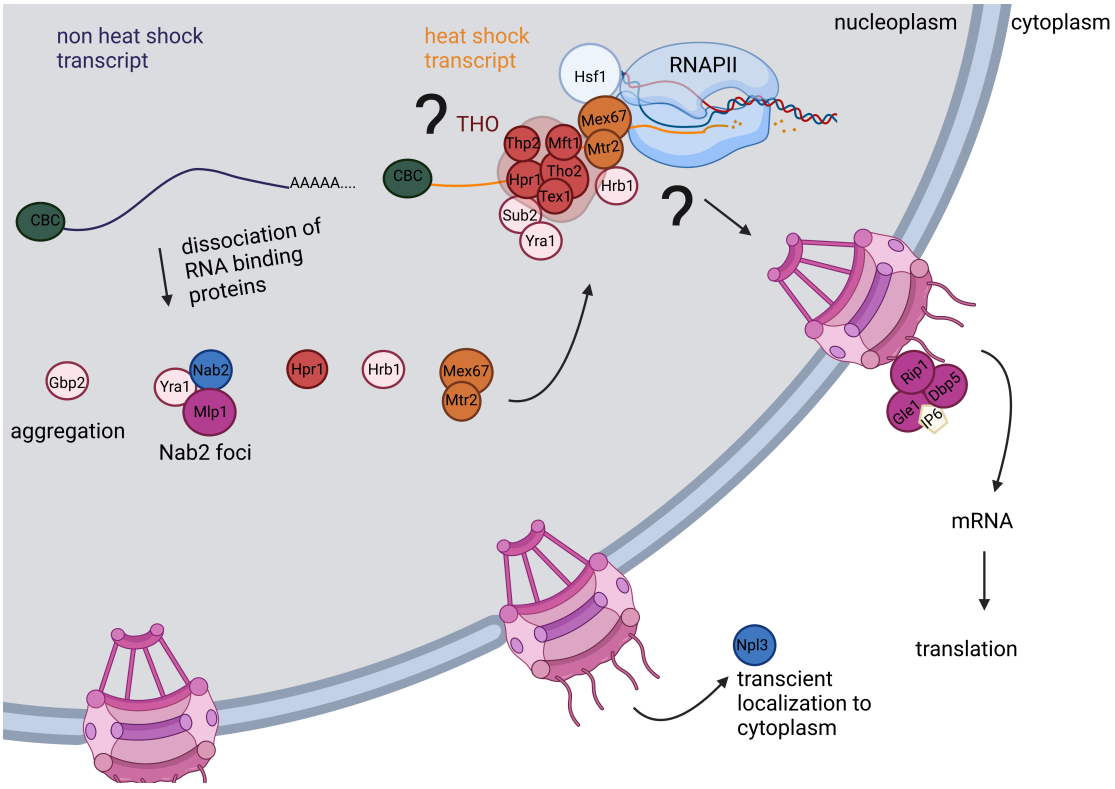

Figure 3.4: **Changes in nuclear mRNA export during stress** The graphic shows the changes known to occur during stress and marks some of the open questions. On the left, the dissociation of known mRNA-binding proteins is depicted. This includes the aggregation of Gbp2 and the formation of nuclear Nab2 foci. The proteins, dissociated from the bulk mRNA, could bind to newly transcribed heat shock mRNAs (orange). This is depicted on the right side. Since it is not clear for all of the shown proteins whether they really bind or are necessary for heat shock mRNA export the transcription site is marked by question marks. Hsf1 is thought to bind and recruit the export receptor Mex67-Mtr2 to the heat shock mRNA, which facilitates the export of the mRNA into the cytoplasm through the NPC. Created with BioRender.com.

The mRNA export block under heat stress was shown to be dependent of Slt2, since a deletion leads to a rescue of the export block [Carmody et al., 2010]. However, mutation of the identified Slt2-dependent phosphorylation sites of Nab2 (T178 and S180) were not sufficient to rescue the mRNA export block. This indicates the importance of posttranslational modifications for the mRNA export block during stress, but also highlights that probably not one single protein is responsible for

the export block.
The changed localization and aggregation of the known adapter proteins correlates with the hypothesis that heat shock mRNAs do not undergo quality control and are therefore exported differently than bulk mRNAs at 30°C [Zander et al., 2016]. Only Sub2, Mex67, Dbp5 and Gle1 were shown to be necessary for heat shock mRNA export [Saavedra et al., 1997, Hurt et al., 2000, Rollenhagen et al., 2004, 2007]. In contrast, the THO complex, Gbp2, Hrb1, Yra1 and Npl3, were reported not to be essential for the export of heat shock mRNAs [Saavedra et al., 1997, Rollenhagen et al., 2007]. However, the deletion of THO complex proteins, TREX2 proteins and some NUPs leads to the accumulation of *SSA4* mRNA within the nucleus [Rollenhagen et al., 2007, Thomsen et al., 2003, 2008]. This indicates that although known mRNA export factors are not essential (eg THO complex), they probably still promote the export of heat shock mRNAs. Zander et al. [2016] identified that the recruitment of the transcription factor Hsf1 leads to export of the transcribed mRNA during heat stress. A direct interaction of Hsf1 with Mex67 could be shown, which is thought to be the reason for the direct export of heat shock mRNAs regulated by Hsf1. Since Saavedra et al. [1996] were not able to detect an export of a *GAL1* mRNA expressed from a *SSA4* promoter during heat stress, more studies are needed to further validate this hypothesis.
The NPC as export channel also plays an important role during the export of heat stress mRNAs. Deletion or mutation of NUPs lead to the accumulation of heat shock transcripts [Saavedra et al., 1996, Thomsen et al., 2008]. The NUP Rip1, which is not required for mRNA export at 30°C, is necessary for the export of heat shock mRNAs. Upon deletion of Rip1 the heat shock mRNA *SSA4* strongly accumulates within the nucleus at its transcription site [Saavedra et al., 1997, Thomsen et al., 2003]. This could be explained by the finding that Dbp5 and Gle1 lose their association with the NPC under heat stress when Rip1 is deleted [Stutz et al., 1997, Rollenhagen et al., 2004]. During ethanol stress, a relocalization of Dbp5 to the nucleus [Takemura et al., 2004, Rollenhagen et al., 2004] could be detected, which is thought to cause the export block during ethanol stress. This change in localization was not observed for Dbp5 under heat stress [Takemura et al., 2004, Adams and Wente, 2020].
In summary, many studies analyzed the export block of bulk mRNA upon stress and the export of heat shock mRNAs. Nevertheless, both mechanisms are not fully understood so far.

Methods to study mRNP composition and structure

In the earlier part of the introduction the focus was on mRNA production, processing and transport as well as changes in these processes during stress. All these mechanisms involve mRNPs. In recent decades, the interaction of mRNA and proteins was studied extensively, reaching from the identification of individual binding proteins of specific RNAs [McHugh et al., 2015, Chu et al., 2015, Iadevaia et al., 2020] to global studies to identify new RNA-binding proteins [Beckmann, 2017, Shchepachev et al., 2019, Backlund et al., 2020, Kilchert et al., 2020]. The identification of binding partners for a specific mRNA is conducted mostly either by a combination of cross-linking followed by purification under denaturing condition or by *in vitro* transcription and subsequent binding of interacting proteins from lysate to the target mRNA [Rieder et al., 2012].

Many studies use structured RNA sequences that have a high affinity to a protein or other ligand. These so-called aptamers can be introduced into the sequence of the RNA of interest. One example for an aptamer heavily used in the past decades is the MS2 aptamer. Originally, the MS2 coat protein (MCP) was derived from the bacteriophages MS2. It binds to an RNA stem-loop structure [Peabody, 1993]. For scientific research different versions of the MS2 system are available. Mutations in the stem-loop sequence, changing numbers of repeats as well as the distance between the repeats can modulate the affinity between the MS2 aptamer and the MCP [Zhou et al., 2002, Tutucci et al., 2018]. The MS2 system has been used for visualization of mRNAs for microscopy for a long time. The RNA of interest is tagged with an array of MS24 loops and the MCP mostly fused to GFP is coexpressed within the cell. By fluorescence microscopy, Mcp-GFP bound to the RNA can be seen and the RNA movement followed by life cell imaging [Bertrand et al., 1998, Grünwald and Singer, 2010, Tutucci et al., 2018]. Tutucci et al. [2018] optimized the structure of the MS2 array further to prevent aggregation of MS2 arrays bound by MCP after degradation of the coding sequence of the aptamer-tagged RNA *in vivo*. This modification further improved the usage of the MS2 system *in vivo*. The MS2 system has also been used successfully to identify RNA-binding proteins from an *in vitro* synthesized RNA [Rieder et al., 2012]. For this, the MCP was fused to a maltose binding protein (MBP). This fusion could be used to immobilize the *in vitro* synthesized, MS2-tagged mRNA on the MCP-MBP fusion bound to amylose beads. Even the assembly of a functional spliceosomes on an *in vitro* synthesized, MS2-tagged RNA was possible, allowing the purification and structure determination of the spliceosome [Zhou et al., 2002]. Slobodin and Gerst

[2010] used the MS2 system in their newly developed method RNA-binding protein purification and identification (RaPID) to purify *in vivo* transcribed RNAs after cross-linking to identify RNA-binding proteins using mass spectrometry (MS).
Other structured RNA elements with corresponding binding partners have been used for similar experiments, for example binding sites for the PP7 coat protein [Larson et al., 2011] or the streptavidin-binding RNA aptamer (4 × S1m) [Leppek and Stoecklin, 2014]. Panchapakesan et al. [2017] aimed to establish an aptamer that could be not only used for purification of an mRNP but also for fluorescenc labeling. They tested the RNA Mango aptamer, which binds to thiazole orange (TO) or its derivates (TO1-Biotin) with nanomolar affinity [Dolgosheina et al., 2014]. The 19 nt aptamer folds into a G-quadruplex which is embedded in a GAAA tetraloop-like motif [TrachmanIii et al., 2017]. The system has been used for purifications, fluorescence based *in vitro* assays and microscopy [Dolgosheina et al., 2014, Panchapakesan et al., 2017, Autour et al., 2018].
All these approaches require a change or even the *in vitro* transcription of the RNA of interest. A strategy where no modification of the RNA is needed is based on the use of antisense oligo nucleotides (ASO). Different ASOs have been used, reaching from DNA over 2´O-methylated RNA [Matia-González et al., 2017] to locked nucleic acid (LNA) ASOs [Rogell et al., 2017]. In most cases the ASO itself is modified, for example biotinylated, which allows the purification of the target RNA after binding [Matia-González et al., 2017, McHugh and Guttman, 2018]. Similar as for single molecule fluorescence *in situ* hybridization (smFISH) ASO probes have been designed to cover the whole RNA sequence [McHugh and Guttman, 2018] or only a single ASO is used for purification [Matia-González et al., 2017]. Also, the ASO size used differs from up to 90mers [McHugh et al., 2015, McHugh and Guttman, 2018] down to around 20 nt-long sequences [Iadevaia et al., 2020, Rogell et al., 2017].
For the identification of RNA-binding proteins, cross-linking is often performed prior to the purification which connects the RNA with close-by proteins. The most common cross-linking methods are either chemical cross-linking [Chu et al., 2015] by formaldehyde, UV or photoactivatable ribonucleoside-enhanced (PAR) cross-linking [Beckmann, 2017]. For PAR cross-linking, photo-activatable nucleoside analogs are incooperated in the transcribed RNA. These can be photo-activated by irradiation at 365 nm. PAR cross-linking yields more cross-linked complexes than conventional cross-linking with UV light at 254 nm [Hafner et al., 2010]. After cross-linking and lysing, the RNA could be purified directly, but many protocols include another purification step to either enrich a certain pool of RNA, for example poly(A)-RNA using Oligo(dT) beads [Iadevaia et al., 2020], or enrich RNAs from one cellular compartment, for example by preparation of a nuclear extract [Back-

lund et al., 2020, McHugh and Guttman, 2018]. Because of the cross-linking prior to purification, the protocols often include stringent washing steps with denaturing buffer conditions and/or incubation steps at elevated temperatures [McHugh et al., 2015, McHugh and Guttman, 2018]. After purification, the cross-linked copurified proteins can be analyzed by immunoblotting or identified by MS analysis.
However, for some purposes, for example structure determination denaturing purification conditions are unwanted. As described above, for the spliceosomes it is possible to perform a purification or reconstruction of RNA-protein complex with an aptamer-tagged, *in vitro* transcribed RNA [Zhou et al., 2002]. Another possibility is to use established protein purification protocols to purify an RNA-binding protein and copurify the RNA. For example Batisse et al. [2009] used a TAP-purification [Puig et al., 2001] and subsequent gradient centrifugation coupled with cross-linking (GraFIX) [Stark, 2010] to purify all Nab2-TAP-containing mRNPs from yeast. The purified particles were analyzed using electron microscopy (EM). The particles held other nuclear RNA-binding proteins like Cbp80, TREX components, Mex67 and over 6000 transcripts. The particle size varied from 20 to 30 nm in length and 5 to 7 nm in thickness.
Besides purification of a complex from the original organism, it can also be overexpressed in an expression system like insect cells [Ren et al., 2017, Schuller et al., 2020]. For expression in a different organism, the proteins can be coexpressed or expressed separately and reconstituted *in vitro*. Defined RNA sequences like a polyU stretch can be added to aid complex assembly and visualize RNA binding. The assembled complexes can be used for structure determination, for example, by using cryo-EM as described for the THO complex together with Sub2 [Ren et al., 2017, Schuller et al., 2020, Pühringer et al., 2020, Xie et al., 2021, Chen et al., 2021].

4. Aim of this thesis

Stress causes a rearrangement of mRNA export with the accumulation of bulk mRNAs within the nucleus and export of stress specific-mRNAs. While many factors involved in mRNA export at 30°C are known the exact composition and structure of an export-competent mRNPs remains unknown. For survival at elevated temperatures studies so far focused mainly on proving that most of these factors are not required for mRNA export during heat stress. The aim of this study is to establish a purification protocol for the purification of a nuclear, transcript-specific mRNP under native conditions. A two-step ASO-based purification based on an initial enrichment of nuclear mRNPs using the nuclear CBC followed by the purification of a transcript-specific mRNP is taken as a starting point for optimization [Wierschem, 2020]. Different RNA-based purifications will be evaluated for the second purification step including the ASO and new aptamer-based approaches. The quality of the purified mRNPs will be assessed by determining the mRNA enrichment and analyzing the copurification of known nuclear mRNA-binding proteins. Then, the structure and composition of the purified mRNPs will be determined by EM and cross-linking MS, respectively. The overall goal is to purify a heat shock mRNP in comparison to a non-heat shock mRNP to investigate not only the composition and structure of the mRNPs but to also pinpoint the differences in both mRNPs and export pathways.

Furthermore, the question should be answered if nuclear accumulation of mRNA is a general reaction to different kinds of stress and how the cell mediates the mRNA export blockade. Therefore, screening of different stress conditions for poly(A) accumulation after stress treatment will be carried out by using Oligo(dT) FISH. Since the mRNA export block is Slt2-dependent during heat stress it will be analyzed if this is also the case for other stresses. Moreover, a phosphoproteome analysis of a *SLT2* deletion mutant under heat stress will be performed with the goal to identify proteins involved in mRNA export that are differentially phosphorylated upon stress. The identified phosphosites will be analyzed towards their involvement in the nuclear accumulation of mRNA. Both, understanding how some mRNAs are retained within the nucleus and how stress-specific transcripts are selectively exported, will improve our understanding of mRNA export and how cells are able to cope with stress.

5. Results

Purification of transcript-specific, nuclear mRNPs

ASO-based mRNP purification

The structure and composition of mRNPs is often studied by overexpression of a complex in another organism or by a combination of cross-linking and purification under denaturing conditions. To determine the structure of a nuclear, transcript-specific mRNP a native purification from yeast needed to be established in order to facilitate structure determination. A two-step purification method was established in a previous study using an ASO for the purification of a transcript-specific mRNP [Wierschem, 2020]. This method should be further optimized and tested for heat shock mRNPs in this study (Figure 5.1 A). In the first purification step, all nuclear mRNAs bound to the nuclear CBC were enriched by purifying the TAP-tagged subunit Cbp20 (blue). To purify one specific mRNA, a 2´O-methylated, biotinylated RNA ASO was added to the TEV eluate from the first purification step. After binding to the mRNA target, the ASO could bind to streptavidin dynabeads via its biotin moiety (green). For further optimization of the method, a denaturing elution for proteins and RNAs was used instead of the native elution. The denaturing elution is faster and more efficient, but the native elution will be needed later on for structure determination. The RNA is analyzed by reverse transcription coupled with qPCR (RT-qPCR). In addition, Western blotting is used to verify the copurification of known nuclear mRNA-binding proteins, like Nab2, Npl3 or Cbp80 [Anderson et al., 1993, Wilson et al., 1994, Fortes et al., 2000].
As mentioned above, the purification of nuclear mRNPs was studied before using the highly expressed mRNA *CCW12* as target mRNA. My colleagues Christoph Wierschem [Wierschem, 2020] and Nataliia Stefanyshena (unpublished data) tested different ASOs to purify *CCW12* mRNPs. Their binding sites are depicted in Figure 5.1 B. In this study only the ASO1 and ASO3 were used for the purification of *CCW12* mRNPs as they were identified to yield the best results for mRNA yield and copurification of proteins, respectively.

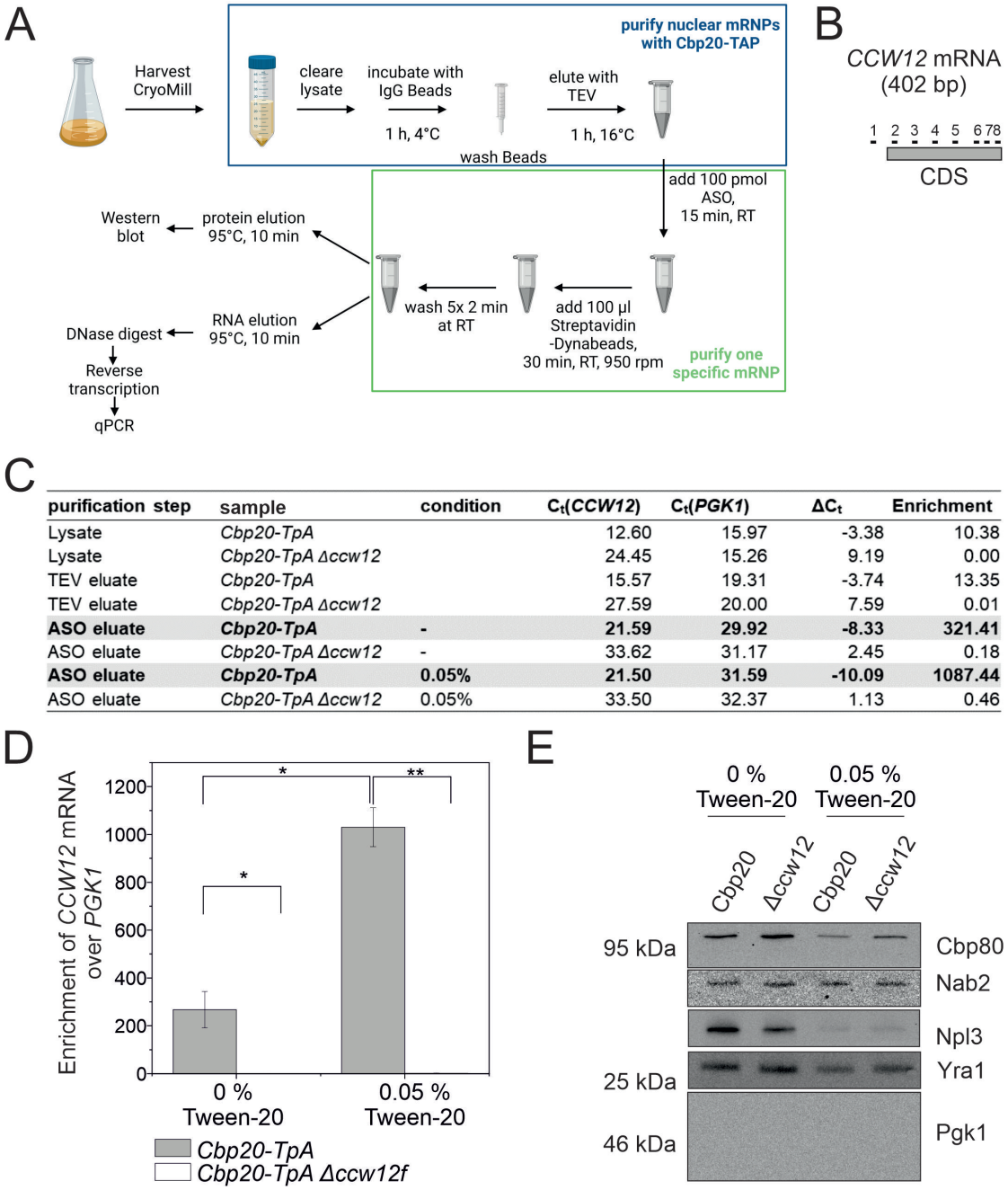

purification step	sample	condition	C_t(*CCW12*)	C_t(*PGK1*)	ΔC_t	Enrichment
Lysate	*Cbp20-TpA*		12.60	15.97	-3.38	10.38
Lysate	*Cbp20-TpA Δccw12*		24.45	15.26	9.19	0.00
TEV eluate	*Cbp20-TpA*		15.57	19.31	-3.74	13.35
TEV eluate	*Cbp20-TpA Δccw12*		27.59	20.00	7.59	0.01
ASO eluate	***Cbp20-TpA***	**-**	**21.59**	**29.92**	**-8.33**	**321.41**
ASO eluate	*Cbp20-TpA Δccw12*	-	33.62	31.17	2.45	0.18
ASO eluate	***Cbp20-TpA***	**0.05%**	**21.50**	**31.59**	**-10.09**	**1087.44**
ASO eluate	*Cbp20-TpA Δccw12*	0.05%	33.50	32.37	1.13	0.46

Figure 5.1: **Nuclear transcript-specific mRNPs can be purified in a two-step purification using ASOs. A** Schema of nuclear transcript-specific mRNP purification steps. **B** Schema showing the binding sites of different ASOs annealing to *CCW12*. ASOs were designed and tested by Christoph Wierschem [Wierschem, 2020]. CDS = coding sequence **C** Representative C_t value table for an ASO purification. The table contains results from a purification comparing the washing step of the streptavidine dynabeads in presence and absence of 0.05 % Tween-20. **D** Fold enrichment of the *CCW12* mRNA in the ASO elution for different Tween-20 concentrations in the wash buffer. Fold enrichment was determined relative to *PGK1* mRNA. The mean ± standard deviation (SD) is illustrated. The p-value was determined using a student's t-test with $\star$ $p < 0.05$ and $\star\star$ $p < 0.01$. **E** Representative Western blot showing the copurification of nuclear mRNA-binding proteins for the ASO purification from C and D.

Table 5.1: Conditions tested to improve ASO purification of *CCW12* mRNA using denaturing RNA and protein elution. The condition and the changes in RNA yield and purity determined by RT-qPCR are listed. The qPCR and Western blot result of the different purification can be found in Supplement A.1 - A.7.

Condition	***CCW12* mRNA yield**	**Enrichment over *PGK1* mRNA**	**Remarks**
1 h 40000 rpm centrifugation to cleare the lysate instead of 16 min at 40000 xg	reduced	reduced	
use of KCl instead of NaCl	no change	no change	
compare annealing at RT with 4°C and 16°C	reduced	reduced	
add random RNA Oligo without biotin	no change	no change	The aim was to reduce unspecific protein binding, but no effect on protein binding was seen.
add random DNA Oligo without biotin	no change	no change	The aim was to reduce unspecific protein binding, but no effect on protein binding was seen.
add 0.05 % Tween to the wash buffer	no change	higher	
use a *Δccw22* strain	no change	no change	*CCW22* is the paralog from *CCW12* which arose from whole genome duplication.
higher Bead amount for ASO purification	no change	no change	
lower Bead amount for ASO purification	decreased	decreased	

To optimize this purification, different approaches and conditions were tested (Table 5.1, Supplement A.1 - A.7). An exemplary purification using ASO1 is shown in Figure 5.1 C - E. In this exemplary purification, it was tested whether the presence of 0.05 % Tween-20 in the binding and wash buffer used for ASO purification increases purity. A *CCW12* deletion strain served as negative control. Figure 5.1 C shows representative C_t values determined by RT-qPCR, the ΔC_t value and the enrichment of *CCW12* mRNA over the negative control mRNA *PGK1*.
Already in the lysate and TEV eluate, the highly transcribed *CCW12* mRNA is more abundant than *PGK1* control mRNA as measured by RT-qPCR. Moreover, for the first purification step a TEV-proteinA tag was used instead of a classical TAP tag consisting of a Calmodulin-binding peptide, TEV cleavage site and protein A. This is possible because the second step of the TAP protocol is replaced by

an ASO purification step. Moreover, it can be observed that even in the *Δccw12* strain, a C_t value of up to 24.45 could be reached possibly because of unspecific binding for example to the *CCW22* paralog. However, this was much lower than the in the strain expressing *CCW12*(C_t of 12.6). In the second purification step, the enrichment of *CCW12* over *PGK1* mRNA increased significantly in the elution sample if Tween-20 was added. The isolated RNA from the eluate contained 1030 ± 81 times more *CCW12* than *PGK1* mRNA, which is depicted in Figure 5.1 D. No signal for *CCW12* mRNA was detected in the *Δccw12* control purification.
The copurification of Cbp80, Nab2, Npl3 and Yra1 was analyzed by Western blot. Pgk1 served as negative control. The protein signal on the Western blot for the *CCW12* deletion strain (negative control) is similar to the strain expressing *CCW12* under both conditions, suggesting that unspecific mRNA-binding proteins copurify with the ASO procedure and contribute significantly to the protein signal. However, addition of Tween-20 strongly reduces the amount of copurified Cbp80 and Npl3. For Yra1, a slight decrease in copurification can be observed (Figure 5.1 E).
All other tested conditions led to a reduced yield or enrichment of *CCW12* mRNA or showed no differences (Table 5.1).

Nuclear heat shock mRNAs and the CBC

For purification of heat shock mRNPs several questions had to be answered. First, the question arose whether the enrichment of nuclear, heat shock-specific mRNPs using a CBC purification was possible. RNA-immunoprecipitation (RIP) was performed to study the binding of heat shock mRNAs to Cbp20 at 30°C and after 15 min at 42°C (heat shock). For *CCW12*, *PGK1* and *YEF3* no difference of binding was observed between 30°C and the heat shock sample (Figure 5.2 A). Several heat shock mRNAs were tested. Even though a slight increase was observed for all tested heat stress mRNAs, only *HSP12* showed a significantly increased mRNA enrichment under heat shock conditions compared to growth conditions at 30°C.
To further verify the importance of the nuclear CBC for heat shock mRNA export from the nucleus a smFISH using probes against the well-studied *SSA4* mRNA [Boorstein and Craig, 1990, Saavedra et al., 1997, Rollenhagen et al., 2007] was performed (Figure 5.2 B). Several cells show an accumulation of nuclear *SSA4* signal in the *CBP80* and/or *CBP20* deletion strain. The deletion of the NUP *RIP1* served as positive control. Since foci formation was obvious, but only present in a minority of cells, the percentage of cells with *SSA4* accumulation was quantified (Figure 5.2 C).

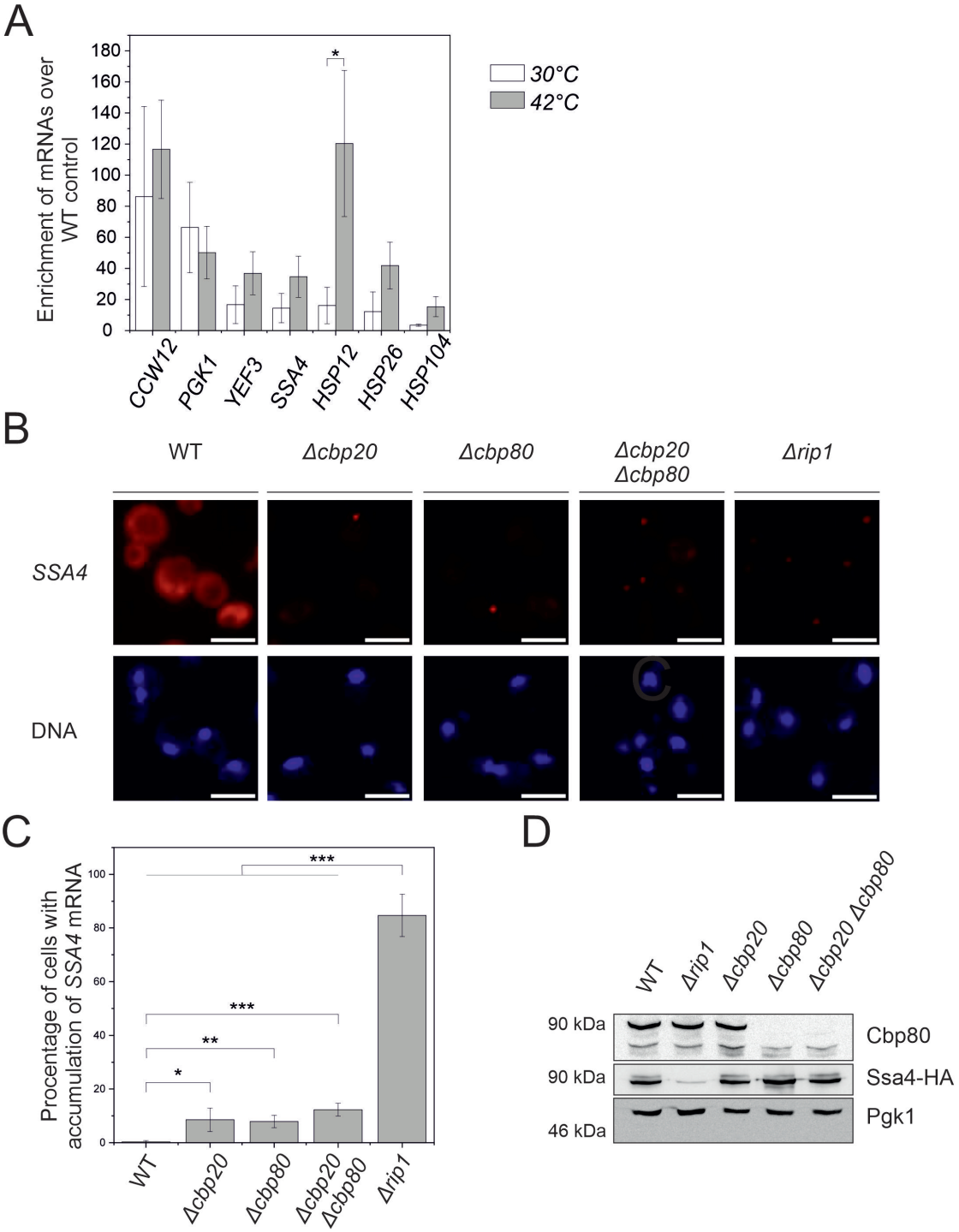

Figure 5.2: **The nuclear CBC binds to heat shock mRNAs and is probably involved in nuclear export of heat shock mRNAs. A** RIP of *Cbp20-FTpA* at 30°C (white) and 42°C (gray). The graph depicts the enrichment of copurified transcripts over an untagged negative control. In addition, the enrichment was normalized over the lysate to correct the differential expression of heat shock transcripts. RNA levels were determined using RT-qPCR for highly transcribed mRNAs (*CCW12*, *PGK1*, *YEF3*) and four heat shock transcripts *SSA4*, *HSP12, HSP26, HSP104*. The mean ± SD is illustrated. The p-value was determined using a student's t-test with $\star$ $p < 0.05$. **B** Representative images of a smFISH using probes against *SSA4* mRNA in a *Δcbp20*, a *Δcbp80* and a *Δcbp20Δcbp80* strain. WT and *Δrip1* served as controls. **C** Quantification of smFISH shown in B. The data represent the percentage of cells containing *SSA4* foci. Data presents the mean ± SD. The p-value was determined using a student's t-test with $\star$ $p < 0.05$, $\star\star$ $p < 0.01$ and $\star\star\star$ $p < 0.001$.

Figure 5.2: **D** Representative Western blot showing the protein levels of Ssa4-3xHA after heat shock in different CBC deletion strains. Pgk1 served as loading control.

For the deletion of *CBP20*, *CBP80* or both, an accumulation of *SSA4* mRNA upon heat shock could be observed in 9, 8 and 12 % of all counted cells, respectively. For the *RIP1* deletion strain, 85 % of the cells formed *SSA4* foci.
Previous studies showed that even if nuclear accumulation of *SSA4* is observed, the protein can still be produced at similar levels as in the WT strain. These proteins were classified as not necessary for the export of heat shock mRNAs (eg. Hpr1) [Rollenhagen et al., 2007]. In cells lacking Rip1 the amount of Ssa4-3xHA is decreased in comparison to the WT (RS453) during heat stress. The deletion of CBC components did not influence protein expression of Ssa4-3xHA in comparison to the WT (Figure 5.2 D).
These results indicate that the nuclear CBC binds heat shock mRNAs in the nucleus during heat stress. Therefore, the two-step nuclear mRNP purification can be suitabled for heat shock mRNPs. However, it appears not to be essential for the nuclear export of heat shock transcripts.

Identification of possible ASO-binding sites for the heat shock mRNA *SSA4*

To test whether the ASO-based mRNP purification, can be used to purify and analyze heat shock mRNPs with regards to their protein content and structure, the heat shock mRNA *SSA4* was chosen as target mRNA. Before testing ASO purification, new ASOs needed to be designed. To test the accessibility of the RNA within a nuclear mRNP, an RNase H assay was performed (Figure 5.3 A). A DNA ASO is incubated with nuclear mRNPs, enriched by Cbp20-TAP purification as described above, followed by digestion with RNase H. RNase H digests the RNA of DNA-RNA hybrids [Donis-Keller, 1979]. Upon binding of one of the 15 tested DNA ASOs (Figure 5.3 B) to *SSA4* mRNA the ASO binding site is digested. This can be analyzed by RT-qPCRs using a primer pair annealing on both sides of the ASO binding site. In theory, the relative amount of uncleaved RNA should be equal to the input in the RNase H-only control, which contains the enzyme, but no DNA ASO. Eventual reduction in the enrichment indicates RNA cleavage and consequently binding of the ASO. For all tested ASOs levels of uncleaved RNA were reduced in comparison to the input (Figure 5.3 C). The enrichment upon incubation and RNase H digestion with ASO6 is not changed significantly compared to the Input. ASOs 1, 2, 4, 5, 8, 12, 15 show the biggest reduction in

levels of uncleaved RNA, indicative of efficient hybridization of the ASO with the RNA.

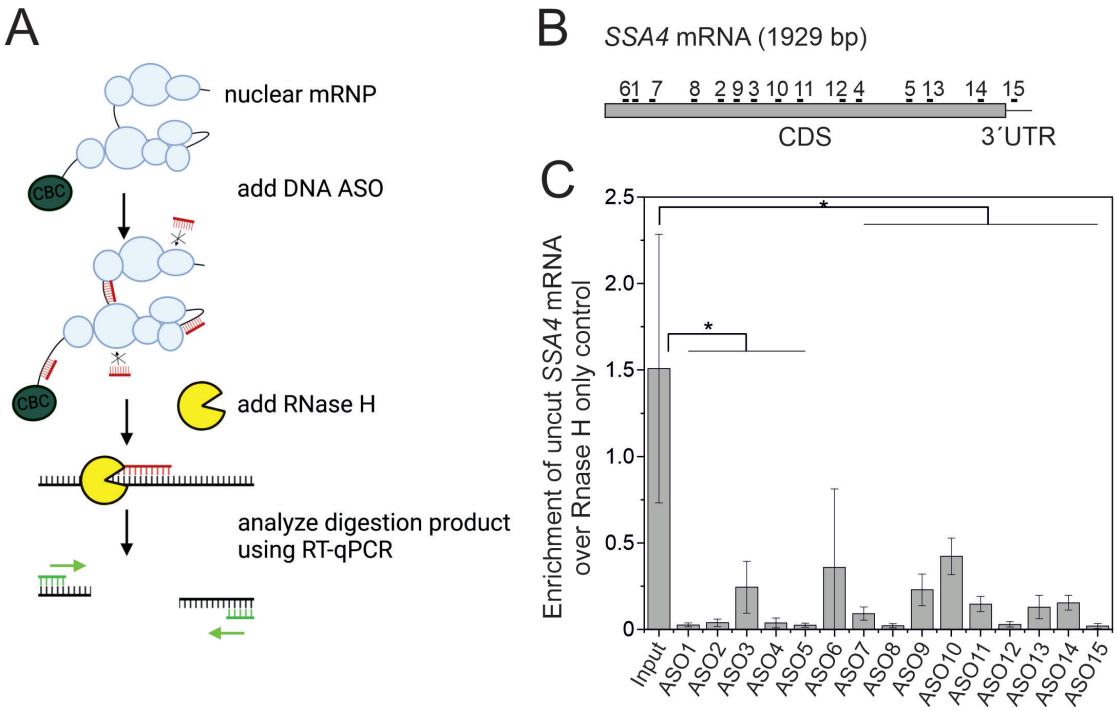

Figure 5.3: **RNase H Assay to determine optimal ASO sequences for *SSA4* purification A** Schematic representation of the RNase H assay: DNA ASOs are depicted in red and the RNase H enzyme in yellow. Primers used for qPCR are shown in light green. Created with BioRender.com. **B** Schematic representation of tested ASOs for *SSA4* mRNA. C Results of RNase H assay using the DNA ASOs depicted in B. Data shows the fold-enrichment over the negative control without addition of a DNA ASO determined by RT-qPCR. The graph contains mean ± SD. The p-value was determined using a student's t-test with $\star$ $p < 0.05$.

ASO-based *SSA4* mRNP purification

For six of the DNA ASOs (ASO1, 4, 5, 8 12 and 15) tested earlier, 2´O-methylated, biotinylated RNA ASOs were used for a test *SSA4* mRNP purification (Figure 5.4). While the purification of *CCW12* mRNA using ASO1 (without Tween-20) led to an enrichment of 189 ± 24-fold, the enrichment of *SSA4* mRNA over *PGK1* for ASO1, ASO4 and ASO5 is 2 ± 1.1, 1.6 ± 2 and 1.4 ± 0.4, respectively (Figure 5.4 A). The proteins Cbp80, Nab2, Npl3, and to a minor extent Sub2, could be copurified. As for a *CCW12* mRNP purification, the protein signal does not show a reproducible difference compared to the negative control (Figure 5.4 B). The most promising ASO is ASO8. In contrast to the other tested ASOs for *SSA4*, ASO8 leads to a significant 17.8 ± 0.6-fold enrichment over *PGK1*. ASO12 and ASO15 do not show an enrichment of *SSA4* mRNA that is significant in comparison to the negative control (Figure 5.4 C). Similar to the other tested ASOs, no reproducible

difference in copurified protein to the negative control could be observed (Figure 5.4 D). A one-step ASO purification using ASO8 and lysate from a *Δrip1* strain, which mainly contains nuclear *SSA4*, did not result in a better enrichment of *SSA4* mRNA (Supplement A.12).

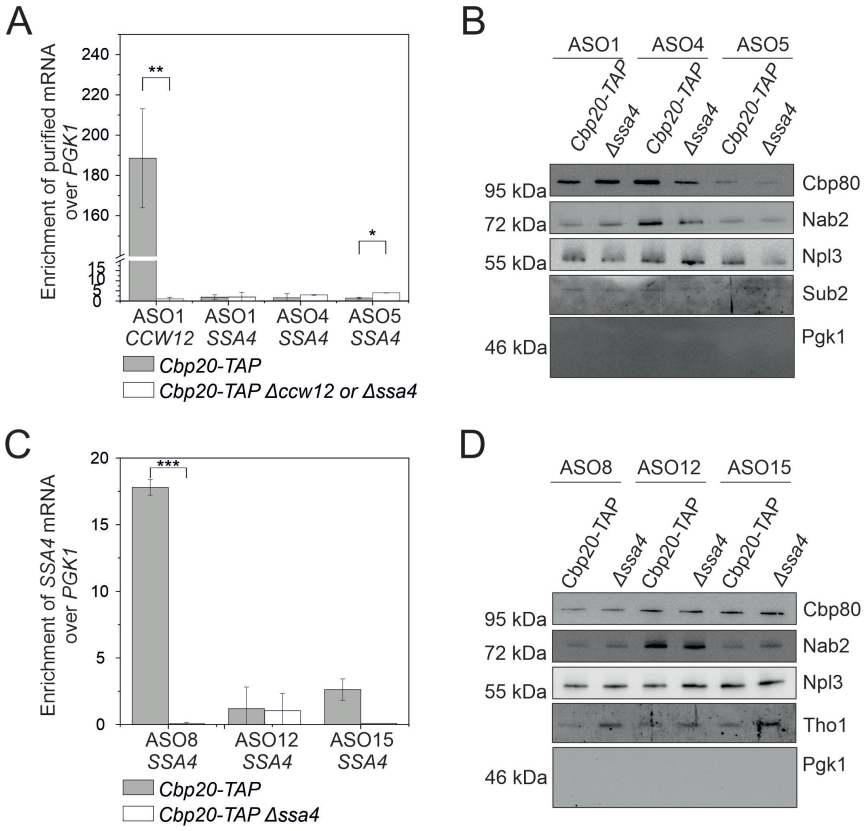

Figure 5.4: **ASO8 can be used for a purification of *SSA4*. A and C** Results for ASO-based *SSA4* mRNP purification to identify ASOs that can be successfully used for heat shock mRNP purification. The enrichment of *SSA4* or *CCW12* mRNA over *PGK1* is shown as indicated. The corresponding negative control, which does not contain *SSA4* or *CCW12*, is shown in white. The data represents mean ± SD. The p-value was determined using a student's t-test with $\star$ $p < 0.05$, $\star\star$ $p < 0.01$ and $\star\star\star$ $p < 0.001$. Representative results for all purification steps can be found in Supplement A.11. **B and D** Representative Western blot for the purifications shown in A and C. The copurification of selected nuclear mRNA-binding proteins is shown. Pgk1 serves as negative control.

Analysis of natively eluted mRNPs

To further analyze the composition of a nuclear mRNP, either the structure of a nuclear mRNP would need to be determined or XL-MS could be performed. In both cases, a native elution from the streptavidin beads is necessary or at least preferable. *CCW12* purifications performed by Christoph Wierschem showed that only a minority of mRNA bound to the beads can be eluted by the addition of biotin-containing elution buffer [Wierschem, 2020]. However, using a desthiobiotinylated ASO3 led to an improved elution as the biotin analogue

desthiobiotin interacts with a lower affinity to streptavidin than biotin [Hirsch et al., 2002], which results in a more efficient elution from streptavidin-beads. Conditions tested in this study to improve the native elution are listed in Table 5.2 and representative purifications can be found in the Supplements A.8 - A.11. The optimization was performed by purification of *CCW12*-containing mRNPs: This purification leads to a higher enrichment over *PGK1* as the purification of *SSA4*-containing mRNPs. For ASO1 it could be shown that no elution is possible with a biotinylated ASO (Supplement A.8). The elution is increased slightly by the replacement of the biotin with a desthiobiotin as shown before for ASO3 [Wierschem, 2020]. It was shown before, that the elution of biotin from streptavidin increases by adding up to 16 mM biotin [Lin et al., 2019]. The elution with 16 mM biotin instead of 5 mM reached an additional mild increase in elution efficiency (Supplement A.9). A native purification with a desthiobiotinylated ASO1 and 16 mM biotin led to a 45.4 ± 6.8-fold enrichment over *PGK1* (Figure 5.5 A).

Table 5.2: Conditions tested to improve ASO purification of *CCW12* mRNA using native RNA and protein elution. Listed are the conditions and the changes in RNA yield and purity determined by RT-qPCR. The qPCR and Western blot results of the different purifications can be found in Supplement A.8- A.10.

Condition	***CCW12* mRNA yield**	**Enrichment over *PGK1* mRNA**	**Remarks**
denaturing vs. native elution	decreased	decreased	Using ASO1 no RNA could be detected after native elution.
test desthiobiotinylated ASO1	increased	increased	Known for ASO3
increase biotin concentration to 16 mM	increased	increased	
Use a concentrator after purification	reduced	reduced	Concentrating the elution samples of six purifications with a centrifugal filter unit

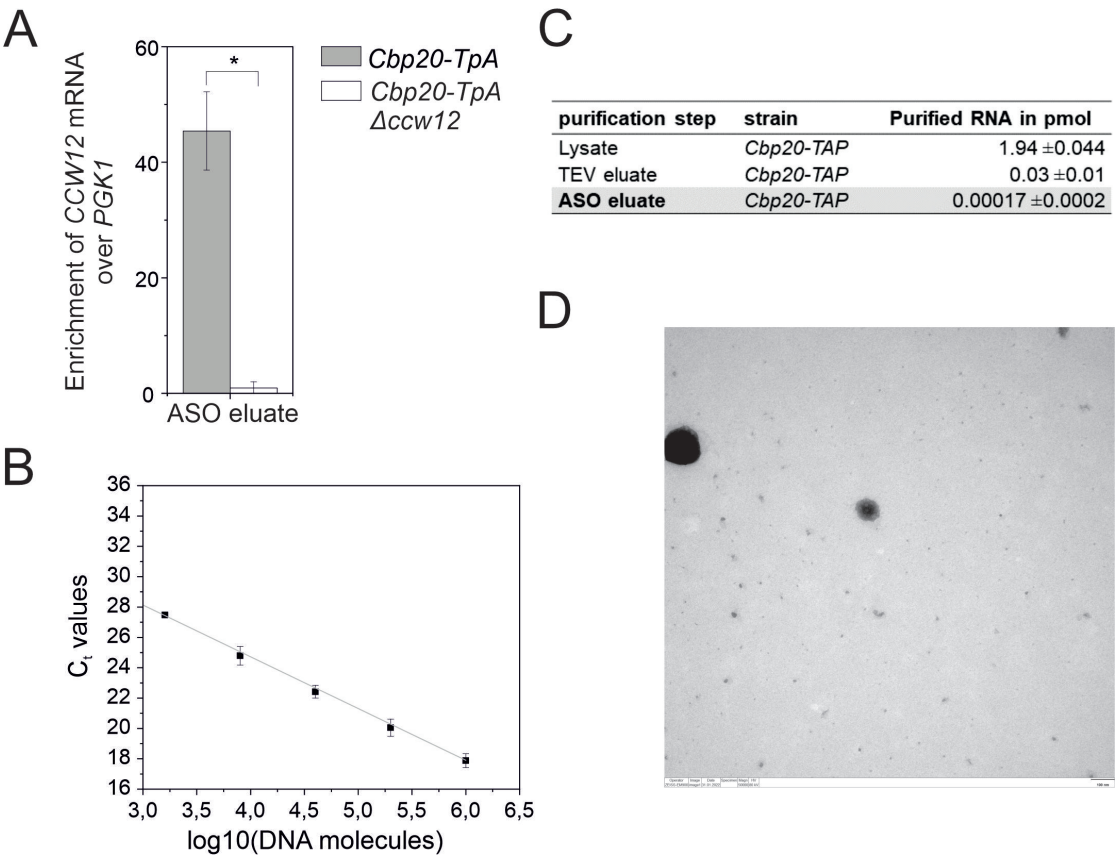

purification step	strain	Purified RNA in pmol
Lysate	*Cbp20-TAP*	1.94 ±0.044
TEV eluate	*Cbp20-TAP*	0.03 ±0.01
ASO eluate	*Cbp20-TAP*	0.00017 ±0.0002

Figure 5.5: **No promising particles could be visualized by EM after native ASO purification of *CCW12* mRNPs.** **A** Enrichment of *CCW12* mRNA over *PGK1* after ASO purification with native elution using 16 mM biotin and desthiobiotinylated ASO1. The graph shows mean ± SD. The p-value was determined using a student's t-test with $\star$ $p < 0.05$. Representative RT-qPCR values of all purification steps are shown in Supplement A.9. **B** qPCR standard curve created with a defined amount of linearized *CCW12* containing plasmid. The graph shows the measured C_t values against the log10 of the number of used DNA molecules. **C** Total amounts of *CCW12* mRNA calculated with a standard curve taking into account the different dilutions and volumes used for purification, RNA analysis and RT-qPCR. **C** Representative EM picture of the elution sample of *CCW12* mRNP purification after native elution. Samples were applied to EM grid and negative staining was used. The picture was taken at a 50000 x magnification.

The analysis of the eluted mRNA with RT-qPCR allows the determination of the relative enrichment over another mRNA. However, no absolute concentration can be deduced from the c_t value. To determine the amount of eluted *CCW12* mRNA more precisely, a *CCW12*-containing plasmid was linearized by restriction digest, purified and a defined number of DNA molecules was added as template for qPCR. The resulting standard curve can be seen in Figure 5.5 B and was used to calculate the total RNA amount in the different samples. The lysate contains around 1.94 ± 0.044 pmol *CCW12* mRNA. The TEV eluate, which should only contain nuclear *CCW12* mRNA, contained around 0.03 ± 0.01 pmol. The final elution sample contains roughly 0.00017 ± 0.0002 pmol *CCW12* mRNA of a purification of 2 l yeast culture (Figure 5.5 C). Purification and EM analysis of 2 l yeast culture were

performed together with Nataliia Stefanyshena and Dr. Ulrich Gärtner from the Institute for Anatomy and Cell Biology (JLU Gießen). The sample was applied to a grid and negatively stained with ammoniumheptamolybdat. At a 50,000x magnification no promising particles at the expected size of around 5-7 nm in thickness and 25-35 nm in length [Batisse et al., 2009] could be identified. A representative image is shown in Figure 5.5 D.
Taken together, while a native, ASO-based, nuclear mRNP purification yields an enrichment of *CCW12* mRNA over *PGK1* of over 40-fold no specific protein copurification could be observed. In addition, no particles were visible during EM. The ASO-based purification strategy appears not to yield enough material or intact particles for structure determination. Therefore, other purification methods need to be explored.

Purification of nuclear mRNPs using the Mango aptamer

The purification of nuclear heat shock mRNPs led to an enrichment of around 17.8 $\pm$ 0.6-fold using ASO8 and is not as effective as for *CCW12*. To test whether other methods lead to a higher enrichment of heat shock mRNA and thereby to a higher amount of *SSA4*-containing nuclear mRNPs, mRNP purifications using a Mango aptamer were tested. The purification protocol was established and optimized by Nataliia Stefanyshena (unpublished data). It is a two-step purification as described before using the Mango aptamer with a TO-biotin ligand and magnetic streptavidine beads instead of a biotinylated ASO for the second purification step. To test this method for *SSA4*-containing mRNPs the Mango aptamer was integrated into the 3´UTR of *SSA4* at three different positions (Figure 5.6). The positions were selected based on secondary structure prediction using the RNAfold WebServer [Gruber et al., 2008, Lorenz et al., 2011]. While the expression of *SSA4* from a plasmid leads to a significantly increased amount of *SSA4* mRNA, the aptamer does not change the mRNA levels of *SSA4* determined by RT-qPCR. (Figure 5.6 B).
A test purification of the three different *SSA4-Mango* constructs in comparison to an untagged *SSA4* was performed. In this experiment *CCW12* mRNA served as negative control for RT-qPCR instead of *PGK1* mRNA. While the integration of the Mango aptamer at position 1 and 24 leads to no enrichment of *SSA4* mRNA over *CCW12*, the enrichment of the construct cantaining the Mango aptamer at position 3 varies. A significant enrichment over CCW12 mRNA and the negative control could be achieved for none of the tested constructs (Figure 5.6 C). Similar

to the ASO purification, the proteins Cbp80, Npl3 and Yra1 could be detected during Western blotting, but the signal shows no difference to the negative control indicating unspecific protein binding (Figure 5.6 D).
To summarize, the purification of *SSA4* mRNA using the Mango aptamer from 2 l culture volume does not lead to a significant enrichment of *SSA4* mRNA.

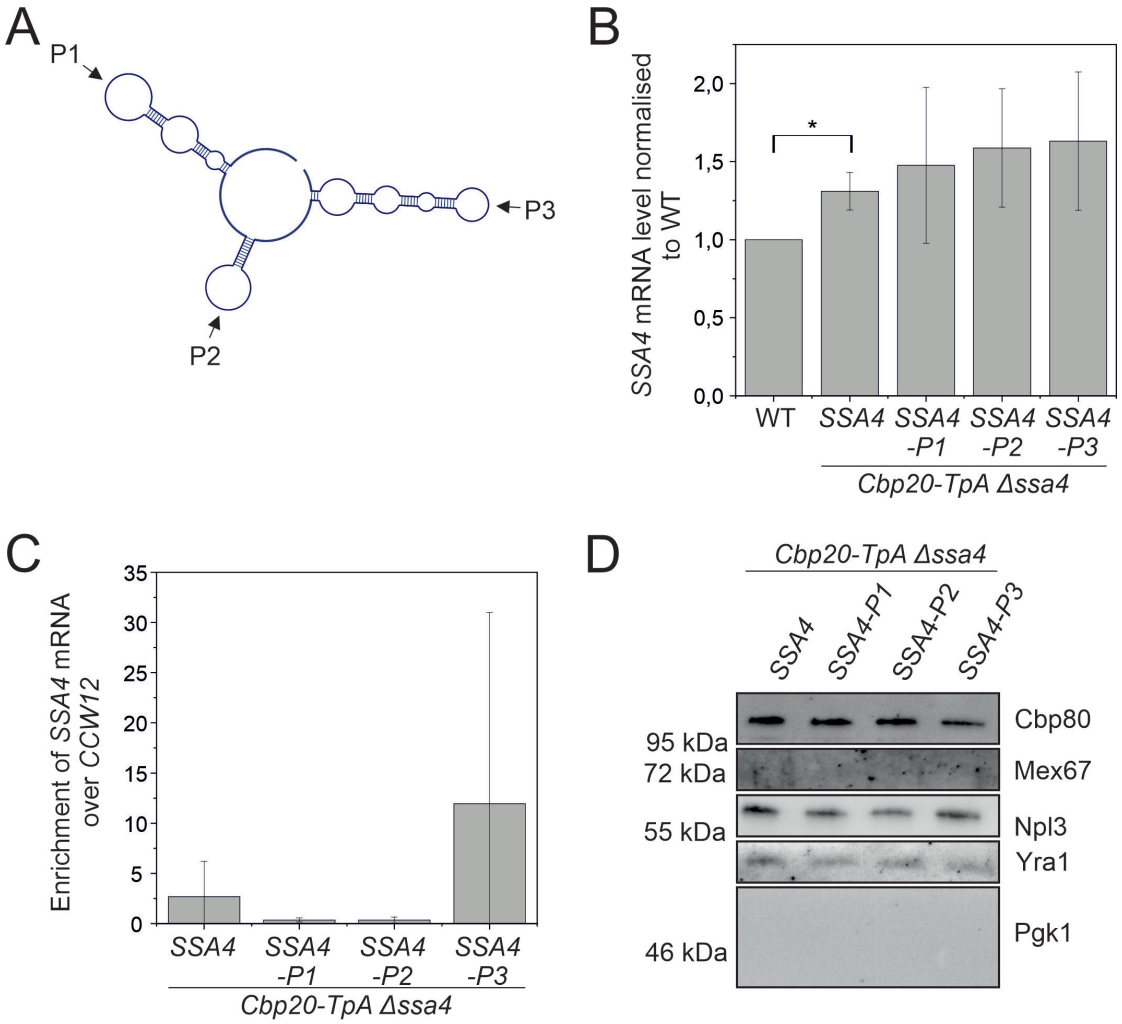

Figure 5.6: **The Mango aptamer could not be successfully used to purify *SSA4* mRNA-containing nuclear mRNPs.** **A** Schematic representation of the *SSA4* 3´UTR structure determined by the use of RNAfold WebServer [Gruber et al., 2008, Lorenz et al., 2011]. The arrows mark the positions where the Mango aptamer was integrated (P1 - P3). Created with BioRender.com. **B** Relative *SSA4* mRNA levels compared to WT after heat shock. RNA levels were determined by RT-qPCR. The data represent the mean ± SD. The p-value was calculated using a student's t-test with $\star$ $p < 0.05$. **C** Enrichment of *SSA4* mRNA over *CCW12* after nuclear mRNP purification using the Mango aptamer. *SSA4* without aptamer serves as negative control. The qPCR values of all purification steps of a representative purification can be found in Supplement C.1. **D** Representative Western blot for Mango purification shown in C. Antibodies against known nuclear mRNA-binding proteins were used. Pgk1 serves as negative control.

Establishment of a nuclear mRNP purification using the MS2 aptamer

Purification of nuclear mRNPs using the 12xMS2V6 aptamer

Since neither the ASO nor the Mango aptamer based purification approach led to a high enrichment of *SSA4* mRNA over a control mRNA, another purification strategy was needed. One concern was the accessibility of the packaged mRNA for the ASO or ligand binding. Therefore, a strategy was tested where the aptamer-binding protein was already coexpressed in the cell. To this purpose, the 12xMS2V6 aptamer was used. For establishing a nuclear, transcript-specific purification based on the 12xMS2V6 aptamer the highly transcribed *CCW12* mRNA was used as *CCW12*-containing mRNPs are highly abundant and no heat shock needed to be carried out for each purification. The aptamer consists of 12 repeats of a modified MS24 loop optimized for *in vivo* expression and microscopy [Tutucci and Stutz, 2011]. The 12xMS2V6 aptamer, here after referred to as 12xMS2, was integrated at three different positions in the 3´UTR of *CCW12* mRNA (Figure 5.7 A). In addition, a gene encoding a fusion protein of the Mbp, Mcp, a nuclear localization sequence and a 3xHA tag was integrated into the *LEU2* locus of the genome under the control of a *CYC1* promoter.
While the amount of *CCW12* mRNA expressed from a plasmid (-) is significantly increased, the MS2 aptamer reduces the mRNA amounts detected by RT-qPCR (Figure 5.7 B). A growth spot assay was performed to determine whether the tagged *CCW12* is still functional and the expression level sufficient (Figure 5.7 C). Deletion of the non essential gene *CCW12* leads to a reduced growth at 30°C, 37°C and 25°C compared to the WT. The growth defect can be rescued by addition of a *CCW12*-containing plasmid. Also the addition of a plasmid containing a MS2 aptamer-tagged version of *CCW12* can rescue the growth phenotype.
For the test purification, nuclear mRNPs were enriched in a initial step by purification of the nuclear CBC using TEV-proteinA tagged Cbp20. In a next step, amylose resin was added to the TEV eluate to purify Mbp. The purification leads to an averaged enrichment of 34-91-fold of *CCW12* mRNA over *PGK1* depending on the used construct. The highest enrichment could be reached by integrating the MS2 tag at position 2 (Figure 5.7 D). Therefore, all following optimizations were performed with this construct.

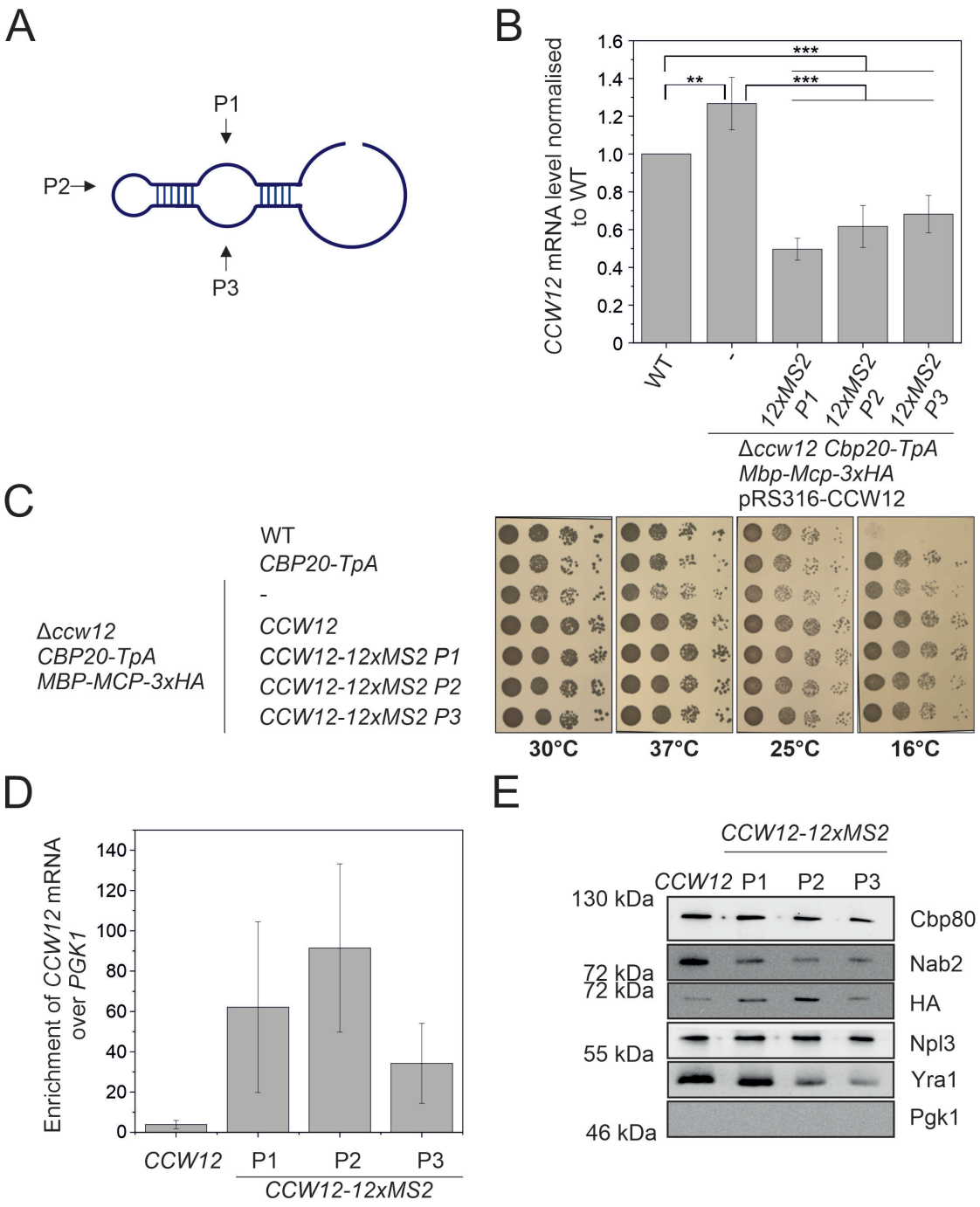

Figure 5.7: ***CCW12* mRNA can be enriched using a MS2 based mRNP purification.** **A** Schematic representation of the secondary structure of the *CCW12* 3´UTR determined by the use of the RNAfold WebServer [Gruber et al., 2008, Lorenz et al., 2011]. Arrows indicate the positions where the 12xMS2 aptamer is inserted into the 3´UTR (Position 1 - 3). Created with BioRender.com. **B** Relative *CCW12* mRNA levels compared to the WT are shown. RNA levels were determined by RT-qPCR. The data show mean ± SD. The p-value was calculated using a student's t-test with ⋆⋆ $p < 0.01$ and ⋆⋆⋆ $p < 0.001$. **C** The growth spot assay shows the influence of the different modifications and aptamers of the corresponding yeast strains. Cells were spotted in 4 serial 1:10 dilutions. Plates were incubated for 2 days at 30°C, 3 days at 37°C and 25°C and 8 days at 16°C. **D** Enrichment of *CCW12* mRNA over *PGK1* after nuclear mRNP purification using the 12xMS2 aptamer. *CCW12* without aptamer serves as negative control. The qPCR values of all purification steps of a representative purification can be found in Supplement D.1.

Figure 5.7: **E** Representative Western blot for 12xMS2 purification shown in D. The Western blot shows the amount of purified Mbp-Mcp-3xHA detected with an HA antibody. Antibodies against known nuclear mRNA-binding proteins were used. Pgk1 serves as negative control.

In addition to the RNA purification, the purification of the Mbp-Mcp-3xHA protein was verified using Western blotting (Figure 5.7 E). Only a minor signal was detected in the negative control, while the *CCW12-12xMS2* P2 variant led to the highest yield of Mbp-Mcp-3xHA. Similar to the other purification strategies, unspecific protein signal can be observed for Cbp80, Nab2, Npl3 and Yra1.

Optimization of the 12xMS2 based nuclear mRNP purification

The possibility of purifying an MS2 aptamer-tagged mRNA by Mbp-Mcp-3xHA in a second purification step relies on the assumption that all Mbp-Mcp-3xHA that are not contained within a nuclear mRNP are removed during the first purification step. Since a band for Mbp-Mcp-3xHA is still visible in the negative control, the protein abundance in the TEV eluate was analyzed using Western blot. It can be seen that the expression of *CCW12-12xMS2* indeed results in an increased copurification of Mbp-Mcp-3xHA, but a minor band is still visible in the negative control (Figure 5.8 A).
To test whether an increased amount of Mbp-Mcp-3xHA would result in a higher amount of copurified mRNA ,the Mbp-Mcp-3xHA protein was expressed under the control of a *CYC1* (P_{CYC1}) and *NOP1* promoter (P_{NOP1}). When Mbp-Mcp-3xHA is expressed under control of P_{NOP1}, the protein level significantly increases by the factor of 1.8 ± 0.2 (Figure 5.8 B, Supplement Figure D.2). The purification was performed with different expression levels of Mbp-Mcp-3xHA and with denaturing versus native elution. For the native elution, the sample was incubated with an elution buffer containing 15 mM maltose. The denaturing elution of a nuclear *CCW12-12xMS2* mRNP purification led to an 85.2 ± 17-fold enrichment over *PGK1* mRNA. The expression of a higher amount of Mbp-Mcp-3xHA led to a significant reduction in *CCW12-12xMS2* enrichment to 11.7 ± 4.2. For the native elution, the significant enrichment over *PGK1* is reduced to around 25.5 ± 3.7 while the purification with higher Mbp-Mcp-3xHA levels leads to no significant enrichment over the negative control as for the denaturing elution (Figure 5.8 C). The enrichment of the copurified *CCW12-12xMS2* mRNA corresponds to the amount of purified Mbp-Mcp-3xHA detected on the Western blot. The amount of purified Mbp-Mcp-3xHA is higher when expressed under the *CYC1* promoter and increased with the denaturing elution in comparison to the native elution.

Generally, it can be observed that more unspecific protein binding occurs in the negative control of the purification where Mbp-Mcp-3xHA is expressed under the *NOP1* promoter.

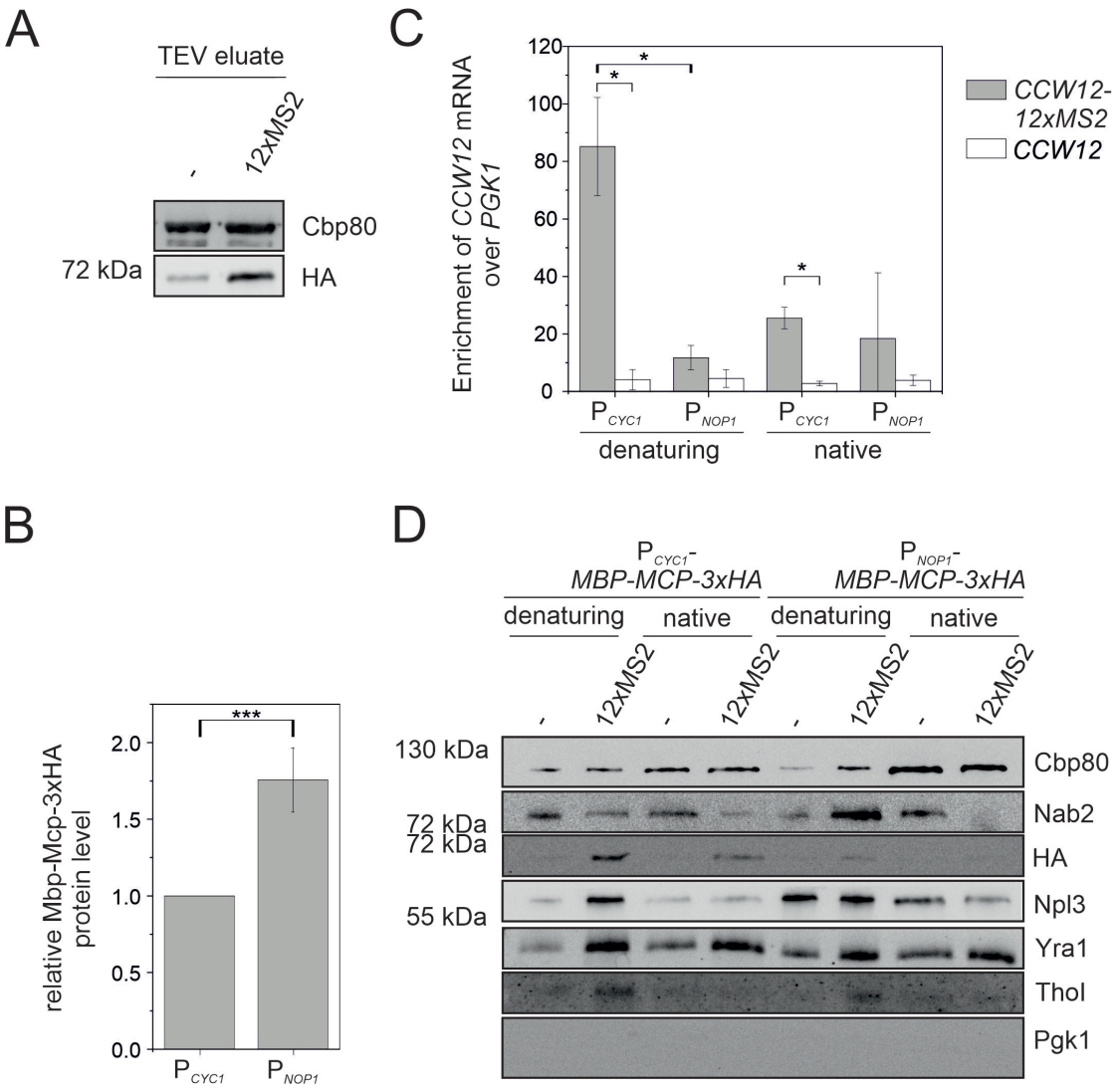

Figure 5.8: **Stronger Mbp-Mcp-3xHA expression hinders the *CCW12-12xMS2V6* nuclear mRNP purification.** **A** Representative Western blot showing the copurification of the Mbp-Mcp-3xHA protein with nuclear CBC during the first step of a nuclear *CCW12* mRNP purification. Cbp80 serves as loading control. **B** Quantification of the Mbp-Mcp-3xHA protein level when it is expressed under the control of the *CYC1* or *NOP1* promoter. The data illustrates the mean ± SD. The p-value was determined using a student's t-test with $\star\star\star$ $p < 0.001$. **C** Enrichment of *CCW12* mRNA over *PGK1* in the elution of a 12xMS2V6-based mRNP purification. Comparison of the different promoters (B) and denaturing or native elution. The graph shows the mean ± SD. The p-value was determined using a student's t-test with $\star$ $p < 0.05$ and $\star\star$ $p < 0.01$.QPCR values of all purification steps of a representative purification can be found in Supplement D.2. **D** Representative Western blot of the purification from C. The Western blot shown in the amount of purified Mbp-Mcp-3xHA detected with an HA antibody. Antibodies against known nuclear mRNA-binding proteins were used. Pgk1 serves as negative control.

The expression from the *CYC1* promoter leads to an increased protein signal of Npl3, Yra1 and Tho1 in comparison to the negative control without aptamer. While the signals of Cbp80 are similar to the control, more Nab2 can be detected in the negative control.

To reduce unspecific protein signals and further enhance enrichment of *CCW12-12xMS2*, magnetic amylose beads were used. The results were compared to the previously used amylose resin. It can be seen that the enrichment of *CCW12-12xMS2* over *PGK1* is significantly enriched over the negative control and seems to be slightly higher than for the amylose resin (Figure 5.9 A). However, the relative yield of both purifications is the same (Supplement D.1 C). The purification using magnetic beads reduced the amount of copurified proteins Cbp80, Npl3 and Yra1 detected by Western blot. Nab2 can not be detected when magnetic beads are used for the mRNP purification. The magnetic beads purification leads to less unspecific protein signal in the negative control (Figure 5.9 B).

To verify if the purification leads to complexes or only mRNA and single proteins, a 24 l purification was performed and the sample was analyzed using electron microscopy together with Nataliia Stefanyshena and Janett Piesker (Max Plank Institute for Heart and Lung Research). The sample was attached to alcian blue treated grids and negative staining was performed with 1 % uranyl acetat. Particles of the expected size could be observed (Figure 5.9 C). However, a similar pattern was observed on an empty grid (Figure 5.9 D).

Taken together, the enrichment of *CCW12* mRNA using a MS2 aptamer is possible and leads to a specific copurification of Cbp80, Npl3 and Yra1 protein. If the particles observed by electron microscopy are *CCW12*-containing nuclear mRNPs remains elusive.

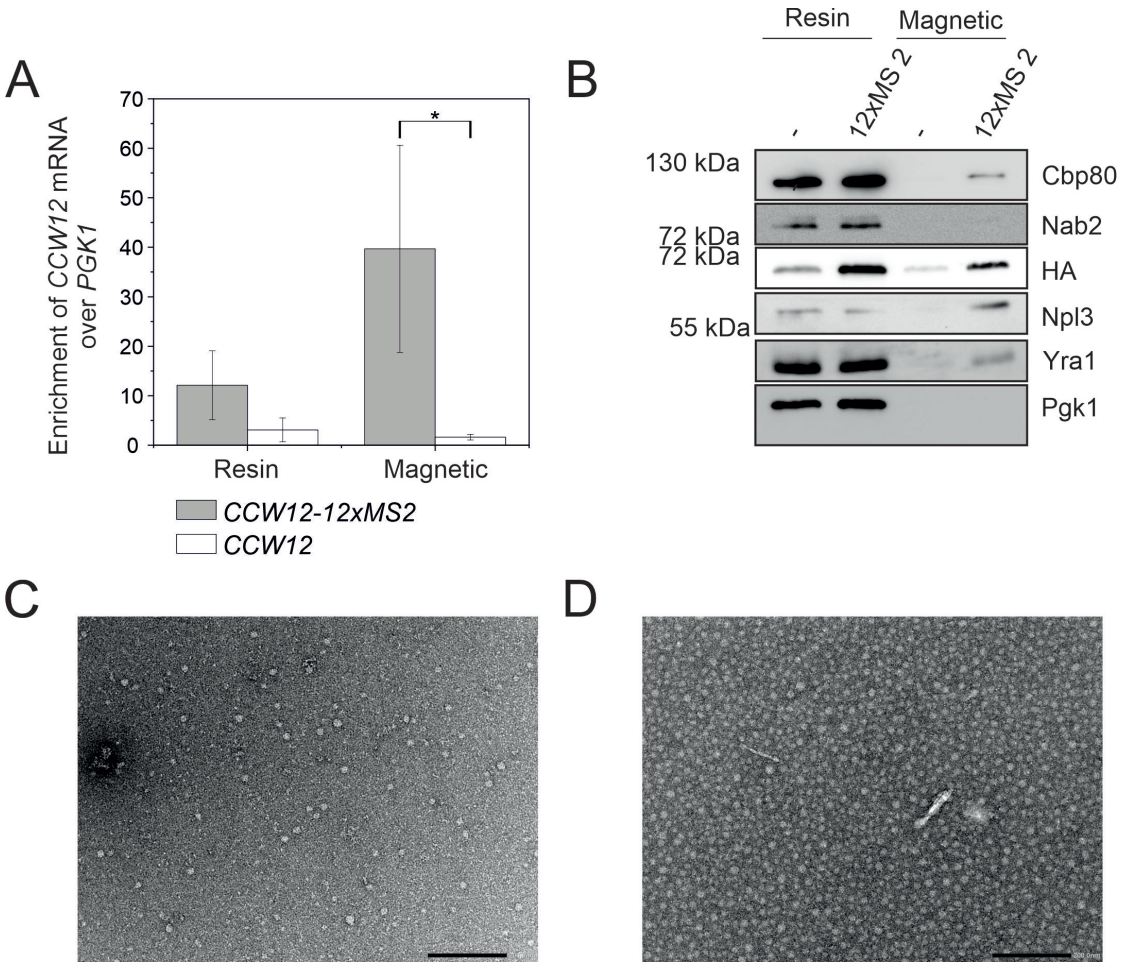

Figure 5.9: **The usage of magnetic beads improves purity of 12xMS2 based purification A** Enrichment of *CCW12* mRNA over *PGK1* in the elution of a nuclear mRNP purification based on 12xMS2. Comparison of the usage of amylose resin or magnetic beads for the purification. The graph shows the mean ± SD. The p-value was determined using a student's t-test with $\star$ $p < 0.05$. The qPCR values of all purification steps of a representative purification can be found in Supplement D.1. **B** Representative Western blot of the purification shown in A. The Western blot shows the amount of purified Mbp-Mcp-3xHA detected with an HA antibody. Antibodies against known nuclear mRNA-binding proteins were used. Pgk1 serves as negative control. **C and D** EM picture of the elution sample of *CCW12* mRNP purification after native elution (**C**) or water as negative control (**D**). Samples were applied to the alcian blue pretreated EM grid and negatively stained with 1 % uranyl acetate. Picture was taken at a 50000 x magnification.

Purification of heat shock mRNPs using the 12xMS2-based purification

To test whether the 12xMS2-based nuclear mRNP purification can be used to purify heat shock mRNA, the aptamer was integrated at the same positions of the 3´UTR as the Mango aptamer before (Figure 5.6 A). RNA levels were quantified using RT-qPCR. The levels of *SSA4* mRNA are only significantly reduced when placing the aptamer at position 2 (Figure 5.10 A). All three constructs were used for a test purification using amylose resin.

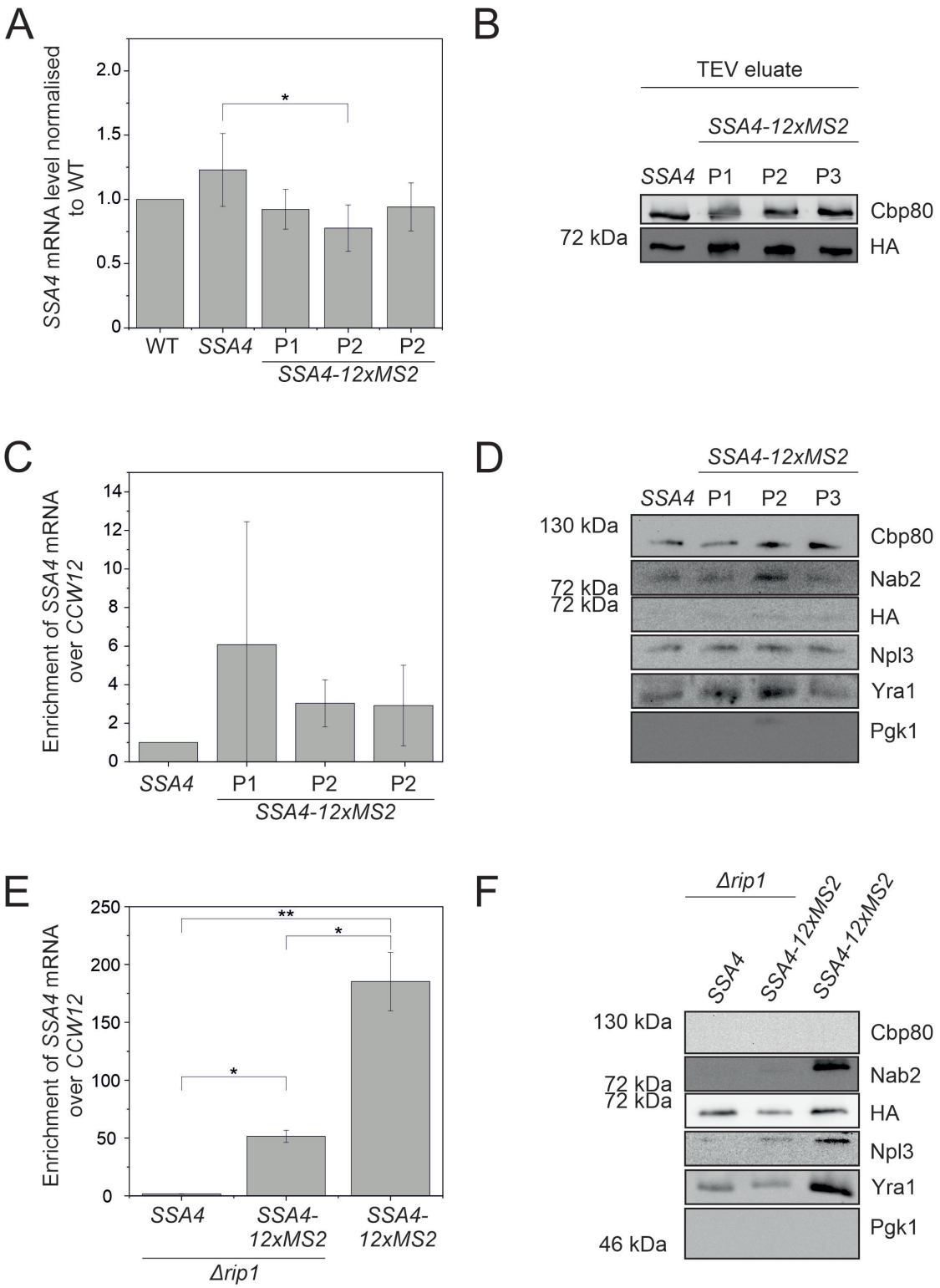

Figure 5.10: **A *Δrip1* strain yields the highest enrichment during purification of nuclear *SSA4* mRNPs using the 12xMS2V6 aptamer. A** Relative *SSA4* mRNA levels compared to WT after heat shock. RNA levels were determined by RT-qPCR. Shown is the mean ± SD. The p-value was calculated using a student's t-test with ⋆ p < 0.05.

Figure 5.10: **B** Representative Western blot showing the copurification of the Mbp-Mcp-3xHA protein with nuclear CBC during the first step of a nuclear *SSA4* mRNP purification. Cbp80 serves as loading control. **C and E** Enrichment of *SSA4* mRNA over *CCW12* after nuclear mRNP purification using the 12xMS2 aptamer in a two-step and one-step purification, respectively. *SSA4* without aptamer serves as negative control. The qPCR values of all purification steps of a representative purification can be found in Supplement D.3. **D and F** Representative Western blot for 12xMS2 purification shown in C and E. The Western blot shows the amount of purified Mbp-Mcp-3xHA detected with an HA antibody. Antibodies against known nuclear mRNA-binding proteins were used. Pgk1 serves as negative control.

In the test purification the TEV eluate shows no clear differences in copurified Mbp-Mcp-3xHA levels between the samples with and without 12xMS2 aptamer (Figure 5.10 B). In the elution sample, a minor enrichment of *SSA4* mRNA over *CCW12* mRNA could be achieved. However, the difference to the negative control is not significant (Figure 5.10 C). The protein levels of copurified Cbp80, Nab2, Npl3 and Yra1 are similar to the negative control except of a higher amount of Nab2 and Yra1 for integration of the aptamer at position 2. No clear bands for the Mbp-Mcp-3xHA protein could be detected.
Since no increased amount of Mbp-Mcp-3xHA over the negative control could be detected, a one-step purification was tested. The idea was to use a *Δrip1* strain, which mainly contains nuclear heat shock mRNAs, as they cannot be exported properly from the nucleus (Figure 5.2 B and C). The gene encoding Mbp-Mcp-3xHA was inserted into the Leu locus. Genomic *SSA4* was deleted and replaced using a plasmid encoding *SSA4* in the *Δrip1 MBP-MCP-3xHA* strain. The magnetic amylose beads were added directly to the cleared lysate, washed and eluted. The purification resulted in 51.5 ± 5.2 times more *SSA4-12xMS2* than *CCW12* mRNA. If the purification was performed in a strain possessing Rip1, which can properly export heat shock mRNAs, the enrichment of *SSA4-12xMS2* was much higher (Figure 5.10 E). The amount of purified Mbp-Mcp-3xHA is lower in the *Δrip1* strain with *SSA4-12xMS2* than for both controls. The Yra1 level is similar to the negative control and the Nab2 and Npl3 bands are very faint. The positive control still expressing Rip1 shows a much stronger copurification of Nab2, Npl3 and Yra1 than the other samples (Figure 5.10 F).
In summary, even though the purification of nuclear *CCW12*-containing mRNPs using the MS2-based approach appears promising for heat shock-specific transcript that is not the case. Only a one-step purification yields promising results. However, either all *SSA4* transcripts were enriched or a mutant altering mRNA export was used. Therefore, the purification of nuclear, stress-specific mRNPs for structure determination will be paused until further results can be achieved with the *CCW12*-containing, nuclear mRNP purification.

Cross-linking of heat shock mRNPs

Different publications state that known mRNA export factors are not essential for the export of heat shock mRNAs [Rollenhagen et al., 2007, Zander et al., 2016]. Above, different strategies for a native purification of nuclear heat shock mRNPs were tested. None of the tested methods could reach an enrichment similar to the yield that was achieved in a *CCW12* mRNP purification. Therefore the aim of this study was shifted to the identification of the proteins that constitute a nuclear heat shock mRNP to identify the proteins that are involved in the export of heat shock mRNPs.

Many methods were established in the recent decades to identify mRNA-binding proteins using a combination of cross-linking and stringent purification conditions. In this study, three different methods were tested: tandem RNA isolation procedure (TRIP) [Matia-González et al., 2017], comprehensive identification of RNA-binding proteins (ChIRP) [Chu et al., 2011, 2015] and RNA antisense purification coupled with MS (RAP-MS) [McHugh et al., 2015, McHugh and Guttman, 2018]. All of them had to be slightly altered to adjust them to the different organism and to focus on nuclear mRNPs. For the RAP-MS method, Table 5.3 shows the differences made in comparison to the original protocol [McHugh and Guttman, 2018].

Table 5.3: Overview of changes applied to the RAP-MS protocol [McHugh and Guttman, 2018] to test the method for the identification of nuclear heat shock mRNA-binding proteins. Changes were applied for the first test of the method.

RAP-MS (RNAi)	major adaptations RAP-MS
UVcross-linking	Chemical cross-linking
90nt ASOs cover whole target (DNA)	One 20 nt ASO (RNA)
Prepare nuclear lysate (cell culture)	First step nuclear mRNP enrichment using Cbp20-TAP
Harsh hybridization buffer: LiCl, DDM, SDS, sodium deoxycholate, urea, TCEP	No DDM (only first try, later added)
Purification at 67°C	Purification at 50°C for shorter RNA ASO
Protein elution using benzonase	Denaturing protein elution

First, chemical cross-linking at 42°C using glutaraldehyde (GA) was used instead of UV cross-linking. First experiments were performed with the 2´O-methylated RNA ASO8 for *SSA4* instead of a DNA ASO mix. Therefore, the annealing temperature had to be adjusted for the much shorter ASO. The adjustments and test

purification for the other two approaches can be found in the Supplement (ChIRP: Table E.2 and Figure E.2 , TRIP: Table E.1 and Figure E.1). Since the test purification did not yield promising results, further experiments in this section focused on the RAP-MS approach.

To cross-link RNA-protein complexes a 15 min heat shock was performed, followed by a cross-linking step at 42°C. Afterwards, a two step purification was performed as described for the native ASO purification. After the purification of the nuclear CBC, the TEV eluate was mixed with a denaturing hybridization buffer and the ASOs. The sample was incubated for 2 h at high temperature, the beads were washed and the RNA and proteins were eluted at 95°C. The enrichment of *SSA4* mRNA over the *CCW12* control reached in the first purification is 38.6 ± 26.6. However, this result was not very reproducible during the first purifications (Figure 5.11 A). Copurification of cross-linked proteins was analyzed using a Dot blot instead of a Western blot since the cross-linked protein complexes could not be separated on SDS-PAGE. As for the previous ASO purification, the protein copurification is similar to the negative control (Figure 5.11 B).

To test whether a mix of different 90mer DNA ASOs as used in the original method [McHugh and Guttman, 2018] could reach a higher enrichment of mRNA, 90mer DNA ASOs were ordered. The 21 ordered ASOs for *SSA4* were mixed. In addition, a mix of all odd and all even numbered ASOs was generated. The DNA ASO mixes were compared to the purification with the RNA ASO8 for *SSA4*. The purification using ASO8 improved in comparison to the first 90mer DNA ASO tests and reached an enrichment over *CCW12* of 79,1 ± 7.1. This is significantly higher than the enrichment reached using the ASO DNA mixes leading to an enrichment below 5. Moreover, a purification with ASOs for *CCW12* was performed. A very high enrichment of *CCW12* mRNA over *PGK1* could be observed (Figure 5.11 D). Even though it has a high SD, this appeared to be very promising. Since the enrichment of *CCW12* over *PGK1* was 1000-fold higher than the enrichment of *SSA4* mRNA over *CCW12*, the enrichment of *SSA4* over *PGK1* was also determined (Figure 5.11 E). The enrichment of *SSA4* mRNA for the mix containing all DNA ASOs is around 3621.9-fold and the odd and even mix led to an enrichment of 2262.8 and 877, respectively. ASO8, which had the highest enrichment over *CCW12*, shows only a minor increase over *PGK1*. This shows that the enrichment of *SSA4* over *PGK1* is much higher than the enrichment over *CCW12*. The enrichment of *SSA4* over other heat shock and highly transcribed mRNAs is similar to the enrichment over *PGK1* mRNA and can be found in Supplement E.4. The great changes in purification levels observed on RNA level cannot be seen in protein level. The Dot blots for all tested proteins look similar for all samples (Figure 5.11 F).

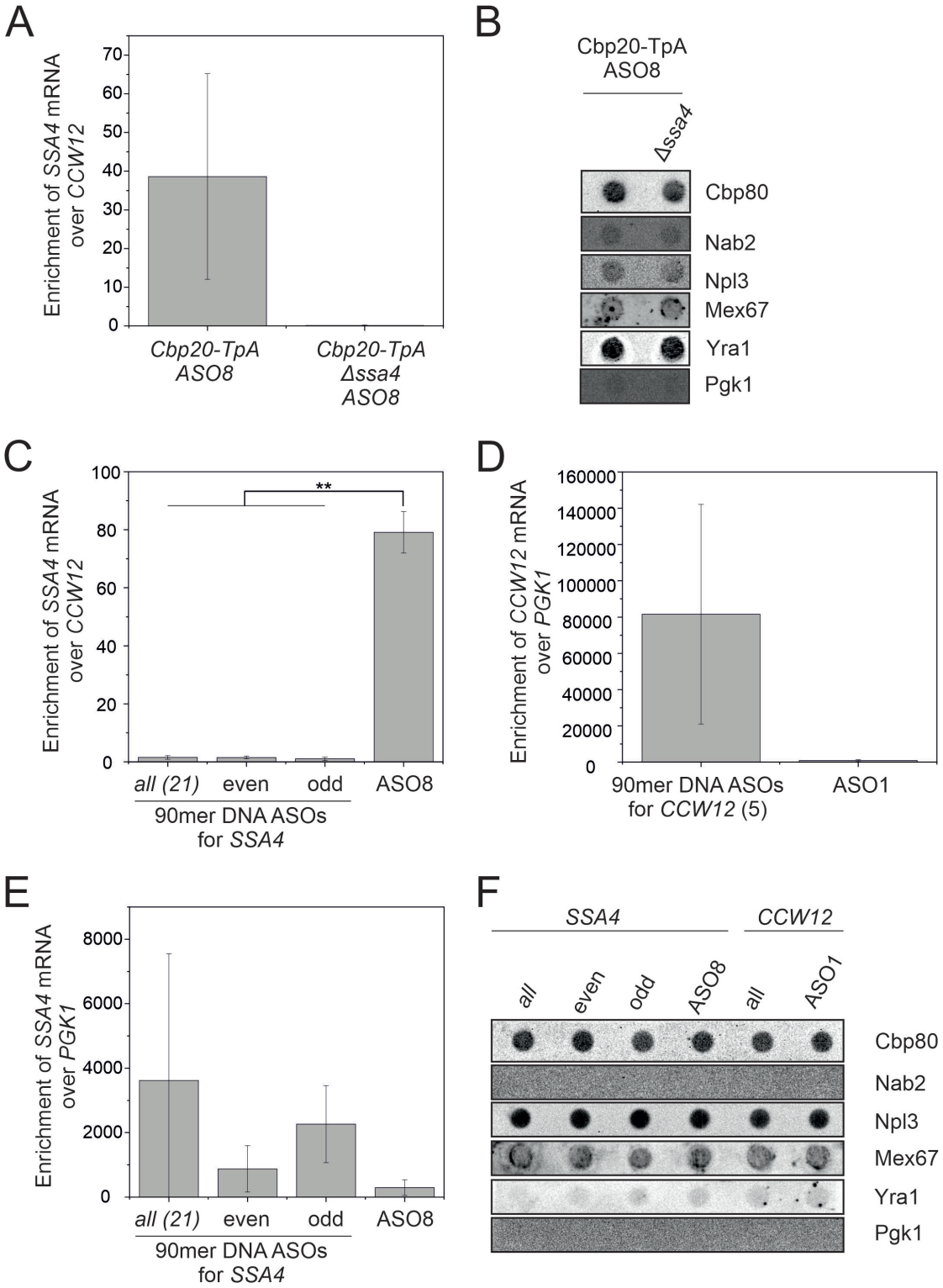

Figure 5.11: **RAP method can be used to purify *SSA4* mRNA A** Enrichment of *SSA4* mRNA over *CCW12* after cross-linking and nuclear mRNP purification using the modified RAP method. A *SSA4* deletion strain served as negative control. The qPCR values of all purification steps of a representative purification can be found in Supplement E.3.

Figure 5.11: **B** Representative Dot blot for the purification shown in A. Antibodies against known nuclear mRNA-binding proteins were used. Pgk1 serves as negative control. **C and E** Enrichment of *SSA4* mRNA over *CCW12* or *PGK1* after cross-linking and RAP purification, respectively. Different ASOs were tested: *SSA4* all: Mix of 21 90mer DNA ASOs covering the whole transcript; *SSA4* odd: Mix of DNA ASOs with odd numbers; *SSA4* even: Mix of DNA ASOs with even numbers; *CCW12* all: Mix of 5 90mer DNA ASOs covering the whole transcript; ASO1 and ASO8: 2'O-Methylated RNA ASOs also used for native purification. **D** Enrichment of *CCW12* mRNA over *PGK1* after cross-linking and RAP purification. A mix of 5 DNA ASOs was compared with ASO1 for *CCW12* purification. **B** Representative Dot blot for the purification shown in C-E. Antibodies against known nuclear mRNA-binding proteins were used. Pgk1 serves as negative control.

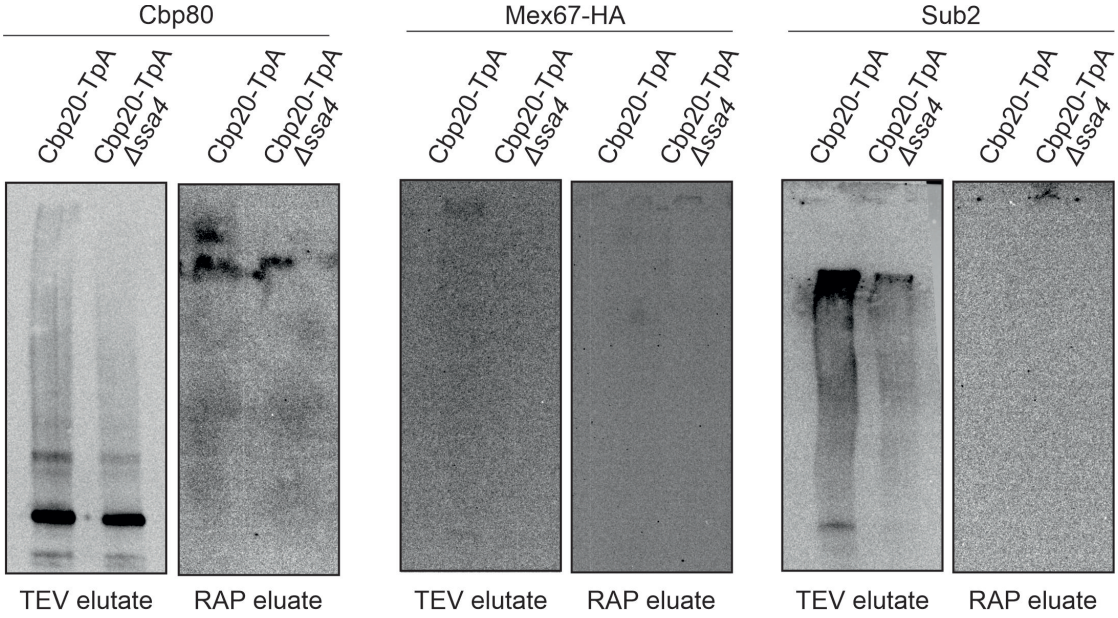

Figure 5.12: **No RNA-binding proteins can be detected using Western blotting for cross-linked proteins.** Representative Western blot for cross-linked proteins of the TEV and RAP eluate. For the Wet blot both the 4 % stacking and 6 % separating gel were used and proteins were transferred for 2.45 h. Antibodies for Cbp80 and Sub2 were used. Mex67-3xHA was detected using a HA antibody.

Taken together, the purification of the *SSA4* mRNA using the RAP method with all 21 ASOs leads to the highest enrichment of *SSA4* mRNA but it also shows the lowest reproducibility. However, further analysis is required to verify the copurification of mRNA-binding proteins.

In the original method [McHugh and Guttman, 2018], the proteins were eluted using benzonase treatment. In a next step, the elution using an RNase mix was tested. The protein samples were used for a Wet Blot with a 2.45 h transfer to see whether cross-linked proteins stuck in the pocket or the stacking gel could be detected. Uncross-linked proteins could be detected in the TEV eluate. In addition, some smear or higher molecular weight bands appeared, which might

be cross-linked proteins since they were only observed in lysate samples treated with GA (Supplement Figure E.5). For the elution sample non-reproducible signal could be detected (Figure 5.12).
A larger purification of 12 l culture was performed, cross-linked with two different GA concentrations and the elution was analyzed by MS. Many proteins could be detected, but the majority of them only with a low amount of measured peptides and a low coverage. The found proteins were divided in 3 categories shown in Venn-diagrams for each GA concentration (Figure 5.13 A). Unique proteins are not found in the negative control where *SSA4* is deleted (white). Proteins identified in both the sample and the negative control and proteins only found in the negative control are colored in dark and light gray, respectively. For both tested GA concentrations, the number of identified proteins in the three classes is similar. Only 17 of the unique proteins were found in both GA concentrations (Figure 5.13 B). Based on annotations, for most of the proteins an involvement in the heat shock mRNA export seems unlikely. Known mRNA export factors like Sub2 and Yra1 were found in both samples (Supplement Figure E.7).
To give a brief summary, the purification of cross-linked heat shock mRNAs using the RAP method is possible. Further comparative MS analysis will be needed for the identification of heat shock mRNA-binding proteins.

A

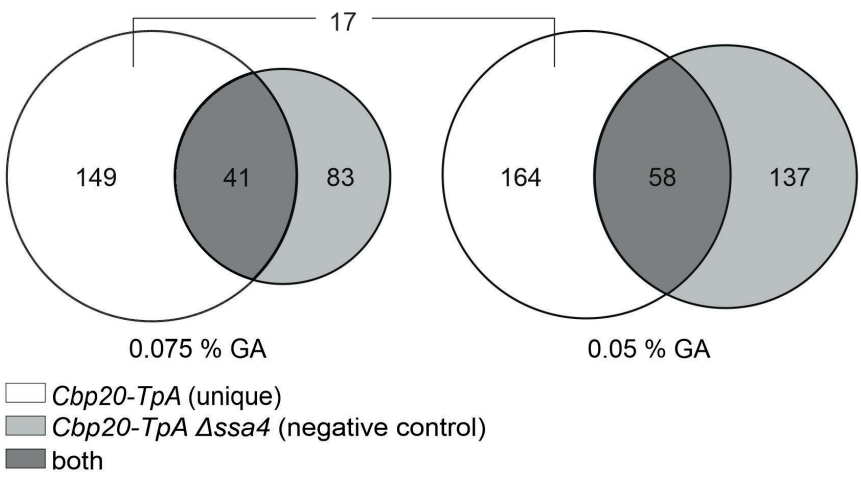

B

Accession	Description	Exp. q-value: Mascot	Coverage [%]	# Peptides	# PSMs	# Unique Peptides
P41895	Transcription initiation factor IIF subunit alpha	0	5	2	3	2
Q02725	Vacuolar transporter chaperone 3	0.037	3	2	4	2
Q06839	PX domain-containing protein YPR097W	0.011	2	2	2	2
P46974	Respiration factor 2	0.01	2	2	2	2
P34241	Nucleolar pre-ribosomal-associated protein 1	0.053	2	3	5	3
Q06680	Condensin complex subunit 3	0.054	3	2	5	2
P22204	Cell cycle protein kinase DBF2	0.033	6	2	4	2
P32898	Mitochondrial presequence protease	0.015	4	2	2	2
P53917	Factor arrest protein 11	0.023	2	2	3	2
Q07454	UPF0592 protein YDL073W	0.013	2	2	2	2
C7GNA4	Guanine-nucleotide exchange factor YEL1	0.012	3	2	2	2
Q06321	Sterol 3-beta-glucosyltransferase	0.032	2	2	4	2
Q06698	Putative ATP-dependent RNA helicase YLR419W	0.012	1	2	2	2
P36052	Protein arginine methyltransferase NDUFAF7 homolog, mitochondrial	0.009	9	2	2	2
P38991	Spindle assembly checkpoint kinase	0.01	4	2	2	2
Q12680	Glutamate synthase [NADH]	0.027	2	3	3	3
P37297	Phosphatidylinositol 4-kinase STT4	0.013	1	2	2	2

Figure 5.13: **RAP-MS results after mass spectrometry of test samples A** Venn-diagram visualizing the distribution of proteins identified by MS for the tested samples and glutaraldehyde (GA) concentrations. **B** Proteins found in the 0.07 % GA cross-linked sample that were also identified in the 0.05 % sample. The proteins were not identified in one of the negative controls (category unique).

Investigation of the mRNA export block mechanism during heat stress

Is the mRNA export block a conserved mechanism to cope with stress?

As discussed earlier, during heat stress bulk poly(A)-RNA accumulates within the nucleus whereas stress-specific transcripts are exported. It is not clear how these different processes occur. First, the question arose whether the RNA export block is a general mechanism in all stress conditions. To investigate this, a FISH was performed for heat shock, hyperosmotic stress, ethanol stress, hypoosmotic stress, rapamycin treatment, oxidative stress (by arsenitee treatment), unfolded protein response (UPR) (due to DTT treatment) and glucose and nitrogen starvation. Oligo(dT)-Cy3 was used to stain the poly(A)-RNA (red) and DAPI to stain the DNA and thereby mark the nucleus (blue). For the untreated WT control, the poly(A)-RNA signal is distributed throughout the cell, with the exception of vacuoles. Heat shock, hyperosmotic stress, ethanol stress and hypoosmotic stress (Figure 5.14 upper panel) lead to an obvious accumulation of nuclear poly(A)-RNA signal, which was already known before for heat shock, hyperosmotic and ethanol stress [Saavedra et al., 1996]. The other stress treatments showed no visible mRNA export block (Figure 5.14 lower panel).
The result was further validated by quantification of the obtained Oligo(dT) signal using a semi-automated quantification protocol that was established together with Dr. Cornelia Kilchert (Figure 5.15 A). After microscopy, the cell and the nucleus can be defined semi-automated using the Oligo(dT)-Cy3 and DAPI signal, respectively. Cells which do not have a assigned nucleus are excluded from the analysis. Afterwards, Fiji ImageJ measures the mean fluorescence of the Oligo(dT)-Cy3 signal within the cell, nucleus and cytoplasm. The calculation and visualization of the nuclear/cytoplasmic ratio was performed with the analysis software R. Quantification was done on a triplicate FISH experiment including at least 100 cells if not stated otherwise. This data analysis allows the detection of minor changes in the poly(A)-RNA distribution not visible by eye on the microscopy images. The quantification of all stress conditions shown previously was performed. While arsenite and DTT treatment resulted in a mild decrease of nuclear mRNA, glucose and nitrogen starvation lead to a minor but significant poly(A)-RNA accumulation in the nucleus.
Since Carmody et al. [2010] published that the deletion of the Slt2 kinase prevents

the mRNA export block during heat stress, the impact of this mutant on the response to various stress conditions was tested. The heat shock-treated *Δslt2* strain served as positive control. The untreated *Δslt2* strain already shows a minor decrease in the nuclear/cytoplasmic mean fluorescence signal (N/C ratio) in comparison to the WT sample (Figure 5.15 C). The N/C ratio is strongly reduced in *Δslt2* in comparison to the WT during heat shock. For hyperosmotic stress, no significant change was observed. In contrast, for ethanol and hypoosmotic stress, the N/C poly(A)-RNA ratio shows a significant reduction for *Δslt2* in comparison to the WT.

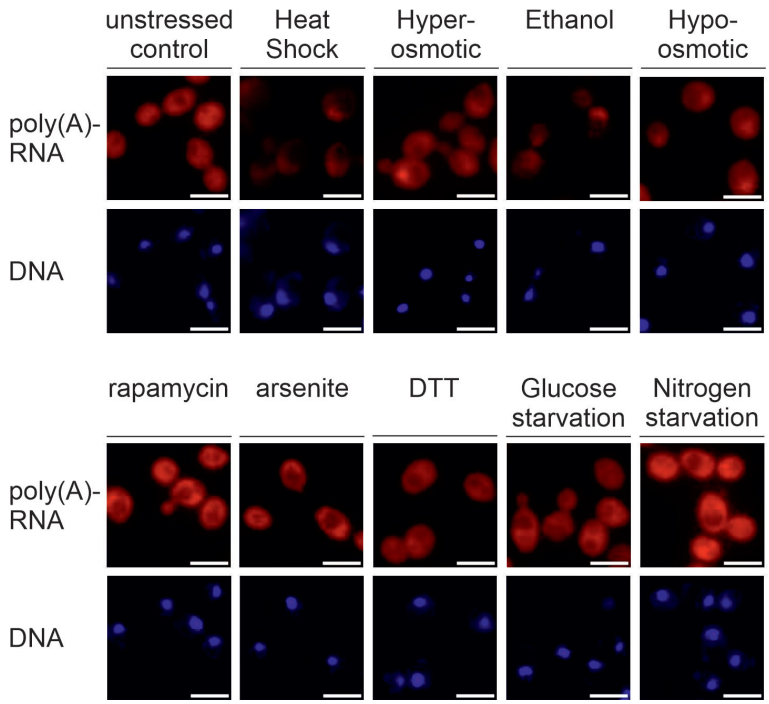

Figure 5.14: **Not all stress treatments tested lead to nuclear poly(A)-RNA accumulation.** Representative microscopy images of FISH performed for several stress conditions. The DNA is stained with DAPI (blue) and the poly(A)-RNA using Oligo(dT)-Cy3 (red). The stress conditions indicated are performed as described in Table 7.13. The scale bar corresponds to 5 µm.

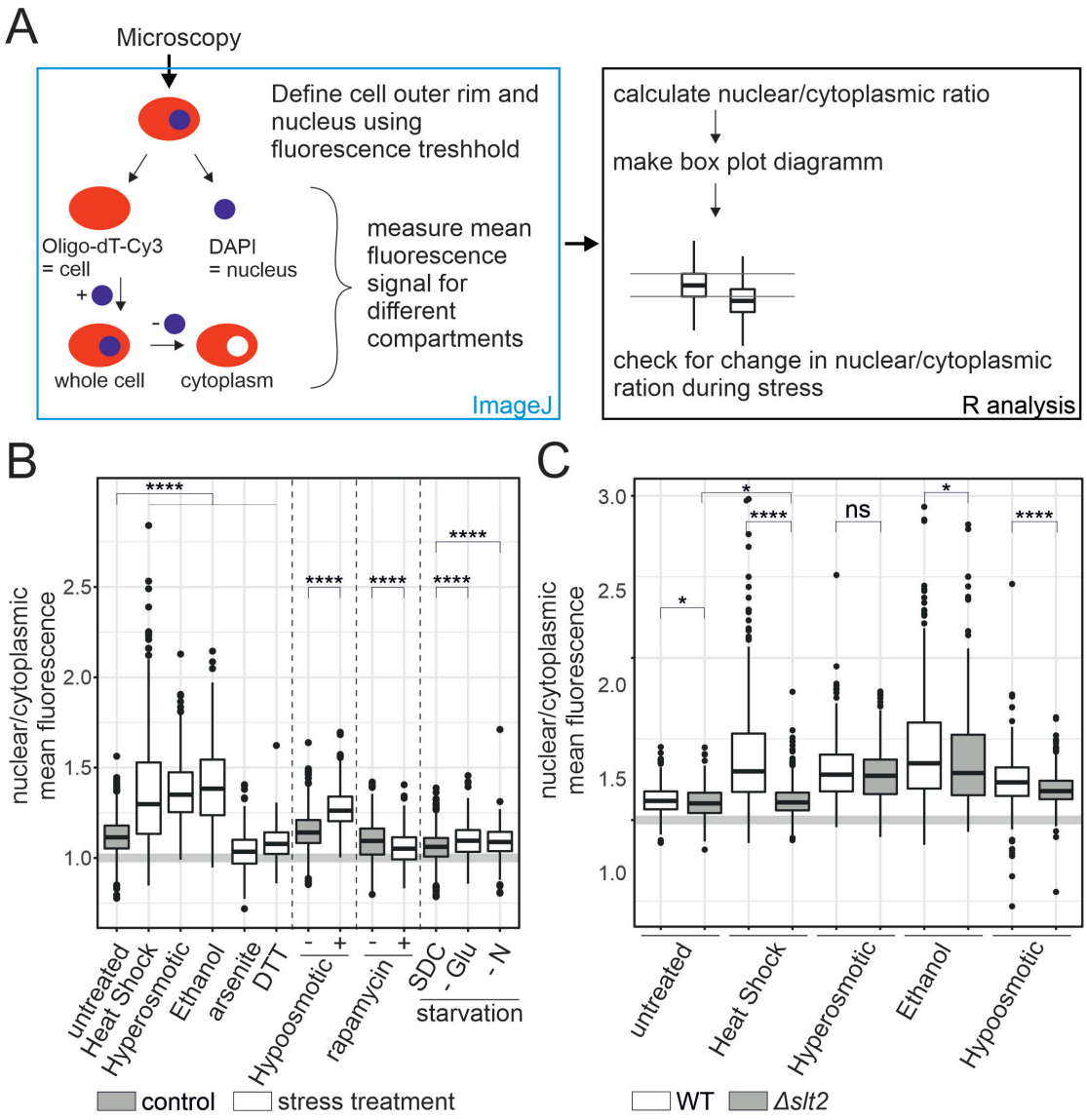

Figure 5.15: **Quantification allows identification of more changes in poly(A)-RNA distribution A** Schematic representation of the quantification process of microscopy images. **B** Quantification of Oligo(dT) FISH for different stress conditions in WT or **C** comparing WT and *Δslt2*. The graphs show a box plot diagram of nuclear/cytoplasmic mean fluorescence for the tested conditions. The stress treatments indicated are performed as described in Table 7.13. Each quantification consists of three experiments with a total of ≥ 300 cells. The p-value was calculated using a Welch t-test with $\star\star\star\star$ $p < 0.0001$.

Nab2 phosphorylation was identified for most tested stress treatments

For all stress conditions tested above, Nab2 phosphorylation was analyzed by Western blot as Slt2-dependent Nab2 phosphorylation was observed upon heat stress and might play a role in mediating the mRNA export bock. Phosphorylated Nab2 migrates more slowly through the gel and is therefore visible as an additional band running above the non-phosphorylated Nab2. These additional Nab2 band vanishes after phosphatase treatment [Carmody et al., 2010]. Nab2

phosphorylation can be observed for all stress conditions that lead to a strong poly(A)-RNA export block (Figure 5.16 A). For glucose and nitrogen starvation, no hiher-running band is detectable instead, Nab2 levels decrease compared to the control grown in minimal media (SDC) (Figure 5.16 B). Upon rapamycin treatment, the shifted band is very pronounced, but only weakly visible after arsenite and DTT treatment, suggesting that phosphorylation levels vary depending on the stress. In addition, no export block was observed for any of these conditions. The phosphorylation of Nab2 does not always correlate with the phosphorylation of Slt2, which was detected using a specific antibody for Slt2 phosphorylation. To examine further under which conditions the Nab2 phosphorylation is dependent on Slt2 stress treatment was performed in a *Δslt2* strain (Figure 5.16 C-E). For heat shock, a reduction in Nab2 phosphorylation can be observed (Figure 5.16 C). For rapamycin, arsenie and DTT treatment (Figure 5.16 D) and for hypoosmotic stress, the Nab2 phosphorylation disappears completely (Figure 5.16 E). Interestingly, for hyperosmotic stress the phosphorylation stays the same even if Slt2 is deleted.

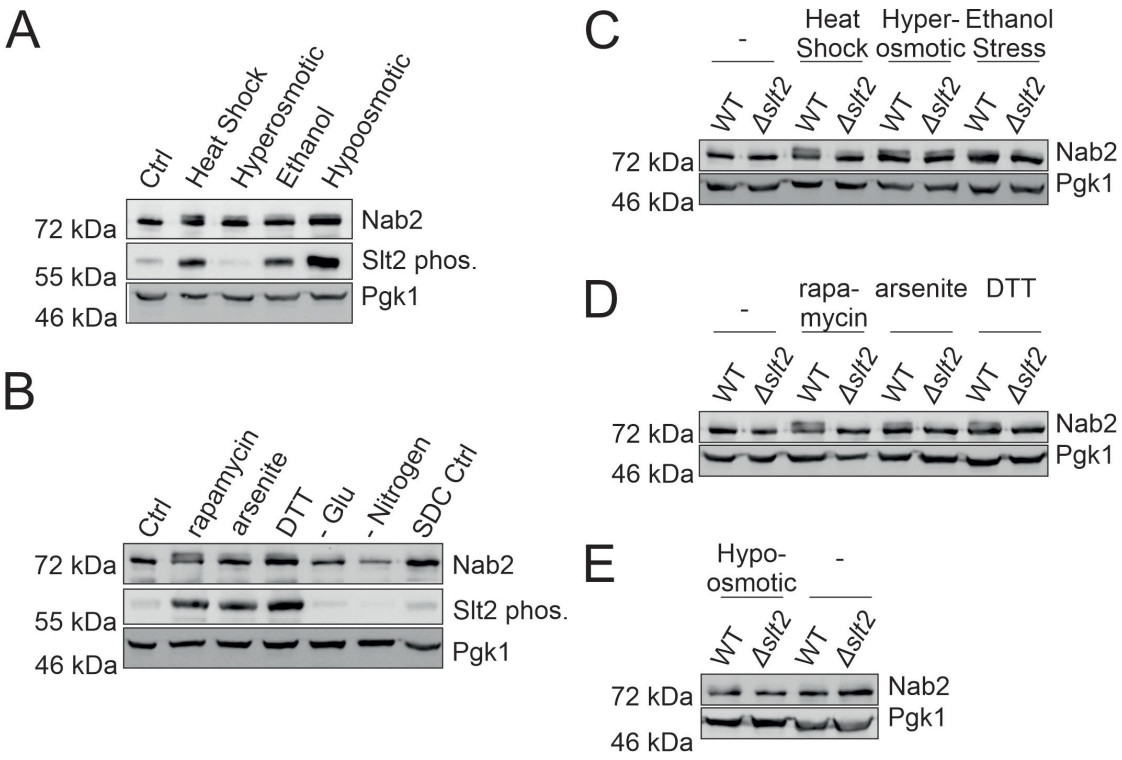

Figure 5.16: **Nab2 phosphorylation can be observed upon many stress treatments A and B** Representative Western blots showing the change in Nab2 phosphorylation. An antibody against Nab2 and phosphorylated Slt2 is used. Pgk1 serves as loading control. **C - E** Representative Western blot to identify the Slt2 dependency of Nab2 phosphorylation by comparing the WT with the *Δslt2* strain. An antibody against Nab2 is used. Pgk1 serves as loading control.

Altogether, many stress conditions lead to a mild or strong poly(A) mRNA export block. In addition, many stress conditions cause phosphorylation of Nab2. However, these two observations do not appear to be dependent on each other. Also, no correlation between the activation of Slt2 and the mRNA export block could be detected (Table 5.4).

Table 5.4: Analysis of Slt2-dependency of mRNA export block and Nab2 phosphorylation for various stress treatments. Summary of the results shown in Figure 5.14, 5.15 and 5.16. ++ strong effect, + detectable effect, - no effect

Stress condition	**mRNA export block**		**Nab2 phosphorylation**	
	WT	***Δslt2***	**WT**	***Δslt2***
Heat stress	++	-	++	-
Hyperosmotic stress	++	++	++	++
ethanol treatment	++	+	+	-
Hypoosmotic stress	++	+	+	-
rapamycin	-		++	-
arsenite	-		+	-
DTT	-		+	-
glucose starvation	+		-	
nitrogen starvation	+		-	

Identification of phosphosites on potential mRNA export regulators during heat and hyperosmotic stress

It was shown that Nab2 phosphorylation alone is not responsible for the mRNA export block during heat stress [Carmody et al., 2010]. However, since no mRNA export block is observed in *Δslt2* upon heat shock maybe other targets of this kinase beside Nab2 are involved in mediating the mRNA export block. To identify other proteins phosphorylated by Slt2 during heat stress, a phosphoproteome analysis was performed. A WT and *Δslt2* mutant were grown at 30°C or a 1 h heat shock was performed at 42°C. In addition, a hyperosmotically stressed WT was added to analyze if the same residues are phosphorylated for both stress conditions that cause an mRNA export block. The phosphoproteome analysis was performed by the lab of Prof. Dr. Johannes Graumann.
A volcano plot shows the log2 fold change of *Δslt2* over the WT sample after heat stress (Figure 5.17 A). The distribution of the volcano plot shows more changes in phosphorylation with a negative log2 fold change (log2FC) than with a positive. This indicates a lower level of residue phosphorylation if the kinase Slt2 is not present.

Other components of the cell wall integrity pathway are shown in red. Proteins possessing phosphorylation sites known to be regulated by the CWI pathway based on a phosphoproteome analysis with protein kinase C overexpression are depicted in blue [Mascaraque et al., 2013]. In addition, some of the top differentially phosphorylated residues belong to proteins which are known to be phosphorylated by Slt2 like RCN2 and Nup145 [Alonso-Rodríguez et al., 2016, Mascaraque et al., 2013].

Pie charts show to which biological processes the proteins with changed phosphorylation state belong (Figure 5.17 B). If comparing the amount of differentially phosphorylated residues assigned to biological processes for heat stress and additional deletion of Slt2 both datasets show a very similar distribution. An exception is a decrease in proteins involved in ribosome biogenesis if Slt2 is deleted. However, if Slt2 is deleted during heat stress a different distribution can be observed for phosphorylated and non-phosphorylated sites (Figure 5.17 C, Supplement Figure G.2 B). More proteins belonging to cytoskeleton organisation and transmembrane transport are phosphorylated if Slt2 is absent. Also the percentage of phosphorylated proteins involved in DNA replication and amino acid metabolic processes is increased. In contrast, phosphorylation levels tend to decrease for proteins associated with vesicle mediated transport and chromatin organization.

Taken together, the deletion of *SLT2* causes a reduction in phosphorylated residues due to heat shock. Biological processes and proteins known to be influenced by Slt2 could be identified in the generated dataset. Therefore, the differentially phosphorylation of residues upon heat shock and their Slt2-dependency can be further analyzed.

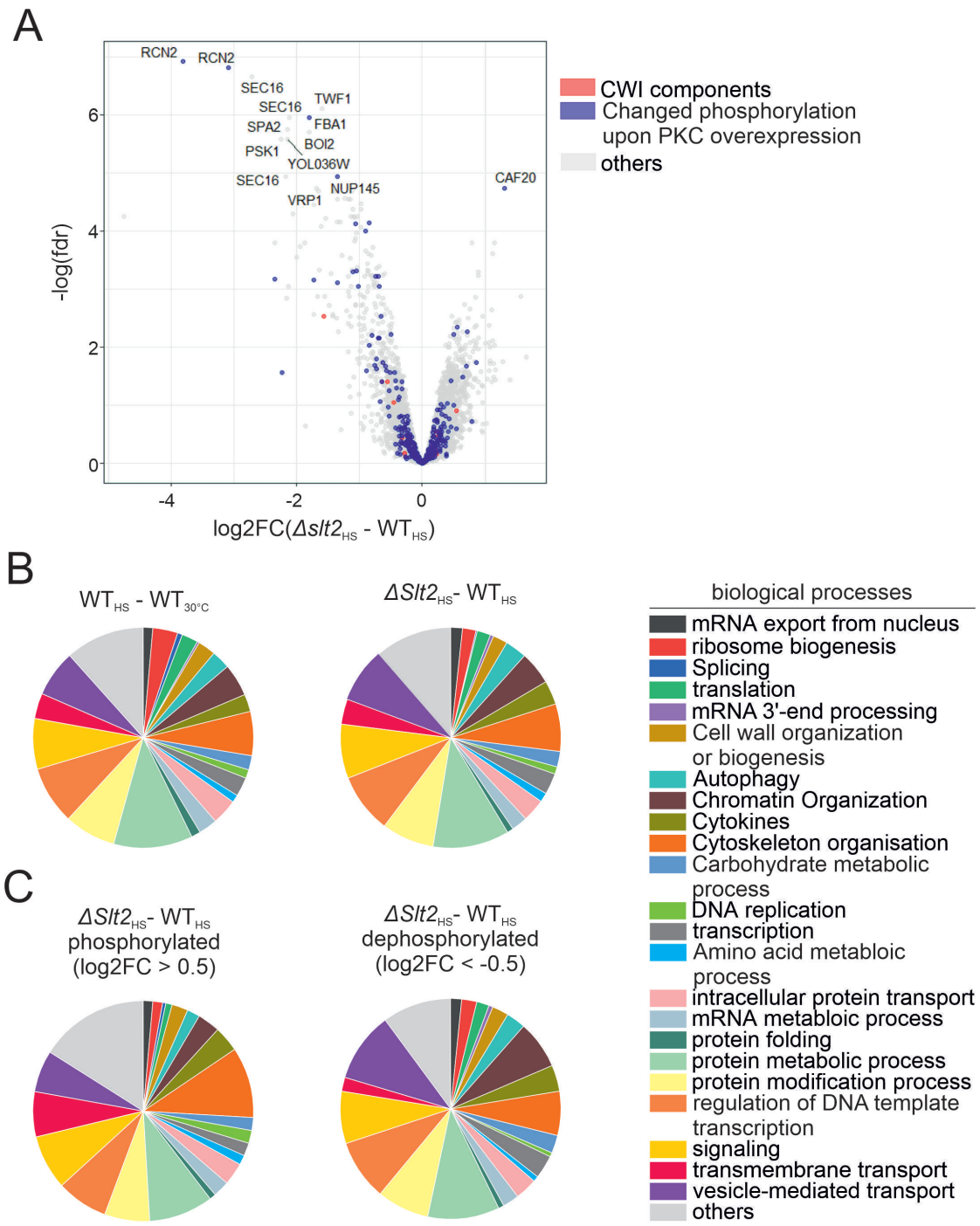

Figure 5.17: **Changes in the phosphoproteome upon deletion of Slt2 during heat stress A** Volcano plot showing the log2 fold change (log2FC) of the level of phosphorylation occupancy of individual phosphosites in a *Δslt2* mutant over the WT during heat shock against the -log(fdr). Cell wall integrity pathway components and proteins that are known Slt2 targets are shown in red and blue, respectively [Mascaraque et al., 2013]. *B and C* Pie chart showing the percentages of residues with changed phosphorylation belonging to proteins of several biological processes. One protein can be associated with several biological processes. The residues of the category "others" could not be assigned to any of the other categories.

To identify proteins that are phosphorylated upon heat stress and might be involved in mediating the mRNA export block the data set was compared with a protein list containing proteins linked to mRNA export (GO:0006406) [The UniProt Consortium, 2021]. In a second step, the changed phosphorylation status of mRNA export factors in the heat shocked *Δslt2* mutant was analyzed for mRNA export factors. The aim of this analysis was the identification of phosphosites involved in altered mRNA export under stress and the identification of a subset of proteins linked to mRNA export that are phosphorylated in a Slt2-dependent manner. Analyzed where either the TREX proteins (red), other mRNP components (Nab2, Npl3, Tho1)(blue), proteins of the NPC (purple) or the remaining export factors (GO:0006406)(other export factors, cyan) [The UniProt Consortium, 2021]. Other export factors are contained within GO:0006406 but are neither TREX components, Nab2, Npl3, Tho1 or NUPs. Examples of this category are Gfd1 and Pin4. Phosphorylated residues contained within these proteins were colored in a volcano plot showing the phosphorylation change upon heat stress (Figure 5.18 A). Many residues show a change in phosphorylation under stress which have a link to mRNA export (GO:0006406) [The UniProt Consortium, 2021]. From all TREX components 4 residues have a -log(fdr) greater than 2.5. But the majority of differentially phosphorylated residues can be found in NPC proteins. For the deletion of Slt2 during heat stress, the top candidates are highlighted in the volcano plot Figure 5.18 B. If Slt2 is deleted, a residue of the TREX component Yra1 with a significantly decreased level of phosphorylation can be seen in red. Other Slt2-dependent changes of phosphorylation status during heat shock are observed for amino acids of NPC proteins like Nup145, Nup159 and Dbp5 (purple). Besides these other proteins of the nuclear basket show a massive change of phosphorylation if Slt2 is deleted (Nup60, Nup1, Nup2, Mlp1).

To compare whether heat and salt stress affect the phosphorylation pattern in a similar way, a heatmap was generated for differentially phosphorylated residues residues within proteins that have been linked to mRNA export (Figure 5.19). If comparing the first two rows, it is clear that the change of phosphorylation is very different between the two stress conditions. No obvious similar pattern can be observed. For hyperosmotic stress, a strong increase in phosphorylation levels can be seen for several residues whereas heat shock seems to lead to a stronger overall reduction in phosphorylation. The *Δslt2* mutant compared to the WT during heat stress shows mostly slight effects in differentially phosphorylation with the exception of some strongly decrease level of phosphorylation of residues within NUPs.

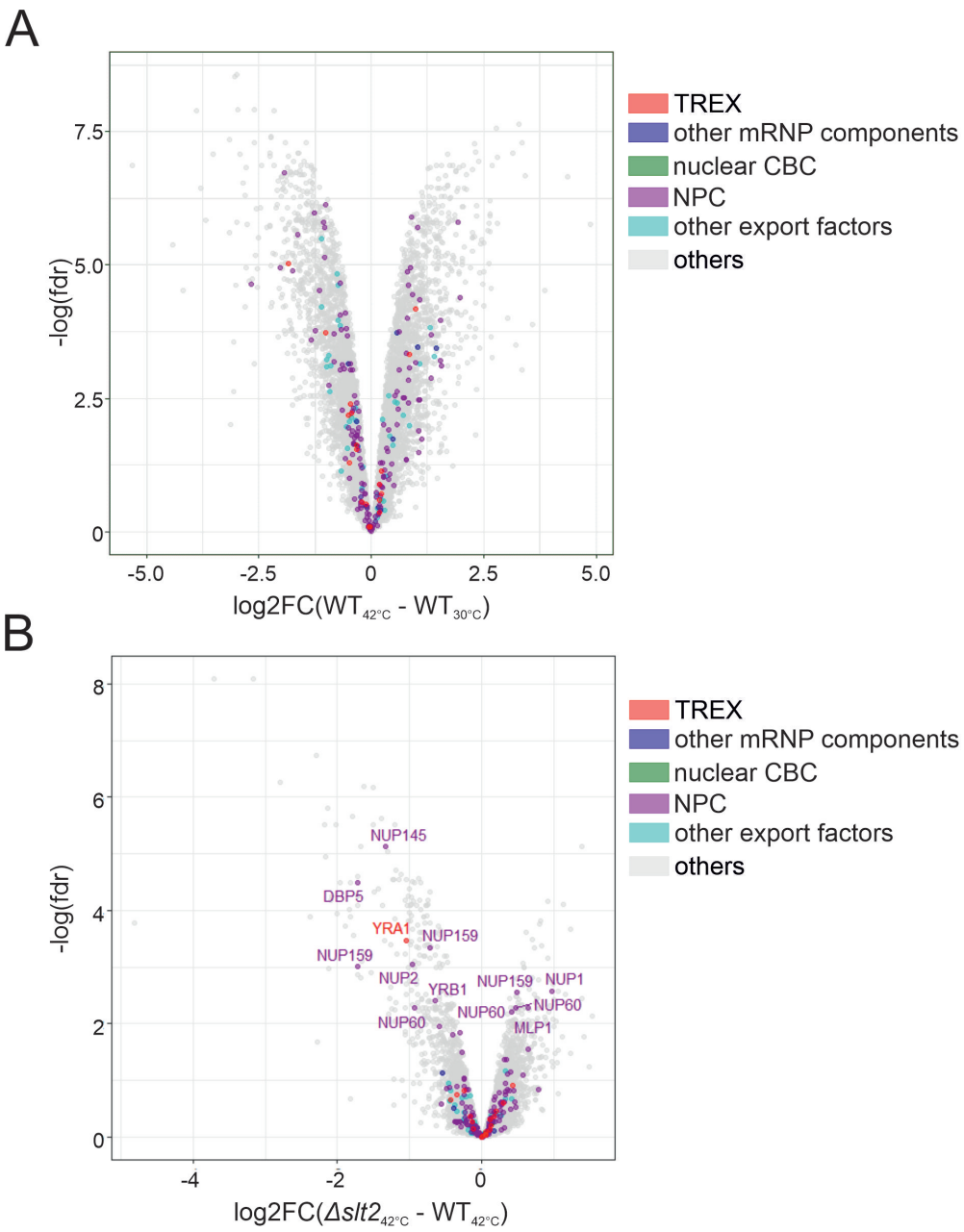

Figure 5.18: **Many mRNA export related proteins have residues with changed phosphorylation upon heat stress A** Volcano plot showing the log2 fold change of the phosphorylation sites of the WT during heat shock against the -log(fdr). **B** Volcano plot showing the log2 fold change of the phosphorylation sites of the *Δslt2* mutant over the WT during heat stress against the -log(fdr). Proteins involved in mRNA export are colored as shown in the figure legend. The residues with the most significant change in phosphorylation in the *Δslt2* mutant are highlighted with the corresponding protein names.

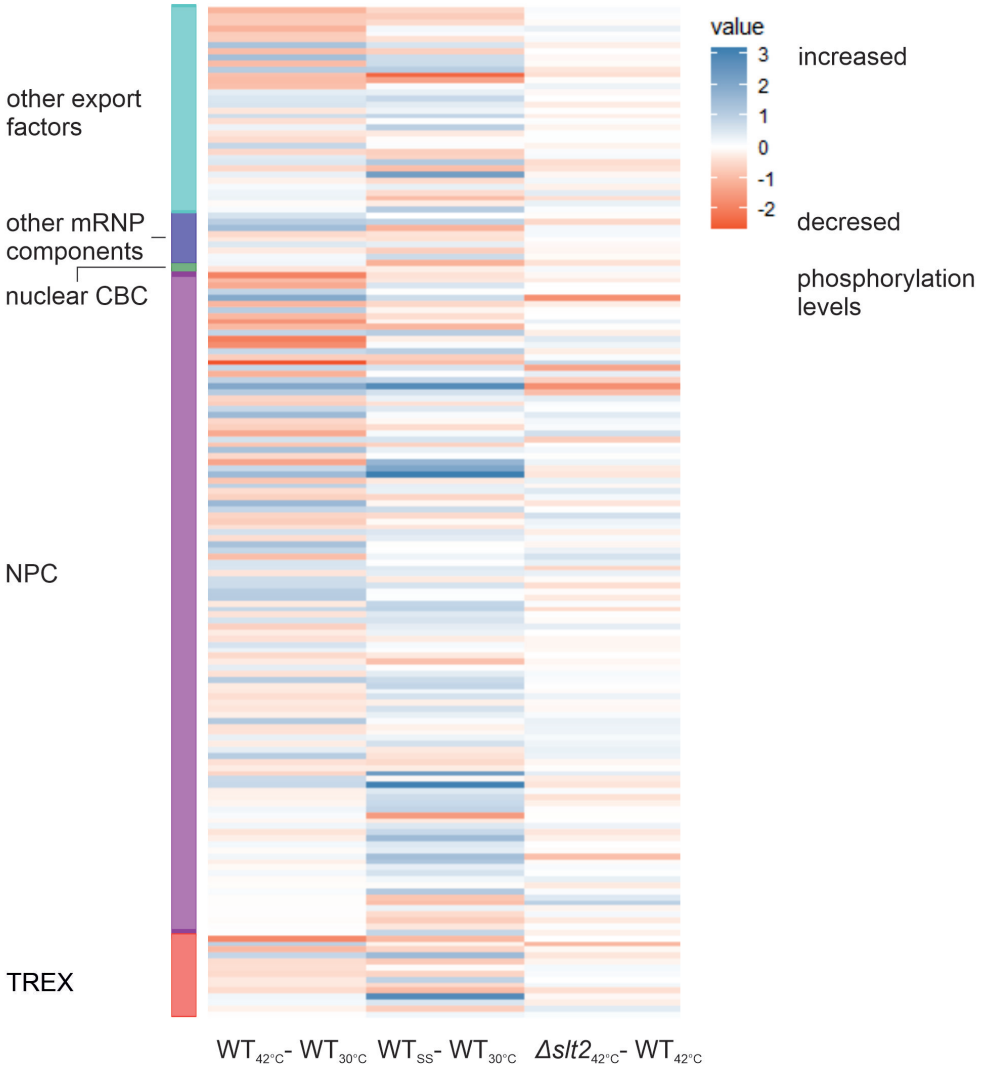

Figure 5.19: **Heat shock and hyperosmotic stress show different changes in phosphorylation of export factors** Heatmap displays the change in phosphorylation upon heat stress ($WT_{42°C}$-$WT_{30°C}$), salt stress (WT_{ss}-$WT_{30°C}$) and in the *Δslt2* mutant during heat stress ($\Delta slt2_{42°C}$-$WT_{42°C}$) for all significant changes (fdr < 0.05).

Influence of differentially phosphorylation of phosphopreoteome candidates on the mRNA export block during heat stress

Phosphorylation of Yra1 enhances protein levels and mRNA retention during heat stress

The TREX complex couples mRNA transcription and export. It could be determined that two components, Yra1 and Hpr1, are differentially phosphorylated under heat stress. Yra1 has two amino acids that are phosphorylated upon heat stress, S8 and S142 (Figure 5.20 A). The phosphorylation of S8 is decreased in the *Δslt2* mutant. During hyperosmotic stress three residues are differentially phosphorylated, the residues S142 and S211 are phosphorylated and S149 is less phosphorylated. The phosphorylation sites within the C- and N-box can be found in regions known to be involved in the interaction with Sub2 and Mex67 [Sträßer and Hurt, 2001], while S142 is located within the RRM domain, which is known for binding to Nab2 [Iglesias et al., 2010] (Figure 5.20 A). Yra1 was also one of the proteins that showed differences in the protein level in the phosphoproteome dataset. A fold change of 0.48 was determined for the *Δslt2* mutant at 42°C over the heat shocked control. The change in protein level could be verified using a quantitative WB at 30°C and 42°C (Figure 5.20 B). The mutant shows a reduction of the relative *Yra1-3xHA* protein level to 0.55 ± 0.08 at 30°C and a further decrease to 0.24 ± 0.05 after heat stress. To determine whether the reduced protein level is a result of the changed phosphorylation profile of Yra1, mutants were generated that either prevent phosphorylation by mutation to an alanine (A) or a phosphomimicry was generated by mutation to an aspartic acid (D). None of the mutations caused any growth defect in a spot assay (Supplement Figure H.1 A). The phosphomimicry single mutants *yra1-S8D-3xHA* and *yra1-S142D-3xHA* lead to an increased protein level of Yra1 during heat stress (Figure 5.20 C). However, preventing the phosphorylation of these residues did not alter protein levels compared to the control. Furthermore, the *yra1-S211A-3xHA* mutant shows a significant increase in protein levels while the corresponding phosphomimicry does not. For the *yra1-S8A-S142A* double mutant, a reduction of Yra1 protein level can be observed at 30°C (Supplement Figure H.2) and at 42°C (Figure 5.20 D). However, only the reduction during heat stress was significant. Mutations of the amino acids phosphorylated during hyperosmotic stress causes no significant change in protein level upon heat stress.

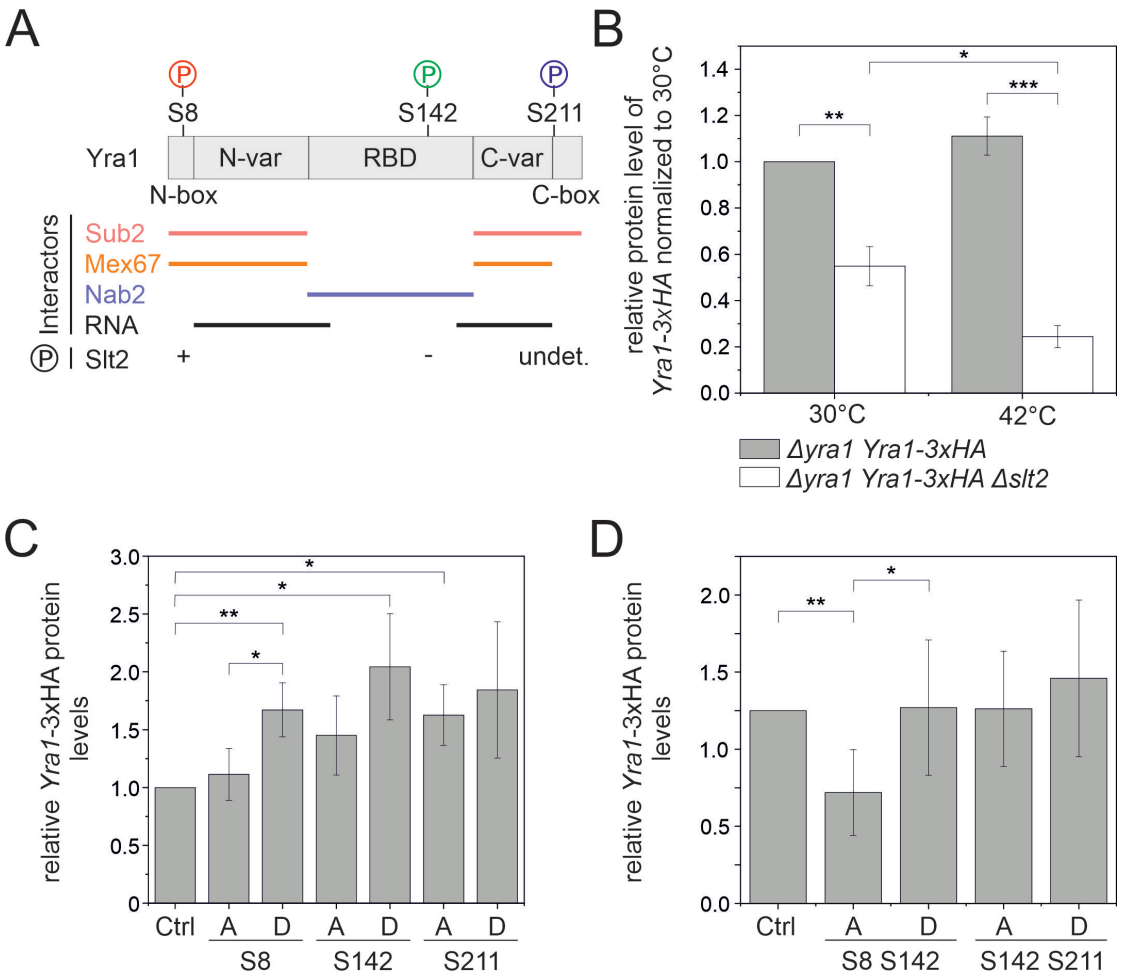

Figure 5.20: **Yra1 levels are dependent on its phosphorylation status A** Schematic representation of Yra1 and the different stress-induced phosphorylation phosphorylated upon heat stress (red), hyperosmotic stress (blue) or both (green). Indicated are known Yra1 interaction sites and Slt2 dependency deduced from the phosphoproteome data. **B** Quantification the relative *Yra1-3xHA* protein level in presence and absence of Slt2 determined by Western blot. Representative Western blot can be found in Supplement Figure H.1. **C and D** Relative *Yra1-3xHA* protein levels for the different Yra1 mutants preventing or imitating phosphorylation after 1 h heat shock at 42°C. Representative Western blot can be found in Supplement Figure H.2. Quantified protein levels are shown as mean ± SD. The p-value was calculated using a student's t-test with $\star$ $p < 0.05$, $\star\star$ $p < 0.01$ and $\star\star\star$ $p < 0.001$.

To investigate whether the phosphorylation profile has an impact not only on Yra1 protein levels but on the nuclear mRNA export block, a FISH was performed at 30°C and after 1 h at 42°C (Figure 5.21 A and B, Supplement H.3). As described above, quantification was performed. For *yra1-S8A*, a significant reduction in the N/C ratio was detected during heat shock, indicating a reduced mRNA export block. No significant difference was observed for the *yra1-S142A* and the *yra1-S211A* compared to the control.

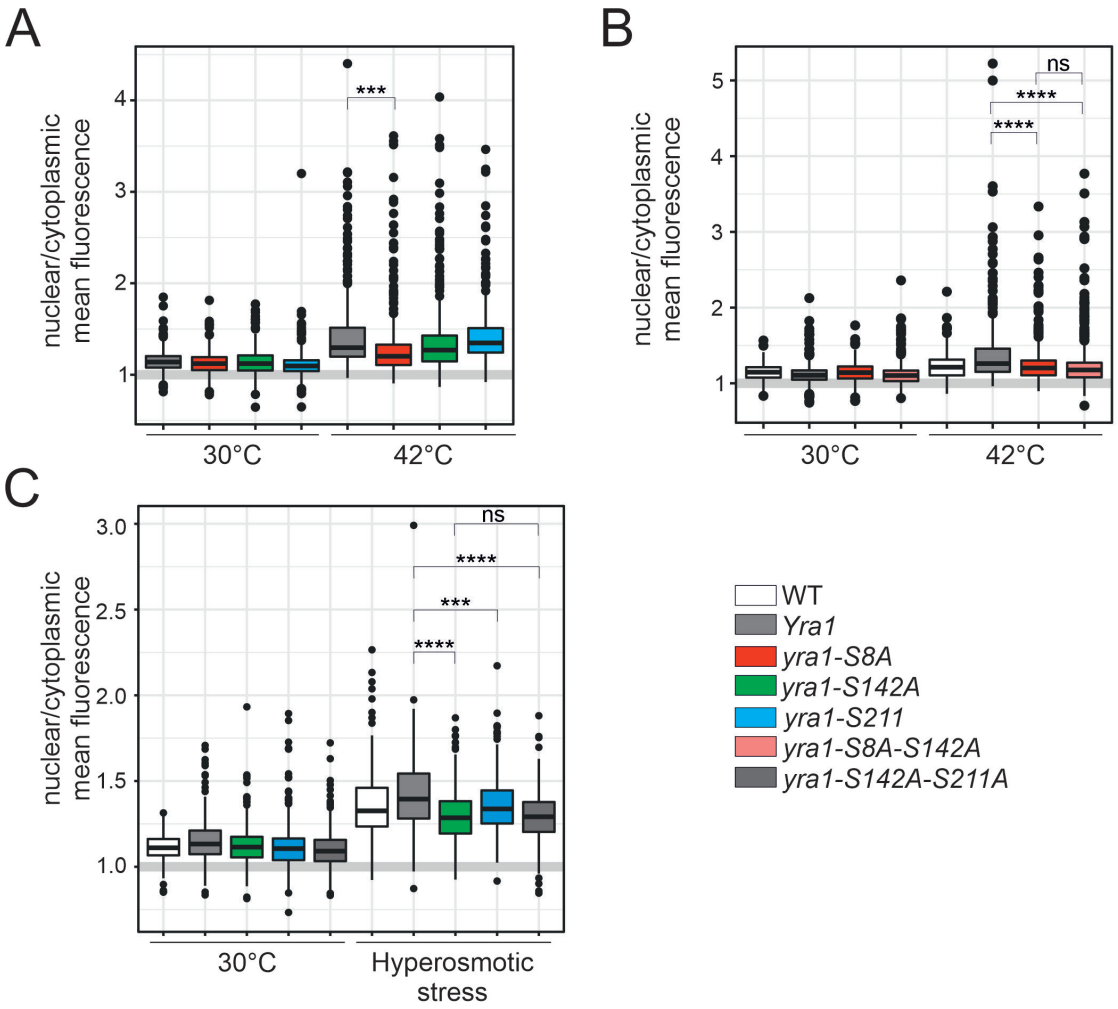

Figure 5.21: **Yra1 phosphosite mutation influences the poly(A)-RNA export block during stress treatment** Quantification of Oligo(dT) FISH for different Yra1 mutants with and without heat (**A and B**) and hyperosmotic stress treatment (**C**). The graphs show a box plot diagram of nuclear/cytoplasmic mean fluorescence for the tested strains. The stress conditions indicated are performed as described in Table 7.13. Each quantification consists of three experiments with a total of ≥ 300 cells. The p-value was calculated using a Welch t-test with $\star\star\star$ $p < 0.001$ and $\star\star\star\star$ $p < 0.0001$. Representative FISH images can be found in Supplement Figure H.3 and H.4.

The *yra1-S8A-S142A* double mutant led to a significantly reduced N/C ratio in comparison to the control but no significant difference was detected compared to the *yra1-S8A* single mutant.

During hyperosmotic stress, both *yra1-S142A* and *yra1-S211A* single mutants result in a reduction of the N/C ratio in comparison to the control (Figure 5.21 C, Supplement H.4). The corresponding double mutant behaves similar to the *yra1-S142A* single mutant and no significant difference can be observed between these two mutants.

Take together, three phosphorylation sites were identified for Yra1 in the phosphoproteome dataset. S8 and S142 are phosphorylated during heat and S142 and S211 during hyperosmotic stress. Preventing the phosphorylation of Yra1 during heat

shock with a *yra1-S8A-S142A* mutant led to reduced protein levels and a reduction in mRNA retention. Mutation of S142 to A led to an reduced N/C poly(A) RNA ratio during hyperosmotic stress.

To determine whether the export block can be further decreased by combining mutants of different export adapters, the *yra1-S8A-S142A* was combined with a *nab2-T178A-S180A*. In this study, the known Nab2 phosphorylation sites identified by Carmody et al. [2010] could not be found. Only minor log2 fold changes could be observed for changes of the phosphorylation status in Nab2 residues. However, a Slt2-independent phosphorylation site (S254) was identified (Figure 5.22 A). *Nab2-T178A-S180A* was used before for heat shock FISH and an mRNA export block could still be observed on the microscopy images [Carmody et al., 2010]. However, a quantification of the heat shock FISH showed a significant reduction in N/C ratio (Supplement Figure H.6). No significant difference could be found between the *nab2-T178A-S180A* and the *nab2-T178A-S180A-S254A* mutant including the Slt2-independent phosphosite identified in our phosphorproteome dataset. Combination of *yra1-S8A-S142A* with *nab2-178A-S180A* does not decrease nuclear poly(A)-RNA retention during heat stress further compared to the *yra1-S8A-S142A* mutant alone (Figure 5.22 B, Supplement H.6 B). In addition, it should be mentioned that the strain carrying both mutations (*yra1-S8A-S142A nab2-T178A-S180A*) already shows a significant increase in N/C ration compared to the control at 30°C.

In summary, combination the two mRNA export adaptor mutants, *yra1-S8A-S142A* and *nab2-T178A-S180A*, is not sufficient to prevent the mRNA export block during heat stress.

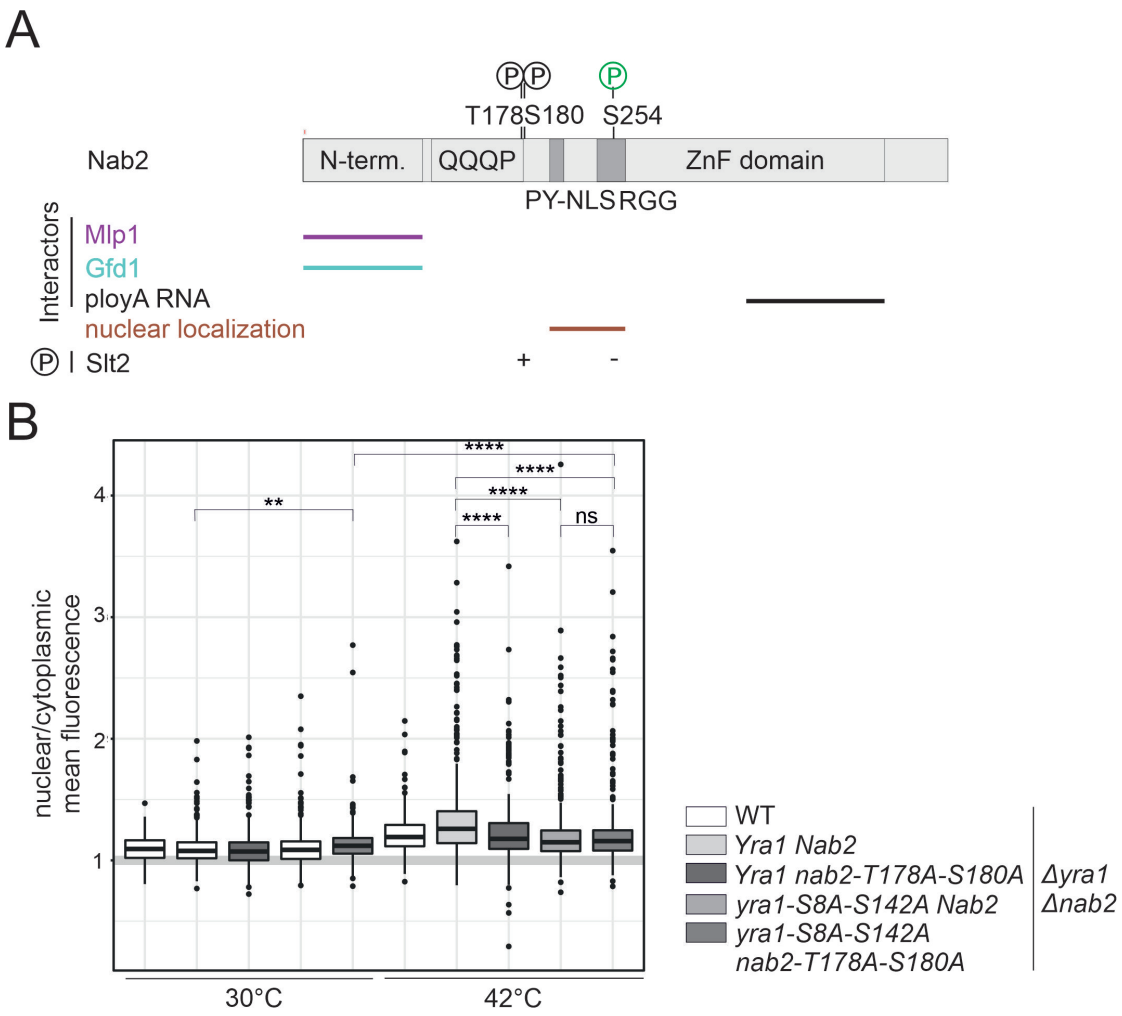

Figure 5.22: **Combination of *yra1-S8A-S142A* and *nab2-T178A-S180A* leads to no further reduction in nuclear poly(A) accumulation upon heat shock A** Schematic representation of Nab2 and the sites that are differentially phosphorylated upon heat and hyperosmotic stress (green). Indicated are known Nab2 interaction sites and Slt2-dependent phosphosites identified by Carmody et al. [2010] (black). **B** Quantification of Oligo(dT) FISH for the combination of Yra1 mutants with Nab2 mutants with and without heat stress. The graph shows a box plot diagram of nuclear/cytoplasmic mean fluorescence for the tested mutants. Each quantification consists of three experiments with a total of ≥ 300 cells. The p-value was calculated using a Welch t-test with $\star\star$ $p < 0.01$ and $\star\star\star\star$ $p < 0.0001$. Representative FISH images can be found in Supplement Figure H.6.

A Hpr1 phosphomimicry mutant enhanced the mRNA export block during heat stress

Another protein of the TREX complex which shows a strong change in its phosphorylation profile upon heat stress (reduced level of phosphorylation, Figure 5.18 A) is Hpr1. During heat stress, the phosphorylation at residue S673, S675 and S694 is decreased (Figure 5.23 A). In contrast to Yra1, the change in phosphorylation is not dependent on Slt2 but for 2 out of 3 sites it can be observed for

heat as well as hyperosmotic stress. To prevent the reduction in phosphorylation upon heat stress, two phosphomimetic mutants *hpr1-S673D*, *hpr1-S673D-S675D* and one mutant that prevents phosphorylation *hpr1-S694A* were generated and tested for changes in protein level and an influence on mRNA export block during heat stress. For none of these three mutants could a significantly changed protein level be observed (Figure 5.23 B).

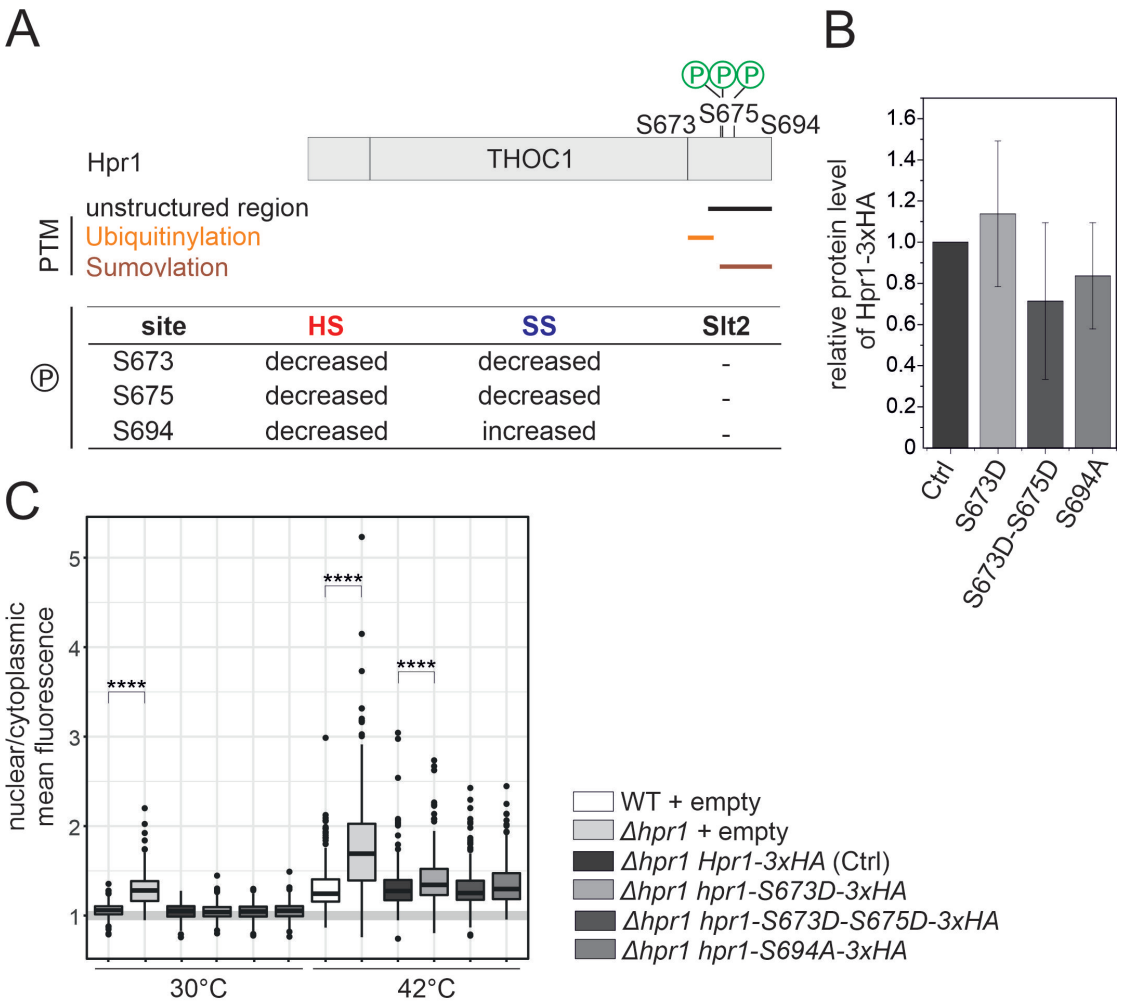

Figure 5.23: ***Hpr1-S673D* mutation leads to an increased poly(A)-RNA export block during heat stress A** Schematic representation of changes in Hpr1 phosphorylation pattern upon stress treatment as identified in our phosphoproteome dataset. Indicated are known sites of posttranslational modifications (PTM) of Hpr1 [Bretes et al., 2014]. **B** Relative *Hpr1-3xHA* protein levels for the different Hpr1 mutants after 1 h heat shock at 42°C. Quantified protein levels are shown as mean ± SD. **C** Quantification of Oligo(dT) FISH for different Hpr1 mutants with and without heat stress. The graph shows a box plot diagram of nuclear/cytoplasmic mean fluorescence for the tested mutants. Each quantification consists of three experiments with a total of ≥ 300 cells. The p-value was calculated using a Welch t-test with ⋆⋆⋆⋆ $p < 0.0001$. Representative Western blot and FISH images can be found in Supplement Figure H.7.

The deletion of Hpr1 leads to an mRNA export block at 30°C [Sträßer et al., 2002] and to an even stronger one during heat stress (Figure 5.23 C). For the three mutants tested, an increase in nuclear RNA retention was detected for *hpr1-S673D* while the other mutants showed no significant difference to the control.
Taken together, three Hpr1 residues are differentially phosphorylated upon heat shock (S673, S675 and S694). The *hpr1-S673D* phosphomimicry mutant led to a significantly enhanced mRNA export block.

Changed phosphorylation status of Dbp5 and Gfd1 leads to no or only minor changes in the nuclear mRNA export block upon heat stress

The strongest change in phosphorylation can be observed in proteins of the NPC. One protein for which a strong, Slt2-dependent change in phosphorylation was identified is the helicase Dbp5. Dbp5 has phosphorylation sites at its N-terminus which are differentially phosphorylated upon heat and hyperosmotic stress (Figure 5.24 A). However, only phosphorylation of S86 is Slt2-dependent. In addition, another protein, Gfd1, which is known to interact with Dbp5 and Nab2 [Christine A. Hodge et al., 1999, Suntharalingam et al., 2004], shows a decrease in phosphorylation. This decrease is enhanced by the absence of Slt2 (Figure 5.25 A).
For both proteins, Dbp5 and Gfd1 mutants were generated to prevent the reduction in phosphorylation mediated by heat shock treatment and tested for a change in poly(A)-RNA export block. None of the mutants showed any growth defect (Supplement Figure H.9 and H.8). The *dbp5-S86A* mutant shows no difference in N/C ration compared to control (Figure 5.24 B). For Gfd1 two mutants, namely *gfd1-S110D* and *gfd1-S106D*, show a mild decrease in the N/C ratio during heat stress compared to control.

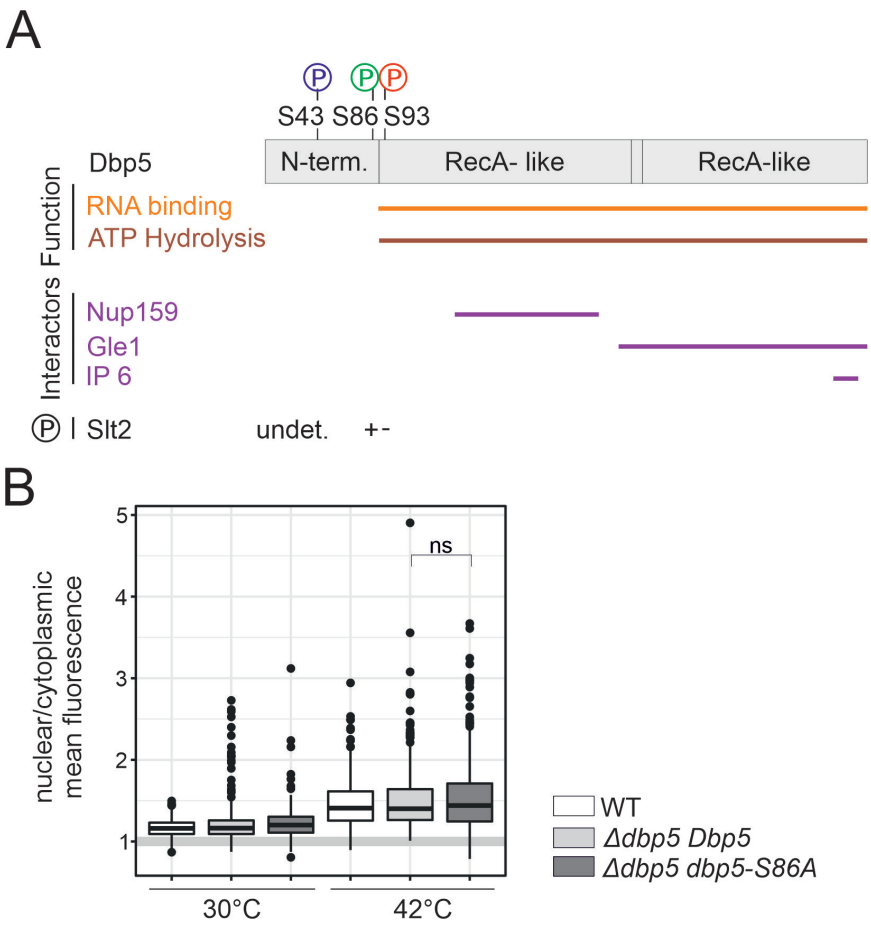

Figure 5.24: **Dbp5 phosphorylation mutant does not change poly(A) mRNA export A** Schematic representation of changes in Dbp5 phosphorylation upon stress treatment as identified in our phosphoproteome data and their dependence of Slt2. Indicated are know interaction sites and functional domains of Dbp5. **B** Quantification of Oligo(dT) FISH for different Dbp5 mutants with and without heat stress. The graph shows a box plot diagram of nuclear/cytoplasmic mean fluorescence for the tested mutants. Each quantification consists of three experiments with a total of $\geq$ 300 cells. Representative FISH images can be found in Supplement Figure H.9.

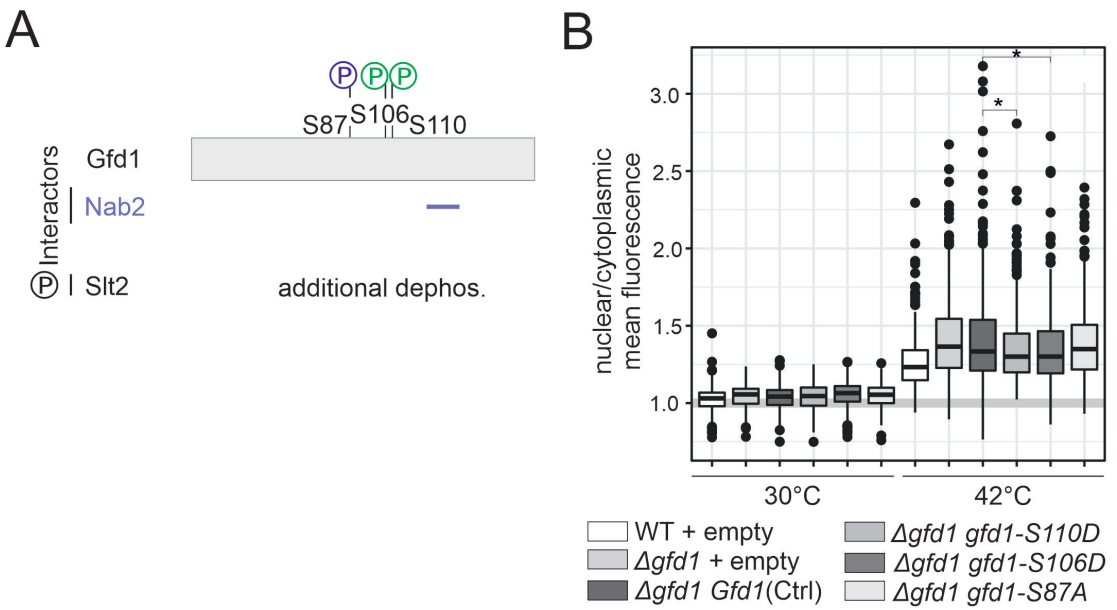

Figure 5.25: **Gfd1 phosphomimetic mutants show a mild effect on poly(A)-RNA export block during heat stress. A** Schematic representation of Gfd1 sites that are less phosphorylated upon stress treatment as identified in our phosphoproteome data and their dependence of Slt2. **B** Quantification of Oligo(dT) FISH for different Gfd1 mutants with and without heat stress. The graph shows a box plot diagram of nuclear/cytoplasmic mean fluorescence for the tested mutants. Each quantification consists of three experiments with a total of ≥ 300 cells. The p-value was calculated using a Welch t-test with $\star$ $p < 0.05$. Representative FISH images can be found in Supplement Figure H.8.

In summary, the mRNA export block appears to be a complex mechanism mediated at least in parts by the phosphorylation of several proteins. The change of phosphorylation of Yra1, Nab2 and Gfd1 appear to all contribute to mediating the mRNA export block, while the reduction of Hpr1 phosphorylation appears to facilitate poly(A)-RNA export during heat stress. So far no mutant or combination of mutants has been found that completely prevents the mRNA export block. The mechanisms of poly(A) mRNA retention still remain elusive and further investigations are needed.

6. Discussion

Purification of transcript-specific, nuclear mRNPs is not sufficient for structure determination

The first aim of this study was the purification of heat shock mRNPs to elucidate the structure of a transcript specific nuclear mRNP. The purification of transcript-specific mRNPs was performed in a two-step purification with an initial enrichment of nuclear mRNPs followed by an RNA purification step to yield only nuclear mRNPs harboring one specific transcript. It was not possible in this study to purify enough nuclear, transcript-specific mRNP particles for structure prediction using electron microscopy.

The unspecific protein copurification observed made it difficult to determine the amount of specifically copurified protein, especially for the ASO-based purification strategy. This unspecific protein purification could be due to unspecific binding of RNA-binding proteins to the ASO. Purification with the addition of random DNA or RNA oligos was performed to investigate whether this would reduce the unspecific purification by saturation of free RNA-binding sites (Supplement Figure A.3 and A.4). However, no change in protein copurification could be detected.

CCW22 is a paralog of *CCW12* in yeast which arose from genome duplication [Byrne and Wolfe, 2005]. Another possibility for detection of nuclear mRNA-binding proteins in the *Cbp20-TpA* Δ*ccw12* negative control could be the additional purification of *CCW22*-containing mRNPs. Deletion of *CCW22* did not cause any change in *CCW12* mRNP purification (Supplement A.5). Also, a *Cbp20-TpA* Δ*ccw12*Δ*ccw22* control resulted in unspecific protein copurification. This indicates that copurification of the *CCW12* paralog is not responsible for the unspecific protein copurification. However, the unspecific copurification does not occur using a 12xMS2 based mRNP purification using magnetic beads (Figure 5.9 B). Specific copurification of the shown proteins can be further increased by a purification from 2 l cultures instead of 24 l (Nataliia Stefanyshena, unpublished data).

The amount of purified nuclear *CCW12* mRNPs was increased in this study using desthiobiotinylated ASO1 [Wierschem, 2020] and increased biotin concentrations to a 45.4 ± 6.8 fold enrichment over *PGK1* (Figure 5.5 A - C, Supplementary

Figure A.9 and A.10). This corresponds to an RNA amount of 0.00017 ± 0.0002 pmol. This constitutes 0.009 % of the *CCW12* molecules of the lysate. A low yield of around 5 % - 1 % was expected because the majority of *CCW12* molecules are cytoplasmic. To increase the total yield of nuclear mRNPs the efficiency of both purification steps should be improved. In this study the initial purification of all nuclear mRNPs is carried out by the purification of the nuclear CBC. In the cytoplasm, the CBC is replaced by the cytoplasmic cap-binding protein eIF4E [Fortes et al., 2000], allowing this complex to be used to enrich nuclear mRNPs. This has also been used in other studies [Philip Keil, 2021, Wierschem, 2020]. Another possibility would be the purification of yeast nuclei. However, the isolation of yeast nuclei in contrast to higher eukaryotes is a difficult process with a low yield [Aris and Blobel, 1991]. In addition, the use of only one ASO instead of multiple that cover the whole transcript was reported to be less successful [Chu et al., 2011]. Therefore, using multiple ASOs could increase the yield of the second purification step.

As mentioned above electron microscopy performed from this purification (Figure 5.5 D) did not yield any promising particles. Particles are expected to have a size of around 20 to 30 nm in length and 5 to 7 nm in thickness based on published data on Nab2-containing mRNPs [Batisse et al., 2009]. Since Nab2-containing mRNPs include Yra1 and Cbp80 the protein composition could be similar to our purification (Figure 5.1 E and Supplement Figure A.1 - A.9). An expected difference might be that more homogeneous particles are observed in our sample as it contains only *CCW12*-specific mRNPs while Batisse et al. [2009] found over 6000 transcripts including *CCW12* in their sample. Expected particles were detected by Wierschem [2020]. However, this result could not be reproduced in this study using an ASO1-based purification.

EM analysis of possible *CCW12* containing nuclear mRNPs purified using a 12xMS2 aptamer revealed roundish particles of the expected size (Figure 5.9 C) but the water-treated grid showed similar particles. There are several ways to explain these observations. First, the observed particles are unspecific and derive either from the grid or the grid preparation. Second, the sample contains too less mRNPs to detect them by eye as reoccurring patterns under the EM. Third, specific particles are there but can not be distinguished from unspecific ones. The first possibility will be tested in future studies by testing different girds and different grid preparation (glow discharged vs. alcian blue treatment). For the second possibility, a purification from a bigger culture volume than 24 l has to be performed. Increasing the concentration of a particle could also be achieved by concentrating the eluate. When concentrating the purified mRNPs with a centrifugal filter unit, *CCW12* mRNA is found in the flow through and no enrichment can be observed

in the concentrate (Supplement A.11). Mild cross-linking could possibly overcome this problem. This could have a further stabilizing advantage of the particles for EM analysis [Schuller et al., 2020]. Alternatively, a different sample preparation could also be beneficial especially for a small amount of purified complex. It has been shown that 1 pmol of the RNA editing complex which was loaded onto a GraFIX gradient and used for EM yields row images with a good quality and enough detectable particles [Stark, 2010].
The third possibility, that nuclear mRNPs are there but can not be distinguished from the unspecific particles, will also be tested by two different strategies. On the one site, proteins previously detected by immunoblotting and the Mbp-Mcp protein will be tagged with GFP. This enables the usage of a GFP-antibodies suitable for EM, which allows to determine if the particles contain the copurified proteins and, indirectly, the RNA tagged with a 12xMS2 aptamer. In a second approach, RNA of different sizes will be purified and analyzed by EM to investigate if a change in particle size can be observed. A bigger particle size could help to distinguish the mRNPs from other particles. Using longer transcripts would be beneficial for the MS2 approach especially because the aptamer is very long. Therefore, it is expected that the impact of the aptamer would be more pronounced for smaller RNAs such as *CCW12* than for longer ones. This may explain why the *CCW12* mRNA shows a decrease in total mRNA level, whereas longer transcripts as *SSA4* or *ILV5* do not (Figure 5.10 A and Supplement Figure D.4 B). The fact that the MS2 aptamer can influence the half-life of the tagged mRNA is known and can be prevented by using the 24xMS2 [Tutucci and Stutz, 2011, Tutucci et al., 2018]. Since this aptamer is twice as large, the shorter 12xMS2 was used in this study due to the relatively small length of the *CCW12* mRNA.
Taken together, the purification of a *CCW12* nuclear mRNP shows a promising enrichment over a *PGK1* negative control. Especially, purification using an MS2 aptamer tag leads to specific copurification of nuclear RNA-binding proteins. However, further EM analysis is required to understand the results and to determine whether mRNAs and single bound mRNA-binding proteins or a correctly assembled nuclear mRNP were purified.
In addition, the exploration of other purification strategies could be carried out in parallel. For example, all *CCW12*-containing mRNPs could be purified using a single step 12xMS2 purification. The resulting complexes could be stabilized and separated on a GraFIX gradient. Afterwards, different fractions could be analyzed by EM under the use of GFP-tagged nuclear mRNA binding proteins and a GFP antibody to distinguish between nuclear and cytoplasmic complexes. In further studies other purification strategies should be developed and explored to reach the difficult goal of the structure determination of a nuclear transcript-specific mRNP.

The main goal of this study was not to analyze a *CCW12* mRNP but a heat shock-specific mRNA, which was especially difficult. The purification was carried out by initial purification of the nuclear CBC and following *SSA4* mRNA purification. The CBC binds to heat shock mRNAs and deletion of CBC components led to the accumulation of *SSA4* in the nucleaus (Figure 5.2 A - C). Rollenhagen et al. [2007] always tested for protein production as well as accumulation of heat shock mRNAs. They used GFP tagging in combination with fluorescence associated cell sorting (FACS). In this study, the presence of the Ssa4-3xHA protein after heat shock was validated by Western blotting (Figure 5.2 D). Another preferable possibility would have been the use of [^{35}S]methionine to label newly synthesized proteins after induction of heat shock. Simple immunoblotting was nevertheless chosen because Izawa et al. [2008] showed no expression of Ssa4 protein on Western blot before. However, all of these data suggest that the nuclear CBC is likely involved but not essential for the export of heat shock mRNAs.

The purification of a nuclear *SSA4*-containing mRNP has been tested with the ASO (Figure 5.4), the Mango (Figure 5.6) and the MS2 aptamer (Figure 5.10) based method. The best enrichment was reached with the ASO purification using ASO8 ($\sim$ 18 fold, Figure 5.4 C) and the one step MS2 purification from a *Δrip1* strain ($\sim$ 50 fold, Figure 5.4 E). The two step MS2-based purification yields nearly no enrichment. The use of another MS2 tag with a higher affinity to Mcp did not result in a more promising enrichment (Supplement Figure D.4). This could either indicate that the purification does not work for the *SSA4* mRNA or that the yield is much lower. Using more starting material or more material for the RT-qPCR could show an enrichment. The length of the transcript, which is around 5x longer than *CCW12*, could decrease the efficiency of the purification. This theory is strengthened by the fact that also purification of *ILV5* (CDS: 1188 bp) yields no significant enrichment compared to the negative control (Supplement Figure D.5). The one step purification from a *Δrip1* strain prevents the necessity of an enrichment of all nuclear mRNPs as heat shock mRNAs accumulate within the nucleus (Figure 5.2 B and C) [Saavedra et al., 1997, Rollenhagen et al., 2007]. However, it is known that the heat shock transcripts accumulate at the site of transcription [Thomsen et al., 2008] which could cause a change in mRNP structure or composition. Analyzing the accumulated nuclear heat shock mRNPs would be very interesting, of course, but in comparison to a proper export competent heat shock mRNP.

For further studies, the focus will be on the optimization and structure determination of *CCW12* mRNPs. After this is achieved, it will be interesting to test the improved and working method for *SSA4* mRNPs.

Cross-linking of heat shock mRNPs could not identify new nuclear heat shock mRNA-binding proteins so far

As mentioned before, many methods have been developed in the last decade to study RNA-binding proteins and to identify new RNA-binding partners. Therefore, the identification of proteins that bind to nuclear heat shock mRNAs and are involved in their export should be possible by adaptation of already developed methods. The RAP protocol reached the highest enrichment of *SSA4* mRNA compared to a negative control [McHugh et al., 2015, McHugh and Guttman, 2018]. The two main differences performed in this study in comparison to the original method [McHugh and Guttman, 2018] were chemical cross-linking and enrichment of nuclear RNA by a Cbp20-TAP purification. In general, cross-linking is beneficial for the identification of heat shock mRNA-binding proteins because it can maintain interactions formed upon heat shock. This led to the decision to use chemical cross-linking at 42°C rather than PAR cross-linking where the cells are harvested and irradiated on ice [Philip Keil, 2021]. For the chemical cross-linking GA had to be used instead of formaldehyde to prevent cross-linking reversion at higher temperatures. It was shown that the use of 90mer DNA ASOs for purification leads to high purity over *PGK1* (Figure 5.11) and other transcripts (Supplement Figure E.4). During ASO design the sequences were compared with the yeast genome to identify of target binding. Some of the designed ASOs had a partial complementary to *KAR2*. However, even *KAR2* mRNA could not be detected in the eluate indicating that full complementary of several ASOs to the target mRNA is required for purification. This in turn leads to a high purity.
Moreover, the protein copurification was either found to be unspecific as with other ASO purifications or no cross-linked proteins were detected at all (Figure 5.12). The unspecific copurification of proteins is unlikely because of the high temperatures (67°C) and highly denaturing buffer (10 mM Tris-HCl pH 7.5. 5 mM EDTA, 500 mM LiCl, 0.5 % DDM, 0.2 % SDS, 0.1 % sodium deoxycholate, 4 M urea and 2.5 mM TCEP) used for purification (Figure 5.3 F) . Since the RNA purification worked and proteins should be cross-linked a test MS analysis from 12 l culture was performed (Figure 5.13). Over 250 proteins were identified including about 150 specific proteins that could not be found in the negative control (category 1). However, comparing the unique hits at both tested GA concentrations showed that both conditions share only a minority of targets which also have a very low coverage and number of (unique) peptides. Again, this could have several causes.

First, the method does not work with the used settings, second the sample amount was too low, the cross-linking did not work, or the analysis was not performed correctly. For the first point the method can be repeated with a positive control. More starting material can be used. Furthermore, the last two options are important to be considered. For *in vitro* experiments it was shown that GA cross-links RNA to RNA at elevated temperatures (46°C and higher) [Hopwood, 1975]. GA cross-linking for *in vivo* experiments has previously been used to purify RNA-DNA-protein complexes [Chu et al., 2011]. This indicates that the cross-linking should work in general, but maybe heat shock at 46°C could be tested. Increased GA concentrations could also be considered but this causes a decrease in *SSA4* mRNA yield (Supplementary Figure E.6). The other option is to further analyze the generated MS data. Over 40 proteins are contained in category 2 (sample and negative control) for both GA concentrations (Supplement Figure E.7). Some of the top hits are Enolase-2, Sub2, Glyceraldehyde-3-phosphoate dehydrogenase 3 and Yra1 with a coverage of 47 %, 26 %, 35 % and 32%, respectively. This shows that category 2 hits shared between the two conditions show a much higher coverage during MS analysis than categroy 1 hits. The enzymes found are known RNA-binding proteins [Dollenmaier and Weitz, 2003, Huppertz et al., 2022]. Sub2 is known to be important for export of heat shock RNAs, while Yra1 was stated as not required for export but able to bind heat shock mRNA by Rollenhagen et al. [2007]. This indicates that another comparative MS and *CCW12* as control would be a good next step to identify heat shock mRNA-binding proteins. Subsequent analysis using smFISH, RIPs and ChIPs can be used to validate the found hits and identify their role in nuclear export of heat shock mRNAs.

mRNA export appears not to be a general stress response mechanism

For several stress treatments, an accumulation of poly(A)-RNA was observed (heat, hyper- and hypoosmotic, ethanol, glucose and nitrogen starvation) while others (rapamycin, arsenite, DTT) lead to no change or even a slight decrease the mRNA export block [Saavedra et al., 1996, Heinrich et al.]. The phosphorylation of the mRNA export adapter protein Nab2 and the activation of the kinase Slt2 appear to be independent events even though it was shown for heat stress that the accumulation of poly(A)-RNA vanishes upon deletion of Slt2 [Carmody et al., 2010] (Figure 5.15 C). Many studies investigated the activation of the cell wall integrity pathway and phosphorylation of Slt2 under various stress conditions [Staleva et al., 2004, Scrimale et al., 2009, Soulard et al., 2010].

Especially interesting are treatment with rapamycin, arsenite and DTT, which lead to TORC1 signaling pathway inhibition. In this study all three conditions caused a Slt2-dependent Nab2 phosphorylation but showed no accumulation of poly(A)-RNA in FISH experiments (Figure 5.15 C and 5.16 B). Both Nab2 phosphorylation and poly(A)-RNA accumulation could vary between experiments because of differences in the treatment (concentration, time) or strain background (W303 instead of RS453). For example, Carmody et al. [2010] could not detect a Nab2 phosphorylation in response to hyperosmotic stress (0.4 M NaCl, 1 h, 30°C) while in this study a phosphorylation could be detected. However, Nab2 phosphorylation analysis and the FISH experiment were performed following exactly the same treatments, which allows the conclusion that Nab2 phosphorylation and an mRNA export block are independent events. In addition, Carmody et al. [2010] determined that a Nab2 phosphomimicry mutant (S to D) is not able to abolish mRNA accumulation upon heat shock which may indicate that the observed Nab2 phosphorylation is not sufficient to cause or is not involved in mRNA accumulation. However, another possibility is that the phosphomimicry mutant cannot substitute the effect of the Nab2 phosphorylation efficiently. The Nab2 phosphorylation sites identified by [Carmody et al., 2010] could not be found in our phosphoproteome dataset. Instead, a Slt2-independent phosphorylation site was detected under heat stress or hyperosmotic conditions (Figure 5.22A). This highlights that Nab2 could be differentially phosphorylated under various conditions involving another kinase. Although no significant difference of the N/C ratio could be detected between the *nab2-T178A-S180A-S254A* and the *nab2-T178A-S180A* mutant (Supplement Figure H.5) it can not be ruled out completely that different Nab2 phosphorylation sites exist that induce a poly(A)-RNA accumulation.

Furthermore, it would be interesting to investigate whether other Slt2-dependent changes occur during any of these treatments and how the cell mediates activation of a specific subset of Slt2 targets under specific stress conditions. For example, the phosphorylation of Yra1 S8 was also identified in a phosphoproteome analyzing phosphorylation under nitrogen and glucose starvation [Rødkær and Færgeman, 2014] but not in a similar study to identify rapamycin dependent phosphorylation sites [Soulard et al., 2010]. This indicates a complex mechanism behind the phosphorylation preferences of kinases like Slt2 under different treatments. It would be beneficial to set up a bioinformatic comparison of different phosphoproteome data sets, which could lead to a better understanding of the activated targets under various conditions and which processes are involved. Moreover, activation of Slt2 is caused by phosphorylation of the T-E-Y motive of the Slt2 activation loop (T190, Y192) [Martín et al., 2000]. Although it is generally excepted that

dual phosphorylation is needed for full activation, the biological function of monophosphorylated Slt2 is still not fully understood [González-Rubio et al., 2021]. This fact adds another layer of complexity to the selection of different Slt2 targets under stress.By using commercial antibodies against dualphosphorylated Slt2, it has been shown that Slt2 is phosphorylated during various stress conditions. However, depending on the antibody, monophosphorylated Slt2 can also be detected [González-Rubio et al., 2021]. Therefore, it would be interesting to analyze if Slt2 is mono- or dual-phosphorylated upon various stress conditions and if this correlates with a defined subset of Slt2 targets.
For hyperosmotic stress it was observed that Nab2 phosphorylation and accumulation of poly(A)-RNA are Slt2-independent, indicating that another kinase is responsible for Nab2 phosphorylation. A likely candidate is the kinase Hog1, which is known to be activated during hyperosmotic stress [Regot et al., 2013]. This could be verified by performing a Nab2 phosphorylation Western blot with samples of a *HOG1* deletion strain. Since many signaling pathway are linked compensation upon deletion of a single component can not be ruled out. For example, cell wall perturbation leads also to the activation of Hog1 in addition to the CWI pathway [Sukegawa et al., 2018]. Also Slt2 activation is not only influenced by the CWI MAPK cascade but also by proteasomal degradation of Msg5 phosphatase [Martín et al., 2000, Liu and Levin, 2018]. This interplay between pathways and various ways of pathway activation and control shows the complexity of cell signaling. Therefore, it is even more complicated to understand causalities and makes intensive research necessary to gain further understanding ot the underlying mechanisms.

Identification of Slt2-dependent phosphosites by phosphoproteome analysis

The phosphoproteome analysis performed in this study aimed to identify more Slt2 dependent phosphorylation sites and patterns during heat stress. Carmody et al. [2010] identified Nab2 phosphorylation sites by Nab2 purification and subsequent MS analysis. Afterwards, an *in vitro* phosphorylation assay was performed to verify the phosphorylation of these residues by Slt2. These sites were thought to serve as positive control. Even though the phosphorylation of Nab2 was verified before by Western blot (Supplement Figure G.1 A), these sites could not be identified in our phosphoproteome dataset. This indicates that not all phosphosites can be identified by this method. However, 7911 changes in phosphosites/-occupancies were identified. The first step was to compare

our data with known Slt2 targets (Figure 5.17 A). Known verified targets like the calcium/calmodulin-dependent protein phosphatase regulator Rcn2 and the translation initiation repressor Caf20 [Mascaraque et al., 2013] belonged to the phosphosites with the highest significance and effect. Spa2, another top target, is known to act as scaffold-like protein of the CWI pathway during polarized cell growth and interacts physically with Slt2 [Fujiwara et al., 1998, van Drogen and Peter, 2002]. Rho1, also part of the CWI pathway, is transported from endoplasmatic reticulum to plasma membrane through the secretory pathway [Abe et al., 2003]. This could be shown by different mutations including deletion of Sec16, which causes a Rho1 mislocalization. Rho1 also influences vesicle transport through its targets [Guo et al., 2001]. In the phosphoproteome dataset, changes in the phosphorylation pattern of proteins involved in vesicle-mediated transport are found during heat stress and upon deletion of Slt2 (Figure 5.17 C). In addition, several highly significant changes were detected in the phosphorylation of Sec16 (Figure 5.18 B), a protein that plays a role in vesicle transport [Supek et al., 2002]. This suggests either a direct effect of Slt2 on vesicle-transport components or an indirect influence due to a feedback loop influencing Rho1 [Guo et al., 2009]. Heat stress causes a change from a polarized to a uniform localization of actin [Lillie and Brown, 1994, Delley and Hall, 1999]. It could be shown that Slt2 is required for the repolarization of actin after cell wall stress [Guo et al., 2009]. This could also be shown for oxidative stress [Pujol-Carrion et al., 2013]. The importance of Slt2 for cytoskeleton organization can be observed in our data (Figure 5.17 C) by a strong change in phosphorylation of proteins involved in cytoskeleton organization. These observations, which are consistent with published data from other groups, show that we were able to identify valid Slt2 targets in our data set although, the expected Nab2 sites could not be found.
Our data shows the change in the phosphorylation of many NUPs, some TREX components and other known export factors during heat and hyperosmotic stress (Figure 5.18 A and Supplement Figure G.1 B). However, the overall effects are quite different between the two conditions 5.19. Modifications observed in both datasets are probably part of a general stress response while the distinct changes are due to stress specific pathways. The two TREX proteins with the strongest effect due to heat stress are Yra1, which will be phosphorylated, and Hpr1, which will be less phosphorylated. Upon deletion of Slt2 highly significant changes in phosphorylation can be observed in proteins from the NPC. These comprise nuclear basket proteins (Nup1, Nup1, Nup60, Mlp1), FG rich proteins (Nup159, Nup145, Nup60, Nup1, Nup2), Dbp5 and YRB1. Interestingly, Yra1 is the only TREX protein identified in this study that is phosphorylated in a Slt2-dependent manner.

In this study, the phosphorylation of NUPs was not analyzed. However, since this class is very prominent in our data (Figure 5.18 A), it definitely hints at the importance of the NPC in stress response and would be an interesting aspect for further studies. Phosphorylation of the NPC is associated with the disassembly of the NPC during mitosis [Glavy et al., 2007, Laurell et al., 2011]. In the fission yeast *Schizosaccharomyces pombe*, it was shown that the NPC remodels during stress [Gallardo et al., 2020]. Deletion of Slt2 caused a change in phosphorylation of proteins of the nuclear basket (Figure 5.18 B). This has also been observed before for hyperosmotic stress [Regot et al., 2013]. Here Hog1 causes phosphorylation of nuclear basket proteins which was shown to be important for the proper export of stress-induced mRNAs [Regot et al., 2013]. Kosako et al. [2009] identified new targets for the human extracellular signal-regulated (ERK) MAPK and found ERK-dependent phosphorylation of Nup50, Nup153 and Nup214, which are the human orthologs of Nup60, Nup1 and Nup159, respectively. Phosphorylation of NUPs was shown to decrease interaction with the nuclear transport receptor importin-β and inhibit nuclear translocation of importin-β in an ERK mediated manner. A bioinformatic analysis based on the yeast NPC indicates that phosphorylation causes extension of FG-NUPs, which leads to a less dense FG-network [Mishra et al., 2019]. This in turn decreases the transport rate of nuclear transport receptors. Further studies would be needed to determine if the effects described above also are true and involved in the mRNA export block and export of stress transcripts during heat stress in yeast.

Yra1 is involved in mediating the mRNA export block during heat stress

In this study, the first analysis of phosphosites that was performed was the further investigation of Yra1 phosphorylation. Yra1 possesses a Slt2-dependent and independent phosphorylation site at S8 and S142, respectively. Upon hyperosmotic stress, the phosphorylation of S211 was identified. It could also be shown that Yra1 protein levels are changed in the *SLT2* deletion mutant (Figure 5.20 B). Mutations of the phosphosites indicate that the phosphorylation influences the protein level at high temperatures (Figure 5.20 C and D). However, exactly how this is mediated is not clear. Increased degradation due to a missing phosphorylation is possible and could be further verified using a cycloheximide assay. Ubiquitinylation of Yra1 by Tom1 is associated with the dissociation of Yra1 from the mRNP rather than with protein degradation [Iglesias et al., 2010]. But Iglesias et al. [2010] state that another unidentified E3 ubiquitin ligase exists that also ubiquitinylates Yra1. It would be interesting to analyze

in further studies if the changed phosphorylation pattern causes a change in ubiquitinylation of Yra1 and if that is the cause for decreased protein levels. Since Yra1 ubiquitinylation is associated with the dissociation of Yra1 from the nuclear mRNP, it would be interesting to investigate if the phosphorylation influences the occurrence of Yra1 within nuclear mRNPs. A purification of the nuclear CBC by Cbp20-TAP could show an influence on the association with nuclear mRNPs.
However, many other open questions still need to be analyzed concerning Yra1 phosphorylation. It could be shown that preventing the phosphorylation of Yra1 at S8 leads to a significant reduction of the N/C ration in Oligo(dT) FISH (Figure 5.21 A and B). Also preventing the phosphorylation of Yra1 during hyperosmotic stress leads to a reduced accumulation of poly(A)-RNA (Figure 5.21 C). To better understand this process, the sites of phosphorylation are very interesting. Yra1 has a conserved C- and N-box [Sträßer and Hurt, 2000]. Gromadzka et al. [2016] identified four conserved motifs for mRNA export factors in humans. The N-box contains a SLDD/E motif, which was termed UAP56 binding motif (UBM). While the N-terminus contains the S_8LDE sequence of a UBM, the C-terminus contains a S_{211}LED sequence similar to the UBM consensus sequence. In addition, the C-terminus contains another motive identified by Gromadzka et al. [2016] the LDxxLD motif (ALY: L_{243}DAQLD; Yra1: L_{215}DKEMA) also found in export factors that interact with Sub2. Taken together, Yra1 is phosphorylated in a N- terminal or C-terminal UMB motif during heat and hyperosmotic stress, respectively. Yra1 cells without the C-box where shown to have a strong growth phenotype [Zenklusen et al., 2001]. Also, deletion of either the N- or the C-box including the respective UBM sequence leads to the accumulation of poly(A)-RNA in the nucleus at 37°C. In recent studies, the structure of the Yra1 C-terminus (185-226) was solved in complex with Sub2 [Ren et al., 2017]. The C-terminus of Yra1 forms a helix (L15-F223) which interacts via polar interactions as well as Van-der-Waals interactions with two helices of Sub2. Mutations of L215D and D216K (part of the LDxxLD motive [Gromadzka et al., 2016]) disrupt the interaction and were found to be insufficient to stimulate the ATPase activity of Sub2 [Ren et al., 2017]. In future studies, it would be important to investigate whether phosphomimicry mutations influence the binding of the C- and N-terminal Yra1 domain shown for Sub2 and Mex67 [Sträßer and Hurt, 2001]. This can be performed using TAP purificationas or an *in vitro* study by GST-pulldown. If a change in Yra1 binding to Sub2 can be detected, it would be interesting to verify if these mutants show a change in Sub2 stimulation. Also, the influence of the mutation on recruitment to the transcription site (ChIP) and on accumulation in nuclear foci together with Nab2 (Live cell imaging) could be analyzed. In addition, cross-links between S211 in the N-terminal region to RNA

were identified, indicating a role for this amino acid in RNA binding [Philip Keil, 2021]. A RIP would give insight into the influence of the phosphorylation on RNA binding.
The reduced phosphorylation of S149 under hyperosmotic stress was not analyzed so far. Similar to the S142 it is part of the RRM domain, which was shown to be important for the interaction with Nab2 [Iglesias et al., 2010]. The reason was the main focus on heat stress and a lower log2 fold change of -0.7 in contrast to 1.8 and 3.3 for the phosphorylation of S142 and S211, respectively. Since the *S142A* mutation appears to cause the decrease of poly(A)-RNA accumulation during hyperosmotic stress, a combination with S149D would be very interesting to analyze using FISH. All this could lead to further understanding of how the Yra1 phosphorylation pattern influences the stress-induced mRNA export block.

Enhanced the mRNA export block during heat stress indicates role of Hpr1 in the nuclear export of heat shock transcripts

The other TREX protein that showed a change in its phosphorylation status upon heat stress is Hpr1. In contrast to Yra1, a decrease in the level of phosphorylation was detected upon heat shock. While the prevention of Yra1 phosphorylation leads to an decrease in nuclear poly(A)-RNA accumulation upon heat stress the phosphomimicry mutant of Hpr1 leads to further accumulation (hpr1-S673D, Figure 5.23). In other phosphoproteome screens, the phosphorylation site S673 was identified as dependent of the cell cycle controlling kinase Cdk1 while S675 was found to be mediated by the kinases Mec1/Tel1 [Holt et al., 2009, Chen et al., 2010]. No change in the phosphorylation status upon *SLT2* deletion was observed, which can be explained by the dependency on the other kinases. Even though it is postulated that Hpr1 dissociates from poly(A)-RNA under heat stress and is not crucial for the export of heat stress mRNA [Rollenhagen et al., 2007, Zander et al., 2016], deletion of Hpr1 causes the accumulation of the heat shock mRNA *SSA* at the site of transcription [Thomsen et al., 2008]. Hpr1 is known to undergo posttranscriptional modification. Hpr1 is ubiquitinylated by Rsp5 which leads to a reduction in Hpr1 protein levels at 37°C [Gwizdek et al., 2005]. Ubiquitinylated Hpr1 interacts directly with Mex67 due to the ubiquitin-associated domain of Mex67 [Gwizdek et al., 2006]. This interaction stabilizes Hpr1 and protects it from degradation. The C-terminus of Hpr1 is also sumoylated (Figure 5.23 A), which was shown to be important for the binding of Hpr1 to mRNA while the recruitment to the transcription site was unchanged [Bretes et al., 2014]. It was found that this sumoylation is necessary for the binding of acidic stress-induced

transcripts and their stabilization. The amino acids (S673, S675, S694), which are less phosphorylated upon heat stress, are within the area of Hpr1 known to be sumoylated. First, it would be important to perform smFISH for *SSA4* to identify if the increase in nuclear poly(A)-RNA accumulation upon heat stress in the *hpr1-S673D* mutant is due to additional accumulation of poly(A) heat shock mRNA [Izawa et al., 2008, Turtola et al., 2021]. Second, it would be interesting to know if the phosphorylation of Hpr1 influences or even causes the sumoylation of Hpr1 or vice versa. To this end a Hpr1-TAP purification could be performed and the copurification of SUMO-His could be analyzed. Alternatively, the generated Hpr1 mutants could be combined with a strain lacking the SUMO-protease Ulp1 and tested for growth, mRNA export block, and *SSA4* localization [Bretes et al., 2014].

Changed phosphorylation status of Dbp5 could be important for its activity or involvement for the nuclear export of heat shock mRNAs

One of the most significant changes in phosphorylation of all known export factors and NPC components upon deletion of Slt2 is Dbp5 S86. Since it was shown that Dbp5 is located in the nucleus during ethanol stress, which is thought to be the main reason for the accumulation of nuclear mRNA [Takemura et al., 2004, Rollenhagen et al., 2004], Dbp5 appears to be a very promising candidate. The phosphorylation of S86 can be observed for both heat and hyperosmotic stress. It was also detected in a phosphoproteome analysis focusing on the phosphorylation under DTT treatment and one that analysed the cross-talk between ubiquitinylation and phosphorylation [Swaney et al., 2013, MacGilvray et al., 2018]. Besides, there is a Slt2 independent site S93 during heat stress and another, S43, during hyperosmotic stress. All stated residues (S43, S86, S93) are located at the N-terminus of Dbp5 (Figure 5.24 A). The N-terminus of Dbp5 shows no similarity with other yeast DEAD-box helicases [Snay-Hodge et al., 1998]. It was postulated that the N-terminus of Dbp5 (9-79) is completely dispensable for function. However, it is known that the N-terminal domain is important for autoregulation of the human ortholog DDX19 [Collins et al., 2009]. Whether phosphorylation has an effect on the helicase activity of Dbp5, could be analyzed with an *in vitro* assay using the phosphomimicry mutants. A recent study states that the absence of Dbp5 causes the accumulation of Nab2 in nuclear foci during glucose starvation [Heinrich et al.]. If the phosphorylation influences the activity of Dbp5 live cell imaging could be performed to investigate whether the Nab2 foci still form during heat shock. The effect of the phosphorylation on the activity of Dbp5 was not assayed so far since the Oligo(dT) FISH did not show

any difference in poly(A) accumulation upon heat stress for the S86A mutation in comparison to the control (Figure 5.24 B). The mutation could be combined with a mutation of the Slt2-independent site or tested during hyperosmotic stress. Another possibility would be to test the effect of *Dbp5-S86A* on the export of heat shock mRNAs using smFISH.
It is unlikely that phosphorylation changes the known protein interactions of Dbp5 mediated by the RecA-like domains [Adams and Wente, 2020] since they are located in another domain. Testing the interaction with Nup159 would be interesting because it was shown that Dbp5 mislocalizes upon deletion of the NUP Rip1 during heat stress [Stutz et al., 1997, Rollenhagen et al., 2004]. Also, different sites in the FG-repeat region of Nup159 show a change phosphorylation pattern in *slt2* at 42°C. Both could influence the interaction of Nup159 and Dbp5 which allows the mislocalization upon *RIP1* deletion.

Gfd1 could be associated with Nab2 foci upon heat stress

Another protein that is less phosphorylated upon heat and hyperosmotic stress is Gfd1, an interactor of Dbp5 and Nab2. The phosphoproteome showed a further decrease in phosphorylation of Gfd1 in the *SLT2* deletion mutant (Figure 5.25 A). Preventing the reduction in Gfd1 phosphorylation Gfd1 leads to a minor decrease in the N/C ratio in comparison to the control after heat shock (Figure 5.25 B). Gfd1 is a promising candidate because it interacts with Dbp5 [Christine A. Hodge et al., 1999] and Nab2 [Suntharalingam et al., 2004, Zheng et al., 2010], which both possess Slt2-dependent phosphorylation sites [Carmody et al., 2010]. In a Nab2 purification comparing the copurification of proteins at 30°C and 42°C, it was found that under heat stress Gfd1 interacts 2.8x stronger with Nab2 [Carmody et al., 2010]. Also Mlp1 (6.8x), Mlp2 (4.5x), Yra1 (2.3x), Pab1 (2x), Stm1 (2x) and Tho2 (1.4x) show an increased copurification while the interaction with Mex67 and other NUPs is decreased. Since Mlp1 and Yra1 have been shown to accumulate together with Nab2 in the nucleus, it is likely that the enriched proteins are also present in these foci. It would be very interesting to confirm this for Gfd1, the stress granule marker Pab1, and the TREX component Tho2.
Taken together, accumulation of poly(A)-RNA in the nucleus was observed in different, but not all stresses tested, implicating a specialized rather than a general mechanism. No direct correlation to phosphorylation of Slt2 and Nab2 could be identified. However, phosphoproteome analysis comparing WT and *SLT2* deletion led to the identification of differentially phosphorylated residues of many proteins linked to mRNA export. Therefore, the CWI pathway appears to be a major

regulator of nuclear export under heat stress. Of the many identified sites with changed levels of phosphorylation only Yra1, Nab2, Gfd1 and Dbp5 were further analyzed in this study. Yra1 phosphorylation influences the nuclear accumulation of mRNA whereas phosphorylation of Dbp5 (at S86) does not. A phosphomimicry mutant of Hpr1 causes an increased amount of nuclear poly(A)-RNA upon heat stress. Further studies are needed to elucidate the exact mechanisms how these phosphorylation events influence the accumulation of mRNA and the export of heat shock mRNAs.

7. Material and Methods

Material

Chemicals and materials

All chemicals, enzymes and equipment are listed in the following Tables 7.1, 7.3 and 7.2, respectively.

Table 7.1: Chemicals used for all experiments

Chemicals and ingredients	Supplier
1 kb Plus DNA Ladder	NEB
2-Propanol	Carl Roth
5-Fluoroorotic acid (5-FOA)	Apollo Scientific Ltd
Acetic acid	VWR Chemicals
Acrylamide (29:1) 40 %	AppliChem
Agar Bacteriology grade	AppliChem
Agarose	Applichem
Ammonium persulfate (APS)	VWR Chemicals
Ampicillin	Applichem
ANTI-FLAG M2 Affinity Gel	Sigma-Aldrich
BactoTM Peptone	BD Biosciences
BactoTM Yeast extract	BD Biosciences
Bicine	Fluka
Bovine serum albumin (BSA)	Carl Roth
Bromophenol blue	Applichem
Calcium chloride ($CaCl_2$)	Fluka
Calmodulin Affinity resin	Agilent Technologies
CheLuminate ECL Solution	Applicem
Chloroform	Merck
Colored prestained ladder	NEB
Coomassie Brilliant Blue G-250	Applichem
Coomassie Brilliant Blue R-250	Applichem
D-Glucose Monohydrate	Sigma-Aldrich
Dextran sulfate	Sigma-Aldrich
Dimethyl sulfoxide (DMSO)	Grüssing

Disodium hydrogenphosphate (Na_2HPO_4)	Sigma-Aldrich
Dithiothreitol (DTT)	Sigma-Aldrich
dNTPs (dATP, dTTP, dCTP, dGTP)	Thermo Fisher Scientific
Dodecyl-β-D-maltosid (DDM)	Sigma-Aldrich
Dynabeads^{TM} M-280 Tosylactivated	Invitrogen
Dynabeads^{TM} M-280 Streptavidin	Invitrogen
ECL Solution	Applichem
E.coli t-RNA	Roche diagnostics
Ethanol	Fisher Chemical
Ethylenediaminetetraacetic acid (EDTA)	Sigma-Aldrich
Ethyleneglycol-bis(aminoethylether)tetraacetic acid EGTA)	Merck
Ficoll 400	Carl Roth
FLAG Peptide	Sigma-Aldrich
Formaldehyde	ORG Laborchemie
Formamide	Merck
Gel loading dye, purple (6x)	NEB
Gel loading dye, purple (6x) w/o SDS	NEB
Genetecin (G418)	ThermoFisher (Gibco)
Glycerol	Carl Roth
Glycine	Labochem international
Herring Sperm DNA	Invitrogen
HDGreen^{TM} DNA stain	Intas
HEPES	Carl Roth
Hydrochloric acid (HCl)	Carl Roth
IGEPAL CA-630	Sigma-Aldrich
IgG Sepharose 6 Fast Flow	GE Healthcare
Indol-3-acetid acid (IAA)	Sigma-aldrich
L-Arginine-HCl	Biomol GmbH
L-Aspartic acid	Sigma-Aldrich
Leupeptin (Hemisulfate)	Carl Roth
L-Histidine	Sigma-Aldrich
L-Isoleucine	Sigma-Aldrich
Lithium acetate ($C_2H_3LiO_2$)	Carl Roth
Lithium chloride (LiCl)	Merck
L-Leucine	Sigma-Aldrich
L-Lysine Monohydrochloride	Sigma-Aldrich
L-Methionine	Sigma-Aldrich

L-Phenylalanine	Sigma-Aldrich
L-Threonine	Sigma-Aldrich
L-Tryptophan	Sigma-Aldrich
L-Tyrosine	Sigma-Aldrich
L-Valine	Biomol GmbH
Magnesium chloride ($MgCl_2$)	Merck
Methanol	Merck-Millipore
Octylphenoxypolyethoxyethanol (IGEPAL CA-630; NP-40)	Sigma-Aldrich
Pepstatin A	Applichem GmbH
Phenylmethane sulfonyl fluoride (PMSF)	Carl Roth
Phosphoric acid	Carl Roth
PhosStop	Roch
Polyethylene glycol (PEG) 3800/4000	Carl Roth
Polyethylene glycol (PEG) 8000	Fluka
Polysorbate 20 (Tween 20)	Merck
Polyvinylpyrrolidone (PVP)	Sigma-Aldrich
Ponceau S	Serva
Potassium acetat (CH_3CO_2K)	Applichem
Potassium chloride (KCl)	ORG Laborchemie
Potassium hydroxide (KOH)	Merck
Powdered milk, fat free, blotting grade	Carl Roth
PowerUp™ SYBR™ Green Master Mix	
Random Hexames	Jena Bioscience
Ribolock	Thermo Fisher Scientific
Rothi-Mount FluorCare DAPI	Carl Roth
Salmon sperm DNA (SSD)	Applichem
Sodium acetate ($C_2H_3NaO_2$)	Merck
Sodium carbonate (Na_2CO_3)	Merck
Sodium chloride (NaCl)	Merck
Sodium citrate	Carl Roth
Sodium deoxycholate	Sigma-Aldrich
Sodium dihydrogenphosphate (NaH_2PO_4)	Sigma-Aldrich
Sodium dodecyl sulfate (SDS)	Serva
Sodium hydroxide (NaOH)	Merck
Sulfosalicylic acid	Merck
SuperSignal West Dura	Thermo Fisher Scientific
Tetramethylethylendiamin (TEMED)	Carl Roth
Tris (2-Carboxyethyl)-Phosphin (TCEP)	Sigma-Aldrich

Trichloroacetic acid (TCA)	Merck
Tris(hydroxymethyl)aminomethane (Tris)	Applichem
Triton X-100	Applichem
Trizol reagent	Thermo Fisher Scientific
Tryptone BioChemica	Applichem
Uracil	Sigma-Aldrich
Urea	Applichem
Yeast nitrogen base, w/o amino acids	Formedium
Yeast nitrogen base, w/o amino acids, w/o ammonium sulphate	Formedium

Table 7.2: Equipment used for all experiments

Equipment	Supplier
Agarose gel electrophoresis system	Southern biological
AM100, micro scale	Mettler-Toledo
Apollo, liquid nitrogen container	Cryotherm
Avanti JXN-26 with JLA-8.1, JA-10	Beckman Coulter
Bio Dot Aparatus	Bio-Rad Laboratories
Bioruptor UCL 200	Diagenode
ChemoCam Imager ECL HR 16-3200	Intas
CME microscope	Leica
CO8000 Cell Density Meter	WPA
Delta Vision Ultra fluorescence microscope	Cytiva
Electrophoresis Power Supply Consort E835	Neolab
Electrophoresis Power Supply EPS 3500	Pharmacia Biotech
Eppendorf centrifuge 5424	Eppendorf
Eppendorf centrifuge 5430R	Eppendorf
Eppendorf centrifuge 5415D	Eppendorf
FastPrep-24^{TM} 5G	MP Biomedicals
Freezer/Mill 6870D	Spex SamplePrep
Frezzer Forma 900 Series	Thermo Scientific
Gel iX20 Transilluminator/gel docu	Intas
Hera safe, laminar flow cabinet	Thermo Fisher Scientific
HeraFreeze HFU T Series	Thermo Fisher Scientific

Heidolph shaker duomax 1030	Neolab
IKA KS 4000 ic control, shaking incubator	IKA Labortechnik
IKAMAG RCT, magnetic stirrer	IKA Labortechnik
Incubators	Memmert
Innova 44 shaking incubator	New Brunswick
LED bluelight transilluminator	Nippon genetics
Megafuge 40R, 75003180R	Thermo Fisher Scientific
Milli-Q integral water purification system	Merck
Mini-Protean Tetra Electrophoresis Cell	Bio-Rad Laboratories
Multitron Pro / Labotron shaker	Infors HT
Nano Drop ND - 1000 Spectrometer	Thermo Fisher Scientific
Optima XPN-80 Ultracentrifuge with 70 Ti	Beckman Coulter
PeqStar XS Thermocycler	Peqlab
Personal Thermocycler	Biometra
Pipetboy acu	IBS Integra Biosciences
Pipettes	Gilson
PM2000, scale	Mettler-Toledo
pH 211 Microprocessor pH meter	HANNA instruments
Pulverisette	Fritsch
Rotator	neoLab
StepOnePlus Real Time PCR System	Applied Biosystems
SW22, shaking waterbath	Julabo
T3 Thermocycler	Biometra
Thermomixer compact	Eppendorf
Thermomixer 5436	Eppendorf
Trans-Blot Turbo Transfer System	Bio-Rad Laboratories
Vakulan CVC 3000	Vacuubrand
VF2, vortex mixer	IKA Labortechnik
VX-150, autoclave	Systec
WT 12, tumbling shaker	Biometra

Table 7.3: Enzymes used for all experiments

enzyme	Supplier
DNaseI	Thermo Fisher Scientific
M-MuLV Reverse Transcriptase	NEB
Phusion High-Fidelity DNA Polymerase	NEB
Proteinase K	NEB
Q5 High-Fidelity DNA Polymerase	NEB
Restriction enzymes	NEB
RNaseA	Thermo Fisher Scientific
RNaseH	NEB
RNaseI	Thermo Fisher Scientific
RNase T1	Thermo Fisher Scientific
T5 exonuclease	NEB
Taq DNA Ligase	NEB
Tobacco etch virus (TEV) protease	Straesser lab self-made
Taq DNA Polymerase	Straesser lab self-made
Zymolyase 100T	Carl Roth
Zymolyase 20T	Carl Roth

Buffer and media

The buffer composition and media recipes are listed in the following Tables 7.4 and 7.5.

Table 7.4: List of the buffers used for all experiments.

buffer	composition
1 x TAE	40 mM TRIS, 2 mM EDTA, pH 8.0; 20 mM acetic acid
1 x PBS	137 mM NaCl, 2.7 mM KCl, 20 mM NaH_2PO_4, 10 mM Na_2HPO_4
1 x TBE	100 mM TRIS; 100 mM H_3BO_3; 2,5 mM EDTA
1 x TBST	137 mM NaCl, 2.7 mM KCl, 12.5 mM TRIS-HCl, 0.1 % (v/v) Tween-20
1 x TE	1 mM EDTA, 10 mM TRIS-HCl, pH 8.0
1x RAP Hybridization buffer	10 mM HEPES-KOH pH 7.5, 5 mM EDTA, 500 mM LiCl, 0.5 % DDM, 0.2 % SDS, 0.1 % sodium deoxycholate, 4 M urea, 2.5 mM TCEP

4 x separating SDS gel buffer	3 M TRIS, 0.4% (w/v) SDS, pH 8.8 (HCl)
4 x stacking SDS-gel buffe	0.5 M TRIS, 0.4% (w/v) SDS, pH 6.8 (HCl)
20x SSC	3 M NaCl, 0.3 M sodium citrate
4 x SDS loading dye	0.2 M TRIS-HCl (pH 6.8), 40% (v/v) glycerol, 8% (w/v), SDS, some mg of bromophenol blue, 0.1 M DTT
30:1 mix	30 ml 100 % ethanol, 1 ml NaOAc pH 5.2
AE buffer	10 mM TRIS-HCl pH 7.4, 50 mM NaOAc, 10 mM EDTA
Binding and Wash buffer	10 mM TRIS-HCl pH 7.5, 150 mM NaCl, 0.5 mM EDTA pH 8.0
Coomassie stain solution	0.25% (w/v) Coomassie Brilliant Blue R-250, 30% (v/v)
Fixation buffer	1.2 M sorbitol, 0.1 M potassium phosphate dibasic pH 7.5
Gibson Master Mix	1x ISO buffer, 4 U/µl T5 exonuclease, 4 U/µl Taq DNA ligase, 25 U/ml Phusion DNA polymerase
ISO buffer	500 mM TRIS pH 7.5, 50 mM $MgCl_2$, 1 mM dATP, 1 mM dGTP, 1 mM dTTP, 1 mM dCTP, 50 mM DTT, 25 % PEG-8000, 5 mM NAD
Maltose elution buffer	100 mM NaCl, 50 mM HEPES-KOH pH 7.5, 15 mM Maltose
NLS elution buffer	20 mM HEPES-KOH pH 7.5, 2 % NLS, 10 mM EDTA, 2.5 mM TCEP
prehybridization buffer	50 % formamide, 10 % dextran sulphate, 125 $\frac{\mu g}{ml}$ *E. coli* tRNA, 500 $\frac{\mu g}{ml}$ hering sperm DNA, 4 x SSC, 0.02 % polyvinyl pyrrolidone, 0.02 % BSA, 0.02 % ficol-400
pre-treatment solution	7.5 % β-mercaptoethanol, 1.85 M NaOH
Protease inhibitor (100x)	8 ng/ml Leupeptin, 137 ng/ml Pepstatin A, 17 ng/ml PMSF, 0.33 mg/ml Benzamidine, solved in 100% EtOH (p.a.)
RNA IP buffer	25 mM TRISpH 7.5, 150 mM NaCl, 2 mM $MgCl_2$, 0.2 % rition-X-100, 500 µM
RNase Mix	2 µg/µl RNase A, 200 U/µl RNase T1, 1 U/µl RNase III, 10 U/µl RNaseH, 10 U/µl RNaseI
SDS-PAGE running buffer	25 mM TRIS, 0.1% (w/v) SDS, 0.19 mM glycine

Semi-Dry-Blotting-buffer	25 mM TRIS, 192 mM glycine, 20% (w/v) methanol
smFISH Hybridization buffer	1 g dextran sulfate, 10 mg *E. coli* tRNA, 1 ml 20x SSC, 20 µl 10 % RNase free BSA, 100 µl 200 mM Vanadyl-Ribonucleoside Complex, 10 % ultrapurde deionized formamide, add autoclaved MilliQ water to 10 ml
Solution 1	1x TE, 100 mM LiAc pH 7.5
Solution 2	1x TE, 100 mM LiAc pH 7.5, 50 % $\frac{w}{v}$ PEG4000
TAP buffer	100 mM NaCl, 50 mM HEPES-KOH pH 7.5, 1.5 mM $MgCl_2$, 0.15 % NP-40
TNN buffer	100 mM TRIS-HCl pH 8.0, 100 mM NaCl, 1 % NP40
wash buffer (FISH)	1.2 M sorbitol, 0.1 M potassium phosphate dibasic pH 6.4
wash buffer A	2 ml 20x SSC, 2 ml formamide, 16 ml DEPC water
wash buffer B	1x PBS
Wet blot transfer buffer	3.28 $\frac{g}{l}$ TRIS base, 14.4 $\frac{g}{l}$ glycine, 10 % $\frac{v}{v}$ methanol

Table 7.5: Recipes for Media and Agar plates used for the cultivation of all organisms.

Media	composition
LB medium	1% (w/v) tryptone; 0.5% (w/v) yeast extract;0.5 % (w/v) NaCl; (2 % (w/v) agar for plates)
Synthetic dropout complete (SDC)	0.67% (w/v) yeast nitrogen base; 0.06% (w/v) complete, synthetic mix of aa; drop out as required; 2% (w/v) glucose; (2% (w/v) agar for plates)
SDC-FAA	0.67% (w/v) yeast nitrogen base; 0.06% (w/v) complete, synthetic mix of aa; drop out as required; 2% (w/v) glucose; 2% (w/v) agar for plates, g 5-FAA
SDC-FOA	0.67% (w/v) yeast nitrogen base; 0.06% (w/v) complete, synthetic mix of aa; drop out as required; 2% (w/v) glucose; 2% (w/v) agar for plates, 1 g 5-FOA
SOC	2 g tryptone, 0.5 g yeast extract, 10 mM NaCl, 0.5 mM KCl, 10 mM $MgCl_2$, 10 mM $MgSO_4$ dissolve in up to 100 ml water and adjust pH to 7.0
Yeast full medium (YPD)	2% (w/v) peptone; 2% (w/v) glucose; 1% (w/v) yeast extract; (2% (w/v) agar for plates)

Antibodies

Primers and secondary antibodies used for immunoblotting are shown in Table 7.6 and 7.7.

Table 7.6: Primary antibodies used for Western blot.

Name	Source	Dilution	Supplier
anti-Cbp80	rabbit, polyclonal	1:20000	Görlich lab, Göttingen, Germany
anti-HA	rabbit, monoclonal	1:1000	R&D Systems, Minneapolis, USA
anti-Nab2	mouse	1:5000	Swanson lab (3F2)
anti-Npl3	rabbit, polyclonal	1:5000	Guthrie lab, California, San Francisco
Peroxidase-anti-peroxidase (PAP)	rabbit, polyclonal	1:5000	Sigma, Taufkirchen, Germany
anti-Pgk1	mouse, monocloncl	1:5000	Abcam
anti-Slt2 phos. (p42/p44 antibody)	rabbit	1:1000	Cell Signaling Technology, Denvers, USA
anti-Sub2	rabbit, polyclonal	1:10000	[Sträßer et al., 2002]
anti-Tho1	rabbit	1:5000	Pineda lab
anti-Yra1	rabbit, polyclonal	1:2000	Straesser lab, Gießen, Germany
anti-Rps8	rabbit, polyclonal	1:5000	G. Dieci lab, Parma, Italy

Table 7.7: List of the used secondary antibodies.

Name	Source	Dilution	Supplier
anti-rabbit-HRPO	goat, monoclonal	1:3000	Bio-Rad, Hercules, Kalifornia
anti-mouse-HRPO	goat, monoclonal	1:3000	Bio-Rad, Hercules, Kalifornia

Oligonucleotid sequences

Oligonucleotides used for PCRs and qPCRs were obtained from Biolegio (Nijmegen, Netherlands) (Table 7.8 and 7.10). Modified DNA and RNA oligonucleotides were obtained from biomers.net (Ulm, Germany)(Table 7.9).

Table 7.8: Primer sequences used for plasmid cloning and creating cassettes for transformations in yeast.

Primer	Sequence 5' - 3'
ssa4 fwd new	GCTCTAGAACTAGTGGATCCACTATTGTCACTTCTC CATTGA
pRS316 ssa4 rev	TCAATGGAGAAGTGACAATAGTGGATCCACTAGTTC TAGAGC
pRS316 ssa4 fwd	TCTGTGGTTTCAGATATAATATCACTCGAGGGGGGG CCCGGTA
ssa4 rev new	TACCGGGCCCCCCCTCGAGTGATATTATATCTGAAA CCACAGA
ssa4 L1 plasmid fwd	CAGAGACCCTCACACGGAAGCAGCATCGAATTTCTT AGTTT
ssa4 L1 plasmid rev	GATTGCCAGGGGGCTCTGACTTCATCGCATCTTTGT ATTTAT
ssa4 L1 MS2 fwd	ATAAATACAAAGATGCGATGAAGTCAGAGCCCCCTG GCAATC
ssa4 L1 MS2 rev	AAACTAAGAAATTCGATGCTGCTTCCGTGTGAGGGT CTCTG
ssa4 L2 plasmid fwd	CAGAGACCCTCACACGGAATAAGTATATATATAAGA TACACAATCA
ssa4 L2 MS2 rev	TGATTGTGTATCTTATATATATACTTATTCCGTGTG AGGGTCTCTG
ssa4 L2 MS2 fwd	TAGTTTTCCCTCTTAACAACTTTTTCAGAGCCCCCT GGCAATC
ssa4 L2 plasmid rev	GATTGCCAGGGGGCTCTGAAAAAGTTGTTAAGAGGG AAAACTA
ssa4 L3 MS2 fwd	ATAAGATACACAATCAGTAATTAGCCAGAGCCCCCT GGCAATC
ssa4 L3 plasmid rev	GATTGCCAGGGGGCTCTGGCTAATTACTGATTGTGTA TCTTAT
ssa4 L3 plasmid fwd	CAGAGACCCTCACACGGAAAATGACTACTATTTGTAC GTTCTC
ssa4 L3 MS2 rev	GAGAACGTACAAATAGTAGTCATTTTCCGTGTGAGG GTCTCTG
ccw124 l1 plasmid fwd	CAGAGACCCTCACACGGAttatttatacattctaaatttttttataaactt
ccw124 l1 MS2 rev	aagtttataaaaaatttagaatgtataaataaTCCGTGTGAGGGTCTCTG

ccw124 l1 plasmid rev	GATTGCCAGGGGGCTCTGtaataaactaagtttacaacaacaaag
ccw124 l1 MS2 fwd	ctttgttgttgtaaacttagtttattaCAGAGCCCCCTGGCAATC
ccw124 l3 MS2 fwd	ttagtttattattatttatacattctaaatttCAGAGCCCCCTGGCAATC
ccw124 l3 plasmid rev	GATTGCCAGGGGGCTCTGaaatttagaatgtataaataataataaactaa
ccw124 l3 plasmid fwd	CAGAGACCCTCACACGGAtttataaacttttttggcatttaacaaat
ccw124 l3 MS2 rev	atttgttaaatgccaaaaaagtttataaaTCCGTGTGAGGGTCTCTG
ccw124 l2 MS2 fwd	ttgtaaacttagtttattattatttatacaCAGAGCCCCCTGGCAATC
ccw124 l2 plasmid rev	GATTGCCAGGGGGCTCTGtgtataaataataataaactaagtttacaa
ccw124 l2 plasmid fwd	CAGAGACCCTCACACGGAttctaaatttttttataaacttttttggc
ccw124 l2 MS2 rev	gccaaaaaagtttataaaaaatttagaaTCCGTGTGAGGGTCTCTG
fwd1 ssa4 Mango	GAAGGGACGGGCGGAGAGGAGAtgctacttGCATCGAA TTTCTTAGTTTTCCC
rev1 ssa4 Mango	TCTCCTCTCCGCCCGTCCCTTCTGCTACTTCATCGCAT CTTTG
fwd2 ssa4 Mango	GAAGGGACGGGCGGAGAGGAGAATAAAAAAGTATATAT ATAAGATACACAATCA
rev2 ssa4 Mango	TCTCCTCTCCGCCCGTCCCTTCATAAAAAGTTGTTAAG AGGGAAAAC
fwd3 ssa4 Mango	GAAGGGACGGGCGGAGAGGAGATTTGCTGACTACTATT TGTACGTTCTCA
rev3 ssa4 Mango	TCTCCTCTCCGCCCGTCCCTTCTTTGCTAATTACTGAT TGTGTATCT
Mango fwd	GAAGGGACGGGCGGAG
Δccw22 HIS3 fwd	GGATAACAAACATCTTCTTTCGTTCGCTTCAAAATAA CTACAAATTAAAAATGACAGAGCAGAAAGCCC
Δccw22 HIS3 rev	AAGTACTTAACCATTTTTCTAAAAATATATTAAAGAA AAGGTTGAGTAAACTACATAAGAACACCTTTG-GTG
Δccw22 colony fwd	GAGCTGCAGGACACGCT
HIS3 colony rev	CTCTATCGCTAGGGGACC
plasmid rev MBP	cagtttaccttcttcgattttcatggatccactagttctagagc
MPB fwd	gctctagaactagtggatccatgaaaatcgaagaaggtaaactg
MCP fwd MBP	cgggatcgagggaaggattATGGCTTCTAACTTTACTCAGTT
MBP rev MCP	AACTGAGTAAAGTTAGAAGCCATaatccttccctcgatcccg

plasmid fwd MCP	AAAAAAAAAAAGAAAAGTTACCGGTTAAgaattcgatatca agcttatcga
MCP rev	tcgataagcttgatatcgaattcTTAACCGGTAACTTTTCTTTTTT TTTTT
Δrip1 HIS3 fwd	AGCTCATCAAGCTATCATTAAATTTCGACCCGAGCAACG ACTCAACTGTAATGACAGAGCAGAAAGCCC
Δrip1 his rev	TTCATATATATTGTTTAAGTTACCATTTTGTATGTTTTT CTTTGACCTTACTACATAAGAACACCTTTGGTG
Δrip colony fwd	GTACTGAGCATTAATCTGGCT
Cyc1 fwd	gctctagaactagtggatccGAGCGTTGGTTGGTGGAT
plasmid pCyc1 rev	ATCCACCAACCAACGCTCggatccactagttctagagc
MBP pCyc1 fwd	CACACACTAAATTAATAGGATCCatgaaaatcgaagaaggtaaactg
Cyc1 rev	cagtttaccttcttcgattttcatGGATCCTATTAATTTAGTGTGTG
HA fwd	AAAAAAAAAAAGAAAAGTTACCGGTtacccatacgatgttcctga
MCP HA rev	tcaggaacatcgtatgggtaACCGGTAACTTTTCTTTTTTTTTTT
plasmid HA fwd	ccagattacgcttctagcTAAgaattcgatatcaagcttatcga
HA rev	tcgataagcttgatatcgaattcTTAgctagaagcgtaatctgg
Nop1 fwd	gctctagaactagtggatccTCCTGTACTTGCTGATATTGTG
plasmid pNop rev	CACAATATCAGCAAGTACAGGAggatccactagttctagagc
MBP Nop1 fwd	AATTAACTCAAATCAACTAAAACAGTAatgaaaatcgaagaagg taaactg
Nop1 MBP rev	cagtttaccttcttcgattttcatTACTGTTTTAGTTGATTTGAGTTA ATT
cbp80 fwd	GCTCTAGAACTAGTGGATCCGATTCTTCGAGTGTGTCT TTTTC
plasmid cbp80 rev	GAAAAAGACACACTCGAAGAATCGGATCCACTAGTTCT AGAGC
plasmid cbp80 fwd	CAAATGTGTAGGCGGTTCGCTCGAGGGGGGGCCCGGTA
cbp80 rev	TACCGGGCCCCCCCTCGAGCGAACCGCCTACACATTTG
cbp80 verif rev	GTCGTTTTGATTAGCAATATACC
cbp20 fwd	GCTCTAGAACTAGTGGATCCCACAAATGATGAGAAATAG TCATC
plasmid cbp20 rev	GATGACTATTTCTCATCATTTGTGGGATCCACTAGTTCT AGAGC
plasmid cbp20 fwd	GGAATTGAGTTTACCAGGGTATACTCGAGGGGGGGC CCGGTA
cbp20 rev	TACCGGGCCCCCCCTCGAGTATACCCTGGTAAACTCAA TTCC
cbp20 verif rev	GATATTAGTCCTTTCGGGACT

cbp80 verif fwd	GAATACGGCTGTATGAAACCA
cbp20 verif fwd	CTAACTAGTATTTACGTTACTAGTA
Δcbp80 fwd	TGGTATACGCGTTTGGGGCTACAATTGCATTTTAAA TATATTTAAGCCTGATTCAAGAAATATCTTGA
Δcbp80 rev	TAAAAAGCGGAGTGATAACGAATGTAGTCCATCCTC CGAATCTTTCGTGTCGTTTCTATTATG
Δcbp20 fwd	GATGACACAAATGATGAGAAATAGTC
Δcbp20 rev	CGCAAAATATTTAGTGATTACTATACCC
12xMS2 ilv5 fwd	CAAGTGCTGGAAACTTTTTCTCcagagccccctggcaatc
ilv5 12xMS2 rev	gattgccaggggctctgGAGAAAAAGTTTCCAGCACTTG
ilv5 12xMS2 fwd	cagagaccctcacacggaTTGGAATTTTTGCAACATCAAGTC
12xMS2 ilv5 rev	GACTTGATGTTGCAAAAATTCCAAtccgtgtgagggtctctg
cbp80 seq	GAGCAACCACAGAAGCAAG
cbp80 seq2	GCCCAATTAATTGCCACTTATG
Δslt2 his fwd	CTATCAAAATAGTAGAAATAATTGAAGGGCGTG TATAACAATTCTGGGAGATGACAGAGCA-GAAAGCCC
Δslt2 his rev	TTACATCTATGGTGATTCTATACTTCCCCGGTT ACTTATAGTTTTTTGTCCTACATAAGAACAC-CTTTGGTG
Δslt2 colony PCR	ATAAATGCATATACTCTAGTTGAAG
Δcbp20 his fwd	ATATCGAATAAAAGTTGCATCCATTAATATACC AATAAATAAAGGGAAAGATGACAGAGCA-GAAAGCCC
Δcbp20 his rev	TATATATATATCTGTGTGTAGAATCTTTCTCAG ATATAAATTGATTGATTCTACATAAGAACAC-CTTTGGTG
Δcbp20 colony PCR	TGGAAGCTGAAACGCAAGG
ssa4-S2	AAACTAAGAAATTCGATGCTGCTACTTCATCGCATC TTTGTATTTATCTAATCGATGAATTCGAGCTCG
ssa4-S3	CAGGCCCCACTGGAGCACCAGACAACGGCCCAACGG TTGAAGAGGTTGATCGTACGCTGCAGGTCGAC
ssa4 M1 Cvar fwd	ATCCGTACACCATCAGGGTACGAGCTAGCCCATGG CGTACACCATCAGGGTACGACTAGTAGATCTCG-TACACCATCAGGGTACGGAGCAGCATC-GAATTTCTTAGTTT
ssa4 plasmid L1	GGCTAGCTCGTACCCTGATGGTGTACGGATACTTCATC
3xMS2 rev2	GCATCTTTGTATTTAT

ssa4 M1 Cvar rev	CCGTACCCTGATGGTGTACGAGATCTACTAGTCGTACC CTGATGGTGTACGCCATGGGCTAGCTCG-TACCCTGATGGTGTACGGATACTTCATCG-CATCTTTGTATTTAT
ssa4 plasmid L1	TAGTAGATCTCGTACACCATCAGGGTACGGAGCAGCAT
3xMS2 fwd2	CGAATTTCTTAGTTT
MS2 Cvar fwd	TCAGGGTACGAGCTAGCC
Δslt2 colony rev	AGTTTGTCCAGTTGGCAATTG
Dbp5 fwd	GCTCTAGAACTAGTGGATCCATGCCAAACACAGGTTT ATCAAA
Dbp5 plasmid rev	TTTGATAAACCTGTGTTTGGCATGGATCCACTAGTTC TAGAGC
Dbp5 rev	TACCGGGCCCCCCCTCGAGACTAAACGGTGCCTTC TTCG
dbp5 plasmid fwd	CGAAGAAGGCACCGTTTAGTCTCGAGGGGGGGCC CGGTA
Dbp5 colonyPCR fwd	CTTCTCAGTTTGTTGATCCAC
Dbp5 S86A fwd	ACCCAAATGCTCCATTGTACA
Dbp55 S86A rev	TGTACAATGGAGCATTTGGGT
Ddbp5 HIS3 fwd	CGATCAGCAACCAAGAACATCTATAAAAATACTTACC ACCTTAGATCGGAatgacagagcagaaagccc
Ddbp5 HIS3 rev	TGAAATTAGATTAAAGCTTTTACGTATTTTGAGGTAT TATGTACTGAATTctacataagaacacctttggtg
Ddbp5 colony fwd	AGAGGGCTGCCATCTGG
Dbp5 Seq	CTGTCTCTTTCTTGTGTCTGT
Yra S8A fwd	ACTTAGATAAAGCTTTAGACGAAAT
Yra S8A rev	ATTTCGTCTAAAGCTTTATCTAAGT
Yra1 S142A fwd	TTTAACGGCGCTCCAATCG
Yra1 S142A rev	CGATTGGAGCGCCGTTAAA
Yra1 S211A fwd	GCTAAGAAAGCTCTTGAAGATC
Yra1 S211A rev	GATCTTCAAGAGCTTTCTTAGC
Yra1 S8D fwd	CTTAGATAAAGATTTAGACGAAATC
Yra1 S8D rev	GATTTCGTCTAAATCTTTATCTAAG
Yra1 S142D fwd	ATTTAACGGCGATCCAATCGA
Yra1 S142D rev	TCGATTGGATCGCCGTTAAAT
Yra1 S211D fwd	GCTAAGAAAGATCTTGAAGATCT
Yra1 S211D rev	AGATCTTCAAGATCTTTCTTAGC
HA fwd yra1	GGCGGACTATTTCGAAAAGAAAtacccatacgatgttcctga

Yra1 rev HA	tcaggaacatcgtatgggtaTTTCTTTTCGAAATAGTCCGCC
plasmid fwd HA yra1	ccagattacgcttctagcTAATTAATTGTCAATTTTTTGTTTG ATTTAATTT
HA rev Yra1	AAATTAAATCAAACAAAAAATTGACAATTAATTAgct agaagcgtaatctgg
HA colony PCR	agcgtaatctggaacgtcatat
Hpr1 S673D S675D fwd	TAA ACG ATG CTG ATC AAA CAG AA
Hpr1 S673D S675D rev	TTCTGTTTGATCAGCATCGTTTA
Hpr1 S694A fwd	GGGAGAAATAGCAGAAGAGAA
Hpr1 S694A rev	TTCTCTTCTGCTATTTCTCCC
Hpr1 S673D fwd	CGTATAAACGATGCTTCTCAA
Hpr1 S673D rev	TTGAGAAGCATCGTTTATACG
HA fwd hpr1	GTTCATCTACCCAAGATATGAAAtacccatacgatgttcctga
Hpr1 rev HA	tcaggaacatcgtatgggtaTTTCATATCTTGGGTAGATGAAC
HA rev Hpr1	AGTTTAAAATTTCTATTAAGAGGATAATTTAgctagaag cgtaatctgg
plasmid fwd Hpr1 HA	ccagattacgcttctagcTAAATTATCCTCTTAATAGAAATTT TAAACT
Hpr1 Seq3	GGCTTTATTGTCGTAATAGTCAT
Hpr1 Seq2	CAGCTTTACAAGAATCTGATAAC
Hpr1 Seq1	GTTTACGTTCATCAAGATGGG
GFD1 S110D fwd	CCACCAGTTGATCCTAGCA
GFD1 S110D rev	TGCTAGGATCAACTGGTGG
GDF S106D fwd	CAGAGATAGATCCTCCACC
GFD S106D rev	GGTGGAGGATCTATCTCTG
GFD1 fwd	GCTCTAGAACTAGTGGATCCAATATATGTCAATATA TCGATGTGTC
GFD1 plasmid rev	GACACATCGATATATTGACATATATTGGATCCACTA GTTCTAGAGC
GFD1 plasmid fwd	CTGACCTTGGATGTCTCCACTCGAGGGGGGGCCCG GTA
GFD1 rev	TACCGGGCCCCCCCTCGAGTGGAGACATCCAAGGT CAG
Dgfd1 kanMX fwd	AAGCTATTTTTGATAGGAGAATACCTTCAATATCAT TTTTACTATTTATCgacatggaggcccagaata
Dgfd1 kanMX rev	ATGTCTCTTCAAGCAAAACGTGCTTAAAAGTGTCCA TGTGATGGGAGGGAcagtatagcgaccagcattc

Dgfd1 colony fwd	AAATGCCTCATGACGGTATCT
gfd1 colony fwd	CAACGTTTGAAGACCTCTTTG
GFD1 S87A fwd	GCAAAATAGCTCCTGTAAGTG
GFD1 S87A rev	CACTTACAGGAGCTATTTTGC
HA fwd gfd1	cgtttgaagacctctttgaaaataTACCCATACGATGTTCCTGA
gfd1 rev HA	TCAGGAACATCGTATGGGTAtattttcaaagaggtcttcaaacg
Gfd1 fwd HA	CCAGATTACGCTTCTAGCtaatccctcccatcacatgga
HA rev gfd1	tccatgtgatgggagggattaGCTAGAAGCGTAATCTGG
Dnab2 TEFpro	TAGTGGTTTCTAATTATCTCTGATCATAAGGAAGTGG AAGTACATCAGAAgacatggaggcccagaata
Dnab2 CycTerm	ATCAAAAGGGTCACAGGAACATGAATTTCGTTCCGTG ATTTTAATAGTAActtcgagcgtcccaaaacc
Nab2 T254 fwd	GAACTTCGCTCCAACCAAGAAAGAG
Nab2 T254 rev	CTCTTTCTTGGTTGGAGCGAAGTTC
Dnab2 colony fwd	GGCTGAACCAACTTATAATTTCT
kanMX plasmid fwd	AAGAAATATCTTGACCGCAGTTGACATGGAGGCCCAG AATA
plasmid kanMX rev	TATTCTGGGCCTCCATGTCAACTGCGGTCAAGATATT TCTT
plasmid kanMX fwd	GAATGCTGGTCGCTATACTGAAAGATTCTCTTTTTTT ATGATATTTGTA
kanMX plasmid rev	TACAAATATCATAAAAAAAGAGAATCTTTCAGTATAG CGACCAGCATTC
plasmid A1 rev	GTGTAAACCTCGCGGAATTAGGATCCACTAGTTCTA GAGC
pBS Vektor rev	TTGTGTGGAATTGTGAGCGG
pBS Vektor fw (M13 fwd)	GTAAAACGACGGCCAGT
LEU fwd	CGGCTGTGATTTCTTGACCA
pRS315 Fwd	GGCCAGTGAATTGTAATACGACTCA
pRS315 Rev	CCCTCACTAAAGGGAACAAAAGCTG
PK25 rev comp	TGAGTCGTATTACAATTCACTGGCC
PK26 rev comp	CAGCTTTTGTTCCCTTTAGTGAGGG

Table 7.9: ASOs sequences for mRNP purification, RNaseH assay and purification of cross-linked mRNPs.

Name	Sequence 5' - 3'
CCW12 ASO1	gtgtttaagcgaatgacaga
CCW12 ASO3	aaagctggggagacagtttc
SSA4 1	cgtcaccaattagcctttctgtgtcag
SSA4 2	ccttctgcgatttcttgtccagccc
SSA4 3	cctcggctagaaagttaaccagcc
SSA4 4	gggatcaactttgtcataataccacctgc
SSA4 5	ccagtacctttttcaacggcagatacg
ssa4 ASO6	ttaccttgatcgttagcgat
ssa4 ASO7	cgaatttacgtccgatcaga
ssa4 ASO8	cgttactacagcatctttca
ssa4 ASO9	ccttcatctatggatagcag
ssa4 ASO10	atagatgtctgagcagacga
ssa4 ASO11	tggctccaatgtagatctaa
ssa4 ASO12	actggtcacccgttaagatg
ssa4 ASO13	cttgaacttttctgcctcag
ssa4 ASO14	ataatggggtttgcaacacc
ssa4 ASO15	attcgatgctgctacttcat
RAP ssa4 1	ttgatcgttagcgataatttcaaccctatcgtttgcaaaatgagcaacacatgaataggttg tacctaaatcaataccaacagcttttga
RAP ssa4 2	gtgggttcatcgcagcttgattcttcgcagcgtcaccaattagcctttctgtgtcagtaaaa gccacataagaaggcgtcgttctattac
RAP ssa4 3	actttgaatgggtaatgcttagcatcgttcgtcacttctggatcatcgaatttacgtccgatc agacgcttagcatcgaatactgtatta
RAP ssa4 4	caagatcattgaggaaatttcttctggagtaaatgtctttgtctcgcctttatattccacttgc actaccggtttacctcccttgtcaat
RAP ssa4 5	tttgtgaatcgttgaaataggctggaaccgttactacagcatctttcacttctgttcctaaaa agttctcagcagtctccttcatctttg
RAP ssa4 6	agcccatacgcaatagcggcagctgtaggttcattaatgatacgaagaacgttcaagcccg cgattgtaccggcatcttttgttgcttgc
RAP ssa4 7	accttcatctatggatagcagagagacatcaaaagtaccaccacctaaatcaaagatcaa gacgttgtgctcctctgcgatttcttgtc
RAP ssa4 8	tgaactcctcggctagaaagttaaccagcctactatcgaaatcttcaccacccaagtgagtg tcaccagcagtagccttaacctcaaaga

RAP ssa4 9	gaagacagagttctcttggccctttcagcggcggtccttaacctccttagggacctttggttag ttgttagatccttttttatttttttctt
RAP ssa4 10	acataattcttcaaatcttgcccttgtaatggaagtatagaaatcgataccctcaaataatga atctatttctatagatgtctgagcaga
RAP ssa4 11	caagtacaatttcatcaatttgtgacttatctaattttgaatcagccaaaacttttttccactgg ctccaatgtagatctaaacaaatcag
RAP ssa4 12	tcatcagggttaatcgaacggtttggttctttaccattgaaaaaatcagaaaccagtttttgt acttttggaattcttgttgaaccacca
RAP ssa4 13	tgcaacatccagcaacagtaaatcttgggtcgtcgacgactggtcacccgttaagatggca gcctgtacggcagcaccataagcgacggc
RAP ssa4 14	acacttccgatttttttgttgggatagtcgaatttcttgggatcaactttgtcataataccacct gcagtttcaatacctagagataatg
RAP ssa4 15	ttacccagtagattgttgtcttttgtccttgtcctttcaccctcaaaaacttgtatcaacacacc aggttggttgtcagcgtaggtggaa
RAP ssa4 16	tacgttcagaataccatttgcatcgatatcaaatgtaacttcaatttgtggtacgcctcttgga gcgggtggaataccgctcaactcaaa
RAP ssa4 17	ccattttatcgatatcttccttcgataatcttcccttatcgttagtaattgtaatcttgttagattt accagtacctttttcaacggcag
RAP ssa4 18	aaagtaaacgcgtacgattctagctgattcttagcttgaacacgttgagcttcttgttcatcttc ggccttgaacttttctgcctcagca
RAP ssa4 19	atttatagcatcttgggcggcggcttccaatttcctggcatcctcttcacccaccttctccttga agttattttcgctcacagaattttt
RAP ssa4 20	atttactcataatggggtttgcaacaccttctagttccttttgcctttccttgtattcctcggtgga ggccgcttgcgaagcatctaacc
RAP ssa4 21	accgttgggccgttgtctggtgctccagtggggcctgctccagcacccggaactgggcctgctc ctggggcaccacctgcagctccgtaa
RAP ccw12 1	agcagcggcagaagcgacagcggcgacagcggcgatagaagcgacagtagaaaattgcatt attgatatagtgtttaagcgaatgacaga
RAP ccw12 2	gggagacagtttcagaacagacgtggtcttcacaagaagtgatggtgaccaaagtggtagatt cttggctgacagtagcagtggtaacgt
RAP ccw12 3	ttctttggggcttcagtggtcaatgggcaccaggtggtgtattgagtgataacgtcatcgac ggtgacggtagcggtggaaaccaaagct
RAP ccw12 4	agtgtaagaggtgacagagtgagttggagcagcagaggtggtgttctttggagcttca gtagaggtaactggagcagcagtagaagtacc
RAP ccw12 5	tataaataataataaactaagtttacaacaacaaagcagcggcaccagccaacaaagca ccagcagctggcaaagccttagcagcagcac

Table 7.10: List of all primer used for qPCR.

Name	Sequence 5' - 3'	Description
CCW12 5´fwd	actgtcgcttctatcgccgc	
CCW12 5´rev	ttggctgacagtagcagtgg	
PGK1 5´fwd	ttgccaaccatcaagtacgttt	
PGK1 5´rev	cccaagtgagaagccaagaca	
fwd SSA4 1	gaacgacgccttcttatgtggc	primer for RNaseH assay
rev SSA4 1	gggttcatcgcagcttgattcttc	primer for RNaseH assay
fwd SSA4 2	gaacctacagctgccgctattg	primer for RNaseH assay
rev SSA4 2	ccaccacctaaatcaaagatcaagacg	primer for RNaseH assay
fwd SSA4 3	cgatagtaggctggttaactttctagcc	primer for RNaseH assay
rev SSA4 3	gggacctttggttagttgttagatcc	primer for RNaseH assay
fwd SSA4 4	gctggatgttgcaccattatctctagg	primer for RNaseH assay
rev SSA4 4	gggatagtcgaatttcttgggatcaac	primer for RNaseH assay
fwd SSA4 5	ggtattctgaacgtatctgccgttg	primer for RNaseH assay
rev SSA4 5	cgataatcttcccttatcg	primer for RNaseH assay
ssa4 6 fwd	gctcattttgcaaacgatagggttg	primer for RNaseH assay
ssa4 7 fwd	cccacataatacagtattcgatgc	primer for RNaseH assay
ssa4 7 rev	gcttagcatcgttcgtcacttct	primer for RNaseH assay
ssa4 8 fwd	gatgaaggagactgctgagaac	primer for RNaseH assay
ssa4 8 rev	gttgcttgcctttgtgaatcgttg	primer for RNaseH assay
ssa4 9 fwd	ggtggtggtacttttgatgtctc	primer for RNaseH assay
ssa4 9 rev	gtgagtgtcaccagcagtagc	primer for RNaseH assay
ssa4 10 fwd	gaaagggccaagagaactctg	primer for RNaseH assay
ssa4 10 rev	ggaagtatagaaatcgataccctc	primer for RNaseH assay
ssa4 11 fwd	gggcaagatttgaagaattatgtgc	primer for RNaseH assay
ssa4 11 rev	cctcatcagggttaatcgaacgg	primer for RNaseH assay
ssa4 12 fwd	tggtgctgccgtacaggctg	primer for RNaseH assay
ssa4 12 rev	ggtgcaacatccagcaacagta	primer for RNaseH assay
ssa4 13 fwd	cgaaggaagatatcgataaaatgg	primer for RNaseH assay
ssa4 13 rev	gcttgaacacgttgagcttcttg	primer for RNaseH assay
ssa4 14 fwd	ccgaggaatacaaggaaaggc	primer for RNaseH assay
ssa4 14 rev	ggcaccacctgcagctccgt	primer for RNaseH assay
ssa4 15 fwd2	ggagcaccagacaacggccc	primer for RNaseH assay
ssa4 15 rev2	gttaagagggaaaactaagaaattcg	primer for RNaseH assay
hsp104 fwd_3	caggttgctgaggaagagagacg	primer used for RAP and RIP
hsp104 rev_3	cagaaatggtgtctgaatcgacc	primer used for RAP and RIP
hsp12 fwd	cctccaaggtgtccacgact	primer used for RAP and RIP

hsp12 rev	ttggttgggtcttcttccc	primer used for RAP and RIP
ilv5 5´ fwd	aagagaacctttgctttggc	primer used for RAP and RIP
ilv5 5´ rev	ttggcttaacgaaacgggca	primer used for RAP and RIP
yef 5´ fwd	gctgacccaactgaagttcc	primer used for RAP and RIP
yef 5´ rev	gggaccatgatggacaaagt	primer used for RAP and RIP
kar2 fwd	gaaaccgccattgctgaaga	primer used for RAP
kar2 rev	gaagtaattggataagcgaccttg	primer used for RAP
RLP8B_fwd	ggtgctaagtccactaagtct	primer used for RAP
RPL8B_rev	cttggccaataccgaagttct	primer used for RAP
YDR524C-B_fwd	tcgctgccttcgctactgt	primer used for RAP
YDR524C-B_rev	gttggaaccgttggtacgg	primer used for RAP

Organisms

All *E. coli* and *S. cerevisiae* strains used for all experiments are listed in Table 7.11 and 7.12, respectively.

Table 7.11: *E. coli* strain list

Name	Genotype	Reference
DH5α	F^- *endA1 glnV44 thi-1 recA1 relA1 gyrA96 deoR nupG θ80dlacZΔM15Δ(lacZYAargG)U169 hsdR17*$_K(r_K^- m_B^+)$ *λ−*	Woodcock et al. [1989]

Table 7.12: *S. cerevisiae strains* strain list

Strain	Genotype	reference
RS453 (WT)	MATa;*ade2-1; his3-11,15; ura3-52; leu2-3,112; trp1-1;can1-100; GAL+*	Sträßer and Hurt [2000]
W303	MATa;*ura3-1; trp1-1; his3-11,15; leu2-3,112;ade2-1,can1-100; GAL+*	Euroscarf
CBP20-TAP	MATa; *ade2-1, his3-11,15, ura3-52, leu2-3,112, trp1-1, can1-100, GAL+; CBP20-FLAG-TEV-protA::HIS3*	Sträßer lab
CBP20-FTpA	MATa; *ade2-1, his3-11,15, ura3-52, leu2-3,112, trp1-1, can1-100, GAL+; CBP20-FLAG-TEV-protA::HIS3*	Philip Keil [2021]

CBP20-FTpA MEX67-HA	MATa; *ade2-1, his3-11,15, ura3-52, leu2-3,112, trp1-1, can1-100, GAL+; MEX67-HA::KanMX4; CBP20-FLAG-TEV-protA::HIS3MX4*	this study
CBP20-TpA	MATa; *ade2-1, his3-11,15, ura3-52, leu2-3,112, trp1-1, can1-100, GAL+; CBP20-TEV-protA::TRP1-KL*	this study
CBP20-TpA *Δccw12*	MATa; *ade2-1, his3-11,15, ura3-52, leu2-3,112, trp1-1, can1-100, GAL+; ccw12::KanMX4; CBP20-TEV-protA::TRP1-KL*	this study
CBP20-TpA *Δccw22*	MATa; *ade2-1, his3-11,15, ura3-52, leu2-3,112, trp1-1, can1-100, GAL+; ccw22::His ; CBP20-TEV-protA::TRP1-KL*	this study
CBP20-TpA *Δccw12 Δccw22*	MATa; *ade2-1, his3-11,15, ura3-52, leu2-3,112, trp1-1, can1-100, GAL+; ccw22::His ; ccw12::KanMX4; CBP20-TEV-protA::TRP1-KL*	this study
Δrip1	MAT a; *ade2-1; his3-11,15; ura3-52; leu2-3,112;trp1-1 can1-100; GAL+; rip1::HIS3*	this study
Δrip1 Δssa4	MAT a; *ade2-1; his3-11,15; ura3-52; leu2-3,112;trp1-1 can1-100; GAL+; ssa4::KanMX4; RIP1::HIS3*	this study
Δssa4 P_{CYC1}-MBP-MCP-3xHA CBP20-TpA	MAT a; *ade2-1; his3-11,15; ura3-52; leu2-3,112;trp1-1 can1-100; GAL+; ssa4::KanMX4; P_{CYC1}-MBP-MCP-3xHA ::LEU2; CBP20-TEV-proteinA::TRP1-KL*	this study
Δccw12 P_{NOP1}-MBP-MCP-3xHA CBP20-TpA	MAT a; *ade2-1; his3-11,15; ura3-52; leu2-3,112;trp1-1 can1-100; GAL+; ccw12::KanMX4; P_{NOP1}-MBP-MCP-3xHA::LEU2; CBP20-TEV-proteinA::TRP1-KL*	this study
Δccw12 P_{CYC1}-MBP-MCP-3xHA CBP20-TpA	MAT a; *ade2-1; his3-11,15; ura3-52; leu2-3,112;trp1-1 can1-100; GAL+; ccw12::KanMX4; P_{CYC1}-MBP-MCP-3xHA ::LEU2; CBP20-TEV-proteinA::TRP1-KL*	this study
Δslt2	MAT a; *ade2-1; his3-11,15; ura3-52; leu2-3,112;trp1-1 can1-100; GAL+; slt2::HIS3*	this study
CBP20-TpA MEX67-HA	MATa; *ade2-1, his3-11,15, ura3-52, leu2-3,112, trp1-1, can1-100, GAL+; CBP20-TEV-proteinA::TRP1-KL, MEX67-HA::HIS3*	this study

CBP20-TpA	MATa; *ade2-1, his3-11,15, ura3-52, leu2-3,112, trp1-1, can1-100, GAL+; MEX67-HA::HIS2MX4; ssa4::KanMX4; CBP20-TEV-protA::TRP1-KL*	this study
*Δ*ssa4 Mex67-HA		
ilv5-shuffle	MATa; *ura3Δ0/ura3Δ0; leu2Δ0/leu2Δ0; his3Δ1/his3Δ1; met15Δ0/MET15; LYS2/lys2Δ0; ilv5::KanMX4; pRS316-ILV5; CBP20-FTpA::HIS3*	Nataliia Stefanyshena
CBP20-FTpA		
Δssa4 Δrip1 P_{CYC1}-MBP-MCP-3xHA Cbp20-TpA	MAT a; *ade2-1; his3-11,15; ura3-52; leu2-3,112;trp1-1 can1-100; GAL+; ssa4::KanMX4; P_{CYC1}-MBP-MCP-3xHA ::LEU2; CBP20-TEV-proteinA::TRP1-KL; rip1::HIS3*	this study
cbp80-shuffle	MAT a; *ade2-1; his3-11,15; ura3-52; leu2-3,112;trp1-1 can1-100; GAL+; cbp80::LEU2; pRS316-CBP80*	this study
cbp20-shuffle	MAT a; *ade2-1; his3-11,15; ura3-52; leu2-3,112;trp1-1 can1-100; GAL+; cbp20::HIS3; pRS316-CBP20*	this study
cbp20-shuffle *Δcbp80*	MAT a; *ade2-1; his3-11,15; ura3-52; leu2-3,112;trp1-1 can1-100; GAL+; cbp20::HIS3; pRS316-CBP20; cbp80::LEU2*	this study
cbp20-shuffle SSA4-HA	MAT a; *ade2-1; his3-11,15; ura3-52; leu2-3,112;trp1-1 can1-100; GAL+; cbp20::HIS3; pRS316-CBP20; SSA4-3xHA::TRP1-KL*	this study
cbp20-shuffle *Δcbp80* SSA4-HA	MAT a; *ade2-1; his3-11,15; ura3-52; leu2-3,112;trp1-1 can1-100; GAL+; cbp20::HIS3; pRS316-CBP20; cbp80::LEU2; SSA4-3xHA::TRP1-KL*	this study
cbp80-shuffle SSA4-HA	MAT a; *ade2-1; his3-11,15; ura3-52; leu2-3,112;trp1-1 can1-100; GAL+;cbp20::LEU2; pRS316-CBP80; SSA4-3xHA::TRP1-KL*	this study
SSA4-HA	MAT a; *ade2-1; his3-11,15; ura3-52; leu2-3,112;trp1-1 can1-100; GAL+; SSA4-3xHA::TRP1-KL*	this study
YRA1-6xHA	MAT a; *ade2-1; his3-11,15; ura3-52; leu2-3,112;trp1-1 can1-100; GAL+; YRA1-6xHA::KanMX4*	this study
YRA1-6xHA *Δslt2*	MAT a; *ade2-1; his3-11,15; ura3-52; leu2-3,112;trp1-1 can1-100; GAL+; YRA1-6xHA::KanMX4; slt2::HIS3*	this study

dbp5-shuffle	MAT a; *ade2-1; his3-11,15; ura3-52; leu2-3,112;trp1-1 can1-100; GAL+; pRS316-DBP5; dbp5::HIS3*	this study
Δgfd1	MAT a; *ade2-1; his3-11,15; ura3-52; leu2-3,112;trp1-1 can1-100; GAL+; gfd1::KanMX4*	this study
yra1-shuffle	MAT a; *ade2-1; his3-11,15; ura3-52; leu2-3,112;trp1-1 can1-100; GAL+; yra1::HIS3; pRS316-YRA1*	
yra1 nab2 double shuffle	MAT a; *ade2-1; his3-11,15; ura3-52; leu2-3,112;trp1-1 can1-100; GAL+; yra1::HIS3; pRS316-YRA1; nab2::HygR; pRS314-NAB2*	this study
nab2-shuffle	MAT a; *ade2-1; his3-11,15; ura3-52; leu2-3,112;trp1-1 can1-100; GAL+; nab2::HygR; pRS314-NAB2*	this study
Δhpr1	MAT a; *ade2-1; his3-11,15; ura3-52; leu2-3,112; trp1-1;can1-100; GAL+; hpr1::KanMX4*	[Sträßer et al., 2002]

Methods

S. cerevisiae specific methods

S. cerevisiae growth

All *S. cerevisiae* strains were stored in a 50 % ($\frac{w}{v}$) glycerol stock at -80°C. For experiments, the strain was streaked out on YPD or selective plates if needed. Cells were grown for 2-3 days at 30°C. For a preculture, 50 ml YPD or selective media were inoculated with yeast cells and grown overnight at 30°C. The main culture was inoculated to an OD_{600} of 0.2 and grown to an OD_{600} of 0.8 for experiments, if not indicated otherwise. Yeast cells were pelleted at 3600 rpm for 3 min.

Stress treatments for *S. cerevisiae*

Yeast strains were grown to an OD_{600} of 0.8 as described above. After cells were diluted back to OD_{600} of 0.2, if not otherwise indicated using the medium or treatment described in table 7.13 for investigation of nuclear poly(A)-RNA accumulation. Heat shock treatment for nuclear mRNP purification was performed similar, but only for 15 min instead of 1 h.

Table 7.13: List of stress conditions tested for export block and used for further experiments

Stress	Treatment
Heat Shock	Add hot media to reach a temperature of 42°C and incubate at 42°C for 1h
Hyperosmotic stress	1.25 M NaCl in YPD for 1 h
Hypoosmotic stress	Shift from 20 % YPD 1 M Sorbitol to 20 % YPD 0.1 M Sorbitol for 5 min
Glucose starvation	SC media without Glu for 1 h
Nitrogen starvation	2 % glucose, 0.19 % (w/v) yeast nitrogen base without amino acids and without ammonium sulphate for 1 h
Ethanol stess	8 % ethanol in YPD for 1 h
Oxidative stress	2 mM arsenite for 1 h
rapamycin treatment	2 $\frac{\mu g}{ml}$ rapamycin in ethanol with 20 % Tween-20 for 1 h
UPR	8 mM DTT in YPD for 1 h

Dot Spot Assay

For each strain, freshly grown yeast cells were resuspended in sterile water, the OD_{600} was adjusted to 0.1, and a serial dilution (1:5) was performed three times. From each dilution, 5 µl cell suspension were pipetted onto a YPD plate or on selective plates. The plates were incubated at 30°C, 37°C and 25°C or 16°C for 2 days, 3 days or a week, respectively.

S. cerevisiae transformation

Yeast cells were grown in 50 ml YPD to an OD_{600} between 0.6 ond 0.8, harvest and washed with 10 ml sterile water. Cells were resuspended in 500 µl Solution 1, spun down, supernatant was removed and the cells resuspended in 250 µl Solution 1. For each transformation, 50 µl cell suspension were mixed with precipitated DNA from 6 PCR reactions or 1 µl plasmid, 5 µl SSD and 300 µl Solution 2. After 30 min incubation at RT on a turning wheel, a 10 min heat shock at 42°C was performed. In case PCR product were transformed, 35 µl DMSO was added before the heat shock. The cells were chilled on ice for 2 min. The transformation solution was diluted with 1 ml water and removed after centrifugation. In case of PCR product transformations, the cells could recover in 1 ml YPD at 30°C shaking for at least 2 h. The cells were then plated on selective plates and could grow for 2-3 days at 30°C. Genomic integration of PCR products were checked by colony PCR or strain verification Western blot.

Yeast Colony PCR

To verify the integration of a marker cassette into the genome, colony PCR was performed. Cells were resuspended in 15 µl 2.5 $\frac{mg}{ml}$ Zymolyase T20 dissolved in 0.1 M KPO_4 pH 7.5 and incubated first for 20 min at RT, following 5 min at 37°C and 95°C, respectively. After dilution with 60 µl water, the mixture was used as template for colony PCR. PCR was performed as described in table 7.14 and 7.15. The resulting DNA fragments were analyzed by agarose gel electrophoresis.

Table 7.14: PCR mix for yeast colony PCR.

PCR mix	
10x Taq buffer	2.5 µl
dNTPs	2 µl
oligo 1 (100 µM)	0.2 µl
oligo 2 (100 µM)	0.2 µl
Taq Polymerase	0.5 µl
template	0.5 µl
water	33.9 µl

Table 7.15: PCR Programme to amplify DNA fragments. The extension time X was calculated with 1 $\frac{kb}{min}$.

Programme		
95°C	5 min	
95°C	30 sec	
57°C	30 sec	
72°C	1 min	back to step 2 25x
72°C	5 min	
12°C	∞	

Molecular biology methods

Polymerase Chaine Reaction

DNA fragments for cloning were amplified by a Q5 PCR reaction as described in Table 7.16. PCR fragments for genomic integration in yeast were amplified with Phusion polymerase as listed in Table 7.17. In both cases, the PCR program shown in table 7.18 was used. The length of the resulting DNA fragments were analyzed by agarose gel electrophoresis (see below).

Table 7.16: PCR mix for a PCR using Q5 DNA polymerase as used for cloning.

PCR mix	
5x Q5 buffer buffer	10 µl
dNTPs	4 µl
oligo 1 (10 µM)	0.3 µl
oligo 2 (10 µM)	0.3 µl
Q5 DNA polymerase	0.5 µl
template (20 - 50 $\frac{ng}{\mu l}$)	1 µl
water	33.9 µl

Table 7.17: PCR mix for a PCR to amlify cassettes for yeast transformation using the Phusion polymerase.

PCR mix	
5x HF buffer	10 µl
dNTPs	4 µl
oligo 1 (10 µM)	0.3 µl
oligo 2 (10 µM)	0.3 µl
Phusion polymerase	0.5 µl
template (20 - 50 $\frac{ng}{\mu l}$)	1 µl
water	33.9 µl

Table 7.18: PCR Programme to amplify DNA fragments. The extension time X was calculated with 2 $\frac{kb}{min}$.

Programme		
98°C	2 min	
98°C	30 sec	
57°C	30 sec	
72°C	X	back to step 2 35x
72°C	10 min	
12°C	∞	

Agarose gel

To verify the correct size of a PCR product, an agarose gel electrophoresis was performed. For a 1 % agarose gel, 0.5 g agarose was dissolved in 50 ml 1x TAE buffer and mixed with 2.5 µl HDgreen for DNA staining. The DNA sample was mixed with 6x DNA loading dye, loaded onto the gel and separated at 120 V for 30 min with the PeqLab PerfectBlue Mini Gel System. Pictures were taken using the Intas Gel iX20 Transilluminator system.

Fluorescence *in situ* hybridization

The cells were grown to an OD_{600} of 0.8 and either fixed for FISH directly or a stress treatment was performed as described in Table 7.13. For fixation, cells were incubated for 90 min with 4.6 % formaldehyde. The cells were washed twice with 0.1 M KPO_4 and once with wash buffer. The cells were permeabilized with 100 µg Zymolyase 100T in wash buffer for 30 min at 30°C. The Zymolyase mixture was removed after centrifuation at 2000 rpm for 4 min and the cells were washed once more with wash buffer. The cells were resuspended in 10 $\frac{\mu l}{OD_{600} unit}$ and 100 µl of the cell suspension was incubated on a poly-lysine coted coverslip for 5 min. After aspiration, the non attached cells were removed by washing with 100 µl 2x SSC for 10 min before adding 12 µl prehybridization buffer. The slides were incubated for 1 h at 37 °C in a humid chamber before adding 0.75 µl of 1 $\frac{pmol}{\mu l}$ Oligo(dT)50-Cy3. The oligo could bind overnight at 37°C. The excess was removed by washing the coverslips in 3 ml 0.5x SSC. The dry slides were mounted on a coverslide with 8 µl Roti Mount FluorCare DAPI. For microscopy the Delta Vision Ultra fluorescence microscope from Cytiva was used. The distribution of poly(A)-RNA was analyzed by defining the whole cell by the RNA signal and the nucleus by the DAPI signal using the software ImageJ (Figure 5.15 A). A R script was used to calculate the rations of mean nuclear to cytoplasmic RNA signal measured

with Fiji ImageJ, display them as box plot diagrams and perform a Welch test to determine significant changes between the samples. Two FISH experiments each were performed by my Bachelor students Elena Bagrin and Cora-Lee Weber under my supervision. The quantification of all experiments was performed by myself.

Single molecule FISH

Yeast cells were grown to an OD_{600} of 0.4 and fixed with 3.7 % formaldehyde for 45 min. Cells were harvested, washed twice with 1 ml ice cold Fixation buffer and the cell wall was permeated with 125 $\frac{mg}{ml}$ Zymolyase T100 for 30 min at 30°C. After centrifugation with 400 xg for 5 min, the Zymolyase was removed and the cells washed twice with ice cold Fixation buffer. The cells were resuspended in Fixation buffer and applied to the coverslip as described above for Fluorescence *in situ* hybridization. The slides were incubated in 70 % ethanol overnight at 4°C. The slides were removed from ethanol and after evaporation, 100 µl hybridization buffer containing 1 µl 125 nM Stellaris Cy3 coupled-probes agains *SSA4* were added. The samples were incubated overnight at 30°C. The sildes were washed with 3 ml wash buffer A for 30 min, shaking at 30°C and for 2 min with 3 ml wash buffer B at RT before mounting on a slide with 8 µl Roti Mount FluorCare DAPI. Mikroskopy was performed as described above.

RNA Immunoprecipitation

For each sample, 400 ml yeast culture were grown to an OD_{600} of 0.8 following stress treatment when indicated. The cells were harvested and washed with 5 ml ice cold PBS. The pellet was flash frozen in liquid nitrogen and stored at -80°C until further use.

The cell pellet was thawed on ice with 1 ml RNA IP buffer containing 20 µl 10x protease inhibitor and lysed with 500 µl glass beads in the FastPrep machine 3 times with 6 $\frac{m}{s}$ for 20 sec and 1 min breaks on ice. The lysate was cleared by two centrifugation steps at 4000 rpm and 13000 rpm for 5 min at 4°C. The DNA was digested with 5.5 µl DNaseI for 30 min on ice before adding 50 µl IgG-coupled tosylactivated Dynabeads. After incubation for 3 h at 4°C, the beads were washed 6 times with RNA IP buffer. For elution of the RNA, Trizol was added and the RNA isolated as described as following in RNA isolation using Trizol.

For protein elution, the organic and interphase from the RNA isolation were mixed with 3x volume of aceton and incubated overnight at -20°C. The proteins were pelleted for 1 h with 15000 rpm for 4°C, the supernatant was removed and the pellet was washed with 500 µl aceton for 30 min. After removing the supernatant,

60 µl SDS loading dye were added. For each Comassie stained protein gel 15 µl protein sample were used. SDS page was performed as described below.

RNA Isolation using Trizol

For RNA isolation the 10 x volume of Trizol was added to the sample and mixed by vortexing. The sample was incubated for either 5 min at RT or for 7 min at 60°C for cross-linked samples or elution from beads. After, 200 $\frac{\mu l}{ml}$ chloroform was added, vortexed and centrifuged for 15 min at 14000 rpm at RT. The upper phase was transferred to a new tube containing 600 µl ice cold isopropanol for RNA precipitation and incubated for 10 min at RT. The RNA was pelleted at 15000 rpm, 20 min at 4°C. The supernatant was removed and the RNA pellet washed with 500 µl 75 % ethanol. The dry pellet was dissolved in 56 µl water at 65°C, 750 rpm for 5 min.

Hot phenol RNA isolation

The cell pellet was resuspended in 500 µl AE buffer with 1 % SDS and 500 µl phenol chloroform isoamylalcohol for RNA isolation were added. The sample was vortexed to mix and incubated at 65°C at 800 rpm for 20 min. The sample was chilled on ice for 1 min before phase separation at 15000 rpm for 5 min at RT. The aequos phase was transferred to a new tube and mixed with 400 µl phenol chloroform isoamylalcohol. After another centrifugation, the upper phase was transferred to a new tube, mixed with 400 µl chloroform, centrifuged again and the upper phase transferred to a tube containing 1 ml 30:1 mix. The RNA was precipitated with a incubation at -20 °C for 30 min up to overnight and pelleted at 15000 rpm, 20 min at 4°C. The RNA pellet was washed with 500 µl 75 % ethanol and after drying dissolved in 56 µl water at 65°C, 750 rpm for 5 min.

DNaseI digest of isolated RNA, reverse transcription and qPCR

To 56 µl RNA solution 7 µl DNase I buffer, 7 µl DNaseI and 1 µl Ribolock were added and the DNA digested for 1 h at 37°C. The enzyme was inactivated for 10 min at 65°C.
Reverse transcription was performed either to compare RNA levels or to validate the mRNP experiment. For comparing RNA levels after hot phenol isolation 100 ng RNA were used for reverse transcription. After an mRNP purification, 7 µl RNA were added for reverse transcription either form 1:10 diluted lysate, TEV eluate or elution sample. The RNA was mixed with 1 µl of 100 nM random hexamer primer,

100 µM Oligo dT_{18}, 10 µM dNTPs and Ribolock each. The mix was incubated for 5 min at 65°C for annealing. To each reaction 2 µl 10x MuLV buffer, 1 µl MuL-V and 6 µl water were added. To check if the DNase digest was efficient a negative control without enzyme was performed. The samples were incubated first 5 min at RT after 1h at 42°C. The reaction was stopped by adding 65 µl 30:1 mix and precipitation of the cDNA at -20°C for 30 min up to overnight. The cDNA was pelleted at full speed at 4°C for 20 min, washed with 75 % ethanol and dried in a speed vac for 10 min at 42°C. The cDNA was dissolved in 100 µl water.
For qPCR, 2.5 µl of the 1:10 diluted or undiluted cDNA sample was used and mixed with 5 µl qPCR Master Mix, 2.3 µl water and 0.1 µl of each primer. The program of the qPCR can be found in Table 7.19.

Table 7.19: Program used for qPCR.

Program		
95°C	10 min	
95°C	15 sec	
60°C	1 min	back to step 2 40x

Cloning

For plasmid cloning, the PCR fragments and plasmid backbones were amplified using PCR with Q5 polymerase (see Polymerase Chain Reaction above). After confirming the correct size of the DNA fragment by agarose gel electrophoresis, the plasmid, used as PCR template was either digested for 3 h at 37°c with 1 µl DpnI or directly purified using the Macherey-Nagel NucleoSpin Gel and PCR Clean up Kit as described in the manual. DNA fragments were assembled using Gibson assembly. Therefore, backbone and insert were added to 15 µl of Gibson Master Mix in a 1:3 ratio with 35 ng backbone and incubated for 1 h at 50°C. For each gibson sample, 3 µl were transformed in DH5α cells and grown on LB plates containing the required antibiotic. The integration of the insert was verified by colony PCR. Plasmids from clones that were positive during colony PCR (see below) were isolated using the Macherey-Nagel NucleoSpin Plasmid (NoLid) Kit and sequenced.

E. coli transfomation

E. coli cells were made competent with the Zymo Mix & Go *E. coli* Transformation Kit as described in the manual. To transform a plasmid, 1 µl plasmid was mixed with 50 µl chemically competent *E. coli* cells on ice. After incubation on ice for

15-30 min a heat shock was performed at 42°C for 60 sec. The cells were chilled on ice for another 2 min, mixed with 250 µl SOC-media and could recover for 1 h at 37°C, shaking. The cells were plated on LB-agar plate containing the appropriate antibiotics.

E. coli colony PCR

Single *E. coli* colonies were tested for successful integration of the insert by colony PCR. Therefore, single clones were restreaked on a new LB plate with antibiotics and the remaining cells were added to a PCR mix (Table 7.20). The used PCR program can be found in Table 7.21. The resulting PCR fragments were analyzed using an agarose gel electrophoresis as described above.

Table 7.20: Reaction mix for *E. coli* colony PCR for plasmid cloning.

PCR mix	
10x Taq buffer	2.5 µl
dNTPs	2 µl
oligo 1 (100 µM)	0.2 µl
oligo 2 (100 µM)	0.2 µl
Taq Polymerase	0.5 µl
template	cells from plater
water	33.9 µl

Table 7.21: PCR program to amplify DNA fragments. The extension time X was calculated with 1 $\frac{kb}{min}$.

Program		
95°C	5 min	
95°C	30 sec	
57°C	30 sec	
72°C	1 min	back to step 2 25x
72°C	5 min	
12°C	∞	

SDS PAGE and Western blot

SDS PAGE

For a SDS PAGE, SDS gels were poured according to Table 7.22 with the BioRad gel system. Samples were mixed with 4x SDS loading dye, boiled at 95°C for 10 min and loaded on the gel. For size comparison, 5 µl Colored prestained ladder were loaded onto the gel. Gel electrophoresis was performed at 200 V for 45 min at RT. The SDS gel was washed with water twice, incubated in Coomassie solution until band are visible. The background was destained by incubation in water. Recipes for Coomassie can be found in Table 7.4.

Table 7.22: Composition of SDS-polyacrylamid gels with different percentages of polyacrylamide for SDS-PAGE. Mixture is sufficient for 12x SDS gels.

	Separating gel 8 %	Separating gel 10 %	Separating gel 12 %	Stacking gel
Water	44 ml	40 ml	36 ml	19.5 ml
Seperating buffer	20 ml	20 ml	20 ml	-
Stacking buffer	-	-	-	7.5 ml
polyacrylamid	16 ml	20 ml	24 ml	3 ml
TEMED	140 µl	140 µl	140 µl	60 µl
10 % APS	700 µl	700 µl	700 µl	180 µl

Western blot

After performing an SDS PAGE without Comassie staining, the proteins were transferred onto a Porablot NCP membrane using the Biorad Trans-Blot Turbo Transfer System with 25 V for 45 min at RT. The membrane was blocked for 1 h in 5 % milk in 1x TBST shaking at RT. The primary antibody was added and incubated overnight at 4°C. The next day, the membrane was washed three times 10 min with 1x TBST and the secondary, HRP coupled antibody was added for 1-2 h. The blot was washed three times to remove the excess of secondary antibody and detected using CheLuminate-HRP ECL or SuperSignal West Dura solution and the Intas ChemoCam Imager system.

Protein Dot blots

Protein Dot blots of cross-linked protein samples were performed using the BioRad Bio Dot-Apparatus as described in the manual.

Quantitative Western blot

Yeast cells were resuspended in 500 µl water, 150 µl pretreatment solution was added, mixed and incubated for 20 min on ice. Then 82 µl 100 % TCA was added, vortex and incubate another 20 min on ice. The lysed cells were centrifuged for 20 min at 15000 rpm at 4°C and the supernatant was removed completely. SDS loading dye containing 21 % 1 M Tris base was added to a final concentration of 1 OD_{600} unit per 21 µl. Pellets were dissolved for 10 min at 95°C with 950 rpm and 5 - 10 µl loaded on a SDS gel. Western blot was performed as described above. In addition to the protein of interest also Pgk1 was detected. Western blot bands

were quantified using Fiji ImageJ and the intensities normalized over the Pgk1 signal.

Mechanical lysis for Western blot

For a strain verification Western blot or for analysis of phosphorylation bands, cells were resuspended in 100 µl 1x SDS loading dye with 100 µl glass beads. Cells were mechanically destroyed for 20 sec with 6 $\frac{m}{s}$ in the FastPrep machine. After, samples were boiled for 10 min at 95°C and 20 µl were loaded onto an SDS gel. Gel electrophoresis and Western blot were performed as described above for strain verification Western blot. To detect phosphorylation-induced protein shifts the samples were separated on a 8 % SDS page for 30 min at 50 V and then at 90 V until the dye front reached the bottom of the gel. The remaining steps of the Western blot were performed as described above.

Wet blot to detect cross-linked proteins

To detect RNA-protein cross-links using a Western blot the samples were separated on a 6 % SDS gel (Table 7.23). Gel electrophoresis was performed until the 55 kDa marker band run off the gel. After, the proteins were transfered to a methanol activated PVDF membrane using the Biorad Mini-Protean Wet blot system. The transfere was performed with 100 V for 2 h and 45 min at 4°C and ice to cool the Wet blot transfer buffer. The blot was blocked, incubated with antibody and detected as described above.

Table 7.23: Composition of SDS-polyacrylamid gels with 6 % separating gel for cross-linked proteins. Mixture is sufficient for 6x SDS gels.

	Separating gel 6 %	Stacking gel
Water	17.7 ml	9.75 ml
Seperating buffer	7.5 ml	-
Stacking buffer	-	3.75 ml
polyacrylamid	4.5 ml	1.5 ml
TEMED	60 µl	30 µl
10 % APS	300 µl	90 µl

Purification of transcript specific nuclear mRNPs

Enrichment of nuclear mRNPs using Cbp20-TAP

The enrichment of nuclear mRNPs was performed by the first step of a TAP purification as published by Puig et al. [2001]. Some alterations were made to shorten the purification. The cells were harvested, pipetted in liquid nitrogen and lysed by cryomilling using the SPEX SamplePrep freezer mill 6870D.
For the purification of the nuclear CBC using *Cbp20-TAP*, the lysate was cleared by centrifugation at 40000 xg for 16 min at 4°C. The lysate was incubated with 500 µl IgG beads for 1 h at a turning wheel at 4°C. After, the beads were pelleted at 1800 rpm for 3 min at 4°C, transferred in a Mobicol with attached syringe and washed with 15 ml TAP buffer. For elution, 160 µl TAP buffer and 5 µl TEV protease were added to the bead. The TEV eluate was used for further experiments either for RNase H assay or for purification of specific transcripts by ASO, Mango or MS2 purification.

RNaseH Assay

The TEV eluate was mixed with 100 µl 10x RNaseH buffer, 60 mM NaCl (final) and water was added up to 1 ml. Half was mixed with 100 pmol DNA ASOs while the other half served as a negative control. Both were incubated for 2 h at 4°C if not indicated otherwise. To digest DNA-RNA hybrids, 2.5 µl RNaseH was added and incubated for 20 min at 37°C.
To isolate the RNA 500 µl Phenol-Chloroform-Isoamylalcohol was added, mixed and centrifuged at 14000 rpm for 10 min at RT. The aqueous phase was mixed with 500 µl chloroform, vortexed and centrifuged. The upper phase was precipitated, DNaseI digested and analyzed with RT-qPCR as described above. For qPCR, a primer pair binding on both sites of the ASO binding site was used to determine if the transcript was bound by the DNA ASO and digested by RNaseH (Figure 5.3 A).

ASO purification

To purify transcript-specific mRNPs by ASOs, 5‘O-methylated RNA ASOs coupled with biotin were used (Table 7.9). Nuclear mRNPs were enriched as described above. For purification of mRNPs containing a specific transcript, 100 pmol ASO for the specific-transcript was added and incubated for 15 min at RT. After, 100 µl

prewashed M280 Streptavidine Dynabeads were added and incubated for 30 min at 25°C with 950 rpm. The beads were washed five times with 750 µl binding and wash buffer for 2 min. For elution, 20 µl of the beads were used for RNA isolation with Trizol following DNaseI digest and RT-qPCR to analyze the purified RNA. The remaining 80 µl beads were mixed with 4x SDS loading dye and used for Western blot as described above.

Mango purification

Enrichment of nuclear mRNAs was performed with TAP buffer containing KCl instead of NaCL to allow the Mango aptamer to form properly. The TEV eluate was mixed with 5 µl TO1-Dtb and incubated for 1h at 4°C in the dark. After, 100 µl prewashed M280 Streptavidine Dynabeads were added and the binding could take place for 15 min at RT. The beads were washed five times with 1 ml 15 mM HEPES-KOH pH 7.5, 150 mM KCl, 1 mM DTT, and 0.05 % Tween-20. For elution the beads were divided and 20 µl used for RNA isolation and 80 µl for protein analysis as described above.

MS2 purification

After enrichment of nuclear mRNPs as described above, 200 µl of TEV eluate were mixed with 25 µl magnetic amylose beads and incubated for 1 h at 4°C on a turning wheel. The bead were washed five times with 1 ml TAP buffer and incubated with 100 µl maltose elution buffer for 30 min at 4°C. The elution was removed from the beads and 20 µl were used for RNA isolation and 80 µl for protein analysis as described above.

EM Analysis of transcript-specific nuclear mRNPs

Purification of the mRNPs for EM was performed by Nataliia Stefanyshena and grid preparation and imaging was performed by myself together with our collaborators. The ASO EM pictures were taken in collaboration with Dr. Gärtner form the Institute for Anatomy and Cell biology (Universität Gießen). For negative staining ammoniumheptamolybdat was used. The Zeiss EM900 was used for imaging. MS2 EM pictures were taken in collaboration with Janett Piesker from the Max Planck Institute for Heart and Lung Research, Bad Nauheim. Grids were pretreated with 1 % alcian blue and 1 % acetic acid and negative staining was performed with 1 % uranyl acetate.

Purification of cross-linked transcript specific mRNPs using the RAP method

For the purification of cross-linked nuclear mRNPs, cells from 2 l yeast culture were heat shocked for 15 min and cross-linked with 0.05 or 0.075 % glutaraldehyde at 42°C for 10 min. To each culture, 25 ml 3 M glycine was added for 10 min before harvesting, flash freezing and cryomilling of the samples. After the cells were lysed, nuclear mRNPs were enriched as described above but with addition of DNaseI to the lysis buffer.
For purification of a specific mRNA and the cross-linked proteins the RAP protocol from the Guttman lab [McHugh and Guttman, 2018] was used. For the purification biotinylated 90mer DNA ASOs were used which cover the whole mRNA sequence. For binding 200 µl 2x RAP Hybridization buffer was mixed with 200 µl TEV eluate and 2.4 µl of a 0.7 $\frac{g}{l}$ASO mix and incubated for 2 h at 67°C with interval shaking for 30 sec at 1100 rpm if not indicated otherwise. For each sample, 100 µl prewashed M280 Streptavidin Dynabeads beads were added and incubated for 30 min at 67°C with interval shaking. Afterwards, the beads were washed 5 times with 750 µl 1x RAP Hybridization buffer. For elution 50 µl beads were used for RNA isolation, resuspended in 50 µl NLS elution buffer, and incubated for 2 min at 95°C. The eluate was removed from the beads and proteins were digested by adding 2.5 µl Proteinase K and incubation at 52°C for 1 h.
The remaining beads were reuspended in 500 µl 10 mM HEPES-KOH pH 7.5 15 mM NaCl and incubation with RNase-Mix for 1 h at 4°C to elute the proteins from the beads. The eluate was concentrated using a AmiconUltra 0.5 3K at 14000 xg for 30 min at 4°C. After addition of 400 µl 50 mM NaCl the sample was concentrated once again. The sample was used for Western blotting of cross-linked proteins or normal Western blot.
For further analysis by mass spectrometry, the proteins were precipitated with 100 % ethanol overnight. After centrifugation for 1 h at 15000 rpm at 4°C, the supernatant was removed and the dry protein analyzed by the group of Prof. Dr. Lochnit from the Universität Gießen using trypsin digest and MALDI-TOF.

Phosphorproteome

For each sample, 400 ml yeast culture was harvest either untreated or following stress treatment as indicated. The cells were resuspended in 1 ml RNA IP buffer containing protease inhibitor and phosphatase inhibitor (PhosStop, Roche) and lysed using a FastPrep-24 5G machine (3 times for 20 sec at 6 m/s). The lysate was cleared by sequential centrifugation steps at 4000 rpm and 13000 rpm, re-

spectively, for 5 min at 4°C. The phosphoproteome analysis was performed by the lab of Prof. Johannes Graumann, Ph.D. (Universität Marburg), then still located at the Max Planck Institute for Heart and Lung Research, Bad Nauheim. For each condition and replicate lysate equating to 1 mg total protein content was processed as described [Dietze et al., 2021] up to isobaric labeling using tandem mass tags (TMT; Thermo Fisher Scientific) and mixing of the isotopically labeled channels into a single sample. While proteome characterization followed the workflow cited above, phosphorylated peptides were enriched using a High Select Re-NTA Phosphopeptide Enrichment Kit (Thermo Fisher Scientific). Half of the resulting peptide sample was further fractionationated into eight fractions using Pierce' High pH Reversed-Phase Peptide Fractionation Kit (Thermo Fischer Scientific). Mass spectrometric and data analytic processing of proteome (8 high ph RP fractions) and phosphoproteome samples (unfractionated as well as eight high pH fractionated fractions) followed again [Dietze et al., 2021]. The generated data can be found on the enclosed CD.

Bibliography

M. Abe, H. Qadota, A. Hirata, and Y. Ohya. Lack of GTP-bound Rho1p in secretory vesicles of *Saccharomyces cerevisiae*. *Journal of Cell Biology*, 162(1), 2003. ISSN 00219525. doi: 10.1083/jcb.200301022.

R. L. Adams and S. R. Wente. Dbp5 associates with RNA-bound Mex67 and Nab2 and its localization at the nuclear pore complex is sufficient for mRNP export and cell viability. *PLoS Genetics*, 16(10), oct 2020. ISSN 15537404. doi: 10.1371/journal.pgen.1009033.

D. Ahmadpour, E. Maciaszczyk-Dziubinska, R. Babazadeh, S. Dahal, M. Migocka, M. Andersson, R. Wysocki, M. J. Tamás, and S. Hohmann. The mitogen-activated protein kinase Slt2 modulates arsenite transport through the aquaglyceroporin Fps1. *FEBS Letters*, 590(20), 2016. ISSN 18733468. doi: 10.1002/1873-3468.12390.

S. Aibara, J. M. Gordon, A. S. Riesterer, S. H. McLaughlin, and M. Stewart. Structural basis for the dimerization of Nab2 generated by RNA binding provides insight into its contribution to both poly(A) tail length determination and transcript compaction in *Saccharomyces cerevisiae*. *Nucleic Acids Research*, 45 (3):1529–1538, feb 2017. ISSN 13624962. doi: 10.1093/nar/gkw1224.

J. D. Aitchison, G. Blobel, and M. P. Rout. Kap104p: A Karyopherin Involved in the Nuclear Transport of Messenger RNA Binding Proteins. *Science*, 274(5287): 624–627, oct 1996. doi: 10.1126/science.274.5287.624.

F. Alber, S. Dokudovskaya, L. M. Veenhoff, W. Zhang, J. Kipper, D. Devos, A. Suprapto, O. Karni-Schmidt, R. Williams, B. T. Chait, A. Sali, and M. P. Rout. The molecular architecture of the nuclear pore complex. *Nature*, 450 (7170), 2007. ISSN 14764687. doi: 10.1038/nature06405.

E. Alonso-Rodríguez, P. Fernández-Piñar, A. Sacristán-Reviriego, M. Molina, and H. Martín. An analog-sensitive version of the protein kinase Slt2 allows identification of novel targets of the yeast cell wall integrity pathway. *Journal of Biological Chemistry*, 291(11):5461–5472, 2016. ISSN 1083351X. doi: 10.1074/jbc.M115.683680.

J. Amin, J. Ananthan, and R. Voellmy. Key features of heat shock regulatory elements. *Molecular and Cellular Biology*, 8(9), 1988. ISSN 0270-7306. doi: 10.1128/mcb.8.9.3761.

M. Amorós and F. Estruch. Hsf1p and Msn2/4p cooperate in the expression of Saccharomyces cerevisiae genes HSP26 and HSP104 in a gene- and stress type-dependent manner. *Molecular Microbiology*, 39(6), 2001. ISSN 0950382X. doi: 10.1046/j.1365-2958.2001.02339.x.

P. R. Andersen, M. Domanski, M. S. Kristiansen, H. Storvall, E. Ntini, C. Verheggen, A. Schein, J. Bunkenborg, I. Poser, M. Hallais, R. Sandberg, A. Hyman,

J. Lacava, M. P. Rout, J. S. Andersen, E. Bertrand, and T. H. Jensen. The human cap-binding complex is functionally connected to the nuclear RNA exosome. *Nature Structural and Molecular Biology*, 20(12), 2013. ISSN 15459993. doi: 10.1038/nsmb.2703.

J. T. Anderson, S. M. Wilson, K. V. Datar, and M. S. Swanson. NAB2: a yeast nuclear polyadenylated RNA-binding protein essential for cell viability. *Molecular and Cellular Biology*, 13(5), 1993. ISSN 0270-7306. doi: 10.1128/mcb.13.5.2730.

J. P. Aris and G. Blobel. Isolation of yeast nuclei. *Methods in Enzymology*, 194 (C), 1991. ISSN 15577988. doi: 10.1016/0076-6879(91)94056-I.

A. Autour, S. C. Jeng, A. D. Cawte, A. Abdolahzadeh, A. Galli, S. S. Panchapakesan, D. Rueda, M. Ryckelynck, and P. J. Unrau. Fluorogenic RNA Mango aptamers for imaging small non-coding RNAs in mammalian cells. *Nature Communications*, 9(1), 2018. ISSN 20411723. doi: 10.1038/s41467-018-02993-8.

M. Backlund, F. Stein, M. Rettel, T. Schwarzl, J. I. Perez-Perri, A. Brosig, Y. Zhou, G. Neu-Yilik, M. W. Hentze, and A. E. Kulozik. Plasticity of nuclear and cytoplasmic stress responses of RNA-binding proteins. *Nucleic Acids Research*, 48(9):4725–4740, may 2020. ISSN 13624962. doi: 10.1093/nar/gkaa256.

C. Baierlein and H. Krebber. *Analysen des SR-Proteins Npl3 in der Translation und Charakterisierung von SR-Domänen-vermittelten Protein-Interaktionen von Npl3*. PhD thesis, Philipps-Universität Marburg, Marburg, 2013.

P. Bangs, B. Burke, C. Powers, R. Craig, A. Purohit, and S. Doxsey. Functional analysis of Tpr: Identification of nuclear pore complex association and nuclear localization domains and a role in mRNA export. *Journal of Cell Biology*, 143 (7), 1998. ISSN 00219525. doi: 10.1083/jcb.143.7.1801.

J. Batisse, C. Batisse, A. Budd, B. Böttcher, and E. Hurt. Purification of nuclear poly(A)-binding protein Nab2 reveals association with the yeast transcriptome and a messenger ribonucleoprotein core structure. *The Journal of biological chemistry*, 284(50):34911–7, dec 2009. doi: 10.1074/jbc.M109.062034.

M. Beck and E. Hurt. The nuclear pore complex: Understanding its function through structural insight. *Nature Reviews Molecular Cell Biology*, 18(2):73–89, 2017. ISSN 14710080. doi: 10.1038/nrm.2016.147.

B. M. Beckmann. RNA interactome capture in yeast. *Methods*, 118-119, 2017. ISSN 10959130. doi: 10.1016/j.ymeth.2016.12.008.

E. Bertrand, P. Chartrand, M. Schaefer, S. M. Shenoy, R. H. Singer, and R. M. Long. Localization of ASH1 mRNA particles in living yeast. *Molecular Cell*, 2 (4), 1998. ISSN 10972765. doi: 10.1016/S1097-2765(00)80143-4.

W. R. Boorstein and E. A. Craig. Structure and regulation of the SSA4 HSP70 gene of Saccharomyces cerevisiae. *Journal of Biological Chemistry*, 265(31): 18912–18921, 1990. ISSN 00219258. doi: 10.1016/s0021-9258(17)30603-8.

E. Boy-Marcotte, M. Perrot, F. Bussereau, H. Boucherie, and M. Jacquet. Msn2p and Msn4p control a large number of genes induced at the diauxic transition which are repressed by cyclic AMP in Saccharomyces cerevisiae. *Journal of Bacteriology*, 180(5), 1998. ISSN 00219193. doi: 10.1128/jb.180.5.1044-1052.1998.

E. Boy-Marcotte, G. Lagniel, M. Perrot, F. Bussereau, A. Boudsocq, M. Jacquet, and J. Labarre. The heat shock response in yeast: Differential regulations and contributions of the Msn2p/Msn4p and Hsf1p regulons. *Molecular Microbiology*, 33(2):274–283, 1999. ISSN 0950382X. doi: 10.1046/j.1365-2958.1999.01467.x.

S. Bresson, V. Shchepachev, C. Spanos, T. W. Turowski, J. Rappsilber, and D. Tollervey. Stress-Induced Translation Inhibition through Rapid Displacement of Scanning Initiation Factors. *Molecular Cell*, 80(3), 2020. ISSN 10974164. doi: 10.1016/j.molcel.2020.09.021.

H. Bretes, J. O. Rouviere, T. Leger, M. Oeffinger, F. Devaux, V. Doye, and B. Palancade. Sumoylation of the THO complex regulates the biogenesis of a subset of mRNPs. *Nucleic Acids Research*, 42(8):5343–5358, 2014. ISSN 13624962. doi: 10.1093/nar/gku124.

C. E. Brown and A. B. Sachs. Poly(A) Tail Length Control in *Saccharomyces cerevisiae* Occurs by Message-Specific Deadenylation. *Molecular and Cellular Biology*, 18(11), 1998. ISSN 0270-7306. doi: 10.1128/mcb.18.11.6548.

J. R. Buchan, D. Muhlrad, and R. Parker. P bodies promote stress granule assembly in Saccharomyces cerevisiae. *Journal of Cell Biology*, 183(3), 2008. ISSN 00219525. doi: 10.1083/jcb.200807043.

M. E. Bucheli and S. Buratowski. Npl3 is an antagonist of mRNA 3' end formation by RNA polymerase II. *The EMBO Journal*, 24(12), 2005. ISSN 02614189. doi: 10.1038/sj.emboj.7600687.

K. P. Byrne and K. H. Wolfe. The Yeast Gene Order Browser: Combining curated homology and syntenic context reveals gene fate in polyploid species. *Genome Research*, 15(10), 2005. ISSN 10889051. doi: 10.1101/gr.3672305.

S. R. Carmody, E. J. Tran, L. H. Apponi, A. H. Corbett, and S. R. Wente. The Mitogen-Activated Protein Kinase Slt2 Regulates Nuclear Retention of Non-Heat Shock mRNAs during Heat Shock-Induced Stress. *Molecular and Cellular Biology*, 30(21):5168–5179, 2010. ISSN 0270-7306. doi: 10.1128/mcb.00735-10.

A. Casañal, A. Kumar, C. H. Hill, A. D. Easter, P. Emsley, G. Degliesposti, Y. Gordiyenko, B. Santhanam, J. Wolf, K. Wiederhold, G. L. Dornan, M. Skehel, C. V. Robinson, and L. A. Passmore. Architecture of eukaryotic mRNA 3'-end processing machinery. *Science*, 358:1056–1059, 2017.

L. M. Castelli, D. Talavera, C. J. Kershaw, S. S. Mohammad-Qureshi, J. L. Costello, W. Rowe, P. F. Sims, C. M. Grant, S. J. Hubbard, M. P. Ashe, and G. D. Pavitt. The 4E-BP Caf20p Mediates Both eIF4E-Dependent and Independent Repression of Translation. *PLoS Genetics*, 11(5), 2015. ISSN 15537404. doi: 10.1371/journal.pgen.1005233.

T. R. Cech. The chemistry of self-splicing RNA and RNA enzymes. *Science*, 236 (4808), 1987. ISSN 00368075. doi: 10.1126/science.2438771.

S. Chavez and A. Aguilera. The yeast HPR1 gene has a functional role in transcriptional elongation that uncovers a novel source of genome instability. *Genes and Development*, 11(24), 1997. ISSN 08909369. doi: 10.1101/gad.11.24.3459.

S. Chavez, T. Beilharz, A. G. Rondon, H. Erdjument-Bromage, P. Tempst, J. Q. Svejstrup, T. Lithgow, and A. Aguilera. A protein complex containing Tho2, Hpr1, Mft1 and a novel protein, Thp2, connects transcription elongation with mitotic recombination in *Saccharomyces cerevisiae*. *The EMBO Journal*, 19(21), 2000. ISSN 02614189. doi: 10.1093/emboj/19.21.5824.

S. Chavez, M. Garcia-Rubio, F. Prado, and A. Aguilera. Hpr1 Is Preferentially Required for Transcription of Either Long or G+C-Rich DNA Sequences in *Saccharomyces cerevisiae*. *Molecular and Cellular Biology*, 21(20), 2001. ISSN 0270-7306. doi: 10.1128/mcb.21.20.7054-7064.2001.

C. Chen, M. Tan, Z. Wu, Y. Zhang, F. He, Y. Lu, S. Li, M. Cao, G. Li, J. Wu, H. Cheng, and M. Lei. Structural and functional insights into R-loop prevention and mRNA export by budding yeast THO-Sub2 complex. *Science Bulletin*, 66 (23), 2021. ISSN 20959281. doi: 10.1016/j.scib.2021.08.004.

S. H. Chen, C. P. Albuquerque, J. Liang, R. T. Suhandynata, and H. Zhou. A proteome-wide analysis of kinase-substrate network in the DNA damage response. *Journal of Biological Chemistry*, 285(17), 2010. ISSN 00219258. doi: 10.1074/jbc.M110.106989.

V. Cherkasov, T. Grousl, P. Theer, Y. Vainshtein, C. Gläßer, C. Mongis, G. Kramer, G. Stoecklin, M. Knop, A. Mogk, and B. Bukau. Systemic control of protein synthesis through sequestration of translation and ribosome biogenesis factors during severe heat stress. *FEBS Letters*, 589(23), 2015. ISSN 18733468. doi: 10.1016/j.febslet.2015.10.010.

E. J. Cho, T. Takagi, C. R. Moore, and S. Buratowski. mRNA capping enzyme is recruited to the transcription complex by phosphorylation of the RNA polymerase II carboxy-terminal domain. *Genes and Development*, 11(24), 1997. ISSN 08909369. doi: 10.1101/gad.11.24.3319.

E. J. Cho, C. R. Rodriguez, T. Takagi, and S. Buratowski. Allosteric interactions between capping enzyme subunits and the RNA polymerase II. Carboxy-terminal domain. *Genes and Development*, 12(22), 1998. ISSN 08909369. doi: 10.1101/gad.12.22.3482.

Christine A. Hodge, Hildur V. Colot, Phillip Stafford, and Charles N.Cole. Rat8p/Dbp5p is a shuttling transport factor that interacts with Rat7p/Nup159p and Gle1p and suppresses the mRNA export defect ofxpo1-1cells. *The EMBO Journal*, 18(20):5778–5788, 1999.

C. Chu, K. Qu, F. Zhong, S. Artandi, and H. Chang. Genomic Maps of Long Noncoding RNA Occupancy Reveal Principles of RNA-Chromatin Interactions. *Molecular Cell*, 44(4):667–678, nov 2011. ISSN 10972765. doi: 10.1016/j.molcel.2011.08.027.

C. Chu, J. Quinn, and H. Y. Chang. Chromatin isolation by RNA purification (ChIRP). *Journal of visualized experiments : JoVE*, (61), 2012. ISSN 1940087X. doi: 10.3791/3912.

C. Chu, Q. C. Zhang, S. T. da Rocha, R. A. Flynn, M. Bharadwaj, J. M. Calabrese, T. Magnuson, E. Heard, and H. Y. Chang. Systematic discovery of Xist RNA binding proteins. *Cell*, 161(2):404–416, apr 2015. ISSN 10974172. doi: 10.1016/j.cell.2015.03.025.

R. Collins, T. Karlberg, L. Lehtiö, P. Schütz, S. van den Berg, L. G. Dahlgren, M. Hammarström, J. Weigelt, and H. Schüler. The DEXD/H-box RNA helicase DDX19 is regulated by an α-helical switch. *Journal of Biological Chemistry*, 284 (16), 2009. ISSN 00219258. doi: 10.1074/jbc.C900018200.

J. L. Corden, D. L. Cadena, J. M. Ahearn, and M. E. Dahmus. A unique structure at the carboxyl terminus of the largest subunit of eukaryotic RNA polymerase II. *Proceedings of the National Academy of Sciences of the United States of America*, 82(23), 1985. ISSN 00278424. doi: 10.1073/pnas.82.23.7934.

P. A. Delley and M. N. Hall. Cell wall stress depolarizes cell growth via hyperactivation of RHO1. *Journal of Cell Biology*, 147(1), 1999. ISSN 00219525. doi: 10.1083/jcb.147.1.163.

J. L. Dermody, J. M. Dreyfuss, J. Villén, B. Ogundipe, S. P. Gygi, P. J. Park, A. S. Ponticelli, C. L. Moore, S. Buratowski, and M. E. Bucheli. Unphosphorylated SR-like protein Npl3 stimulates RNA polymerase II elongation. *PLoS ONE*, 3 (9), sep 2008. ISSN 19326203. doi: 10.1371/journal.pone.0003273.

C. P. Derrer, R. Mancini, P. Vallotton, S. Huet, K. Weis, and E. Dultz. The RNA export factor Mex67 functions as a mobile nucleoporin. *Journal of Cell Biology*, 218(12):3967–3976, dec 2019. ISSN 15408140. doi: 10.1083/JCB.201909028.

R. Dietze, M. K. Hammoud, M. Gómez-Serrano, A. Unger, T. Bieringer, F. Finkernagel, A. M. Sokol, A. Nist, T. Stiewe, S. Reinartz, V. Ponath, C. Preußer, E. P. Von Strandmann, S. Müller-Brüsselbach, J. Graumann, and R. Müller. Phosphoproteomics identify arachidonic-acid-regulated signal transduction pathways modulating macrophage functions with implications for ovarian cancer. *Theranostics*, 11(3), 2021. ISSN 18387640. doi: 10.7150/thno.52442.

E. V. Dolgosheina, S. C. Jeng, S. S. S. Panchapakesan, R. Cojocaru, P. S. Chen, P. D. Wilson, N. Hawkins, P. A. Wiggins, and P. J. Unrau. RNA Mango aptamer-fluorophore: A bright, high-affinity complex for RNA labeling and tracking. *ACS Chemical Biology*, 9(10), 2014. ISSN 15548937. doi: 10.1021/cb500499x.

G. Dollenmaier and M. Weitz. Interaction of glyceraldehyde-3-phosphate dehydrogenase with secondary and tertiary RNA structural elements of the hepatitis A virus 3' translated and non-translated regions, 2003. ISSN 00221317.

M. S. Domínguez-Sánchez, S. Barroso, B. Gómez-González, R. Luna, and A. Aguilera. Genome instability and transcription elongation impairment in human cells

depleted of THO/TREX. *PLoS Genetics*, 7(12), 2011. ISSN 15537390. doi: 10.1371/journal.pgen.1002386.

H. Donis-Keller. Site specific enzymatic cleavage of RNA. *Nucleic Acids Research*, 7(1), 1979. ISSN 03051048. doi: 10.1093/nar/7.1.179.

Y. Du, L. Walker, P. Novick, and S. Ferro-Novick. Ptc1p regulates cortical ER inheritance via Slt2p. *The EMBO Journal*, 25(19), 2006. ISSN 02614189. doi: 10.1038/sj.emboj.7601319.

F. Estruch and C. N. Cole. An early function during transcription for the yeast mRNA export factor Dbp5p/Rat8p suggested by its genetic and physical interactions with transcription factor IIH components. *Molecular Biology of the Cell*, 14:1664–1676, 2003. doi: 10.1091/mbc.e02-09-0602.

C. Fabrega, V. Shen, S. Shuman, and C. D. Lima. Structure of an mRNA capping enzyme bound to the phosphorylated carboxy-terminal domain of RNA polymerase II. *Molecular Cell*, 11(6), 2003. ISSN 10972765. doi: 10.1016/S1097-2765(03)00187-4.

H.-Y. Fan, R. J. Merker, and H. L. Klein. High-Copy-Number Expression of Sub2p, a Member of the RNA Helicase Superfamily, Suppresses hpr1 -Mediated Genomic Instability. *Molecular and Cellular Biology*, 21(16), 2001. ISSN 0270-7306. doi: 10.1128/mcb.21.16.5459-5470.2001.

M. B. Fasken, M. Stewart, and A. H. Corbett. Functional significance of the interaction between the mRNA-binding protein, Nab2, and the nuclear pore-associated protein, mlp1, in mRNA export. *Journal of Biological Chemistry*, 283(40), 2008. ISSN 00219258. doi: 10.1074/jbc.M803649200.

T. Fischer, K. Sträßer, A. Rácz, S. Rodriguez-Navarro, M. Oppizzi, P. Ihrig, J. Lechner, and E. Hurt. The mRNA export machinery requires the novel Sac3p-Thp1p complex to dock at the nucleoplasmic entrance of the nuclear pores. *The EMBO Journal*, 21(21), 2002. ISSN 02614189. doi: 10.1093/emboj/cdf590.

T. Fischer, S. Rodríguez-Navarro, G. Pereira, A. Rácz, E. Schiebel, and E. Hurt. Yeast centrin Cdc31 is linked to the nuclear mRNA export machinery. *Nature Cell Biology*, 6(9), 2004. ISSN 14657392. doi: 10.1038/ncb1163.

S. M. Flaherty, P. Fortes, E. Izaurralde, I. W. Mattaj, and G. M. Gilmartin. Participation of the nuclear cap binding complex in pre-mRNA 3' processing. *Proceedings of the National Academy of Sciences of the United States of America*, 94(22), 1997. ISSN 00278424. doi: 10.1073/pnas.94.22.11893.

J. Fleckner, M. Zhang, J. Valcircel, and M. R. Green. U2AF 6s recruits a novel human DEAD box protein required for the U2 snRNP-branchpoint interaction. *Genes and Development*, 11:1864–1872, 1997. doi: 10.1101/gad.11.14.1864.

P. Fortes, T. Inada, T. Preiss, M. W. Hentze, I. W. Mattaj, and A. B. Sachs. The yeast nuclear cap binding complex can interact with translation factor eIF4G and mediate translation initiation. *Molecular Cell*, 6(1), 2000. ISSN 10972765. doi: 10.1016/S1097-2765(05)00003-1.

T. Fujiwara, K. Tanaka, A. Mino, M. Kikyo, K. Takahashi, K. Shimizu, and Y. Takai. Rho1p-Bni1p-Spa2p interactions: Implication in localization of Bni1p at the bud site and regulation of the actin cytoskeleton in Saccharomyces cerevisiae. *Molecular Biology of the Cell*, 9(5), 1998. ISSN 10591524. doi: 10.1091/mbc.9.5.1221.

Y. Furuichi, A. LaFiandra, and A. J. Shatkin. 5'-Terminal structure and mRNA stability. *Nature*, 266(5599), 1977. ISSN 00280836. doi: 10.1038/266235a0.

M. Gallardo, R. Luna, H. Erdjument-Bromage, P. Tempst, and A. Aguilera. Nab2p and the Thp1p-Sac3p complex functionally interact at the interface between transcription and mRNA metabolism. *Journal of Biological Chemistry*, 278(26): 24225–24232, jul 2003. ISSN 00219258. doi: 10.1074/jbc.M302900200.

P. Gallardo, P. Real-Calderón, I. Flor-Parra, S. Salas-Pino, and R. R. Daga. Acute Heat Stress Leads to Reversible Aggregation of Nuclear Proteins into Nucleolar Rings in Fission Yeast. *Cell Reports*, 33(6), 2020. ISSN 22111247. doi: 10.1016/j.celrep.2020.108377.

V. Galy, O. Gadal, M. Fromont-Racine, A. Romano, A. Jacquier, and U. Nehrbass. Nuclear Retention of Unspliced mRNAs in Yeast Is Mediated by Perinuclear Mlp1. *Cell*, 116(1), 2004. ISSN 00928674. doi: 10.1016/S0092-8674(03)01026-2.

H. Garreau, R. N. Hasan, G. Renault, F. Estruch, E. Boy-Marcotte, and M. Jacquet. Hyperphosphorylation of Msn2p and Msn4p in response to heat shock and the diauxic shift is inhibited by cAMP in *Saccharomyces cerevisiae*. *Microbiology*, 146(9), 2000. ISSN 13500872. doi: 10.1099/00221287-146-9-2113.

W. Gilbert and C. Guthrie. The Glc7p Nuclear Phosphatase Promotes mRNA Export by Facilitating Association of Mex67p with mRNA export in S. cerevisiae and for viral RNA export in HIV-infected cells, indicated that a similar mechanism could direct messenger RNA export (for review see Fornerod and Ohno, 2002, and references therein). However, sub-sequent work suggests that the role of Xpo1/Crm1p in. Technical report, 2004.

W. Gilbert, C. W. Siebel, and C. Guthrie. Phosphorylation by Sky1p promotes Npl3p shuttling and mRNA dissociation. *RNA*, 7(2):302–313, feb 2001. doi: 10.1017/s1355838201002369.

J. S. Glavy, A. N. Krutchinsky, I. M. Cristea, I. C. Berke, T. Boehmer, G. Blobel, and B. T. Chait. Cell-cycle-dependent phosphorylation of the nuclear pore Nup107-160 subcomplex. *Proceedings of the National Academy of Sciences of the United States of America*, 104(10), 2007. ISSN 00278424. doi: 10.1073/pnas.0700058104.

J. R. Glover and S. Lindquist. Hsp104, Hsp70, and Hsp40: A novel chaperone system that rescues previously aggregated proteins. *Cell*, 94(1), 1998. ISSN 00928674. doi: 10.1016/S0092-8674(00)81223-4.

G. González-Rubio, Á. Sellers-Moya, H. Martín, and M. Molina. Differential role of threonine and tyrosine phosphorylation in the activation and activity of the

yeast MAPK Slt2. *International Journal of Molecular Sciences*, 22(3), 2021. ISSN 14220067. doi: 10.3390/ijms22031110.

W. Görner, E. Durchschlag, M. T. Martinez-Pastor, F. Estruch, G. Ammerer, B. Hamilton, H. Ruis, and C. Schüller. Nuclear localization of the C2H2 zinc finger protein Msn2p is regulated by stress and protein kinase A activity. *Genes and Development*, 12(4):586–597, 1998. ISSN 08909369. doi: 10.1101/gad.12.4.586.

O. Gozani, J. Potashkin, and R. Reed. A Potential Role for U2AF-SAP 155 Interactions in Recruiting U2 snRNP to the Branch Site. *Molecular and Cellular Biology*, 18(8), 1998. ISSN 0270-7306. doi: 10.1128/mcb.18.8.4752.

R. P. Grant, E. Hurt, D. Neuhaus, and M. Stewart. Structure of the C-terminal FG-nucleoporin binding domain of Tap/NXF1. *Nature Structural Biology*, 9(4), 2002. ISSN 10728368. doi: 10.1038/nsb773.

R. P. Grant, N. J. Marshall, J. C. Yang, M. B. Fasken, S. M. Kelly, M. T. Harreman, D. Neuhaus, A. H. Corbett, and M. Stewart. Structure of the N-Terminal Mlp1-Binding Domain of the Saccharomyces cerevisiae mRNA-Binding Protein, Nab2. *Journal of Molecular Biology*, 376(4), 2008. ISSN 00222836. doi: 10.1016/j.jmb.2007.11.087.

J. V. Gray, J. P. Ogas, Y. Kamada, M. Stone, D. E. Levin, and I. Herskowitz. A role for the Pkc1 MAP kinase pathway of *Saccharomyces cerevisiae* in bud emergence and identification of a putative upstream regulator. *The EMBO Journal*, 16(16), 1997. ISSN 02614189. doi: 10.1093/emboj/16.16.4924.

D. M. Green, C. P. Johnson, H. Hagan, and A. H. Corbett. The C-terminal domain of myosin-like protein 1 (Mlp1p) is a docking site for heterogeneous nuclear ribonucleoproteins that are required for mRNA export. *Proceedings of the National Academy of Sciences of the United States of America*, 100(3), 2003. ISSN 00278424. doi: 10.1073/pnas.0336594100.

A. M. Gromadzka, A. L. Steckelberg, K. K. Singh, K. Hofmann, and N. H. Gehring. A short conserved motif in ALYREF directs cap- and EJC-dependent assembly of export complexes on spliced mRNAs. *Nucleic Acids Research*, 44(5), 2016. ISSN 13624962. doi: 10.1093/nar/gkw009.

A. R. Gruber, R. Lorenz, S. H. Bernhart, R. N. Ck, and I. L. Hofacker. The Vienna RNA Websuite. *Nucleic Acids Research*, 36, 2008. doi: 10.1093/nar/gkn188.

D. Grünwald and R. H. Singer. In vivo imaging of labelled endogenous B-actin mRNA during nucleocytoplasmic transport. *Nature*, 467(7315), 2010. ISSN 00280836. doi: 10.1038/nature09438.

S. Guo, X. Shen, G. Yan, D. Ma, X. Bai, S. Li, and Y. Jiang. A MAP kinase dependent feedback mechanism controls Rho1 GTPase and actin distribution in yeast. *PLoS ONE*, 4(6), 2009. ISSN 19326203. doi: 10.1371/journal.pone.0006089.

W. Guo, F. Tamanoi, and P. Novick. Spatial regulation of the exocyst complex by Rho1 GTPase. *Nature Cell Biology*, 3(4), 2001. ISSN 14657392. doi: 10.1038/35070029.

C. Gwizdek, M. Hobeika, B. Kus, B. Ossareh-Nazari, C. Dargemont, and M. S. Rodriguez. The mRNA nuclear export factor Hpr1 is regulated by Rsp5-mediated ubiquitylation. *Journal of Biological Chemistry*, 280(14):13401–13405, apr 2005. ISSN 00219258. doi: 10.1074/jbc.C500040200.

C. Gwizdek, N. Iglesias, M. S. Rodriguez, B. Ossareh-Nazari, M. Hobeika, G. Divita, F. Stutz, and C. Dargemont. Ubiquitin-associated domain of Mex67 synchronizes recruitment of the mRNA export machinery with transcription. *PNAS*, 103(44):16376–16381, 2006.

A. Hackmann, H. Wu, U. M. Schneider, K. Meyer, K. Jung, and H. Krebber. Quality control of spliced mRNAs requires the shuttling SR proteins Gbp2 and Hrb1. *Nature communications*, 5:3123, 2014. ISSN 20411723. doi: 10.1038/ncomms4123.

M. Hafner, M. Landthaler, L. Burger, M. Khorshid, J. Hausser, P. Berninger, A. Rothballer, M. Ascano, A. C. Jungkamp, M. Munschauer, A. Ulrich, G. S. Wardle, S. Dewell, M. Zavolan, and T. Tuschl. PAR-CliP - A method to identify transcriptome-wide the binding sites of RNA binding proteins. *Journal of Visualized Experiments*, (41), 2010. ISSN 1940087X. doi: 10.3791/2034.

R. E. Hector, K. R. Nykamp, S. Dheur, J. T. Anderson, P. J. Non, C. R. Urbinati, S. M. Wilson, L. Minvielle-Sebastia, and M. S. Swanson. Dual requirement for yeast hnRNP Nab2p in mRNA poly(A) tail length control and nuclear export. *The EMBO Journal*, 21(7), 2002. ISSN 02614189. doi: 10.1093/emboj/21.7.1800.

S. Heinrich, M. Hondele, D. Marchand, C. P. Derrer, M. Zedan, A. Oswald, F. Uliana, R. Mancini, D. Grunwald, and K. Weis. Condensation of a nuclear mRNA export factor regulates mRNA transport during stress. doi: 10.1101/2022.01.30.478372.

J. D. Hirsch, L. Eslamizar, B. J. Filanoski, N. Malekzadeh, R. P. Haugland, J. M. Beechem, and R. P. Haugland. Easily reversible desthiobiotin binding to streptavidin, avidin, and other biotin-binding proteins: Uses for protein labeling, detection, and isolation. *Analytical Biochemistry*, 308(2), 2002. ISSN 00032697. doi: 10.1016/S0003-2697(02)00201-4.

L. J. Holt, B. B. Tuch, J. Villen, A. D. Johnson, S. P. Gygi, and D. O. Morgan. Global analysis of cdk1 substrate phosphorylation sites provides insiqhts into evolution. *Science*, 325(5948), 2009. ISSN 00368075. doi: 10.1126/science.1172867.

K. B. Hooks, D. Delneri, and S. Griffiths-Jones. Intron evolution in Saccharomycetaceae. *Genome Biology and Evolution*, 6(9), 2014. ISSN 17596653. doi: 10.1093/gbe/evu196.

D. Hopwood. The reactions of glutaraldehyde with nucleic acids. *The Histochemical Journal*, 7(3), 1975. ISSN 00182214. doi: 10.1007/BF01003595.

I. Horvathova, F. Voigt, A. V. Kotrys, Y. Zhan, C. G. Artus-Revel, J. Eglinger, M. B. Stadler, L. Giorgetti, and J. A. Chao. The Dynamics of mRNA Turnover Revealed by Single-Molecule Imaging in Single Cells. *Molecular Cell*, 68(3), 2017. ISSN 10974164. doi: 10.1016/j.molcel.2017.09.030.

A. Hubstenberger, M. Courel, M. Bénard, S. Souquere, M. Ernoult-Lange, R. Chouaib, Z. Yi, J. B. Morlot, A. Munier, M. Fradet, M. Daunesse, E. Bertrand, G. Pierron, J. Mozziconacci, M. Kress, and D. Weil. P-Body Purification Reveals the Condensation of Repressed mRNA Regulons. *Molecular Cell*, 68(1), 2017. ISSN 10974164. doi: 10.1016/j.molcel.2017.09.003.

I. Huppertz, J. I. Perez-Perri, P. Mantas, T. Sekaran, T. Schwarzl, F. Russo, D. Ferring-Appel, Z. Koskova, L. Dimitrova-Paternoga, E. Kafkia, J. Hennig, P. A. Neveu, K. Patil, and M. W. Hentze. Riboregulation of Enolase 1 activity controls glycolysis and embryonic stem cell differentiation. *Molecular Cell*, 82 (14):2666–2680.e11, jul 2022. ISSN 10974164. doi: 10.1016/j.molcel.2022.05.019.

E. Hurt, K. Sträßer, A. Segref, S. Bailer, N. Schlaich, C. Presutti, D. Tollervey, and R. Jansen. Mex67p Mediates Nuclear Export of a Variety of RNA Polymerase II Transcripts*. Technical report, 2000. doi: 10.1074/jbc.275.12.8361.

V. Iadevaia, M. D. Wouters, A. Kanitz, A. M. Matia-González, E. E. Laing, and A. P. Gerber. Tandem RNA isolation reveals functional rearrangement of RNA-binding proteins on CDKN1B/p27 Kip1 3'UTRs in cisplatin treated cells. *RNA Biology*, 17(1):33–46, 2020. doi: 10.1080/15476286.2019.1662268.

N. Iglesias, E. Tutucci, C. Gwizdek, P. Vinciguerra, E. Von Dach, A. H. Corbett, C. Dargemont, and F. Stutz. Ubiquitin-mediated mRNP dynamics and surveillance prior to budding yeast mRNA export. *Genes and Development*, 24(17): 1927–1938, sep 2010. ISSN 08909369. doi: 10.1101/gad.583310.

K. Irie, M. Takase, K. S. Lee, D. E. Levin, H. Araki, K. Matsumoto, and Y. Oshima. MKK1 and MKK2, which encode *Saccharomyces cerevisiae* mitogen-activated protein kinase-kinase homologs, function in the pathway mediated by protein kinase C. *Molecular and Cellular Biology*, 13(5), 1993. ISSN 0270-7306. doi: 10.1128/mcb.13.5.3076-3083.1993.

S. Izawa, T. Kita, K. Ikeda, and Y. Inoue. Heat shock and ethanol stress provoke distinctly different responses in 3'-processing and nuclear export of HSP mRNA in *Saccharomyces cerevisiae*. *Biochemical Journal*, 414(1):111–119, 2008. ISSN 02646021. doi: 10.1042/BJ20071567.

A. Jacewicz, L. Chico, P. Smith, B. Schwer, and S. Shuman. Structural basis for recognition of intron branchpoint RNA by yeast Msl5 and selective effects of interfacial mutations on splicing of yeast pre-mRNAs. *RNA*, 21(3), 2015. ISSN 14699001. doi: 10.1261/rna.048942.114.

J. J. Jacoby, S. M. Nilius, and J. J. Heinisch. A screen for upstream components of the yeast protein kinase C signal transduction pathway identifies the product of the SLG1 gene. *Molecular and General Genetics*, 258(1-2), 1998. ISSN 00268925. doi: 10.1007/s004380050717.

M. Jacquet, G. Renault, S. Lallet, J. De Mey, and A. Goldbeter. Oscillatory nucleocytoplasmic shuttling of the general stress response transcriptional activators Msn2 and Msn4 in Saccharomyces cerevisiae. *Journal of Cell Biology*, 161(3), 2003. ISSN 00219525. doi: 10.1083/jcb.200303030.

S. Jimeno, A. G. Rondón, R. Luna, and A. Aguilera. The yeast THO complex and mRNA export factors link RNA metabolism with transcription and genome instability. *The EMBO Journal*, 21(13), 2002. ISSN 02614189. doi: 10.1093/emboj/cdf335.

S. A. Johnson, G. Cubberley, and D. L. Bentley. Cotranscriptional Recruitment of the mRNA Export Factor Yra1 by Direct Interaction with the 3' End Processing Factor Pcf11. *Molecular Cell*, 33(2):215–226, jan 2009. ISSN 10972765. doi: 10.1016/j.molcel.2008.12.007.

U. S. Jung and D. E. Levin. Genome-wide analysis of gene expression regulated by the yeast cell wall integrity signalling pathway. *Molecular Microbiology*, 34 (5), 1999. ISSN 0950382X. doi: 10.1046/j.1365-2958.1999.01667.x.

Y. Kamada, H. Qadota, C. P. Python, Y. Anraku, Y. Ohya, and D. E. Levin. Activation of yeast protein kinase C by Rhol GTPase. *Journal of Biological Chemistry*, 271(16), 1996. ISSN 00219258. doi: 10.1074/jbc.271.16.9193.

N. Kedersha, S. Chen, N. Gilks, W. Li, I. J. Miller, J. Stahl, and P. Anderson. Evidence that ternary complex (eIF2-GTP-tRNAiMet)-Deficient preinitiation complexes are core constituents of mammalian stress granules. *Molecular Biology of the Cell*, 13(1), 2002. ISSN 10591524. doi: 10.1091/mbc.01-05-0221.

S. M. Kelly, S. W. Leung, L. H. Apponi, A. M. Bramley, E. J. Tran, J. A. Chekanova, S. R. Wente, and A. H. Corbett. Recognition of polyadenosine RNA by the zinc finger domain of nuclear poly(A) RNA-binding protein 2 (Nab2) is required for correct mRNA 3'-end formation. *Journal of Biological Chemistry*, 285(34), 2010. ISSN 00219258. doi: 10.1074/jbc.M110.141127.

T. Ketela, R. Green, and H. Bussey. *Saccharomyces cerevisiae* Mid2p is a potential cell wall stress sensor and upstream activator of the PKC1-MPK1 cell integrity pathway. *Journal of Bacteriology*, 181(11), 1999. ISSN 00219193. doi: 10.1128/jb.181.11.3330-3340.1999.

A. Khong, T. Matheny, S. Jain, S. F. Mitchell, J. R. Wheeler, and R. Parker. The Stress Granule Transcriptome Reveals Principles of mRNA Accumulation in Stress Granules. *Molecular Cell*, 68(4), 2017. ISSN 10974164. doi: 10.1016/j.molcel.2017.10.015.

E. Kiesler, F. Miralles, and N. Visa. HEL/UAP56 binds cotranscriptionally to the Balbiani ring pre-mRNA in an intron-independent manner and accompanies the BR mRNP to the nuclear pore. *Current Biology*, 12(10), 2002. ISSN 09609822. doi: 10.1016/S0960-9822(02)00840-0.

C. Kilchert, T. Kecman, E. Priest, S. Hester, E. Aydin, K. Kus, O. Rossbach, A. Castello, S. Mohammed, and L. Vasiljeva. System-wide analyses of the fission yeast poly(A)+RNA interactome reveal insights into organization and function

of RNA-protein complexes. *Genome Research*, 30(7), 2020. ISSN 15495469. doi: 10.1101/gr.257006.119.

K.-Y. Kim, A. W. Truman, and D. E. Levin. Yeast Mpk1 Mitogen-Activated Protein Kinase Activates Transcription through Swi4/Swi6 by a Noncatalytic Mechanism That Requires Upstream Signal. *Molecular and Cellular Biology*, 28 (8), 2008. ISSN 0270-7306. doi: 10.1128/mcb.01795-07.

S. Kim and D. S. Gross. Mediator recruitment to heat shock genes requires dual Hsf1 activation domains and Mediator tail subunits Med15 and Med16. *Journal of Biological Chemistry*, 288(17):12197–12213, 2013. ISSN 00219258. doi: 10.1074/jbc.M112.449553.

A. L. Kistler and C. Guthrie. Deletion of MUD2, the yeast homolog of U2AF65, can bypass the requirement for Sub2, an essential spliceosomal ATPase. *Genes and Development*, 15(1), 2001. ISSN 08909369. doi: 10.1101/gad.851301.

H. Kosako, N. Yamaguchi, C. Aranami, M. Ushiyama, S. Kose, N. Imamoto, H. Taniguchi, E. Nishida, and S. Hattori. Phosphoproteomics reveals new ERK MAP kinase targets and links ERK to nucleoporin-mediated nuclear transport. *Nature Structural and Molecular Biology*, 16(10):1026–1035, oct 2009. ISSN 15459993. doi: 10.1038/nsmb.1656.

H. Krebber, T. Taura, M. S. Lee, and P. A. Silver. Uncoupling of the hnRNP Npl3p from mRNAs during the stress-induced block in mRNA export. Technical report, 1999. doi: 10.1101/gad.13.15.1994.

T. L. Kress, N. J. Krogan, and C. Guthrie. A Single SR-like Protein, Npl3, Promotes Pre-mRNA Splicing in Budding Yeast. *Molecular Cell*, 32(5), 2008. ISSN 10972765. doi: 10.1016/j.molcel.2008.11.013.

S. Kroschwald, S. Maharana, D. Mateju, L. Malinovska, E. Nüske, I. Poser, D. Richter, and S. Alberti. Promiscuous interactions and protein disaggregases determine the material state of stress-inducible RNP granules. *eLife*, 4 (AUGUST2015), 2015. ISSN 2050084X. doi: 10.7554/eLife.06807.

D. R. Larson, D. Zenklusen, B. Wu, J. A. Chao, and R. H. Singer. Real-time observation of transcription initiation and elongation on an endogenous yeast gene. *Science*, 332(6028), 2011. ISSN 00368075. doi: 10.1126/science.1202142.

E. Laurell, K. Beck, K. Krupina, G. Theerthagiri, B. Bodenmiller, P. Horvath, R. Aebersold, W. Antonin, and U. Kutay. Phosphorylation of Nup98 by multiple kinases is crucial for NPC disassembly during mitotic entry. *Cell*, 144(4), 2011. ISSN 00928674. doi: 10.1016/j.cell.2011.01.012.

K. S. Lee and D. E. Levin. Dominant mutations in a gene encoding a putative protein kinase (BCK1) bypass the requirement for a *Saccharomyces cerevisiae* protein kinase C homolog. *Molecular and Cellular Biology*, 12(1), 1992. ISSN 0270-7306. doi: 10.1128/mcb.12.1.172.

K. S. Lee, K. Irie, Y. Gotoh, Y. Watanabe, H. Araki, E. Nishida, K. Matsumoto, and D. E. Levin. A yeast mitogen-activated protein kinase homolog (Mpk1p) mediates signalling by protein kinase C. *Molecular and Cellular Biology*, 13(5), 1993. ISSN 0270-7306. doi: 10.1128/mcb.13.5.3067-3075.1993.

K. Leppek and G. Stoecklin. An optimized streptavidin-binding RNA aptamer for purification of ribonucleoprotein complexes identifies novel ARE-binding proteins. *Nucleic Acids Research*, 42(2), 2014. ISSN 13624962. doi: 10.1093/nar/gkt956.

X. Li, Y. Du, S. Siegel, S. Ferro-Novick, and P. Novick. Activation of the mitogen-activated protein kinase, Slt2p, at bud tips blocks a late stage of endoplasmic reticulum inheritance in *Saccharomyces cerevisiae*. *Molecular Biology of the Cell*, 21(10), 2010. ISSN 10591524. doi: 10.1091/mbc.E09-06-0532.

S. H. Lillie and S. S. Brown. Immunofluorescence localization of the unconventional myosin, Myo2p, and the putative kinesin-related protein, Smy1p, to the same regions of polarized growth in *Saccharomyces cerevisiae*. *Journal of Cell Biology*, 125(4), 1994. ISSN 00219525. doi: 10.1083/jcb.125.4.825.

K. Lin, Q. Yan, A. Mitchell, N. Funk, C. Lu, and H. Xiao. A simple method for non-denaturing purification of biotin-tagged proteins through competitive elution with free biotin. *BioTechniques*, 68(1), 2019. ISSN 19409818. doi: 10.2144/btn-2019-0088.

D. L. Lindstrom, S. L. Squazzo, N. Muster, T. A. Burckin, K. C. Wachter, C. A. Emigh, J. A. McCleery, J. R. Yates, and G. A. Hartzog. Dual Roles for Spt5 in Pre-mRNA Processing and Transcription Elongation Revealed by Identification of Spt5-Associated Proteins. *Molecular and Cellular Biology*, 23(4), 2003. ISSN 0270-7306. doi: 10.1128/mcb.23.4.1368-1378.2003.

L. Liu and D. E. Levin. Intracellular mechanism by which genotoxic stress activates yeast SAPK Mpk1. *Molecular Biology of the Cell*, 29(23), 2018. ISSN 19394586. doi: 10.1091/mbc.E18-07-0441.

X. Liu, D. A. Bushnell, D. Wang, G. Calero, and R. D. Kornbergt. Structure of an RNA polymerase II-TFIIB complex and the transcription initiation mechanism. *Science*, 327(5962), 2010. ISSN 00368075. doi: 10.1126/science.1182015.

R. Lorenz, S. H. Bernhart, C. Höner Zu Siederdissen, H. Tafer, C. Flamm, P. F. Stadler, and I. L. Hofacker. ViennaRNA Package 2.0. Technical report, 2011.

M. K. Lund and C. Guthrie. The DEAD-box protein Dbp5p is required to dissociate Mex67p from exported mRNPs at the nuclear rim. *Molecular Cell*, 20(4): 645–651, nov 2005. ISSN 10972765. doi: 10.1016/j.molcel.2005.10.005.

M.-J. Luo, Z. Zhou, K. Magni, C. Christoforides, J. Rappsilber[2], M. Mann[2], and R. Reed. Pre-mRNA splicing and mRNA export linked by direct interactions between UAP56 and Aly. Technical report, 2001. doi: 10.1038/35098106.

M. E. MacGilvray, E. Shishkova, D. Chasman, M. Place, A. Gitter, J. J. Coon, and A. P. Gasch. Network inference reveals novel connections in pathways regulating growth and defense in the yeast salt response. *PLoS Computational Biology*, 14 (5), may 2018. ISSN 15537358. doi: 10.1371/journal.pcbi.1006088.

X. Mao, B. Schwer, and S. Shuman. Yeast mRNA cap methyltransferase is a 50-kilodalton protein encoded by an essential gene. *Molecular and Cellular Biology*, 15(8), 1995. ISSN 00225282. doi: 10.1128/MCB.15.8.4167.

G. Marchler, C. Schuller, G. Adam, and H. Ruis. A *Saccharomyces cerevisiae* UAS element controlled by protein kinase A activates transcription in response to a variety of stress conditions. *The EMBO Journal*, 12(5), 1993. ISSN 02614189. doi: 10.1002/j.1460-2075.1993.tb05849.x.

K. A. Marfatia, E. B. Crafton, D. M. Green, and A. H. Corbett. Domain Analysis of the *Saccharomyces cerevisiae* Heterogeneous Nuclear Ribonucleoprotein, Nab2p. *Journal of Biological Chemistry*, 278(9), 2003. ISSN 00219258. doi: 10.1074/jbc.m207571200.

H. Martin, J. Arroyo, M. Sánchez, M. Molina, and C. Nombela. Activity of the yeast MAP kinase homologue Slt2 is critically required for cell integrity at 37° C. *MGG Molecular and General Genetics*, 241(1-2), 1993. ISSN 00268925. doi: 10.1007/BF00280215.

H. Martín, J. M. Rodríguez-Pachón, C. Ruiz, C. Nombela, and M. Molina. Regulatory mechanisms for modulation of signaling through the cell integrity Slt2-mediated pathway in *Saccharomyces cerevisiae*. *Journal of Biological Chemistry*, 275(2), 2000. ISSN 00219258. doi: 10.1074/jbc.275.2.1511.

M. T. Martínez-Pastor, G. Marchler, C. Schüller, A. Marchler-Bauer, H. Ruis, and F. Estruch. The *Saccharomyces cerevisiae* zinc finger proteins Msn2p and Msn4p are required for transcriptional induction through the stress-response element (STRE). *The EMBO Journal*, 15(9), 1996. ISSN 02614189. doi: 10.1002/j.1460-2075.1996.tb00576.x.

V. Mascaraque, M. L. Hernaez, M. Jimenez-Sanchez, R. Hansen, C. Gil, H. Martín, V. J. Cid, and M. Molina. Phosphoproteomic analysis of protein kinase c signaling in *Saccharomyces cerevisiae* reveals Slt2 mitogen-activated protein kinase (mapk)-dependent phosphorylation of eisosome core components. *Molecular and Cellular Proteomics*, 12(3):557–574, mar 2013. ISSN 15359476. doi: 10.1074/mcp.M112.020438.

P. B. Mason and K. Struhl. Distinction and relationship between elongation rate and processivity of RNA polymerase II in vivo. *Molecular Cell*, 17(6), 2005. ISSN 10972765. doi: 10.1016/j.molcel.2005.02.017.

A. M. Matia-González, V. Iadevaia, and A. P. Gerber. A versatile tandem RNA isolation procedure to capture in vivo formed mRNA-protein complexes. *Methods*, 118-119:93–100, apr 2017. ISSN 10959130. doi: 10.1016/j.ymeth.2016.10.005.

A. Mayer, M. Lidschreiber, M. Siebert, K. Leike, J. Söding, and P. Cramer. Uniform transitions of the general RNA polymerase II transcription complex. *Nature Structural and Molecular Biology*, 17(10), 2010. ISSN 15459993. doi: 10.1038/nsmb.1903.

A. Mayer, M. Heidemann, M. Lidschreiber, A. Schreieck, M. Sun, C. Hintermair, E. Kremmer, D. Eick, and P. Cramer. CTD Tyrosine phosphorylation impairs termination factor recruitment to RNA polymerase II. *Science*, 336 (6089), 2012a. ISSN 10959203. doi: 10.1126/science.1219651.

A. Mayer, A. Schreieck, M. Lidschreiber, K. Leike, D. E. Martin, and P. Cramer. The Spt5 C-Terminal Region Recruits Yeast 3' RNA Cleavage Factor I. *Molecular and Cellular Biology*, 32(7), 2012b. ISSN 0270-7306. doi: 10.1128/mcb.06310-11.

C. Mazzoni, P. Zarzov, A. Rambourg, and C. Mann. The SLT2 (MPK1) MAP kinase homolog is involved in polarized cell growth in *Saccharomyces cerevisiae*. *Journal of Cell Biology*, 123(6 II), 1993. ISSN 00219525. doi: 10.1083/jcb.123.6.1821.

C. A. McHugh and M. Guttman. RAP-MS: A Method to Identify Proteins that Interact Directly with a Specific RNA Molecule in Cells. *Methods in molecular biology (Clifton, N.J.)*, 1649:473–488, 2018. ISSN 1940-6029. doi: 10.1007/978-1-4939-7213-5_31.

C. A. McHugh, C.-K. Chen, A. Chow, C. F. Surka, C. Tran, P. Mcdonel, A. Pandya-Jones, M. Blanco, C. Burghard, A. Moradian, M. J. Sweredoski, A. A. Shishkin, J. Su, E. S. Lander, S. Hess, K. Plath, and M. Guttman. The Xist lncRNA interacts directly with SHARP to silence transcription through HDAC3. *Nature*, 521:232–236, 2015. doi: 10.1038/nature14443.

D. M. Meinel, C. Burkert-Kautzsch, A. Kieser, E. O'Duibhir, M. Siebert, A. Mayer, P. Cramer, J. Söding, F. C. Holstege, and K. Sträßer. Recruitment of TREX to the Transcription Machinery by Its Direct Binding to the Phospho-CTD of RNA Polymerase II. *PLoS Genetics*, 9(11), 2013. ISSN 15537390. doi: 10.1371/journal.pgen.1003914.

A. Mishra, W. Sipma, L. M. Veenhoff, E. Van Der Giessen, and P. R. Onck. The effect of FG-nup phosphorylation on NPC selectivity: A one-bead-per-amino-acid molecular dynamics study. *International Journal of Molecular Sciences*, 20 (3), feb 2019. ISSN 14220067. doi: 10.3390/ijms20030596.

M. Moreno-Torres, M. Jaquenoud, and C. De Virgilio. TORC1 controls G 1 -S cell cycle transition in yeast via Mpk1 and the greatwall kinase pathway. *Nature Communications*, 6, sep 2015. ISSN 20411723. doi: 10.1038/ncomms9256.

D. F. Nathan, M. H. Vos, and S. Lindquist. In vivo functions of the *Saccharomyces cerevisiae* Hsp90 chaperone. *Proceedings of the National Academy of Sciences of the United States of America*, 94(24), 1997. ISSN 00278424. doi: 10.1073/pnas.94.24.12949.

H. H. Ng, F. Robert, R. A. Young, and K. Struhl. Targeted recruitment of Set1 histone methylase by elongating Pol II provides a localized mark and memory of recent transcriptional activity. *Molecular Cell*, 11(3), 2003. ISSN 10972765. doi: 10.1016/S1097-2765(03)00092-3.

S. M. Noble and C. Guthrie. Transcriptional pulse-chase analysis reveals a role for a novel snRNP-associated protein in the manufacture of spliceosomal snRNPs. Technical Report 16, 1996. *The EMBO Journal*, 15(16), 1996. doi: 10.1002/j.1460-2075.1996.tb00810.x.

M. Pabis, N. Neufeld, M. C. Steiner, T. Bojic, Y. Shav-Tal, and K. M. Neugebauer. The nuclear cap-binding complex interacts with the U4/U6·U5 tri-snRNP and promotes spliceosome assembly in mammalian cells. *RNA*, 19(8), 2013. ISSN 13558382. doi: 10.1261/rna.037069.112.

S. S. S. Panchapakesan, M. L. Ferguson, E. J. Hayden, X. Chen, A. A. Hoskins, and P. J. Unrau. Ribonucleoprotein purification and characterization using RNA Mango. *RNA*, 23(10), 2017. ISSN 14699001. doi: 10.1261/rna.062166.117.

D. A. Parselt, Y. Sanchez, J. D. Stitzel, and S. Lindquist. Hsp104 is a highly conserved protein with two essential nucleotide-binding sites. *Nature*, 353(6341), 1991. ISSN 00280836. doi: 10.1038/353270a0.

D. S. Peabody. The RNA binding size of bacteriophage MS2 coat protein. *The EMBO Journal*, 12(2), 1993. ISSN 02614189. doi: 10.1002/j.1460-2075.1993.tb05691.x.

L. Pérez-Martínez, M. Öztürk, F. Butter, and B. Luke. Npl3 stabilizes R-loops at telomeres to prevent accelerated replicative senescence. *The EMBO reports*, 21 (3), 2020. ISSN 1469-221X. doi: 10.15252/embr.201949087.

B. Philip and D. E. Levin. Wsc1 and Mid2 Are Cell Surface Sensors for Cell Wall Integrity Signaling That Act through Rom2, a Guanine Nucleotide Exchange Factor for Rho1. *Molecular and Cellular Biology*, 21(1), 2001. ISSN 0270-7306. doi: 10.1128/mcb.21.1.271-280.2001.

P. Keil. *Function of the RNA-binding activity of the nuclear mRNA-binding protein Npl3 in nuclear mRNA packaging*. Dr. rer. nat., Justus-Liebig University Giessen, Giessen, jul 2021.

C. Plaschka, P. C. Lin, and K. Nagai. Structure of a pre-catalytic spliceosome. *Nature*, 546(7660):617–621, jun 2017. ISSN 14764687. doi: 10.1038/nature22799.

D. S. Portman, J. P. O'Connor, and G. Dreyfuss. YRA1, an essential *Saccharomyces cerevisiae* gene, encodes a novel nuclear protein with RNA annealing activity. *RNA*, 3(5), 1997. ISSN 13558382.

T. Pühringer, U. Hohmann, L. Fin, B. Pacheco-Fiallos, U. Schellhaas, J. Brennecke, and C. Plaschka. Structure of the human core transcription-export complex reveals a hub for multivalent interactions. *eLife*, 9, 2020. ISSN 2050084X. doi: 10.7554/eLife.61503.

O. Puig, F. Caspary, G. Rigaut, B. Rutz, E. Bouveret, E. Bragado-Nilsson, M. Wilm, and B. Séraphin. The tandem affinity purification (TAP) method: A general procedure of protein complex purification. *Methods*, 24(3):218–229, 2001. ISSN 10462023. doi: 10.1006/meth.2001.1183.

N. Pujol-Carrion, M. I. Petkova, L. Serrano, and M. A. de la Torre-Ruiz. The MAP kinase Slt2 is involved in vacuolar function and actin remodeling in *Saccharomyces cerevisiae* mutants affected by endogenous oxidative stress. *Applied and Environmental Microbiology*, 79(20), 2013. ISSN 00992240. doi: 10.1128/AEM.01692-13.

R. Rauhut, P. Fabrizio, O. Dybkov, K. Hartmuth, V. Pena, A. Chari, V. Kumar, C. T. Lee, H. Urlaub, B. Kastner, H. Stark, and R. Lúhrmann. Molecular architecture of the *Saccharomyces cerevisiae* activated spliceosome. *Science*, 353(6306):1399–1405, sep 2016. ISSN 10959203. doi: 10.1126/science.aag1906.

D. S. Reading, R. L. Hallberg, and A. M. Myers. Characterization of the yeast HSP60 gene coding for a mitochondrial assembly factor. *Nature*, 337(6208), 1989. ISSN 00280836. doi: 10.1038/337655a0.

M. Régnacq and H. Boucherie. Isolation and sequence of HSP30, a yeast heat-shock gene coding for a hydrophobic membrane protein. *Current Genetics*, 23 (5-6), 1993. ISSN 01728083. doi: 10.1007/BF00312631.

S. Regot, E. De Nadal, S. Rodrigúez-Navarro, A. GonzaĺEz-Novo, J. Peŕez-Fernandez, O. Gadal, G. Seisenbacher, G. Ammerer, and F. Posas. The Hog1 stress-activated protein kinase targets nucleoporins to control mrna export upon stress. *Journal of Biological Chemistry*, 288(24):17384–17398, jun 2013. ISSN 00219258. doi: 10.1074/jbc.M112.444042.

Y. Ren, P. Schmiege, and G. Nter Blobel. Structural and biochemical analyses of the DEAD-box ATPase Sub2 in association with THO or Yra1. *eLife*, 2017. doi: 10.7554/eLife.20070.001.

L. M. Reuter, D. M. Meinel, and K. Sträßer. The poly(A)-binding protein Nab2 functions in RNA polymerase III transcription. *Genes and Development*, pages 1565–1575, 2015. doi: 10.1101/gad.266205.

M. Rexach and G. Blobel. Protein import into nuclei: association and dissociation reactions involving transport substrate, transport factors, and nucleoporins. *Cell*, 83(5), 1995. ISSN 00928674. doi: 10.1016/0092-8674(95)90181-7.

R. Rieder, R. Reinhardt, C. Sharma, and J. Vogel. Experimental tools to identify RNA-protein interactions in Helicobacter pylori. *RNA biology*, 9(4):520 – 531, 2012. doi: 10.4161/rna.20331.

S. V. Rødkær and N. J. Færgeman. Glucose- and nitrogen sensing and regulatory mechanisms in *Saccharomyces cerevisiae*. *FEMS Yeast Research*, 14(5):683–696, 2014. ISSN 15671364. doi: 10.1111/1567-1364.12157.

S. Rodríguez-Navarro, T. Fischer, M. J. Luo, O. Antúnez, S. Brettschneider, J. Lechner, J. E. Pérez-Ortín, R. Reed, and E. Hurt. Sus1, a Functional Component of the SAGA Histone Acetylase Complex and the Nuclear Pore-Associated mRNA Export Machinery. *Cell*, 116(1), 2004. ISSN 00928674. doi: 10.1016/S0092-8674(03)01025-0.

B. Rogell, B. Fischer, M. Rettel, J. Krijgsveld, A. Castello, and M. W. Hentze. Specific RNP capture with antisense LNA/DNA mixmers. *RNA*, 23:1290–1302, 2017. doi: 10.1261/rna.060798.117.

C. Rollenhagen, C. A. Hodge, and C. N. Cole. The Nuclear Pore Complex and the DEAD Box Protein Rat8p/Dbp5p Have Nonessential Features Which Appear To Facilitate mRNA Export following Heat Shock. *Molecular and Cellular Biology*, 24(11):4869–4879, 2004. ISSN 0270-7306. doi: 10.1128/mcb.24.11.4869-4879.2004.

C. Rollenhagen, C. A. Hodge, and C. N. Cole. Following temperature stress, export of heat shock mRNA occurs efficiently in cells with mutations in genes normally important for mRNA export. *Eukaryotic Cell*, 6(3):505–513, 2007. ISSN 15359778. doi: 10.1128/EC.00317-06.

M. P. Rout, J. D. Aitchison, A. Suprapto, K. Hjertaas, Y. Zhao, and B. T. Chait. The yeast nuclear pore complex: Composition, architecture, transport mechanism. *Journal of Cell Biology*, 148(4), 2000. ISSN 00219525. doi: 10.1083/jcb.148.4.635.

C. Saavedra, K. S. Tuug, D. C. Amberg, A. K. Hopper, and C. N. Cole. Regulation of mRNA export in response to stress in Saccharomyces cerevisiae. *Genes and Development*, 10(13):1608–1620, 1996. ISSN 08909369. doi: 10.1101/gad.10.13.1608.

C. A. Saavedra, C. M. Hammell, C. V. Heath, and C. N. Cole. Yeast heat shock mRNAs are exported through a distinct pathway defined by Rip1p. *Genes and Development*, 11(21):2845–2856, 1997. ISSN 08909369. doi: 10.1101/gad.11.21.2845.

M. A. Saroufim, P. Bensidoun, P. Raymond, S. Rahman, M. R. Krause, M. Oeffinger, and D. Zenklusen. The nuclear basket mediates perinuclear mRNA scanning in budding yeast. *Journal of Cell Biology*, 211(6):1131–1140, 2015. ISSN 15408140. doi: 10.1083/jcb.201503070.

A. P. Schmitt and K. Mcentee. Msn2p, a zinc finger DNA-binding protein, is the transcriptional activator of the multistress response in *Saccharomyces cerevisiae*. *Proceedings of the National Academy of Sciences of the United States of America*, 93(12), 1996. ISSN 00278424. doi: 10.1073/pnas.93.12.5777.

C. Schmitt, C. Von Kobbe, A. Bachi, N. Panté, J. P. Rodrigues, C. Boscheron, G. Rigaut, M. Wilm, B. Séraphin, M. Carmo-Fonseca, and E. Izaurralde. Dbp5, a DEAD-box protein required for mRNA export, is recruited to the cytoplasmic fibrils of nuclear pore complex via a conserved interaction with CAN/Nup159p. *The EMBO Journal*, 18(15), 1999. ISSN 02614189. doi: 10.1093/emboj/18.15.4332.

S. K. Schuller, J. M. Schuller, J. R. Prabu, M. Baumgärtner, F. Bonneau, J. Basquin, and E. Conti. Structural insights into the nucleic acid remodeling mechanisms of the yeast tho-SUB2 complex. *eLife*, 9:1–51, oct 2020. ISSN 2050084X. doi: 10.7554/eLife.61467.

T. Scrimale, L. Didone, K. L. De Mesy Bentley, and D. J. Krysan. The unfolded protein response is induced by the cell wall integrity mitogen-activated protein kinase signaling cascade and is required for cell wall integrity in *Saccharomyces cerevisiae*. *Molecular Biology of the Cell*, 20(1), 2009. ISSN 10591524. doi: 10.1091/mbc.E08-08-0809.

A. Segref, K. Sharma, V. Doye, A. Hellwig, J. Huber, R. Lührmann, and E. Hurt. Mex67p, a novel factor for nuclear mRNA export. Binds to both poly(A)+ RNA and nuclear pores. *The EMBO Journal*, 16(11):3256–3271, jun 1997. ISSN 02614189. doi: 10.1093/emboj/16.11.3256.

B. Séraphin. Sm and Sm-like proteins belong to a large family: Identification of proteins of the U6 as well as the U1, U2, U4 and U5 snRNPs. *The EMBO Journal*, 14(9), 1995. ISSN 02614189. doi: 10.1002/j.1460-2075.1995.tb07200.x.

B. Séraphin, L. Kretzner, and M. Rosbash. A U1 snRNA:pre-mRNA base pairing interaction is required early in yeast spliceosome assembly but does not uniquely define the 5' cleavage site. *The EMBO journal*, 7(8), 1988. ISSN 02614189. doi: 10.1002/j.1460-2075.1988.tb03101.x.

V. Shchepachev, S. Bresson, C. Spanos, E. Petfalski, L. Fischer, J. Rappsilber, and D. Tollervey. Defining the RNA interactome by total RNA -associated protein purification. *Molecular Systems Biology*, 15(4), 2019. ISSN 1744-4292. doi: 10.15252/msb.20188689.

B. Slobodin and J. E. Gerst. A novel mRNA affinity purification technique for the identification of interacting proteins and transcripts in ribonucleoprotein complexes. *RNA*, 16(11):2277–2290, nov 2010. ISSN 13558382. doi: 10.1261/rna.2091710.

A. Smith, M. P. Ward, and S. Garrett. Yeast PKA represses Msn2p/Msn4p-dependent gene expression to regulate growth, stress response and glycogen accumulation. *The EMBO Journal*, 17(13), 1998. ISSN 02614189. doi: 10.1093/emboj/17.13.3556.

M. B. Smolka, C. P. Albuquerque, S. H. Chen, and H. Zhou. Proteome-wide identification of in vivo targets of DNA damage checkpoint kinases. *Proceedings of the National Academy of Sciences of the United States of America*, 104(25), 2007. ISSN 00278424. doi: 10.1073/pnas.0701622104.

C. A. Snay-Hodge, H. V. Colot, A. L. Goldstein, and C. N. Cole. Dbp5p/Rat8p is a yeast nuclear pore-associated DEAD-box protein essential for RNA export. Technical Report 9, 1998. *The EMBO Journal*, 17(9), 1998. doi: 10.1093/emboj/17.9.2663..

M. Soniat, P. Sampathkumar, G. Collett, A. S. Gizzi, R. N. Banu, R. C. Bhosle, S. Chamala, S. Chowdhury, A. Fiser, A. S. Glenn, J. Hammonds, B. Hillerich, K. Khafizov, J. D. Love, B. Matikainen, R. D. Seidel, R. Toro, P. Rajesh Kumar, J. B. Bonanno, Y. M. Chook, and S. C. Almo. Crystal structure of human Karyopherin β2 bound to the PY-NLS of *Saccharomyces cerevisiae* Nab2. *Journal of Structural and Functional Genomics*, 14(2):31–35, jun 2013. ISSN 1345711X. doi: 10.1007/s10969-013-9150-1.

P. K. Sorger and H. R. Pelham. Purification and characterization of a heat-shock element binding protein from yeast. *The EMBO Journal*, 6(10), 1987. ISSN 02614189. doi: 10.1002/j.1460-2075.1987.tb02609.x.

P. K. Sorger and H. R. Pelham. Yeast heat shock factor is an essential DNA-binding protein that exhibits temperature-dependent phosphorylation. *Cell*, 54 (6), 1988. ISSN 00928674. doi: 10.1016/S0092-8674(88)91219-6.

A. Soulard, A. Cremonesi, S. Moes, F. Schü Tz, P. Jenö, and M. N. Hall. The Rapamycin-sensitive Phosphoproteome Reveals That TOR Controls Protein Kinase A Toward Some But Not All Substrates. *Molecular Biology of the Cell*, 21: 3475–3486, 2010. doi: 10.1091/mbc.E10.

S. Souquere, S. Mollet, M. Kress, F. Dautry, G. Pierron, and D. Weil. Unravelling the ultrastructure of stress granules and associated P-bodies in human cells. *Journal of Cell Science*, 122(20), 2009. ISSN 00219533. doi: 10.1242/jcs.054437.

L. Staleva, A. Hall, and S. J. Orlow. Oxidative stress activates FUS1 and RLM1 transcription in the yeast *Saccharomyces cerevisiae* in an oxidant-dependent manner. *Molecular Biology of the Cell*, 15(12), 2004. ISSN 10591524. doi: 10.1091/mbc.E04-02-0142.

H. Stark. GraFix: Stabilization of fragile macromolecular complexes for single particle Cryo-EM. *Methods in Enzymology*, 481(C), 2010. ISSN 00766879. doi: 10.1016/S0076-6879(10)81005-5.

K. Sträßer and &. E. Hurt. Splicing factor Sub2p is required for nuclear mRNA export through its interaction with Yra1p. *Nature*, 413, 2001.

K. Sträßer and E. Hurt. Yra1p, a conserved nuclear RNA-binding protein, interacts directly with Mex67p and is required for mRNA export. Technical Report 3, 2000. *The EMBO Journal*, 19(3), 2000. doi: 10.1093/emboj/19.3.410..

K. Sträßer, J. Baßler, and E. Hurt. Binding of the Mex67p/Mtr2p heterodimer to FXFG, GLFG, and FG repeat nucleoporins is essential for nuclear mRNA export. *Journal of Cell Biology*, 150(4), 2000. ISSN 00219525. doi: 10.1083/jcb.150.4.695.

K. Sträßer, S. Masuda, P. Mason, J. Pfannstiel, M. Oppizzi, S. Rodriguez-Navarro, A. G. Rondón, A. Aguilera, K. Struhl, R. Reed, and E. Hurt. TREX is a conserved complex coupling transcription with messenger RNA export. *Nature*, 417(6886):304–308, 2002. ISSN 00280836. doi: 10.1038/nature746.

L. A. Strawn, T. Shen, N. Shulga, D. S. Goldfarb, and S. R. Wente. Minimal nuclear pore complexes define FG repeat domains essential for transport. *Nature Cell Biology*, 6(3), 2004. ISSN 14657392. doi: 10.1038/ncb1097.

F. Stutz, J. Kantor, D. Zhang, T. McCarthy, M. Neville, and M. Rosbash. The yeast nucleoporin Rip1p contributes to multiple export pathways with no essential role for its FG-repeat region. *Genes and Development*, 11(21):2857–2868, 1997. ISSN 08909369. doi: 10.1101/gad.11.21.2857.

F. Stutz, A. Bachi, T. Doerks, I. Braun, B. Seraphin, M. Wilm, P. Bork, and E. Izaurralde. REF, an evolutionary conserved family of hnRNP-like proteins, interacts with TAP/Mex67p and participates in mRNA nuclear export. *RNA*, 6, 2000. doi: 10.1017/s1355838200000078.

Y. Sukegawa, T. Negishi, Y. Kikuchi, K. Ishii, M. Imanari, F. Ghanegolmohammadi, S. Nogami, and Y. Ohya. Genetic dissection of the signaling pathway required for the cell wall integrity checkpoint. *Journal of Cell Science*, 131(13), 2018. ISSN 14779137. doi: 10.1242/jcs.219063.

M. Suntharalingam, A. R. Alcázar-Román, and S. R. Wente. Nuclear export of the yeast mRNA-binding protein Nab2 is linked to a direct interaction with Gfd1 and to Gle1 function. *Journal of Biological Chemistry*, 279(34):35384–35391, aug 2004. ISSN 00219258. doi: 10.1074/jbc.M402044200.

F. Supek, D. T. Madden, S. Hamamoto, L. Orci, and R. Schekman. Sec16p potentiates the action of COPII proteins to bud transport vesicles. *Journal of Cell Biology*, 158(6), 2002. ISSN 00219525. doi: 10.1083/jcb.200207053.

D. L. Swaney, P. Beltrao, L. Starita, A. Guo, J. Rush, S. Fields, N. J. Krogan, and J. Villén. Global analysis of phosphorylation and ubiquitylation cross-talk in protein degradation. *Nature Methods*, 10(7), 2013. ISSN 15487091. doi: 10.1038/nmeth.2519.

B. R. Szymczyna, J. Bowman, S. McCracken, A. Pineda-Lucena, Y. Lu, B. Cox, M. Lambermon, B. R. Graveley, C. H. Arrowsmith, and B. J. Blencowe. Structure and function of the PWI motif: A novel nucleic acid-binding domain that facilitates pre-MRNA processing. *Genes and Development*, 17(4), 2003. ISSN 08909369. doi: 10.1101/gad.1060403.

R. Takemura, Y. Inoue, and S. Izawa. Stress response in yeast mRNA export factor: Reversible changes in Rat8p localization are caused by ethanol stress but not heat shock. *Journal of Cell Science*, 117(18):4189–4197, aug 2004. ISSN 00219533. doi: 10.1242/jcs.01296.

D. Teixeira and R. Parker. Analysis of P-body assembly in *Saccharomyces cerevisiae*. *Molecular Biology of the Cell*, 18(6), 2007. ISSN 10591524. doi: 10.1091/mbc.E07-03-0199.

A. G. Thakurta, G. Gopal, J. H. Yoon, T. Saha, and R. Dhar. Conserved Nuclear Export Sequences in *Schizosaccharomyces pombe* Mex67 and Human TAP Function in mRNA Export by Direct Nuclear Pore Interactions. *Journal of Biological Chemistry*, 279(17), 2004. ISSN 00219258. doi: 10.1074/jbc.M309731200.

The UniProt Consortium. UniProt: the universal protein knowledgebase in 2021 The UniProt Consortium. *Nucleic Acids Research*, 49, 2021. doi: 10.1093/nar/gkaa1100.

R. Thomsen, D. Libri, J. Boulay, M. Rosbash, and T. H. Jensen. Localization of nuclear retained mRNAs in *Saccharomyces cerevisiae*. *RNA*, 9(9):1049–1057, 2003. ISSN 13558382. doi: 10.1261/rna.5170303.

R. Thomsen, C. Saguez, T. Nasser, and T. H. Jensen. General, rapid, and transcription-dependent fragmentation of nucleolar antigens in S. cerevisiae mRNA export mutants. *RNA*, 14(4):706–716, 2008. ISSN 13558382. doi: 10.1261/rna.718708.

J. R. Tietjen, D. W. Zhang, J. B. Rodríguez-Molina, B. E. White, M. S. Akhtar, M. Heidemann, X. Li, R. D. Chapman, K. Shokat, S. Keles, D. Eick, and A. Z. Ansari. Chemical-genomic dissection of the CTD code. *Nature Structural and Molecular Biology*, 17(9), 2010. ISSN 15459993. doi: 10.1038/nsmb.1900.

R. J. TrachmanIii, N. A. Demeshkina, M. W. Lau, S. S. S. Panchapakesan, S. C. Jeng, P. J. Unrau, and A. R. Ferré-D'Amaré. Structural basis for high-affinity fluorophore binding and activation by RNA Mango. *Nature Chemical Biology*, 13(7), 2017. ISSN 15524469. doi: 10.1038/nchembio.2392.

A. C. Tuck and D. Tollervey. XA transcriptome-wide atlas of RNP composition reveals diverse classes of mRNAs and lncRNAs. *Cell*, 154(5), 2013. ISSN 10974172. doi: 10.1016/j.cell.2013.07.047.

M. Turtola, C. M. Manav, A. Kumar, A. Tudek, S. Mroczek, P. S. Krawczyk, A. Dziembowski, M. Schmid, L. A. Passmore, A. Casanal, and T. H. Jensen. Three-layered control of mRNA poly(A) tail synthesis in *Saccharomyces cerevisiae*. *Genes and Development*, 35(17-18), 2021. ISSN 15495477. doi: 10.1101/GAD.348634.121.

E. Tutucci and F. Stutz. Keeping mRNPs in check during assembly and nuclear export, jun 2011. ISSN 14710072. *Nat Rev Mol Cell Biol*, 12(6), 2011. doi: 10.1038/nrm3119..

E. Tutucci, M. Vera, and R. H. Singer. Single-mRNA detection in living S. cerevisiae using a re-engineered MS2 system. *Nature Protocols*, 13(10):2268–2296, oct 2018. ISSN 17502799. doi: 10.1038/s41596-018-0037-2.

F. van Drogen and M. Peter. Spa2p functions as a scaffold-like protein to recruit the Mpk1p MAP kinase module to sites of polarized growth. *Current Biology*, 12(19), 2002. ISSN 09609822. doi: 10.1016/S0960-9822(02)01186-7.

D. Varol, V. Purutçuoğlu, and R. Yılmaz. Transcriptomic analysis of the heat stress response for a commercial baker's yeast *Saccharomyces cerevisiae*. *Genes and Genomics*, 40(2):137–150, 2018. ISSN 20929293. doi: 10.1007/s13258-017-0616-6.

J. Verna, A. Lodder, K. Lee, A. Vagts, and R. Ballester. A family of genes required for maintenance of cell wall integrity and for the stress response in *Saccharomyces cerevisiae*. *Proceedings of the National Academy of Sciences of the United States of America*, 94(25), 1997. ISSN 00278424. doi: 10.1073/pnas.94.25.13804.

P. Vinciguerra, N. Iglesias, J. Camblong, D. Zenklusen, and F. Stutz. Perinuclear Mlp proteins downregulate gene expression in response to a defect in mRNA export. *The EMBO Journal*, 24(4), 2005. ISSN 02614189. doi: 10.1038/sj.emboj.7600527.

N. Viphakone, F. Voisinet-Hakil, and L. Minvielle-Sebastia. Molecular dissection of mRNA poly(A) tail length control in yeast. *Nucleic Acids Research*, 36(7), 2008. ISSN 13624962. doi: 10.1093/nar/gkn080.

E. W. Wallace, J. L. Kear-Scott, E. V. Pilipenko, M. H. Schwartz, P. R. Laskowski, A. E. Rojek, C. D. Katanski, J. A. Riback, M. F. Dion, A. M. Franks, E. M. Airoldi, T. Pan, B. A. Budnik, and D. A. Drummond. Reversible, Specific, Active Aggregates of Endogenous Proteins Assemble upon Heat Stress. *Cell*, 162(6):1286–1298, 2015. ISSN 10974172. doi: 10.1016/j.cell.2015.08.041.

C. Wang, F. Schmich, S. Srivatsa, J. Weidner, N. Beerenwinkel, and A. Spang. Context-dependent deposition and regulation of mRNAs in P-bodies. *eLife*, 7, 2018. ISSN 2050084X. doi: 10.7554/eLife.29815.

C. S. Weirich, J. P. Erzberger, J. M. Berger, and K. Weis. The N-terminal domain of Nup159 forms a β-propeller that functions in mRNA export by tethering the helicase Dbp5 to the nuclear pore. *Molecular Cell*, 16(5), 2004. ISSN 10972765. doi: 10.1016/j.molcel.2004.10.032.

C. S. Weirich, J. P. Erzberger, J. S. Flick, J. M. Berger, J. Thorner, and K. Weis. Activation of the DExD/H-box protein Dbp5 by the nuclear-pore protein Gle1 and its coactivator InsP6 is required for mRNA export. *Nature Cell Biology*, 8 (7), 2006. ISSN 14657392. doi: 10.1038/ncb1424.

C. Wierschem. *A twostep affinity purification of nuclear mRNPs*. PhD thesis, Justus-Liebig-University Giessen, Giessen, 2020.

J. H. Wilbertz, F. Voigt, I. Horvathova, G. Roth, Y. Zhan, and J. A. Chao. Single-Molecule Imaging of mRNA Localization and Regulation during the Integrated Stress Response. *Molecular Cell*, 73(5), 2019. ISSN 10974164. doi: 10.1016/j.molcel.2018.12.006.

S. M. Wilson, K. V. Datar, M. R. Paddy, J. R. Swedlow, and M. S. Swanson. Characterization of Nuclear Polyadenylated RNA-binding Proteins in *Saccharomyces cerevisiae*. *Journal of Cell Biology*, 127(5):1173–1184, 1994. doi: 10.1083/jcb.127.5.1173.

D. M. Woodcock, P. J. Crowther, J. Doherty, S. Jefferson, E. Decruz, M. Noyer-Weidner, S. S. Smith, M. Z. Michael, and M. W. Graham. Quantitative evaluation of Escherichia coli host strains for tolerance to cytosine methylation in plasmid and phage recombinants. *Nucleic Acids Research*, 17(9), 1989. ISSN 03051048. doi: 10.1093/nar/17.9.3469.

Y. Xie, B. P. Clarke, Y. J. Kim, A. L. Ivey, P. S. Hill, Y. Shi, and Y. Ren. Cryo-EM structure of the yeast TREX complex and coordination with the SR-like protein Gbp2. *eLife*, 10, 2021. ISSN 2050084X. doi: 10.7554/eLife.65699.

A. Yamamoto, Y. Mizukami, and H. Sakurai. Identification of a novel class of target genes and a novel type of binding sequence of heat shock transcription factor in Saccharomyces cerevisiae. *Journal of Biological Chemistry*, 280(12): 11911–11919, 2005. ISSN 00219258. doi: 10.1074/jbc.M411256200.

N. Yurko, X. Liu, T. Yamazaki, M. Hoque, B. Tian, and J. L. Manley. MPK1/SLT2 Links Multiple Stress Responses with Gene Expression in Budding Yeast by Phosphorylating Tyr1 of the RNAP II CTD. *Molecular Cell*, 68(5), 2017. ISSN 10974164. doi: 10.1016/j.molcel.2017.11.020.

G. Zander, A. Hackmann, L. Bender, D. Becker, T. Lingner, G. Salinas, and H. Krebber. MRNA quality control is bypassed for immediate export of stress-responsive transcripts. *Nature*, 540(7634):593–596, 2016. ISSN 14764687. doi: 10.1038/nature20572.

A. J. Zaug, P. J. Grabowski, and T. R. Cech. Autocatalytic cyclization of an excised intervening sequence RNA is a cleavage-ligation reaction. *Nature*, 301 (5901), 1983. ISSN 00280836. doi: 10.1038/301578a0.

D. Zenklusen, P. Vinciguerra, Y. Strahm, and F. Stutz. The Yeast hnRNP-Like Proteins Yra1p and Yra2p Participate in mRNA Export through Interaction with Mex67p. *Molecular and Cellular Biology*, 21(13), 2001. ISSN 0270-7306. doi: 10.1128/mcb.21.13.4219-4232.2001.

C. Zheng, M. B. Fasken, N. J. Marshall, C. Brockmann, M. E. Rubinson, S. R. Wente, A. H. Corbett, and M. Stewart. Structural basis for the function of the *Saccharomyces cerevisiae* Gfd1 protein in mRNA nuclear export. *Journal of Biological Chemistry*, 285(27):20704–20715, jul 2010. ISSN 00219258. doi: 10.1074/jbc.M110.107276.

Z. Zhou, J. Sim, J. Griffith, and R. Reed. Purification and electron microscopic visualization of functional human spliceosomes. *PNAS*, 99(19):12203–12207, 2002. doi: 10.1073/pnas.182427099.

List of Figures

List of Tables

List of Abbreviations

12xMS2V6	12xMS2
5-FAA	2-Amino-5-Fluorobenzoic acid
5-FOA	5-Fluoroorotic acid
APD	Ammonium persulfate
ASO	Antisense oligo nucleotid
BS	Branch site
BSA	Bovine serim albumin
CBC	Cap bindingcomplex
ChIP	Chromatin immunoprecipitation
ChIRP	Comprehensive identification of RNA binding proteins
CPF	Cleavage and poly(A)denylation factor
CTD	C-terminal domain (Rpb1)
CTR	C-terminal region (Spt5)
CWI	Cell wall integrity
Dbp5	DEAD box protein 5
DDM	Dodecyl-β-D-maltosid
DMSO	Dimethyl sulfoxide
DTT	Dithiothreitol
EDTA	Ethylenediaminetetraacetic acid
EM	Electron microscopy
ERK	Extracellular signal-regulated kinase
FACS	Fluorescence associated cell sorting
FG	Phenylalanien and glycine rich
FISH	Fluorescence *in situ* hybridization
GA	Glutaraldehyde
Gag1	Golgi-associated protein 1
Gfd1	Good for Dbp5
GraFIX	Gradient centrifuation with cross-linking
HS	Heat shock
Hsf1	Heat shock factor 1
HSP	Heat shock prptein
IGEPAL	Octylphenoxypolyethoxyethanol
IP6	Inositol-6-phosphate
MAPK	Mitogen-activated protein kiase
MBP	Maltose binding protein
MCP	MS2 coat protein
min	Minutes
Mlp1	Myosin-like protein 1
mRNA	Messenger RNA
mRNP	Messenger ribonucleoprotein partice
MS	Mass spectrometry
N/C ratio	Nuclear/cytoplasmic mean fluorescence signal
Nab2	Nuclear abundant poly(A)-RNA binding protein 2

NPC	Nuclear pore complex
NUP	Nuclear pore protein
Pab1	poly(A)-binding prtein 1
PAN	Pab1-dependent polyadenylation nuclease
PAR	Photoactivatable ribonucleosid-enhanced
PCR	Polymerase Chaine Reaction
PEG	Polyethylen glycol
PMSF	Phenylmethane sulfonyl fluoride
poly(A)	poly(A)denosine
PTM	Posttranslational modification
qPCR	Quantitative PCR
RAP-MS	RNA antisense purification coupled with MS
RIP	RNA immunoprecipitation
RNAPII	RNA polymerase II
RT	Room temperature
RT-qPCR	Reverse transcription coupled with qPCR
SDC	Synthetic dropout complete
SDS	Sodium dodecyl sulfate
smFISh	Single molecule FISH
snRNP	Small nuclear RNP
SR-like	Serine-Arginine-rich like
ss	Splice site
SSD	Salmon sperm DANN
TAP	Tandem affinity purification
TCA	Trichloroacetic acid
TCEP	Tris (2-Carboxyethyl)-Phosphin
TEMED	Tetramethylethylendiamin
TEV protease	Tobacco etch virus protease
TMT	Tandem mass tag
TO	Thiazole organe
TREX	Transcription and export
TRIP	Tandem RNA isolation procedure
Tris	Tris(hydroxymethyl)aminomethane
Ub	Ubiquitin
UBM	UAB56 binding motif
UPR	Unfolded protein response
YPD	Yeast full medium
Yra1	Yeast RNA annealing protein 1
ZnF	Zink finger domain

A. ASO purifications

A

purification step	strain	condition	C_t(*CCW12*)	C_t(*PGK1*)	ΔC_t	Enrichment
Lysate	*Cbp20-TAP*	NaCl	17.60	18.60	-1.00	2.00
Lysate	*Cbp20-TAP*	KCl	16.40	17.70	-1.30	2.46
TEV eluate	*Cbp20-TAP*	NaCl	24.50	26.30	-1.80	3.48
TEV eluate	*Cbp20-TAP*	KCl	22.30	24.70	-2.40	5.28
ASO eluate	*Cbp20-TAP*	**ASO NaCl**	**25.70**	**31.40**	**-5.70**	**51.98**
ASO eluate	*Cbp20-TAP*	Mock NaCl	29.70	31.70	-2.00	4.00
ASO eluate	*Cbp20-TAP*	**ASO KCl**	**26.20**	**31.40**	**-5.20**	**36.76**
ASO eluate	*Cbp20-TAP*	Mock KCl	30.90	30.90	0.00	1.00

B

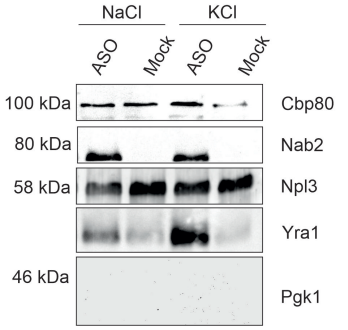

Figure A.1: **Usage of KCl instead of NaCl does not change the yield of *CCW12* mRNA. A** Representative C_t value table for an ASO3 purification comparing the usage of KCl with NaCl in the used buffer. **E** Representative Western blot showing the copurification of nuclear mRNA-binding proteins for the ASO purification from A.

A

purification step	strain	condition	C_t(*CCW12*)	C_t(*PGK1*)	ΔC_t	Enrichment
Lysate	*Cbp20-TAP*		14.80	16.90	-2.10	4.29
Lysate	*Cbp20-TAP Δccw12*		23.50	16.50	7.00	0.01
TEV eluate	*Cbp20-TAP*		20.00	22.50	-2.50	5.66
TEV eluate	*Cbp20-TAP Δccw12*		30.50	24.50	6.00	0.02
ASO eluate	***Cbp20-TAP***	**RT**	**22.20**	**28.70**	**-6.50**	**90.51**
ASO eluate	*Cbp20-TAP Δccw12*	RT	31.40	30.10	1.30	0.41
ASO eluate	***Cbp20-TAP***	**16°C**	**23.00**	**27.80**	**-4.80**	**27.86**
ASO eluate	*Cbp20-TAP Δccw12*	16°C	31.40	29.30	2.10	0.23
ASO eluate	***Cbp20-TAP***	**4°C**	**24.10**	**28.40**	**-4.30**	**19.70**
ASO eluate	*Cbp20-TAP Δccw12*	4°C	32.20	28.10	4.10	0.06

B

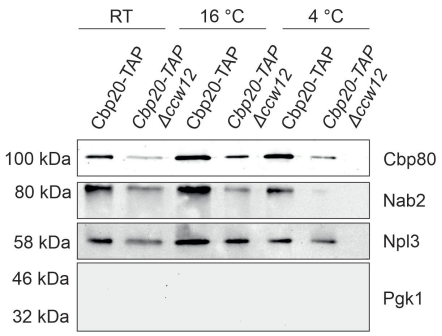

Figure A.2: **Lower annealing temperatures reduce the yield and purity of *CCW12* during ASO purification. A** Representative C_t value table for an ASO purification comparing the annealing of ASO3 at RT, 4°C and 16°C. **E** Representative Western blot showing the copurification of nuclear mRNA-binding proteins for the ASO purification from A.

A

purification	strain	condition	C_t(*CCW12*)	C_t(*PGK1*)	ΔC_t	Enrichment
Lysate	*Cbp20-TAP*		16.6	17.8	-1.2	2.3
Lysate	*Cbp20-TAP Δccw12*		24.4	17.4	7	0.008
TEV eluate	*Cbp20-TAP*	-	18.2	20.6	-2,4	5.3
TEV eluate	*Cbp20-TAP Δccw12*	-	26.2	20.6	5.6	0.02
TEV eluate	*Cbp20-TAP*	10x DNA	18.1	20.4	-2.3	4.9
TEV eluate	*Cbp20-TAP Δccw12*	10x DNA	22.3	20.4	1.9	0.3
TEV eluate	*Cbp20-TAP*	20x DNA	23.8	25.3	-1.5	2.8
TEV eluate	*Cbp20-TAP Δccw12*	20x DNA	25.6	25.3	0.3	0.8
ASO eluate	***Cbp20-TAP***	**-**	**25.4**	**31.6**	**-6.2**	**73.5**
ASO eluate	*Cbp20-TAP Δccw12*	-	31.0	30.7	0.3	0.8
ASO eluate	***Cbp20-TAP***	**10x DNA**	**26.7**	**31.5**	**-4.8**	**27.9**
ASO eluate	*Cbp20-TAP Δccw12*	10x DNA	27.2	28.9	-1.7	3.2
ASO eluate	***Cbp20-TAP***	**20x DNA**	**23.0**	**28.2**	**-5.2**	**36.8**
ASO eluate	*Cbp20-TAP Δccw12*	20x DNA	31.2	30.5	0.7	0.6

B

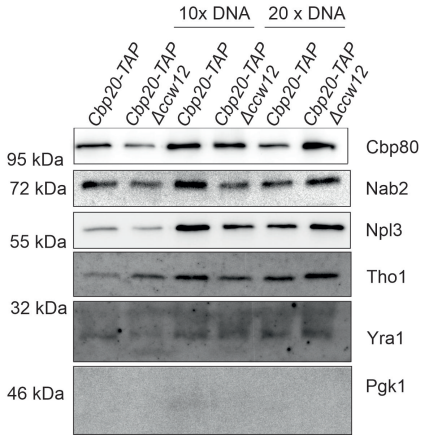

Figure A.3: **Addition of random DNA Oligos does not reduce the unspecific copurification of RNA-binding proteins. A** Representative C_t value table for an ASO purification of *CCW12* mRNPs using ASO3. The influence of the addition of unbiotinylated random DNA oligos on the unspecific protein copurification was tested. **E** Representative Western blot showing the copurification of nuclear mRNA-binding proteins for the ASO purification from A.

A

Purification step	strain	condition	C_t(*CCW12*)	C_t(*PGK1*)	ΔC_t	Enrichment
Lysate	*Cbp20-TAP*		15.28	16.52	-1.24	2.36
Lysate	*Cbp20-TAP Δccw12*		26.00	16.88	9.12	0.00
TEV eluate	*Cbp20-TAP*	-	20.03	21.45	-1.42	2.67
TEV eluate	*Cbp20-TAP Δccw12*	-	28.98	21.86	7.12	0.01
TEV eluate	*Cbp20-TAP*	5x R20	19.55	20.81	-1.26	2.39
TEV eluate	*Cbp20-TAP Δccw12*	5x R20	28.20	21.29	6.92	0.01
TEV eluate	*Cbp20-TAP*	10x R20	19.76	21.02	-1.26	2.40
TEV eluate	*Cbp20-TAP Δccw12*	10x R20	29.34	22.47	6.87	0.01
TEV eluate	*Cbp20-TAP*	20x R20	20.00	21.05	-1.04	2.06
TEV eluate	*Cbp20-TAP Δccw12*	20x R20	29.28	21.79	7.49	0.01
ASO eluate	***Cbp20-TAP***	**-**	**24.98**	**31.85**	**-6.87**	**117.14**
ASO eluate	*Cbp20-TAP Δccw12*	-	32.06	31.63	0.44	0.74
ASO eluate	***Cbp20-TAP***	**5x R20**	**24.76**	**31.97**	**-7.22**	**148.90**
ASO eluate	*Cbp20-TAP Δccw12*	5x R20	32.51	33.52	-1.01	2.01
ASO eluate	***Cbp20-TAP***	**10x R20**	**26.57**	**33.92**	**-7.35**	**163.09**
ASO eluate	*Cbp20-TAP Δccw12*	10x R20	33.18	34.06	-0.88	1.84
ASO eluate	***Cbp20-TAP***	**20x R20**	**25.84**	**33.61**	**-7.77**	**219.00**
ASO eluate	*Cbp20-TAP Δccw12*	20x R20	28.06	33.20	-5.13	35.05

B

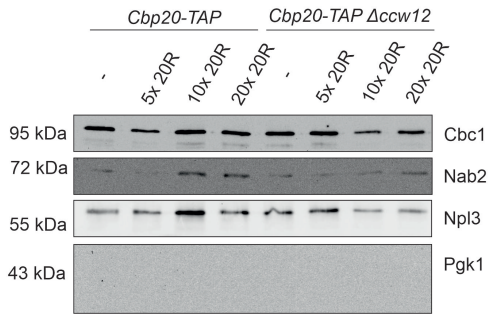

Figure A.4: **Addition of random RNA Oligos does not reduce the unspecific copurification of RNA-binding proteins. A** Representative C_t value table for an ASO purification of *CCW12* mRNPs using ASO3. Tested was the influence of adding unbiotinylated random RNA oligos (R20) to the TEV eluate on the unspecific protein copurification. **E** Representative Western blot showing the copurification of nuclear mRNA-binding proteins for the ASO purification from A.

A

purification step	strain	C_t(*CCW12*)	C_t(*PGK1*)	ΔC_t	Enrichment
Lysate	*Cbp20-TAP*	11.6	14.0	-2.37	5.18
Lysate	*Cbp20-TAP Δccw12*	24.0	15.4	8.60	0.00
Lysate	*Cbp20-TAP Δccw22*	13.4	14.7	-1.36	2.57
Lysate	*Cbp20-TAP Δccw12 Δccw22*	23.3	15.7	7.65	0.00
TEV eluate	*Cbp20-TAP*	16.8	19.6	-2.84	7.17
TEV eluate	*Cbp20-TAP Δccw12*	26.5	19.0	7.54	0.01
TEV eluate	*Cbp20-TAP Δccw22*	16.7	18.4	-1.77	3.40
TEV eluate	*Cbp20-TAP Δccw12 Δccw22*	26.5	19.3	7.20	0.01
ASO eluate	***Cbp20-TAP***	**23.7**	**31.5**	**-7.82**	**226.20**
ASO eluate	*Cbp20-TAP Δccw12*	31.5	30.3	1.12	0.46
ASO eluate	***Cbp20-TAP Δccw22***	**24.0**	**31.7**	**-7.71**	**209.10**
ASO eluate	*Cbp20-TAP Δccw12 Δccw22*	31.7	30.7	1.02	0.49

B

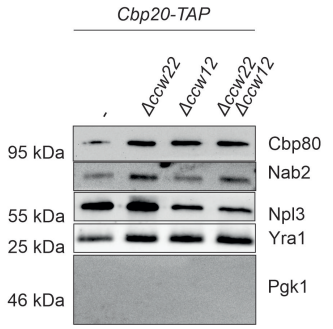

Figure A.5: **The enrichment of *CCW12* after mRNP purification does not change in a *Δccw22* strain.** **A** Representative C_t value table for an ASO purification of *CCW12* mRNPs using ASO1 in strains where the *CCW12* paralog *CCW22* is deleted. **E** Representative Western blot showing the copurification of nuclear mRNA-binding proteins for the ASO purification from A.

A

purification step	strain	condition	C_t(*CCW12*)	C_t(*PGK1*)	ΔC_t	Enrichment
Lysate	*Cbp20-TAP*	60 min	20.86	22.63	-1.77	3.41
Lysate	WT	60 min	20.18	22.03	-1.86	3.62
Lysate	*Cbp20-TAP*	16 min	19.26	19.73	-0.47	1.38
Lysate	WT	16 min	18.57	19.86	-1.29	2.44
TEV eluate	*Cbp20-TAP*	60 min	18.01	19.23	-1.22	2.33
TEV eluate	WT	60 min	21.33	23.36	-2.03	4.09
TEV eluate	*Cbp20-TAP*	16 min	17.05	18.51	-1.46	2.75
TEV eluate	WT	16 min	19.85	20.93	-1.09	2.12
ASO eluate	***Cbp20-TAP***	**60 min**	**22.11**	**28.30**	**-6.19**	**73.14**
ASO eluate	WT	60 min	26.07	31.70	-5.63	49.44
ASO eluate	***Cbp20-TAP***	**16 min**	**20.58**	**27.76**	**-7.18**	**144.95**
ASO eluate	WT	16 min	27.59	34.23	-6.63	99.31

B

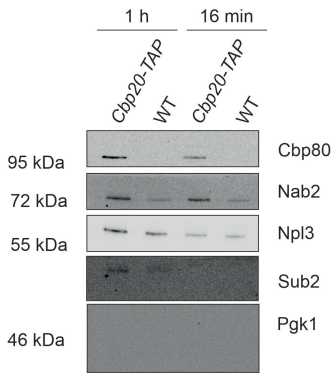

Figure A.6: **Longer centrifugation of the lysate reduces the yield of the *CCW12* mRNP purification.** **A** Representative C_t value table for an ASO1 purification of *CCW12* mRNPs with 1h 40000 rpm centrifugation to clear the lysate instead of 16 min at 40000 xg. **E** Representative Western blot showing the copurification of nuclear mRNA-binding proteins for the ASO purification from A.

A

purification step	strain	condition	C_t(*CCW12*)	C_t(*PGK1*)	ΔC_t	Enrichment
Lysate	*Cbp20-TAP*		18.90	20.50	-1.60	3.03
Lysate	*Cbp20-TAP Δccw12*		24.30	16.30	8.00	0.00
TEV eluate	*Cbp20-TAP*		16.30	18.60	-2.30	4.92
TEV eluate	*Cbp20-TAP Δccw12*		30.30	24.10	6.20	0.01
ASO eluate	***Cbp20-TAP***	**100 µl**	**22.51**	**30.92**	**-8.41**	**341.12**
ASO eluate	*Cbp20-TAP*	100 µl Mock	28.37	30.29	-1.92	3.79
ASO eluate	*Cbp20-TAP Δccw12*	100 µl	32.18	31.02	1.16	0.45
ASO eluate	***Cbp20-TAP***	**200 µl**	**23.34**	**31.78**	**-8.44**	**347.93**
ASO eluate	*Cbp20-TAP*	200 µl Mock	31.92	30.52	1.40	0.38
ASO eluate	*Cbp20-TAP Δccw12*	200 µl	32.26	30.63	1.63	0.32
ASO eluate	***Cbp20-TAP***	**50 µl**	**24.81**	**31.57**	**-6.76**	**108.03**
ASO eluate	*Cbp20-TAP*	50 µl Mock	31.26	30.55	0.71	0.61
ASO eluate	*Cbp20-TAP Δccw12*	50 µl	29.26	30.45	-1.19	2.28

B

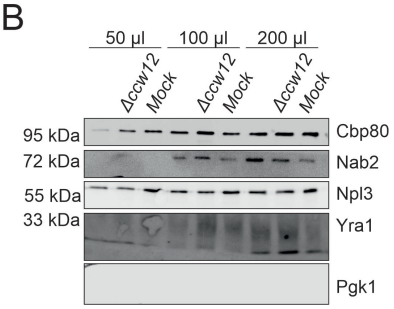

Figure A.7: **Increased bead amount does not increase the yield of *CCW12* mRNA. A** Representative C_t value table for an ASO1 purification of *CCW12* mRNPs comparing the use of 50 µl, 100 µl and 200 µl M280 Streptavidine Dynabeads for the second purification step. **E** Representative Western blot showing the copurification of nuclear mRNA-binding proteins for the ASO purification from A.

A

purification step	strain	condition	C_t(*CCW12*)	C_t(*PGK1*)	ΔC_t	Enrichment
Lysate	*Cbp20-TAP*		19.9	20.2	-0.30	1.23
Lysate	*Cbp20-TAP Δccw12*		27.3	18.7	8.60	0.00
TEV eluate	*Cbp20-TAP*		17.7	19.0	-1.30	2.46
TEV eluate	*Cbp20-TAP Δccw12*		27.5	18.3	9.20	0.00
ASO eluate	***Cbp20-TAP***	**ASO1**	**31.3**	**34.0**	**-2.70**	**6.50**
ASO eluate	*Cbp20-TAP Δccw12*	ASO1	32.0	32.7	-0.70	1.62
ASO eluate	***Cbp20-TAP***	**ASO3**	**27.6**	**31.0**	**-3.40**	**10.56**
ASO eluate	*Cbp20-TAP Δccw12*	ASO3	30.2	28.9	1.30	0.41
ASO eluate	***Cbp20-TAP***	**ASO3-D**	**26.0**	**30.2**	**-4.20**	**18.38**
ASO eluate	*Cbp20-TAP Δccw12*	ASO3-D	30.7	31.3	-0.60	1.52

B

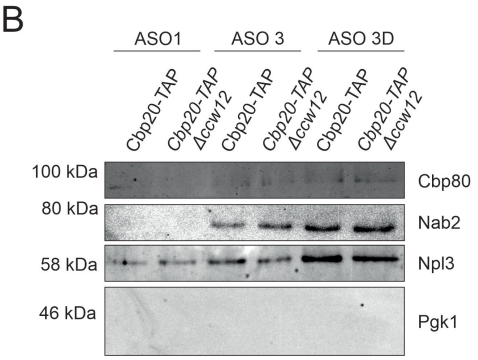

Figure A.8: **Native elution with biotinylated ASO1 is not efficient. A** Representative C_t value table for an ASO1 purification of *CCW12* mRNPs using native elution. **E** Representative Western blot showing the copurification of nuclear mRNA-binding proteins for the ASO purification from A.

A

purification step	strain	condition	C_t(*CCW12*)	C_t(*PGK1*)	ΔC_t	Enrichment
Lysate	*Cbp20-TAP*		17.17	18.89	-1.73	3.31
Lysate	*Cbp20-TAP Δccw12*		27.68	19.78	7.91	0.00
TEV eluate	*Cbp20-TAP*		17.32	21.20	-3.89	14.78
TEV eluate	*Cbp20-TAP Δccw12*		29.33	26.43	2.90	0.13
ASO eluate	***Cbp20-TAP***	**ASO1-D, 5 mM biotin**	**27.64**	**31.19**	**-3.54**	**11.65**
ASO eluate	*Cbp20-TAP Δccw12*	ASO1-D, 5 mM biotin	34.74	32.06	2.68	0.16
ASO eluate	***Cbp20-TAP***	**ASO1-D, 16mM biotin**	**25.56**	**31.21**	**-5.65**	**50.21**
ASO eluate	*Cbp20-TAP Δccw12*	ASO1-D, 16mM biotin	33.09	30.61	2.48	0.18
ASO eluate	***Cbp20-TAP***	**ASO3-D, 5 mM biotin**	**27.42**	**32.11**	**-4.69**	**25.72**
ASO eluate	*Cbp20-TAP Δccw12*	ASO3-D, 5 mM biotin	34.45	30.76	3.70	0.08
ASO eluate	***Cbp20-TAP***	**ASO3-D, 16mM biotin**	**26.27**	**32.08**	**-5.81**	**56.22**
ASO eluate	*Cbp20-TAP Δccw12*	ASO3-D, 16mM biotin	35.82	30.76	5.06	0.03

B

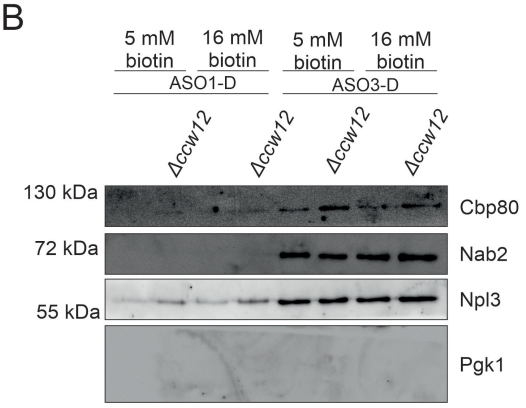

Figure A.9: **Increased biotin concentration results in an increased elution of *CCW12* ASO1-D und ASO3-D. A** Representative C_t value table for a native ASO purification of *CCW12* mRNPs using different ASOs for the elution with 5 mM and 16 mM biotin. ASO: biotinylated ASO; ASO-D: desthiobiotinylated ASO **E** Representative Western blot showing the copurification of nuclear mRNA-binding proteins for the ASO purification from A.

A

purification step	strain	condition	C_t(*CCW12*)	C_t(*PGK1*)	ΔC_t	Enrichment
Lysate	*Cbp20-TAP*		18.64	19.39	-0.76	1.69
Lysate	*Cbp20-TAP Δccw12*		26.52	19.43	7.09	0.01
TEV eluate	*Cbp20-TAP*		18.38	20.54	-2.15	4.45
TEV eluate	*Cbp20-TAP Δccw12*		26.62	20.06	6.56	0.01
ASO eluate	***Cbp20-TAP***	**2 L**	**27.31**	**34.69**	**-7.38**	**166.19**
ASO eluate	*Cbp20-TAP Δccw12*	2 L	32.99	32.56	0.44	0.74
ASO eluate	***Cbp20-TAP***	**12 L**	**27.65**	**34.99**	**-7.34**	**161.98**
ASO eluate	*Cbp20-TAP Δccw12*	12 L	36.33	36.33	0.00	1.00
FT concentrator	***Cbp20-TAP***	**12 L**	**28.23**	**33.83**	**-5.60**	**48.52**
FT concentrator	*Cbp20-TAP Δccw12*	12 L	33.53	30.90	2.63	0.16
Concentrated elution	***Cbp20-TAP***	**12 L**	**26.97**	**34.66**	**-7.69**	**205.90**
Concentrated elution	*Cbp20-TAP Δccw12*	12 L	31.70	34.77	-3.06	8.36

B

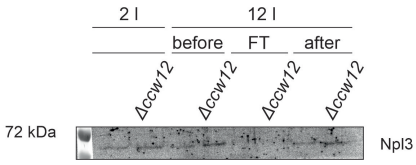

Figure A.10: **Test concentration of the eluate with centrifugal filter unit is not successful. A** Representative C_t value table for an desthiobiotinylated ASO1 purification of *CCW12* mRNPs from 2 and 24 l cultures. The eluate from the 24 l purification was concentrated using a centrifugal filter unit after purification. Ft: Flow through **E** Representative Western blot showing the copurification of nuclear mRNA-binding proteins for the ASO purification from A.

A

purification step	strain	condition	C_t(*SSA4*)	C_t(*CCW12*)	C_t(*PGK1*)	ΔC_t	Enrichment
Lysate	*Cbp20-TAP*		22.46	17.02	17.89		
Lysate	*Cbp20-TAP Δccw12*		23.94	27.62	17.06		
Lysate	*Cbp20-TAP*	HS	19.09	18.71	17.76		
Lysate	*Cbp20-TAP Δssa4*	HS	Undet.	18.95	18.16		
TEV eluate	*Cbp20-TAP*		22.53	16.44	17.84		
TEV eluate	*Cbp20-TAP Δccw12*		23.99	25.74	18.19		
TEV eluate	*Cbp20-TAP*	HS	19.30	17.58	17.40		
TEV eluate	*Cbp20-TAP Δssa4*	HS	30.57	18.10	18.17		
ASO eluate	***Cbp20-TAP***	***CCW12* ASO1**	**35.46**	**24.33**	**32.01**	**-7.69**	**205.90**
ASO eluate	*Cbp20-TAP Δccw12*	*CCW12* ASO1	33.06	32.93	31.59	1.34	0.39
ASO eluate	***Cbp20-TAP***	**HS, ASO 1**	**29.60**	**30.05**	**29.85**	**-0.25**	**1.19**
ASO eluate	*Cbp20-TAP Δssa4*	HS, ASO 1	29.54	30.05	29.62	-0.08	1.06
ASO eluate	***Cbp20-TAP***	**HS, ASO 4**	**28.70**	**31.20**	**30.28**	**-1.58**	**2.99**
ASO eluate	*Cbp20-TAP Δssa4*	HS, ASO 4	34.02	31.20	28.50	5.53	0.02
ASO eluate	***Cbp20-TAP***	**HS, ASO 5**	**28.91**	**25.78**	**29.10**	**-0.19**	**1.14**
ASO eluate	*Cbp20-TAP Δssa4*	HS, ASO 5	35.14	26.43	30.07	5.07	0.03

B

purification step	strain	condition	C_t(*SSA4*)	C_t(*CCW12*)	C_t(*PGK1*)	ΔC_t	Enrichment
Lysate	*Cbp20-TAP*		23.8	20.4	20.8		
Lysate	*Cbp20-TAP Δccw12*		25.1	30.0	20.1		
Lysate	*Cbp20-TAP*	HS	20.3	21.7	20.8		
Lysate	*Cbp20-TAP Δssa4*	HS	34.6	22.0	21.6		
TEV eluate	*Cbp20-TAP*		24.4	19.5	21.0		
TEV eluate	*Cbp20-TAP Δccw12*		25.0	28.5	21.2		
TEV eluate	*Cbp20-TAP*	HS	20.4	20.0	20.7		
TEV eluate	*Cbp20-TAP Δssa4*	HS	33.5	19.8	20.7		
ASO eluate	***Cbp20-TAP***	***CCW12* ASO1**	**32.7**	**23.0**	**30.2**	**-7.16**	**142.93**
ASO eluate	*Cbp20-TAP Δccw12*	*CCW12* ASO1	33.6	32.3	30.4	1.92	0.26
ASO eluate	***Cbp20-TAP***	**HS, ASO 8**	**26.6**	**29.4**	**30.7**	**-4.12**	**17.39**
ASO eluate	*Cbp20-TAP Δssa4*	HS, ASO 8	33.4	29.0	30.4	3.06	0.12
ASO eluate	***Cbp20-TAP***	**HS, ASO 12**	**35.5**	**30.7**	**30.7**	**4.86**	**0.03**
ASO eluate	*Cbp20-TAP Δssa4*	HS, ASO 12	28.9	31.0	29.9	-0.97	1.96
ASO eluate	***Cbp20-TAP***	**HS, ASO 15**	**28.7**	**29.6**	**30.4**	**-1.68**	**3.20**
ASO eluate	*Cbp20-TAP Δssa4*	HS, ASO 15	Undet.	30.1	30.8		

Figure A.11: **Test *SSA4* mRNP purifications using different ASOs**. Representative C_t value table for a *SSA4* mRNPs with different ASOs. The purification of *CCW12* mRNPs with ASO1 serves as positive control. Tested were ASOs 1, 4 and 5 (**A**) as well as ASOs 8, 12 and 15 (**B**). Binding sites of the ASOs can be found in Figure 5.3 B.

A

purification step	strain	condition	C_t(*SSA4*)	C_t(*CCW12*)	ΔC_t	Enrichment
Lysate	*WT*	HS	20.3	17.9		
Lysate	*Δrip1*	HS	24.1	18.0		
Lysate	*Δssa4*	HS	27.8	19.6		
Lysate	*Δrip1*		26.2	16.7		
ASO eluate	***WT***	***SSA4 ASO8***	**26.6**	**27.3**	**-0.75**	**1.68**
ASO eluate	***Δrip1***	***SSA4 ASO8***	**26.5**	**26.6**	**-0.07**	**1.05**
ASO eluate	*Δssa4*	*SSA4 ASO8*	27.4	28.7	-1.26	2.40
ASO eluate	*Δrip1*	*CCW12 ASO1*	28.9	24.2	-4.66	25.26

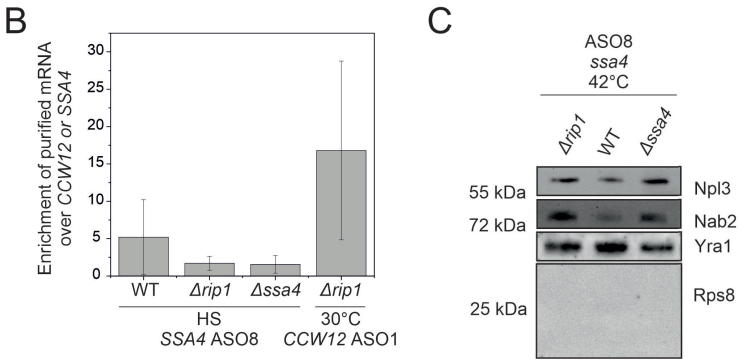

Figure A.12: ***SSA4* ASO purification in *Δrip1*** **A** Representative C_t value table for an *SSA4* ASO8 purification. The table contains results from a purification testing a one step purification from a strain where *RIP1* was deleted. ASO1 purification of *CCW12* mRNPs serves as control. **B** Fold change of the *SSA4* mRNA in the ASO elution for the different strains. Fold change was determined relative to *PGK1* mRNA by RT-qPCR. The mean ± SD is illustrated. **C** Representative Western blot showing the copurification of nuclear mRNA-binding proteins for the ASO purification from A and B.

B. mRNA export block in CBC deletion strains

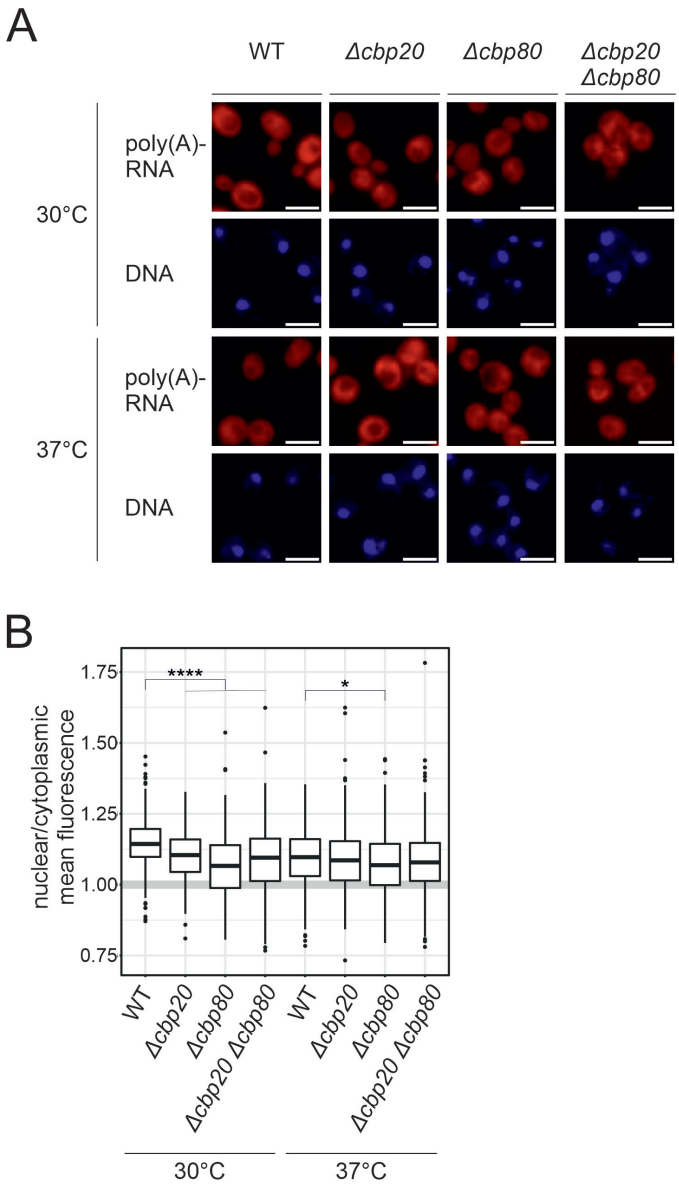

Figure B.1: **CBC mutants show a decreased nuclear/cytoplasmic poly(A)-RNA ratio at 30°C A** Representative microscopy images of an Oligo(dT) FISH performed for several CBC mutants. The DNA is stained with DAPI and depicted in blue. Poly(A)-RNA is stained using Oligo(dT)-Cy3 and depicted in red. The scale bar corresponds to 5 µm. **B** Quantification of Oligo(dT) FISH for different CBC mutants shown in A at 30°C and 37°C. The graph shows a box plot diagram of nuclear/cytoplasmic mean fluorescence for the tested mutants. Each quantification consists of three experiments with a total of $\geq$ 300 cells. The p-value was calculated using a Welch t-test with $\star$ $p < 0.05$ and$\star\star\star\star$ $p < 0.0001$.

C. Mango purification

purification step	strain	C_t(*SSA4*)	C_t(*CCW12*)	ΔC_t	Enrichment
Lysate	*Cbp20-TpA Δssa4 pRS316-SSA4*	22.15	21.06	1.09	0.47
Lysate	*Cbp20-TpA Δssa4 pRS316-SSA4-M1*	21.14	20.94	0.20	0.87
Lysate	*Cbp20-TpA Δssa4 pRS316-SSA4-M2*	20.67	20.86	-0.20	1.14
Lysate	*Cbp20-TpA Δssa4 pRS316-SSA4-M3*	20.37	21.45	-1.07	2.11
TEV eluate	*Cbp20-TpA Δssa4 pRS316-SSA4*	22.06	19.48	2.58	0.17
TEV eluate	*Cbp20-TpA Δssa4 pRS316-SSA4-M1*	20.97	18.84	2.12	0.23
TEV eluate	*Cbp20-TpA Δssa4 pRS316-SSA4-M2*	20.72	19.06	1.66	0.32
TEV eluate	*Cbp20-TpA Δssa4 pRS316-SSA4-M3*	20.99	20.12	0.87	0.55
Mango eluate	***Cbp20-TpA Δssa4 pRS316-SSA4***	**26.87**	**29.63**	**-2.75**	**6.74**
Mango eluate	***Cbp20-TpA Δssa4 pRS316-SSA4-P1***	**31.87**	**30.93**	**0.94**	**0.52**
Mango eluate	***Cbp20-TpA Δssa4 pRS316-SSA4-P2***	**31.43**	**30.76**	**0.67**	**0.63**
Mango eluate	***Cbp20-TpA Δssa4 pRS316-SSA4-P3***	**32.13**	**31.94**	**0.19**	**0.88**

Figure C.1: **The purification of *SSA4* mRNPs using the Mango aptamer yields no *SSA4* mRNA. A** Representative C_t value table for an *SSA4* Mango purification. The table contains results from test purification comparing integration of the Mango aptamer at three different positions of the 3'UTR. *SSA4* without aptamer serves as negative control.

D. MS2 purification

A

purification step	strain	C_t(*CCW12*)	C_t(*PGK1*)	ΔC_t	Enrichment
Lysate	*Cbp20-TpAΔccw12CCW12*	17.13	18.71	-1.58	2.98
Lysate	*Cbp20-TpAΔccw12CCW12-12xMS2V6P1*	18.43	18.92	-0.49	1.41
Lysate	*Cbp20-TpAΔccw12CCW12-12xMS2V6P2*	17.12	18.32	-1.21	2.31
Lysate	*Cbp20-TpAΔccw12CCW12-12xMS2V6P3*	17.48	19.02	-1.55	2.93
TEV eluate	*Cbp20-TpAΔccw12CCW12*	17.55	20.38	-2.83	7.12
TEV eluate	*Cbp20-TpAΔccw12CCW12-12xMS2V6P1*	17.87	19.28	-1.41	2.65
TEV eluate	*Cbp20-TpAΔccw12CCW12-12xMS2V6P2*	16.50	18.85	-2.35	5.08
TEV eluate	*Cbp20-TpAΔccw12CCW12-12xMS2V6P3*	16.36	19.12	-2.75	6.75
MS2 eluate	***Cbp20-TpAΔccw12CCW12***	**26.32**	**28.71**	**-2.39**	**5.25**
MS2 eluate	***Cbp20-TpAΔccw12CCW12-12xMS2V6P1***	**24.21**	**30.74**	**-6.53**	**92.14**
MS2 eluate	***Cbp20-TpAΔccw12CCW12-12xMS2V6P2***	**21.25**	**28.17**	**-6.92**	**121.02**
MS2 eluate	***Cbp20-TpAΔccw12CCW12-12xMS2V6P3***	**22.01**	**27.60**	**-5.59**	**48.26**

B

purification step	plasmid	condition	C_t(*CCW12*)	C_t(*PGK1*)	ΔC_t	Enrichment
Lysate	*CCW12*		20.0	21.2	-1.21	2.31
Lysate	*CCW12-MS2*		19.6	19.7	-0.04	1.02
TEV eluate	*CCW12*		17.7	20.7	-3.00	8.02
TEV eluate	*CCW12-MS2*		18.2	19.4	-1.10	2.15
MS2 eluate (nativ)	*CCW12*	Resin	26.5	29.0	-2.54	5.83
MS2 eluate (nativ)	***CCW12-MS2***	**Resin**	**24.9**	**29.3**	**-4.33**	**20.13**
MS2 eluate (nativ)	*CCW12*	Magnetic	29.9	31.1	-1.19	2.28
MS2 eluate (nativ)	***CW12-MS2***	**Magnetic**	**24.8**	**30.8**	**-5.97**	**62.87**

Figure D.1: **Optimization of the *CCW12* nuclear mRNP purification using the 12xMS2 based method.** **A** Representative C_t value table for an *CCW12* 12xMS2 purification. The table contains results from a purification testing the purification after integration of the 12xMS2 aptamer at three different positions of the 3'UTR. *CCW12* without aptamer serves as negative control. **B** Representative C_t value table for an *CCW12* 12xMS2 purification comparing the purification using amylose resin with magnetic amylose beads.

A

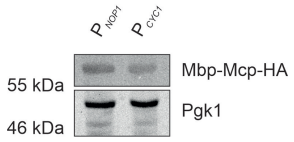

B

purification step	strain	C_t(*CCW12*)	C_t(*PGK1*)	ΔC_t	Enrichment
Lysate	P_{CYC1}-*MBP-MCP-3xHA CCW12*	20.3	21.0	-0.64	1.56
Lysate	P_{CYC1}-*MBP-MCP-3xHA CCW12-MS2*	19.6	20.1	-0.49	1.40
Lysate	P_{NOP1}-*MBP-MCP-3xHA CCW12*	19.3	19.9	-0.65	1.57
Lysate	P_{NOP1}-*MBP-MCP-3xHA CCW12-MS2*	21.2	20.0	1.19	0.44
TEV eluate	P_{CYC1}-*MBP-MCP-3xHA CCW12*	18.8	21.2	-2.36	5.14
TEV eluate	P_{CYC1}-*MBP-MCP-3xHA CCW12-MS2*	20.7	22.3	-1.59	3.01
TEV eluate	P_{NOP1}-*MBP-MCP-3xHA CCW12*	17.6	20.1	-2.53	5.78
TEV eluate	P_{NOP1}-*MBP-MCP-3xHA CCW12-MS2*	19.5	19.8	-0.31	1.24
MS2 eluate (denat.)	P_{CYC1}-*MBP-MCP-3xHA CCW12*	29.9	32.6	-2.73	6.62
MS2 eluate (denat.)	P_{CYC1}-***MBP-MCP-3xHA CCW12-MS2***	**24.8**	**31.4**	**-6.60**	**97.22**
MS2 eluate (denat.)	P_{NOP1}-*MBP-MCP-3xHA CCW12*	25.8	28.5	-2.74	6.69
MS2 eluate (denat.)	P_{NOP1}-***MBP-MCP-3xHA CCW12-MS2***	**26.6**	**30.5**	**-3.88**	**14.73**
MS2 eluate (nativ)	P_{CYC1}-*MBP-MCP-3xHA CCW12*	28.0	29.7	-1.75	3.36
MS2 eluate (nativ)	P_{CYC1}-***MBP-MCP-3xHA CCW12-MS2***	**28.2**	**32.7**	**-4.52**	**22.88**
MS2 eluate (nativ)	P_{NOP1}-*MBP-MCP-3xHA CCW12*	27.3	29.6	-2.35	5.10
MS2 eluate (nativ)	P_{NOP1}-***MBP-MCP-3xHA CCW12-MS2***	**25.0**	**30.1**	**-5.11**	**34.58**

Figure D.2: **The usage of the *NOP1* instead of the *CYC1* promoter increases the Mbp-Mcb-3xHA level but reduced yield of *CCW12* during mRNP purification. A** Representative Western blot for the quantification of the Mbp-Mcp-3xHA protein expressed under the control of the *CYC1* or *NOP1* promoter. Pgk1 served as loading control. **B** Representative C_t value table for an *CCW12* 12xMS2 purification comparing native and denaturing purification from strains expressing the Mbp-Mcp-3xHA protein either from a *CYC1* or a *NOP1* promoter.

A

purification step	strain	C_t(*SSA4*)	C_t(*CCW12*)	ΔC_t	Enrichment
Lysate	*Cbp20-TpA Δssa4 pRS316-SSA4*	21.6	22.1	-0.47	1.38
Lysate	*Cbp20-TpA Δssa4 pRS316-SSA4-M1*	21.6	21.9	-0.36	1.28
Lysate	*Cbp20-TpA Δssa4 pRS316-SSA4-M2*	21.7	21.7	0.01	0.99
Lysate	*Cbp20-TpA Δssa4 pRS316-SSA4-M3*	22.1	22.2	-0.11	1.08
TEV eluate	*Cbp20-TpA Δssa4 pRS316-SSA4*	22.0	21.4	0.51	0.70
TEV eluate	*Cbp20-TpA Δssa4 pRS316-SSA4-M1*	24.8	23.9	0.90	0.54
TEV eluate	*Cbp20-TpA Δssa4 pRS316-SSA4-M2*	20.4	19.1	1.29	0.41
TEV eluate	*Cbp20-TpA Δssa4 pRS316-SSA4-M3*	20.0	18.8	1.20	0.44
MS2 eluate	***Cbp20-TpA Δssa4 pRS316-SSA4***	**27.7**	**27.7**	**0.00**	**1.00**
MS2 eluate	***Cbp20-TpA Δssa4 pRS316-SSA4-M1***	**26.3**	**29.7**	**-3.40**	**10.58**
MS2 eluate	***Cbp20-TpA Δssa4 pRS316-SSA4-M2***	**27.0**	**28.9**	**-1.96**	**3.89**
MS2 eluate	***Cbp20-TpA Δssa4 pRS316-SSA4-M3***	**26.8**	**29.0**	**-2.14**	**4.40**

B

purification step	strain	C_t(*SSA4*)	C_t(*CCW12*)	ΔC_t	Enrichment
Lysate	*Δrip pRS316-SSA4*	23.2	21.8	1.42	0.37
Lysate	*pRS316-SSA4-12xMS2*	21.2	21.9	-0.67	1.60
Lysate	*Δrip pRS316-SSA4-12xMS2*	23.1	21.2	1.84	0.28
MS2 eluate	*Δrip pRS316-SSA4*	29.68	30.34	-0.66	1.58
MS2 eluate	*pRS316-SSA4-12xMS2*	21.5	29.1	-7.67	203.04
MS2 eluate	***Δrip pRS316-SSA4-12xMS2***	**24.5**	**30.3**	**-5.79**	**55.19**

C

purification step	plasmid	C_t(*SSA4*)	C_t(*CCW12*)	ΔC_t	Enrichment
Lysate	*pRS316-SSA4*	24.9	23.3	1.57	0.34
Lysate	*pRS316-SSA4-3xMS2*	20.0	19.9	0.06	0.96
Lysate	*pRS316-SSA4-12xMS2*	20.3	20.6	-0.29	1.22
TEV eluate	*pRS316-SSA4*	22.2	20.8	1.37	0.39
TEV eluate	*pRS316-SSA4-3xMS2*	20.3	20.8	-0.57	1.48
TEV eluate	*pRS316-SSA4-12xMS2*	20.3	19.5	0.80	0.58
MS2 eluate	*pRS316-SSA4*	30.6	31.9	-1.33	2.52
MS2 eluate	***pRS316-SSA4-3xMS2***	**27.4**	**28.6**	**-1.14**	**2.20**
MS2 eluate	***pRS316-SSA4-12xMS2***	**29.8**	**32.1**	**-2.32**	**5.01**

Figure D.3: **The purification of nuclear *SSA4* mRNP yields the best results when used as a one step purification from *Δrip1* cells. A** Representative C_t value table for a 12xMS2 based *SSA4* mRNP purification. The table contains results from a purification testing the purification after integration of the 12xMS2 aptamer at three different positions of the 3'UTR. *SSA4* without aptamer serves as negative control. **B** Representative C_t value table of a one step *SSA4* 12xMS2 purification from a *Δrip1* strain. **C** Representative C_t value table for an *SSA4* MS2 purification comparing the purification using a 12xMS2V6 with a 3xMS2 variant.

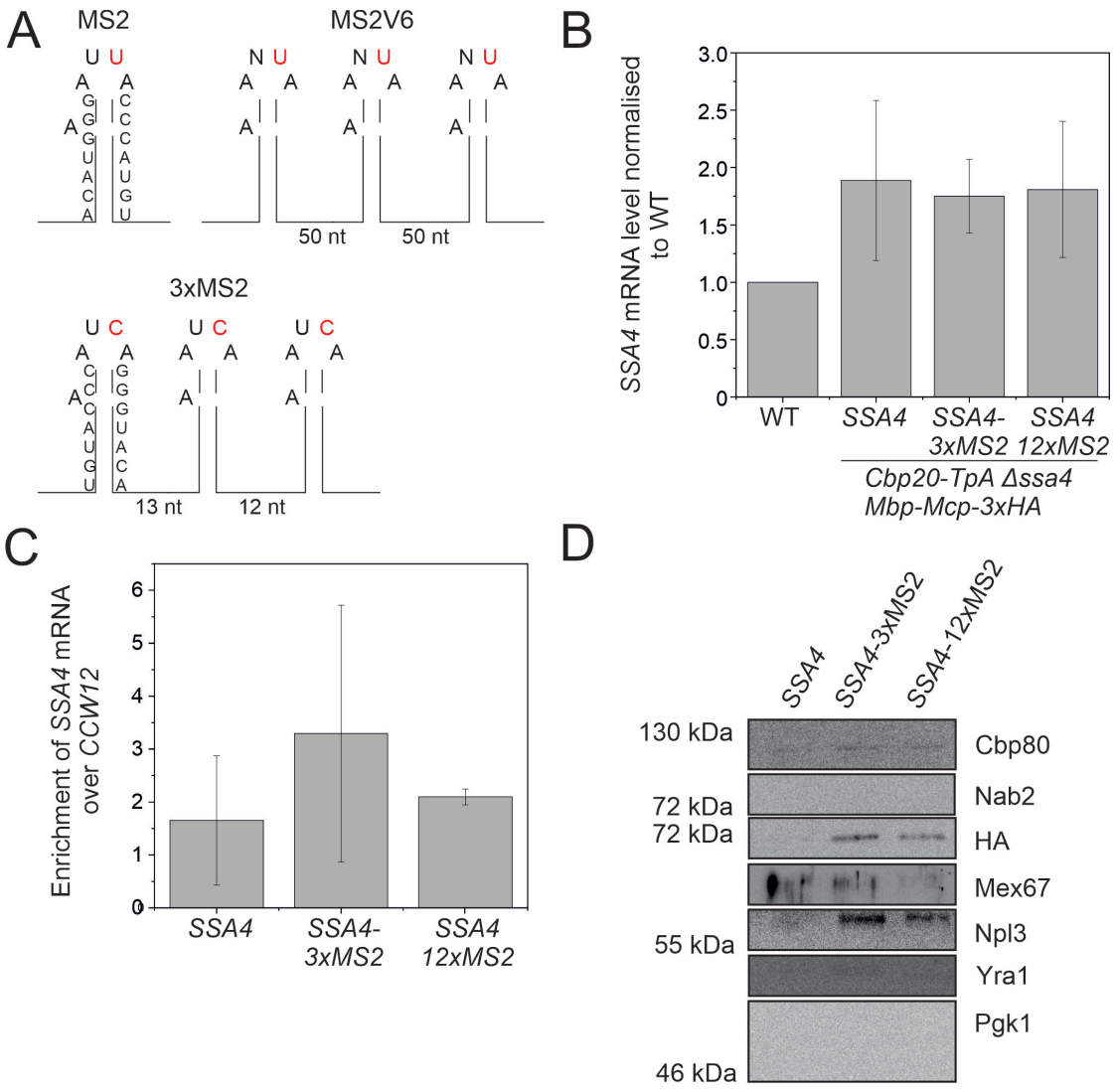

Figure D.4: **Using an 3xMS24 loop with higher affinity to the Mcp does not improve the purification of *SSA4* mRNPs.** **A** Schematic representation of the different MS2 stem loops used in this study. The MS2 and MS2V6 stem loop taken from Tutucci et al. [2018]. The 3xMS24 loop is based on the system used by Zhou et al. [2002] for splicosome purifications. **B** Relative *SSA4* mRNA levels compared to WT after heat shock. RNA levels were determined by RT-qPCR. The data represents the mean ± SD. **C** Enrichment of *SSA4* mRNA over *CCW12* after nuclear mRNP purification using the different MS2 aptamers. *SSA4* without aptamer serves as negative control. The qPCR values of all purification steps of a representative purification can be found in Supplement D.3. **D** Representative Western blot for the purification shown in D. The Western blot shows the amount of purified Mbp-Mcp-3xHA detected with an HA antibody. Antibodies against known nuclear mRNA-binding proteins were used. Pgk1 serves as negative control.

A

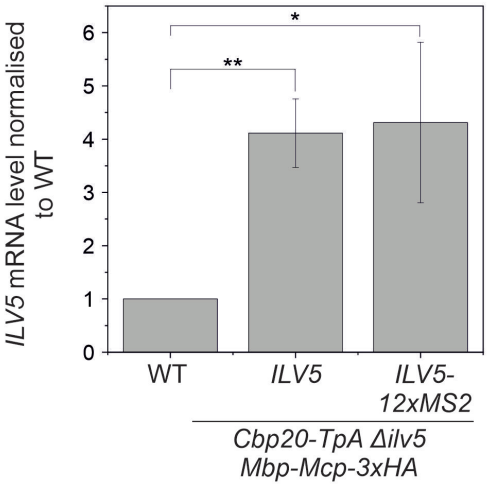

B

purification step	strain	C_t(*SSA4*)	C_t(*PGK*)	ΔC_t	Enrichment
Lysate	*Δilv5* pRS314-*ILV5*	21.8	19.6	2.26	0.21
Lysate	*Δilv5* pRS314-*ILV5-12xMS2*	22.3	20.0	2.25	0.21
TEV eluate	*Δilv5* pRS314-*ILV5*	22.7	21.8	0.91	0.53
TEV eluate	*Δilv5* pRS314-*ILV5-12xMS2*	22.8	21.0	1.80	0.29
eluate	***Δilv5 pRS314-ILV5***	**28.3**	**32.0**	**-3.70**	**13.00**
eluate	*Δilv5 pRS314-ILV5-12xMS2*	34.1	31.3	2.80	0.14

C

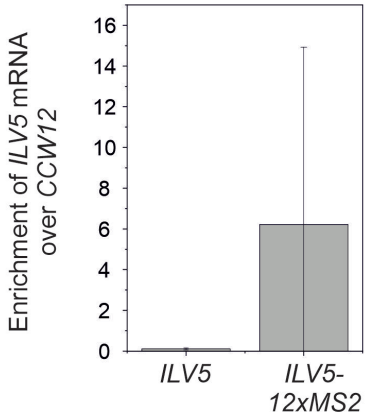

D

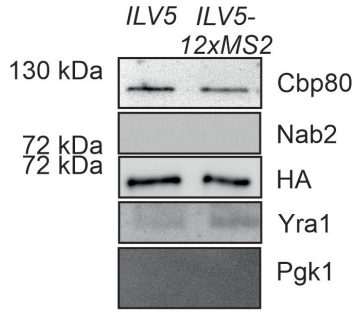

Figure D.5: **Purification of *ILV5* mRNPs using the 12xMS2 based method.** **B** Relative *ILV5* mRNA levels compared to WT after heat shock. RNA levels were determined by RT-qPCR. The data represents the mean ± SD. **B** Representative C_t value table for an *ILV5* 12xMS2 purification. **C** Enrichment of *ILV5* mRNA over *CCW12* after nuclear mRNP purification using the 12xMS2 based purification method. *ILV5* without aptamer serves as negative control. **D** Representative Western blot for the purification shown in B and C. The Western blot shows the amount of purified Mbp-Mcp-3xHA detected with an HA antibody. Antibodies against known nuclear mRNA-binding proteins were used. Pgk1 serves as negative control.

E. Cross-linking of heat shock mRNPs

Table E.1: Overview of changes applied to TRIP to test the method for the identification of nuclear heat shock mRNA-binding proteins. The original method was published by Matia-González et al. [2017].

TRIP	major adaptations TRIP
UV/PAR cross-linking	Chemical cross-linking
Single ASOs	
First step mRNA purification using Oligo(dT) beads	First step nuclear mRNP enrichment using *Cbp20-TAP*
Binding and Wash buffer similar to our ASO protocol	
Annealing: 70 -50 °C	Annealing: 37°C (Formaldehyde)
Wash buffer preheated at 50°C	Wash buffer preheated at 37°C

A

purification step	strain	C_t(*SSA4*)	C_t(*CCW12*)	C_t(*PGK1*)	ΔC_t	Enrichment
Lysate	*Cbp20-TpA*	28.0	20.7	22.3	-1.54	2.90
Lysate	*Cb20-TpA Δccw12*	27.0	32.8	21.9	10.81	0.00
Lysate	*Cbp20-TpA*	26.3	23.4	22.7	3.57	0.08
Lysate	*Cb20-TpA Δssa4*	34.1	21.7	22.2	11.94	0.00
TEV eluate	*Cbp20-TpA*	25.3	18.5	20.0	-1.55	2.93
TEV eluate	*Cb20-TpA Δccw12*	24.7	28.5	19.9	8.59	0.00
TEV eluate	*Cbp20-TpA*	23.8	21.7	21.0	2.80	0.14
TEV eluate	*Cb20-TpA Δssa4*	32.3	19.4	22.6	9.63	0.00
eluate	***Cbp20-TpA***	**28.5**	**21.3**	**24.11**	**-2.80**	**6.94**
eluate	*Cb20-TpA Δccw12*	24.8	28.2	23.40	4.77	0.04
eluate	***Cbp20-TpA***	**26.2**	**24.5**	**25.25**	**1.00**	**0.50**
eluate	*Cb20-TpA Δssa4*	33.4	22.2	23.52	9.93	0.00

B

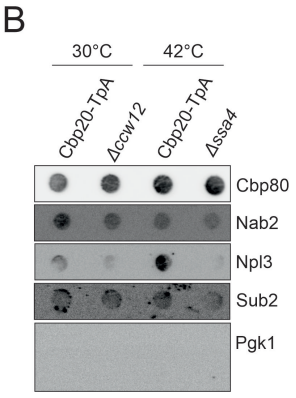

Figure E.1: **Test cross-linking and purification of heat shock mRNPs using the TRIP protocol A** Representative C_t value table for an TRIP purification of *CCW12* and *SSA4* mRNPs. **B** Representative Dot blot showing the copurification of nuclear mRNA-binding proteins for the TRIP purification from A.

Table E.2: Overview of changes applied to ChIRP to test the method for the identification of nuclear heat shock mRNA-binding proteins. The original method was published by Chu et al. [2012].

ChIRP	major adaptations ChIRP
Chemical cross-linking ASO-Mix 1 step purification from lysate Harsh buffer conditions in hybridization and wash buffer (high salt, SDS) Annealing and purification at 37°C	Chemical cross-linking Single ASO First step nuclear mRNP enrichment using *Cbp20-TAP*

A

purification step	strain	C_t(*SSA4*)	C_t(*CCW12*)	C_t(*PGK1*)	ΔC_t	Enrichment
Lysate	*Cbp20-TpA*		15.2	16.77	-1.55	2.93
Lysate	*Cb20-TpA Δccw12*		23.9	16.65	7.26	0.01
Lysate	*Cbp20-TpA*	*16.5*	15.9	16.49	-0.01	1.01
Lysate	*Cb20-TpA Δssa4*	*26.8*	16.2	16.91	9.86	0.00
TEV eluate	*Cbp20-TpA*		15.6	18.04	-2.46	5.49
TEV eluate	*Cb20-TpA Δccw12*		24.2	18.01	6.17	0.01
TEV eluate	*Cbp20-TpA*	*18.1*	17.4	18.35	-0.28	1.22
TEV eluate	*Cb20-TpA Δssa4*	*26.8*	17.0	18.30	8.48	0.00
eluate	***Cbp20-TpA***		**19.0**	**23.56**	**-4.56**	**23.58**
eluate	*Cb20-TpA Δccw12*		28.5	25.36	3.16	0.11
eluate	***Cbp20-TpA***	**21.1**	**23.6**	**23.68**	**-2.60**	**6.08**
eluate	*Cb20-TpA Δssa4*	29.0	23.3	23.39	5.63	0.02

B

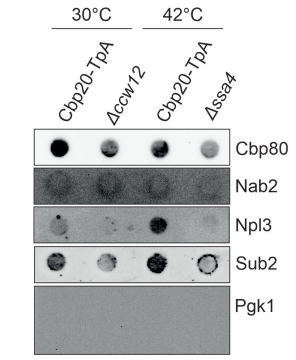

Figure E.2: **Test cross-linking and purification of heat shock mRNPs using the ChIRP protocol. A** Representative C_t value table for an ChIRP purification of *CCW12* and *SSA4* mRNPs. **B** Representative Dot blot showing the copurification of nuclear mRNA-binding proteins for the ChIRP purification from A.

A

purification step	strain	C_t(*SSA4*)	C_t(*CCW12*)	ΔC_t	Enrichment
Lysate	*Cbp20-TpA*	*18.2*	17.9	0.28	0.82
Lysate	*Cb20-TpA Δssa4*	*32.1*	21.8	10.29	0.00
TEV eluate	*Cbp20-TpA*	*22.4*	22.3	0.04	0.97
TEV eluate	*Cb20-TpA Δssa4*	*30.1*	20.2	9.91	0.00
RAP eluate	***Cbp20-TpA***	**25.0**	**30.8**	**-5.84**	**57.40**
RAP eluate	*Cb20-TpA Δssa4*	31.7	29.4	2.33	0.20

B

purification step	strain	condition	C_t(*SSA4*)	C_t(*CCW12*)	C_t(*PGK1*)
Lysate	*Cbp20-TpA (HS)*		20.6	18.8	19.5
Lysate	*Cbp20-TpA (30°C)*		22.9	16.8	19.4
TEV eluate	*Cbp20-TpA (HS)*		21.1	19.6	21.2
TEV eluate	*Cbp20-TpA (30°C)*		22.0	16.8	20.5
RAP eluate	*Cbp20-TpA (HS)*	***SSA4* all (21)**	**20.8**	**21.8**	**33.5**
RAP eluate	*Cbp20-TpA (HS)*	***SSA4* even**	**22.3**	**23.2**	**32.8**
RAP eluate	*Cbp20-TpA (HS)*	***SSA4* odd**	**21.2**	**21.7**	**32.8**
RAP eluate	*Cbp20-TpA (HS)*	***SSA4* ASO8**	**25.4**	**31.8**	**32.3**
RAP eluate	*Cb20-TpA* (30°C)	*CCW12* all (5)		16.2	33.1
RAP eluate	*Cb20-TpA Δssa4*	*CCW12* ASO1		21.9	32.1

purification step	strain	condition	ΔCt(-*CCW12*)	Enrichment over *CCW12*	ΔCt(-PGK1)	Enrichment over *PGK1*
Lysate	*Cbp20-TpA (HS)*					
Lysate	*Cbp20-TpA (30°C)*					
TEV eluate	*Cbp20-TpA (HS)*					
TEV eluate	*Cbp20-TpA (30°C)*					
RAP eluate	*Cbp20-TpA (HS)*	***SSA4* all (21)**	**-1.0**	**2.0**	**-12.64**	**6399.23**
RAP eluate	*Cbp20-TpA (HS)*	***SSA4* even**	**-0.9**	**1.8**	**-10.44**	**1384.72**
RAP eluate	*Cbp20-TpA (HS)*	***SSA4* odd**	**-0.5**	**1.5**	**-11.60**	**3107.02**
RAP eluate	*Cbp20-TpA (HS)*	***SSA4* ASO8**	**-6.4**	**84.2**	**-6.95**	**123.73**
RAP eluate	*Cb20-TpA* (30°C)	*CCW12* all (5)			-16.92	124411.79
RAP eluate	*Cb20-TpA Δssa4*	*CCW12* ASO1			-10.23	1199.54

Figure E.3: **Test cross-linking and purification of heat shock mRNPs using the RAP-MS protocol. A** Representative C_t value table for the purification of cross-linked, nuclear *SS4* mRNPs using the modified RAP-MS protocol (Table 5.3) with ASO8. **B** Representative C_t value table for an RAP-MS purification of *SSA4* mRNPs testing different ASOs: *SSA4* all: Mix of 21 90mer DNA ASOs covering the whole transcript; *SSA4* odd: Mix of DNA ASOs with odd numbers; *SSA4* even: Mix of DNA ASOs with even numbers; *CCW12* all: Mix of 5 90mer DNA ASOs covering the whole transcript; ASO1 and ASO8: 2'O-Methylated RNA ASOs also used for native purification.

purification step	strain	condition	C_t(*SSA4*)	C_t(*CCW12*)	C_t(*PGK1*)	Ct(*ILV5*)
Lysate	*Cbp20-TpA*		21.2	19.9	19.7	28.8
Lysate	*Cbp20-TpA Δssa4*		30.6	19.4	19.7	29.0
TEV eluate	*Cbp20-TpA*		24.9	24.1	23.6	31.4
TEV eluate	*Cbp20-TpA Δssa4*		30.5	23.6	23.3	31.0
RAP eluate	*Cbp20-TpA*	***SSA4* all (21)**	**22.6**	**23.9**	**32.2**	**35.4**
RAP eluate	*Cb20-TpA Δssa4*	*SSA4* all (21)	29.6	22.4	31.4	34.7

purification step	strain	condition	C_t(*HSP105*)	C_t(*HSP12*)	C_t(*KAR2*)	Ct(*RPL28*)
Lysate	*Cbp20-TpA*		22.1	20.0	25.4	32.3
Lysate	*Cbp20-TpA Δssa4*		22.1	20.5	25.4	31.5
TEV eluate	*Cbp20-TpA*		25.6	24.3	27.3	33.2
TEV eluate	*Cbp20-TpA Δssa4*		25.1	24.2	27.0	32.5
RAP eluate	*Cbp20-TpA*	***SSA4* all (21)**	**35.3**	**36.8**	**34.9**	**35.6**
RAP eluate	*Cb20-TpA Δssa4*	*SSA4* all (21)	35.2	34.3	35.4	35.3

purification step	strain	condition	C_t(*SSA4*)	C_t(*YEF3*)
Lysate	*Cbp20-TpA*		21.4	26.9
Lysate	*Cbp20-TpA Δssa4*		30.5	27.1
TEV eluate	*Cbp20-TpA*		23.1	29.4
TEV eluate	*Cbp20-TpA Δssa4*		26.8	28.9
RAP eluate	*Cbp20-TpA*	***SSA4* all (21)**	**20.7**	**34.4**
RAP eluate	*Cb20-TpA Δssa4*	*SSA4* all (21)	25.3	35.1

purification step	strain	condition	C_t(*SSA4*)	C_t(YDR524C-B)
Lysate	*Cbp20-TpA*		20.5	21.5
Lysate	*Cbp20-TpA Δssa4*		28.0	22.4
TEV eluate	*Cbp20-TpA*		23.8	25.1
TEV eluate	*Cbp20-TpA Δssa4*		28.2	24.5
RAP eluate	*Cbp20-TpA*	***SSA4* all (21)**	**24.9**	**33.0**
RAP eluate	*Cb20-TpA Δssa4*	*SSA4* all (21)	28.9	33.6

Figure E.4: **The purification of nuclear, *SSA4* mRNPs using the RAP-MS method yields a high enrichment of *SSA4* mRNA over all tested mRNAs except *CCW12*.** Representative C_t value table for the purification of cross-linked, nuclear *SS4* mRNPs using the modified RAP-MS protocol with all ASOs. The copurification of other transcripts was analyzed using RT-qPCR.

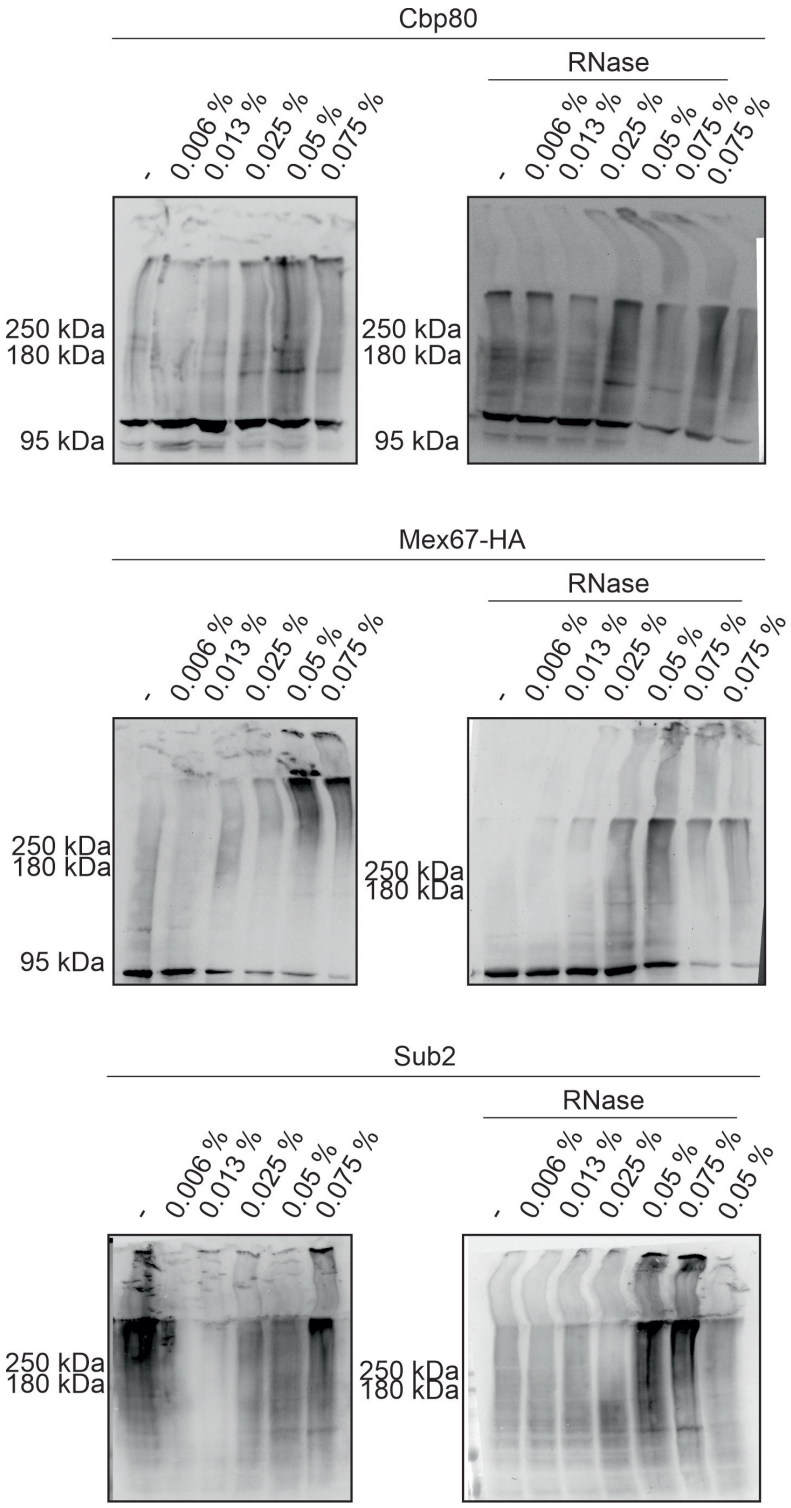

Figure E.5: **Cross-linked proteins can be detected in lysate samples using Wet blot.** Wet blot to detect RNA-protein cross-links. Cells were treated with different concentrations of GA, lysed and half of the sample was incubated with an RNase Mix (RNase). Lysate samples were used for Wet blot to detect cross-linked Cbp80, Mex67 and Sub2.

purification step	GA concentraion	C_t(*SSA4*)	C_t(*CCW12*)
Lysate	*0*	28.0	20.7
Lysate	*0.05*	27.0	32.8
Lysate	*0.1*	26.3	23.4
Lysate	*0.5*	34.1	21.7
eluate	*0*	20.9	21.4
eluate	*0.05*	20.3	21.5
eluate	*0.1*	22.9	23.6
eluate	*0.5*	30.1	31.0

Figure E.6: **Purified *SSA4* mRNA yield reduces with increased GA concentration.** Representative C_t value table containing the values of lysate and elution of a RAP-MS purification testing the yield of *SSA4* mRNA after cross-linking the cells with different concentrations of GA.

Accession	Description	Exp. q-value: Mascot	Coverage [%]	# Peptides	# PSMs	# Unique Peptides
P00925	Enolase 2	0	47	14	20	5
Q07478	ATP-dependent RNA helicase SUB2	0	26	12	27	12
P06169	Pyruvate decarboxylase isozyme 1	0	20	7	11	7
P00359	Glyceraldehyde-3-phosphate dehydrogenase 3	0	35	9	11	9
P00549	Pyruvate kinase 1	0	14	6	6	6
P00330	Alcohol dehydrogenase 1	0	28	7	7	7
Q12159	RNA annealing protein YRA1	0	32	7	8	7
P60010	Actin	0	12	5	6	5
P10592	Heat shock protein SSA2	0	7	3	3	3
P02994	Elongation factor 1-alpha	0	14	6	6	6
P0CH08	Ubiquitin-60S ribosomal protein L40	0	14	2	2	2
P00560	Phosphoglycerate kinase	0	12	4	4	4
P14127	40S ribosomal protein S17-B	0	15	2	2	2
P38766	ATP-dependent DNA helicase RRM3	0	5	3	3	3
P53076	Vacuolar import and degradation protein 30	0.071	2	2	5	2
Q01454	DNA polymerase alpha-binding protein	0.025	2	2	3	2
Q06412	Rho1 guanine nucleotide exchange factor TUS1	0.02	2	2	2	2
P54784	Origin recognition complex subunit 1	0.043	7	4	5	4
P53112	Peroxisomal membrane protein PEX14	0.059	10	2	6	2
P35209	Protein SPT21	0.043	2	2	5	2
P33314	Inhibitory regulator protein BUD2/CLA2	0.05	2	2	5	2
P07702	L-2-aminoadipate reductase	0.026	1	3	3	3
Q06078	U3 small nucleolar RNA-associated protein 21	0.017	2	2	2	2
P15938	Pre-mRNA-splicing factor ATP-dependent RNA helicase PRP16	0.063	2	2	7	2
P41832	Protein BNI1	0.039	3	4	4	4
Q08118	Uncharacterized protein IRC10	0.012	6	2	2	2
P02829	ATP-dependent molecular chaperone HSP82	0.047	5	3	5	3
P33892	eIF-2-alpha kinase activator GCN1	0.014	1	2	2	2
P20424	Signal recognition particle subunit SRP54	0.061	18	4	6	4
P39013	Actin cytoskeleton-regulatory complex protein END3	0.056	13	3	5	3
P32492	Myosin-4	0.065	2	2	10	2
Q04195	E3 SUMO-protein ligase SIZ1	0.031	3	2	4	2
Q99207	Nucleolar complex protein 14	0.032	5	2	4	2
P36069	Probable phosphoglycerate mutase PMU1	0.01	9	2	2	2
P34237	Protein CASP	0.029	2	3	4	3
P53844	Phosphatidylinositol transfer protein PDR17	0.01	5	2	2	2
P17065	Rab guanine nucleotide exchange factor SEC2	0.014	3	2	2	2
Q12019	Midasin	0.013	0	2	2	2
P32333	TATA-binding protein-associated factor MOT1	0.013	1	2	2	2
P04051	DNA-directed RNA polymerase III subunit RPC1	0.038	1	2	4	2
C8ZDL9	Heme-responsive zinc finger transcription factor HAP1	0.069	3	2	13	2

Figure E.7: **Proteins identified by RAP-MS for both samples and both tested GA concentrations.** List of proteins identified by RAP-MS for the heat shock treated sample with 0.075 % GA which were also found in the 0.05 % GA treated sample as well as in both negative control samples.

F. FISH of different stress conditions in WT and *Δslt2*

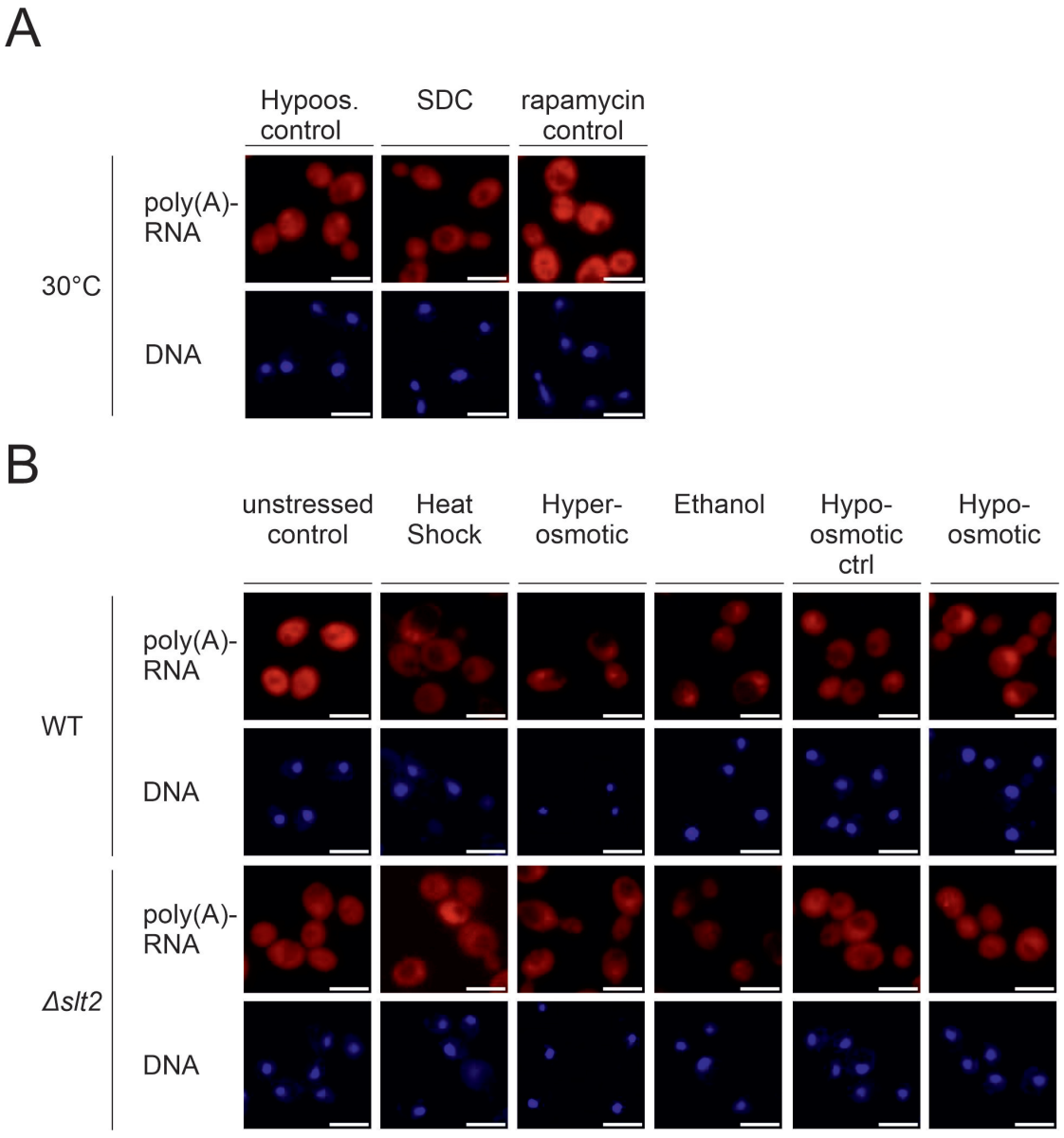

Figure F.1: **Deletion of *Slt2* does not prevent the mRNA export block observed for all tested stress conditions. A** Representative FISH images for additional controls not shown in Figure 5.16. **B** Representative FISH images for WT and *Δslt2* cells treated with heat shock, hyperosmotic stress, ethanol and hypoosmotic stress and the corresponding controls. The DNA is stained with DAPI and depicted in blue. Poly(A)-RNA is stained using Oligo(dT)-Cy3 and depicted in red. The scale bar corresponds to 5 µm.

G. Phosphoproteome

The whole data from the generated phosphoproteome analysis is saved on the enclosed CD.

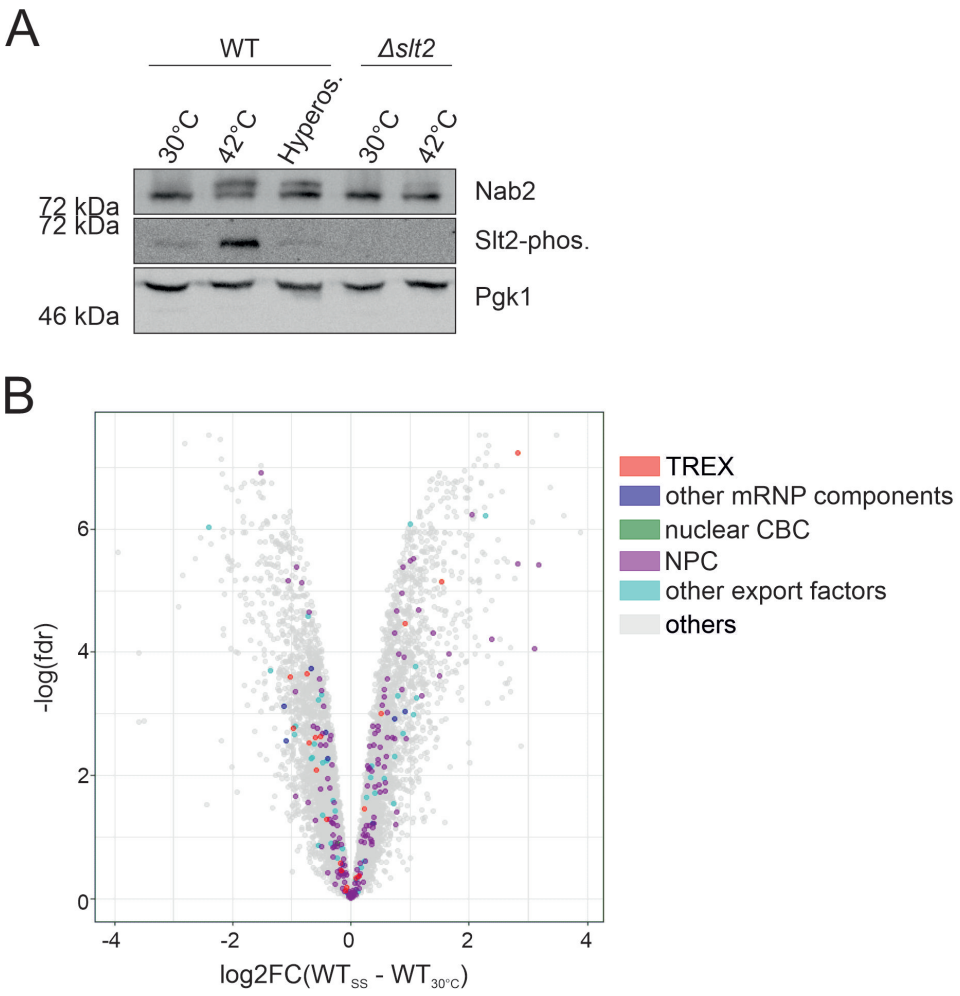

Figure G.1: **Export factors are differentially phosphorylated durign hyperosmotic stress A** Western blot of phosphoproteome samples showing the phosphorylation of Nab2 after heat stress and hyperosmotic stress. **B** Volcano plot showing the log2 fold change of the phosphorylation of the WT during hyperosmotic stress (WT_{SS} - WT_{30C}) against the -log(fdr). Export factors are colored: TREX component = red, other mRNP components (Nab2, Npl3, Tho1) = blue, nuclear CBC = green, NPC = purple, remaining export factors (eg. Gfd1) = cyan

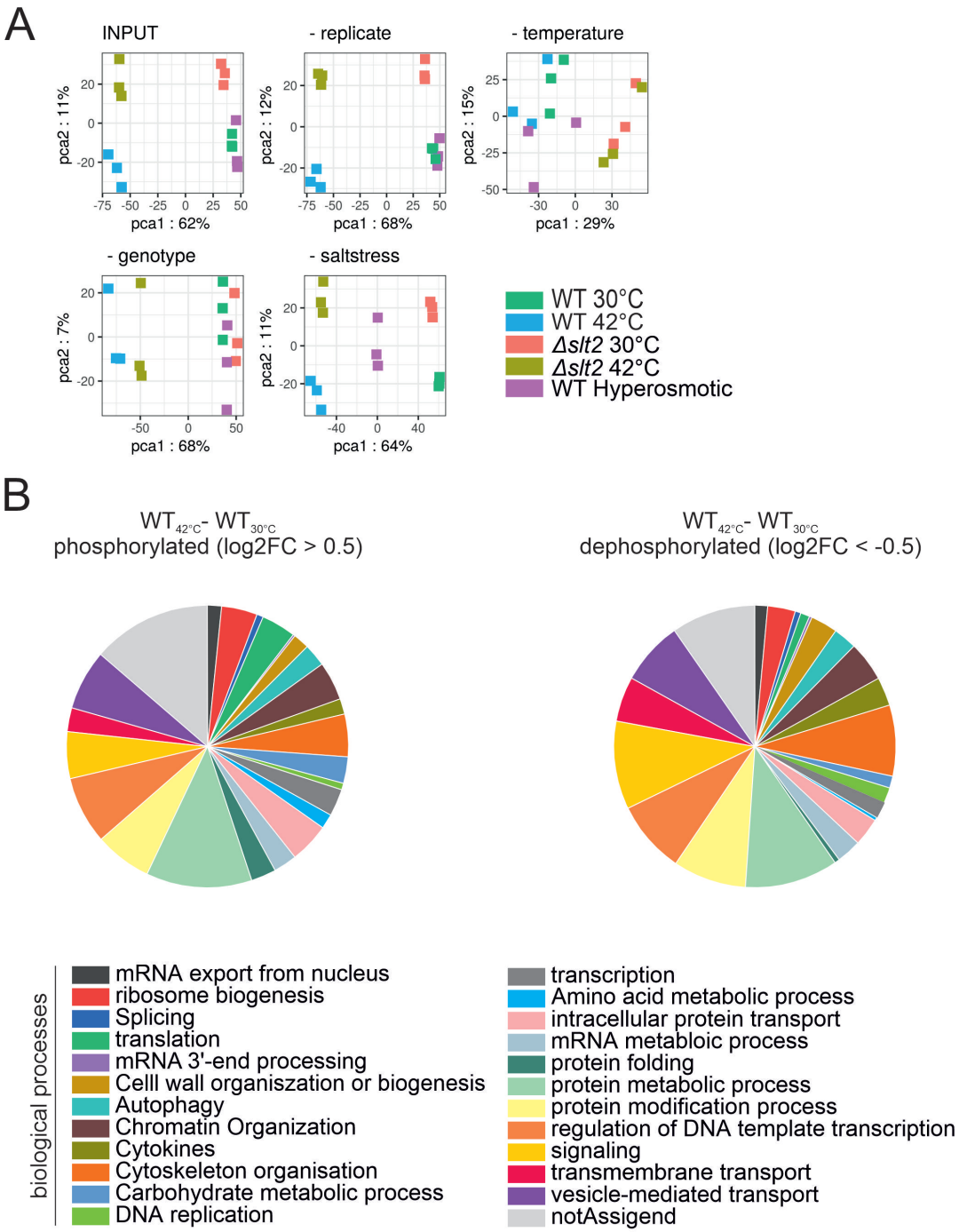

Figure G.2: **Principle component analysis Phosphoproteome data A** Principle component analysis of the different phosphoproteome samples. **B** Pie chart showing the percentages of residues with changed phosphorylation belonging to proteins of several biological processes during heat stress. One protein(or site) can be associated with several biological processes. The residues of the category "others" could not be assigned to any of the other categories.

H. Influence of phosphorylation of export factors on mRNA export block during heat stress

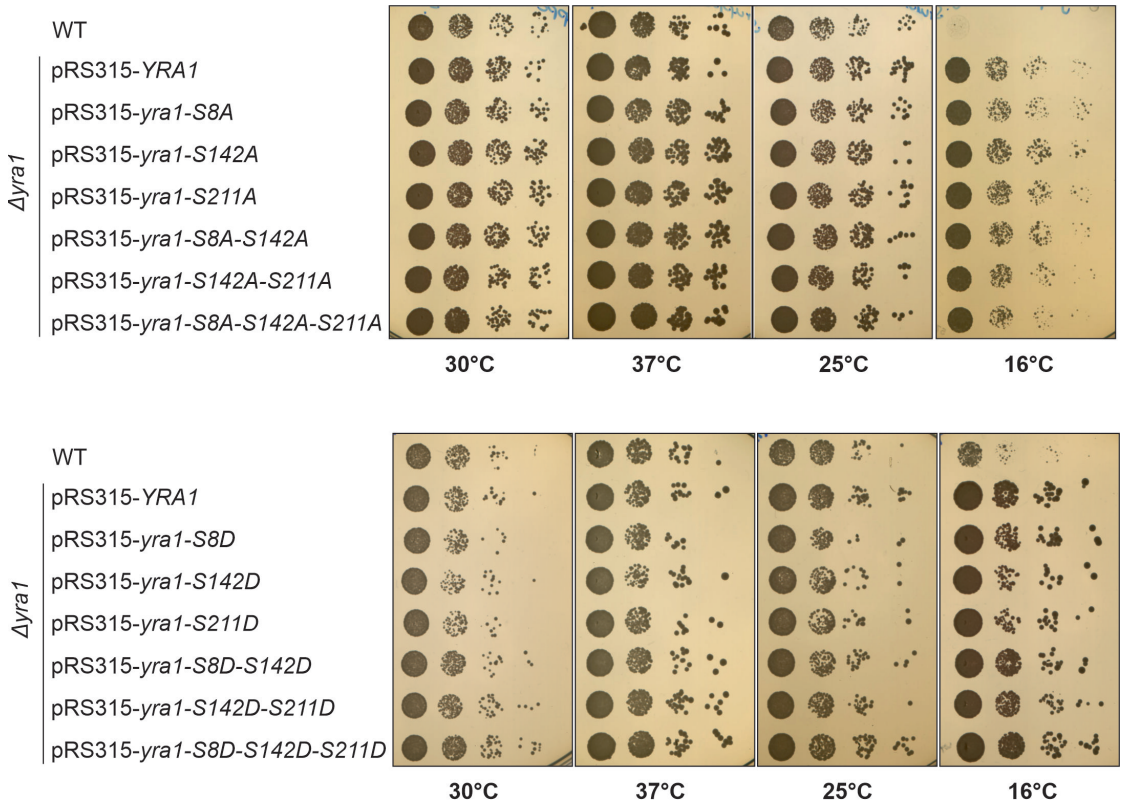

Figure H.1: **Yra1 mutants show no effect on growth. A** Representative growth spot assay showing the influence of the different mutations on the corresponding yeast strain. Cells were spotted in 4 serial 1:10 dilutions. Plates were incubated for 2 days at 30°C, 3 days at 37°C and 25°C and 8 days at 16°C.

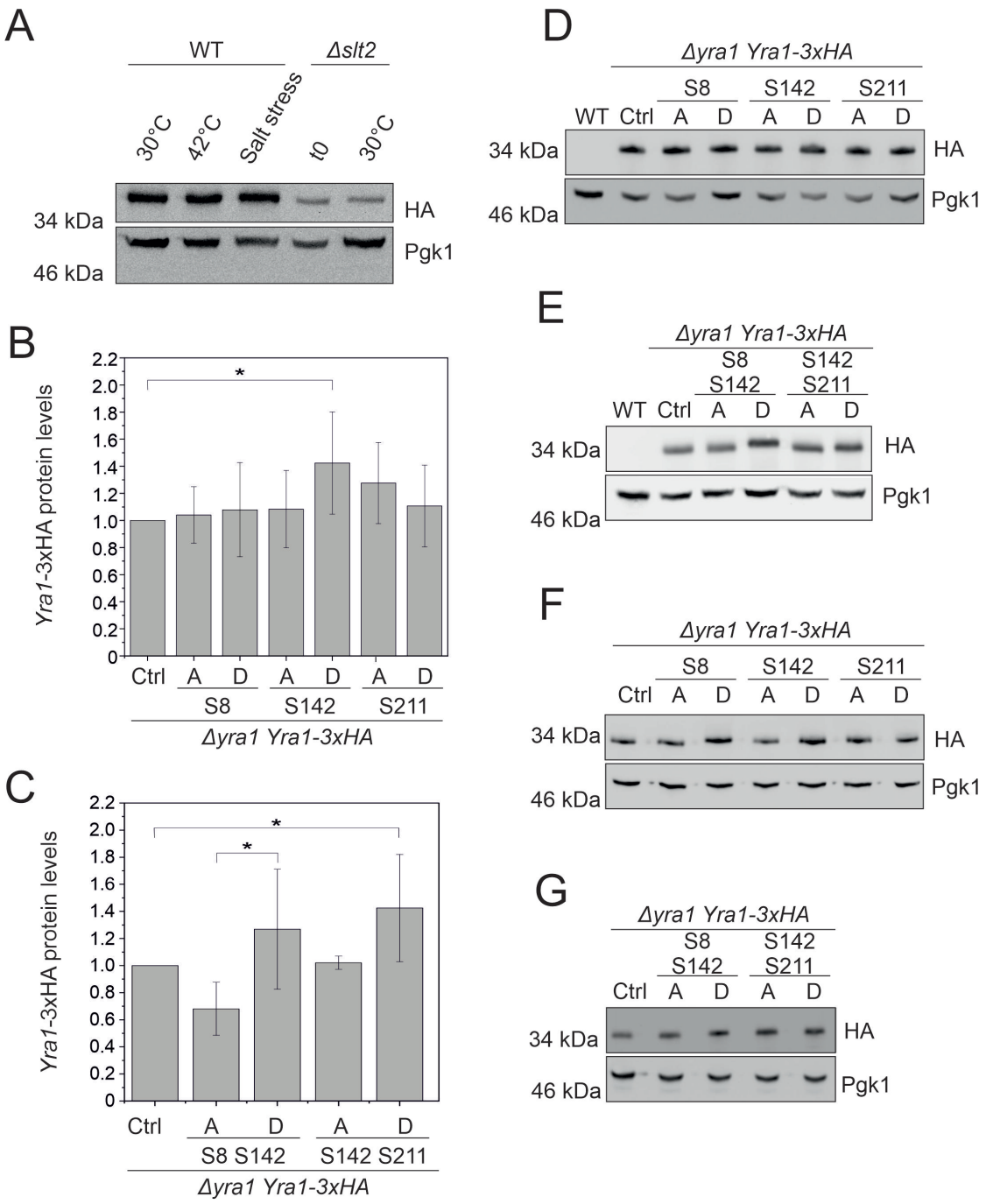

Figure H.2: **Preventing Yra1 phosphorylation influences the Yra1 protein level.** **A** Representative Western blot illustrating the reduction of Yra1 protein levels observed in the phosphoproteome data. Pgk1 serves as loading control.*B* - *E* Quantification and representative Western blot showing the *Yra1-3xHA* protein level of different Yra1 mutants at 30°C. *F* -*G* Representative Western blot showing the *Yra1-3xHA* protein level of different Yra1 mutants at after 1h heat shock. Pgk1 serves as loading control.

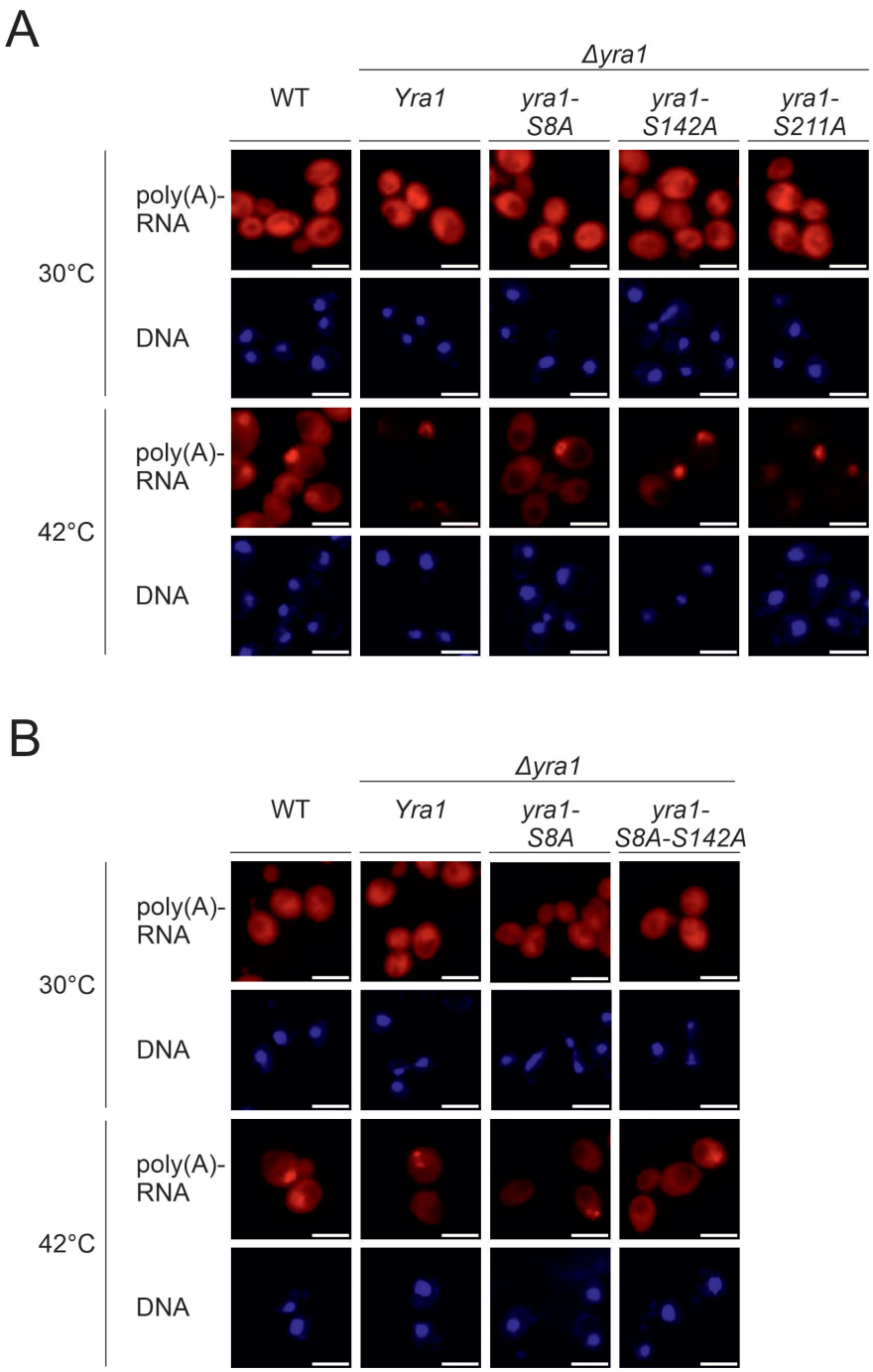

Figure H.3: **The *yra1-S8A* and *yra1-S8A-S142A* mutant show a decrease in nuclear poly(A)-RNA accumulation during heat stress.** Representative microscopy images of an Oligo(dT) FISH comparing the poly(A)-RNA export block of different Yra1 mutants at 30°C and heat stress. The 3 single mutants *yra1-S8A*, *yra1-S142A* and *yra1-S211A* are shown in *A* and the *yra1-S8A-S142A* double mutant in *B*. The DNA is stained with DAPI and depicted in blue. Poly(A)-RNA is stained using Oligo(dT)-Cy3 and depicted in red. The scale bar corresponds to 5 µm.

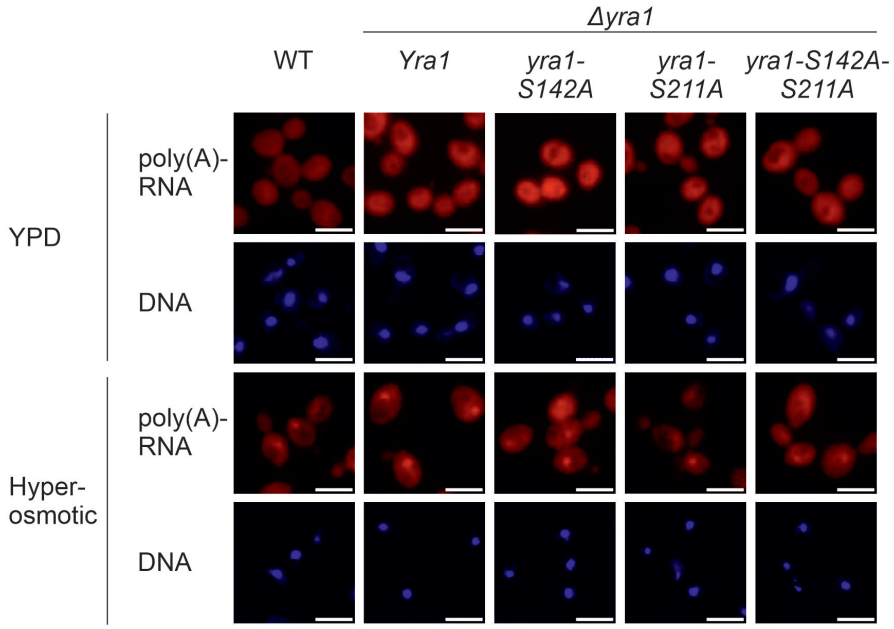

Figure H.4: **The *yra1-S142A* and *yra1-S142A-S211A* mutant show a decrease in nuclear poly(A)-RNA accumulation during hyperosmotic stress.** Representative microscopy images of an Oligo(dT) FISH comparing the poly(A)-RNA export block of different Yra1 mutants at 30°C and hyperosmotic stress. The DNA is stained with DAPI and depicted in blue. Poly(A)-RNA is stained using Oligo(dT)-Cy3 and depicted in red. The scale bar corresponds to 5 µm.

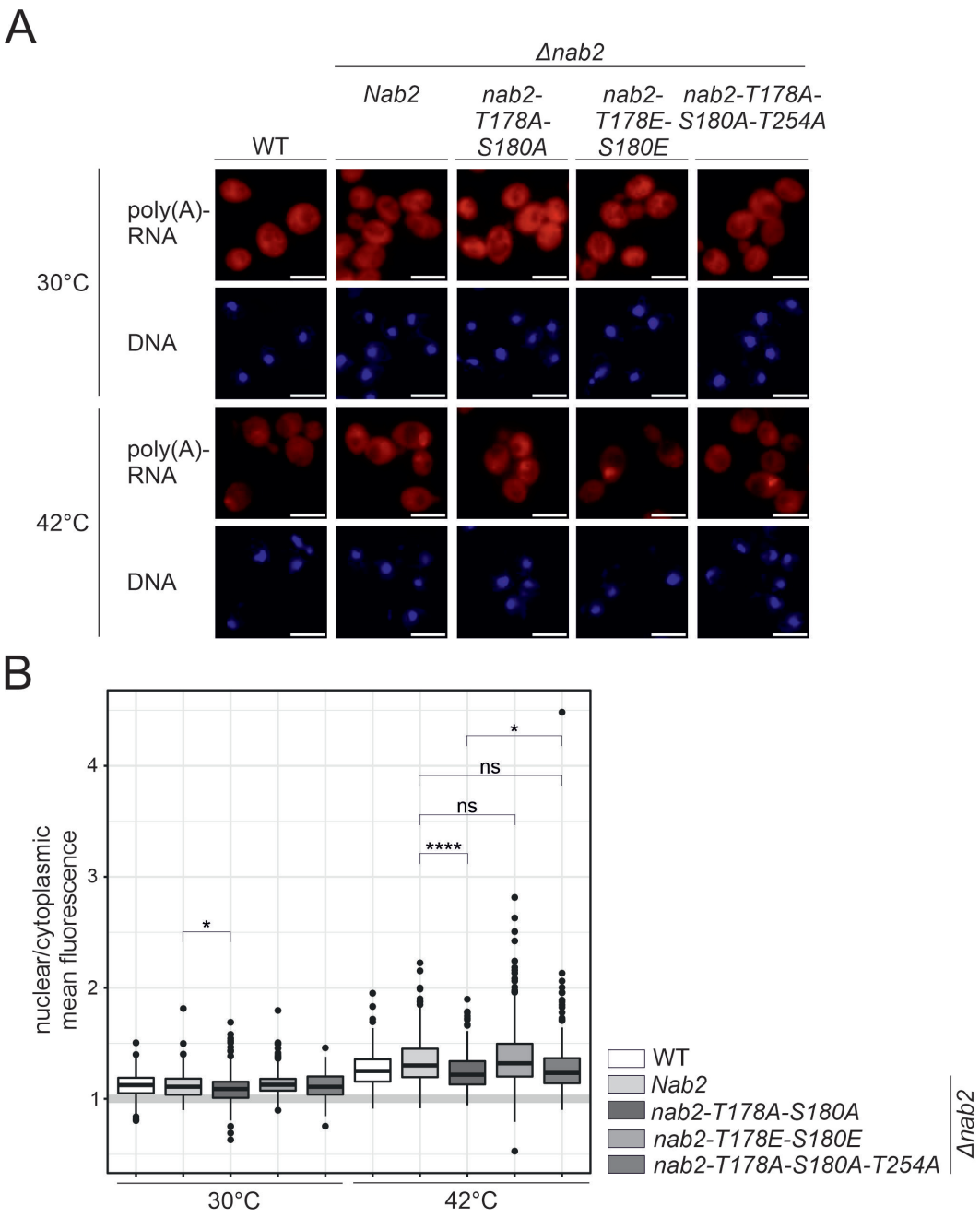

Figure H.5: **Additional Nab2 mutation of T254A leads to no further reduction in the poly(A)-RNA accumulation during heat shock.** Representative microscopy images (**A**) and quantification **B**) of an Oligo(dT) FISH comparing the poly(A)-RNA distribution in different Nab2 mutants at 30°C and during heat stress. **A** The DNA is stained with DAPI and depicted in blue. Poly(A)-RNA is stained using Oligo(dT)-Cy3 and depicted in red. The scale bar corresponds to 5 µm. **B** The graph shows a box plot diagram of nuclear/cytoplasmic mean fluorescence for the tested mutants. The quantification consists of two experiments with a total of ≥ 200 cells. The p-value was calculated using a Welch t-test with $\star$ $p < 0.05$ and $\star\star\star\star$ $p < 0.0001$.

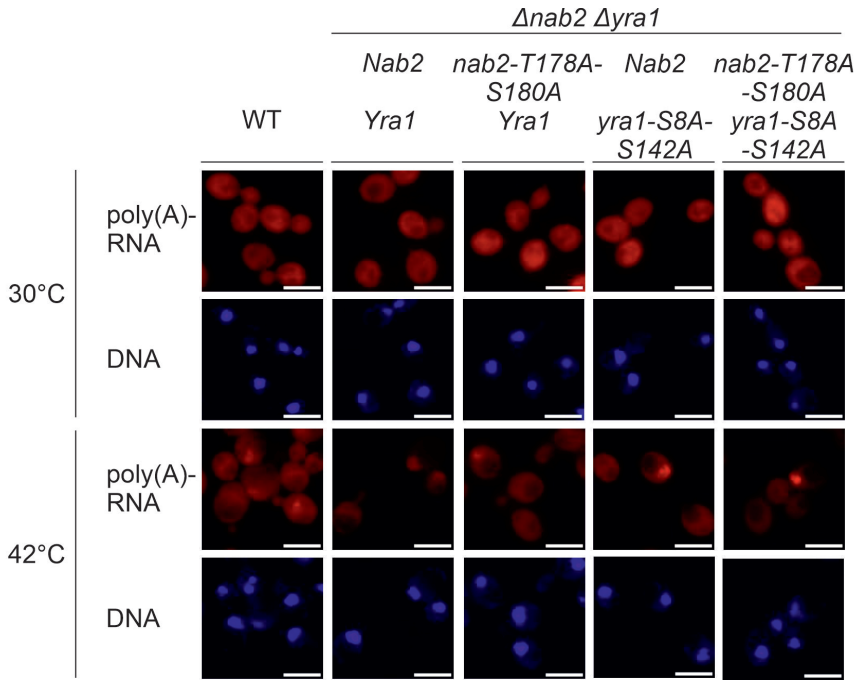

Figure H.6: **Additional Nab2 mutation leads to no further reduction in the poly(A)-RNA accumulation during heat shock compared to the *yra1-S8A-S142A* mutation alone.** Representative microscopy images of an Oligo(dT) FISH investigating the poly(A)-RNA accumulation in a *yra1-S8A-S142A nab2-T178A-S180A* strain heat stress. The DNA is stained with DAPI and depicted in blue. Poly(A)-RNA is stained using Oligo(dT)-Cy3 and depicted in red. The scale bar corresponds to 5 µm.

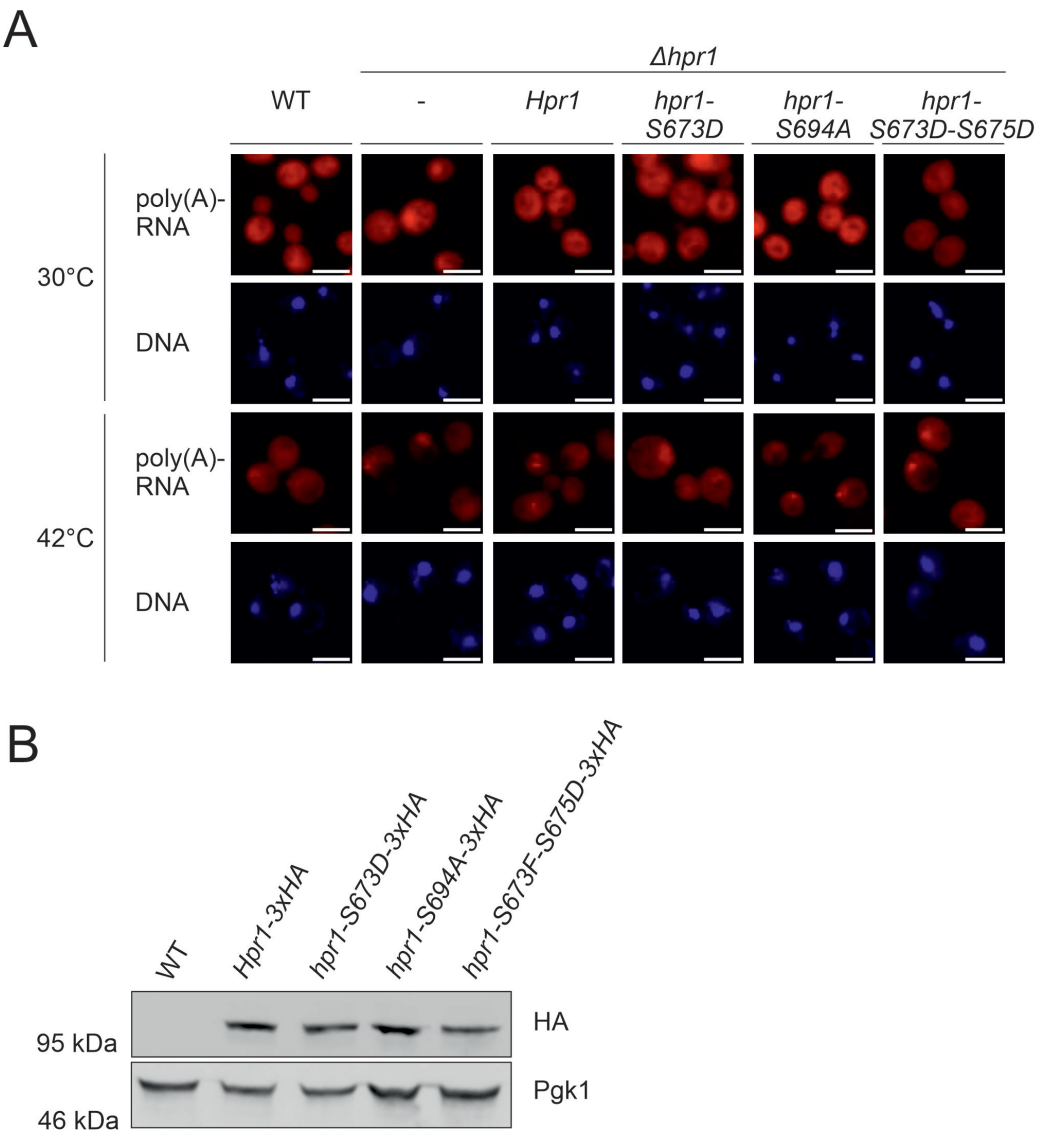

Figure H.7: **Preventing the reduction of Hpr1 phosphorylation leads to an increased poly(A)-RNA accumulation during heat stress. A** Representative microscopy images of an Oligo(dT) FISH analyzing the poly(A)-RNA accumulation for different Hpr1 mutants at 30°C and during heat stress. **B** Representative Western blot showing the *Hpr1-3xHA* protein levels of the different Hpr1 mutants during heat stress. Pgk1 serves as loading control.

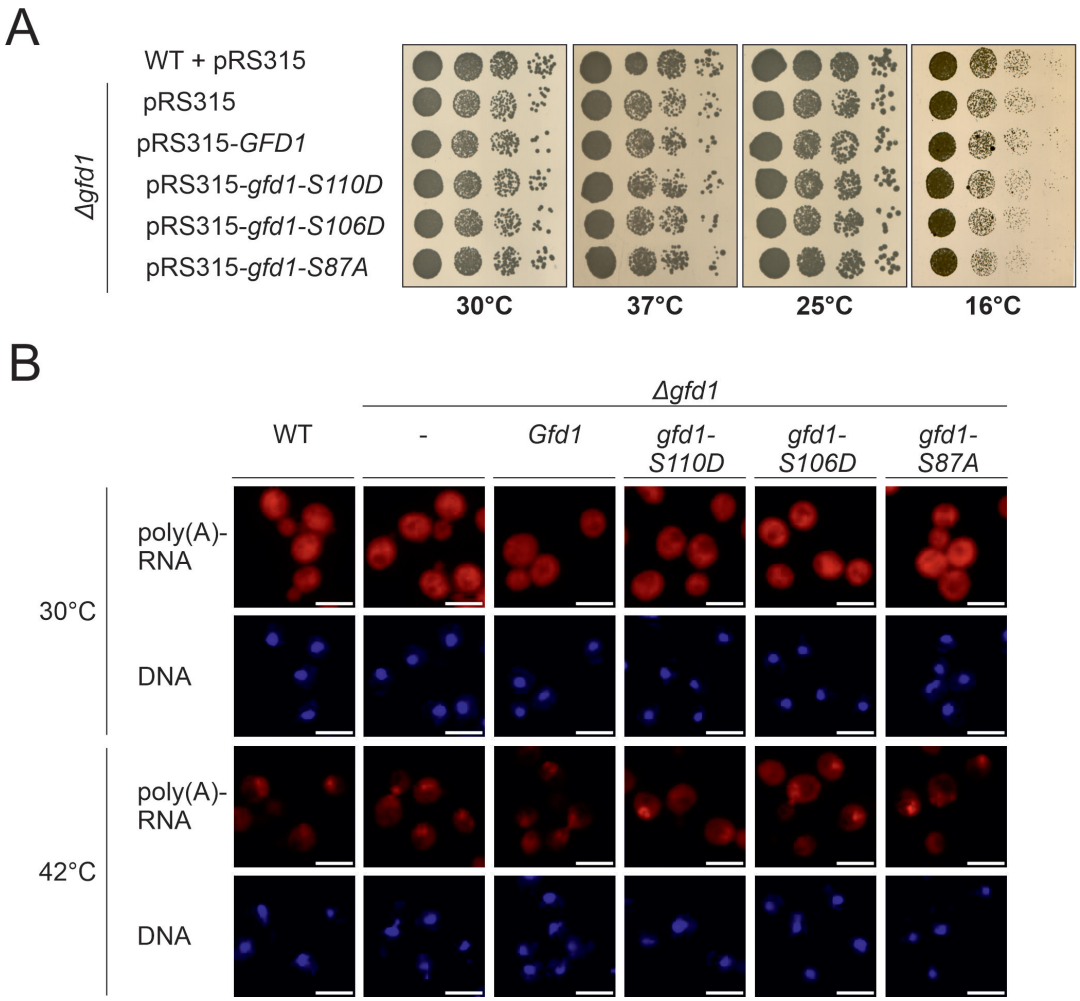

Figure H.8: **Preventing the reduction of Gfd1 phosphorylation leads to no visible growth defect. A** Representative growth spot assay showing the influence of the different mutations of Gfd1 on the corresponding yeast strain. Cells were spotted in 4 serial 1:10 dilutions. Plates were incubated for 2 days at 30°C, 3 days at 37°C and 25°C and 8 days at 16°C.**B** Representative microscopy images of an Oligo(dT) FISH analyzing the poly(A)-RNA accumulation for different Gfd1 mutants at 30°C and during heat stress.

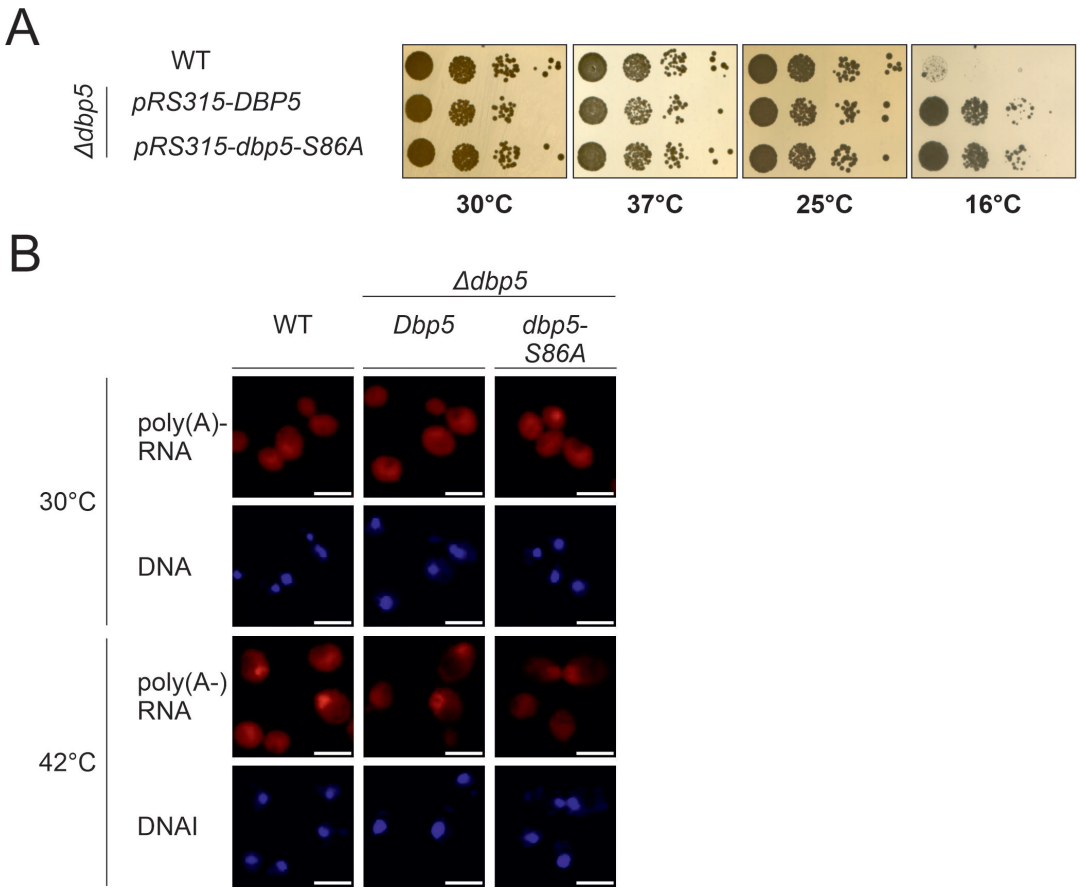

Figure H.9: **The *dbp5-S86A* mutation has no effect on cell growth or poly(A)-RNA accumulation during heat stress. A** Representative growth spot assay showing the influence of the S86A mutation of Dbp5 on the corresponding yeast strain. Cells were spotted in 4 serial 1:10 dilutions. Plates were incubated for 2 days at 30°C, 3 days at 37°C and 25°C and 8 days at 16°C.**B** Representative microscopy images of an Oligo(dT) FISH analyzing the poly(A)-RNA accumulation for *dbp5-S86A* and the corresponding controls at 30°C and during heat stress.

Eidesstattliche Erklärung

Ich erkläre: Ich habe die vorgelegte Dissertation selbstständig und ohne unerlaubte fremde Hilfe und nur mit den Hilfen angefertigt, die ich in der Dissertation angegeben habe. Alle Textstellen, die wörtlich oder sinngemäß aus veröffentlichten Schriften entnommen sind, und alle Angaben, die auf mündlichen Auskünften beruhen, sind als solche kenntlich gemacht. Ich stimme einer evtl. Überprüfung meiner Dissertation durch eine Antiplagiat-Software zu. Bei den von mir durchgeführten und in der Dissertation erwähnten Untersuchungen habe ich die Grundsätze guter wissenschaftlicher Praxis, wie sie in der „Satzung der Justus-Liebig-Universität Gießen zur Sicherung guter wissenschaftlicher Praxis“ niedergelegt sind, eingehalten.

Gießen, den